

Iridium Complexes for Intracellular Transfer Hydrogenation and Their Potential Biological Applications

A Dissertation Presented to
the Faculty of the Department of Chemistry
University of Houston

In Partial Fulfillment
of the Requirements for the Degree
Doctor of Philosophy

By
Anh Hong Ngo
May 2019

Iridium Complexes for Intracellular Transfer Hydrogenation and Their Potential Biological Applications

Anh Hong Ngo

APPROVED:

Dr. Loi H. Do, Chairman

Dr. Chengzhi Cai

Dr. Olafs Daugulis

Dr. Shoujun Xu

Dr. Shaun X. Zhang

**Dr. Dan Wells, Dean, College of
Natural Sciences and Mathematics**

ACKNOWLEDGEMENTS

I would like to express my sincerest gratitude to my advisor, Professor Loi H. Do. His guidance and support throughout this endeavor is invaluable. He is my role model and motivator for becoming a real scientist. His passion in pursuing great science, his critical thinking and patience in solving problems, and his time management to finish many works flawlessly in limited time are truly inspirational.

I appreciate all my Ph.D. committee members, Dr. Olafs Daugulis, Dr. Chengzhi Cai, Dr. Shoujun Xu, and Dr. Shaun X. Zhang for their insightful comments, valuable suggestions, as well as all the instructive questions about my research and this dissertation.

I gratefully acknowledge Dr. Maria Bondesson and her students for zebrafish studies, Dr. Chengzhi Cai and his students for cell experiments and instrumental usage, and Dr. Yongjun Gao for ICP-MS analysis.

My sincere thanks go to my group members: Lu Yang, Zhongzheng Cai, Mike Adams, Sohini Bose, Dawei Xiao, Thi Tran, Huong Nguyen, Dat Nguyen, Miguel Ibañez, and Yennie Nguyen. They are not only great lab mates to discuss about my research, but also great friends to share all the ups and downs in my life. Special thanks to Sohini Bose, Mike Adams, Lu Yang, and Miguel Ibañez for their collaboration in our shared projects.

I would also like to thank my friends in the Chemistry Department at the University of Houston, Ha Le, Truong Nguyen, Tung Nguyen, Ngoc Truong, Areej Siddig, and Chia-wei Hsu, who supported me along the way with hard courses, failed experiments, and difficult times in graduate school.

I am grateful to my parents, and my brother, who always believe in me and support my choices unconditionally. Without them, I could not go this far in my academic career.

My deepest appreciation goes to my husband, Hung Tran. He is the closest friend, the dearest companion, the most patient teacher/mentor, and the most faithful supporter in my life. I am thankful to him for sharing 24+ years and helping me become the better me every day.

Last but not least, I thank my sweet daughters, Giang and Anna, for their smiles and hugs which make me feel loved and recharge my energy to overcome any stress and difficulties.

Iridium Complexes for Intracellular Transfer Hydrogenation and Their Potential Biological Applications

An Abstract of a Dissertation

Presented to

the Faculty of the Department of Chemistry

University of Houston

In Partial Fulfillment

of the Requirements for the Degree

Doctor of Philosophy

By

Anh Hong Ngo

May 2019

ABSTRACT

Transfer hydrogenation is a transformation that has been studied for over 100 years and used widely in chemical synthesis. Although transfer hydrogenation can be performed by natural enzymes such as dehydrogenases, small-molecule intracellular metal catalysts (SIMCats) that are capable of catalyzing such reactions inside living systems have recently been discovered by our research group and others. We found that pentamethylcyclopentadienyl iridium(III) (Cp*Ir) complexes bearing 2-pyridinecarboxamidate ligands are capable of mediating catalytic hydride transfer from either NADH or formate to aldehydes in PBS buffer and cell culture media. These iridium catalysts are tolerant of moderate concentrations of biological nucleophiles, including thiols such as glutathione and cysteine.

To design more efficient catalysts for intracellular transfer hydrogenation, we performed structure-activity relationship (SAR) studies of a series of Cp*Ir pyridinecarboxamidate complexes. Chemical functionalization of the pyridine ring was found to have larger effects on the catalytic activity of the iridium complexes than functionalization of the *N*-amide substituent. Our NMR and UV-vis spectroscopic experiments showed that adding electron donating groups to the pyridine ring increased the hydride donor ability of the corresponding Ir-H complexes, which could enhance the rates of hydride transfer from Ir-H species to benzaldehyde by up to 28x, and lower the activation energy associated with the transfer hydrogenation process by up to 3 kcal/mol. More electron-rich Ir complexes were also found to have greater chemical stability under physiological conditions.

We have also discovered that our Cp*Ir complexes can efficiently reduce cytotoxic α,β -unsaturated aldehydes to non-toxic alcohols in cell culture media. Inductively coupled plasma-mass spectrometry (ICP-MS) analysis demonstrated that these iridium complexes could be retained inside NIH 3T3 and SH-SY5Y cells, as well as zebrafish. In our aldehyde detoxification experiments, cells that were pre-treated with our iridium complexes showed up to 30% greater survival compared to those that were pre-treated with conventional aldehyde scavengers such as carnosine or phloretin. The Ir complexes could also increase the viability of zebrafish in acrolein contaminated water by up to 40%. Our work could lead to the creation of new therapeutic methods in treating diseases associated with cytotoxic aldehydes such as metabolic disorders, neurodegenerative disorders, or cancers.

TABLE OF CONTENTS

Table of Contents	viii
List of Figures.....	x
List of Schemes.....	xiii
List of Tables	xiv
List of Abbreviations	xv
Chapter 1. Small-Molecule Intracellular Metal Catalysts (SIMCats) for Biological Studies	1
1.1. Introduction	2
1.2 Challenges in SIMCat-Promoted Chemistry.....	4
1.3 Achievements of SIMCat-Promoted Chemistry	5
1.3.1. A Brief History	5
1.3.2. Copper-Catalyzed Azide-Alkyne Cycloaddition (CuAAC)	8
1.3.3. Allylcarbamate Cleavage.....	11
1.3.4. Transfer Hydrogenation.....	14
1.4. The Future of SIMCat-Promoted Chemistry.....	18
1.5. References	23
Chapter 2. Iridium Complexes for Aqueous Alcohol Dehydrogenation.....	33
2.1 Introduction	34
2.2 Catalytic Activity Check and Substrate Scope Study	35
2.3 Mechanistic Studies.....	41
2.4 Conclusion.....	43
2.5 Experimental	44
2.6 References	45
Chapter 3. Iridium Complexes for Aldehyde Hydrogenation in Cell Culture Media	49
3.1 Introduction	50
3.2 Synthesis of Iridium Complexes and Catalytic Activity Study.....	51
3.3 Aldehyde Hydrogenation Study under Biological Conditions.....	56
3.4 Substrate Scope Studies	59
3.5 Mechanistic Studies.....	62
3.6 Hydrogenation of Cytotoxic Aldehyde	64
3.7 Conclusion.....	66
3.8 Experimental	66
3.9 References	72
Chapter 3 Appendix	77

Chapter 4. Optimization of Iridium Transfer Hydrogenation Catalysts Guided by Structure-Activity Relationship Studies	84
4.1 Introduction	85
4.2 Structural Modifications and Catalyst Activity Comparison	86
4.3 Thermodynamic Hydricity Measurement	90
4.4 Kinetic Studies	94
4.5 Temperature Dependence of the Reaction Rate Studies	101
4.6 Conclusion.....	103
4.7 Experimental	104
4.8 References	120
Chapter 4 Appendix	124
Chapter 5. Iridium Complexes for Aldehyde Detoxification in Living Cells	145
5.1 Introduction	146
5.2 Iridium Complexes Synthesis and In Vitro Transfer Hydrogenation of Toxic Aldehydes.....	148
5.3 Accumulation of Iridium Complexes in Cells.....	150
5.4 Toxicity of Iridium Complexes.....	152
5.5 Toxicity of Aldehydes, Their Alcohol Products and Aldehyde Scavengers.....	155
5.6 Aldehyde Detoxification by Iridium Complexes and Aldehyde Scavengers.....	157
5.7 Conclusion and Future Work	162
5.8 Experimental	163
5.9 References	168
Chapter 5 Appendix	172
Chapter 6. Iridium Complexes for Aldehyde Detoxification in Zebrafish.....	176
6.1 Introduction	177
6.2 Accumulation of Iridium Complexes in Zebrafish	178
6.3 Toxicity of Iridium Complexes.....	180
6.4 Toxicity of Acrolein and Alcohol Products	182
6.5 Aldehyde Detoxification by Iridium Complexes in Zebrafish.....	183
6.6 Conclusion and Future Work	184
6.7 Experimental	185
6.8 References	187

LIST OF FIGURES

Figure 1.1. Ideal properties of synthetic catalysts and SIMCats.....	4
Figure 1.2. Timelines for the development of biocompatible reactions.	9
Figure 1.3. Evolution of tris(triazole)amine ligands used in CuAAC reactions.	10
Figure 2.1. Representative GC plots from alcohol dehydrogenation studies.....	38
Figure 2.2. ¹³ C NMR spectral comparison of the product from reaction of cyclohex-2-en-1-ol/ Ir3 to those of authentic standards.....	39
Figure 2.3. ¹ H NMR spectrum of reaction of Ir3 with 3-methylcyclohex-2-en-1-ol	41
Figure 2.4. GC-TCD traces analysis of by-products.....	42
Figure 3.1. Catalytic comparison in hydrogenation of benzaldehyde.....	53
Figure 3.2. Recyclability study of Ir4 in the hydrogenation of benzaldehyde.	54
Figure 3.3. Effect of formate equivalence on the hydrogenation efficiency of Ir4	54
Figure 3.4. Effect of NADH equivalence on the hydrogenation efficiency of Ir4	55
Figure 3.5. Hydrogenation of benzaldehyde by Ir4 /NADH in the presence of biologically relevant additives.....	56
Figure 3.6. Effect of solvent on the hydrogenation of benzaldehyde by Ir4 /NADH.	57
Figure 3.7. Reaction of benzaldehyde/sodium formate in the presence of metal ions. ...	58
Figure 3.8. ¹ H NMR spectra from the reaction of the iridium complexes with NADH. .	63
Figure 3.9. ¹ H NMR spectra of Ir-H complexes and benzaldehyde	64
Figure 3.10. Hydrogenation of 4-hydroxynon-2-enal by Ir4 /NADH.....	65
Figure A3.1. Representative GC plots from the hydride transfer studies.	77
Figure A3.2. GC traces from the reaction of Ir-H with benzaldehyde in D ₂ O	78
Figure A3.3. GC traces from the reaction of Ir-H with benzaldehyde in CD ₃ OD.....	78
Figure A3.4. GC plot from the reaction of 4-hydroxynon-2-enal, NADH, and Ir4	78
Figure A3.5. ¹ H NMR spectra of Ir2-H and benzaldehyde.....	79
Figure A3.6. ¹ H NMR spectra of Ir9-H and benzaldehyde.....	80
Figure A3.7. ¹ H NMR spectra of Ir4-H and benzaldehyde.....	80
Figure A3.8. ¹ H NMR spectrum of complex Ir4-H	82
Figure A3.9. ¹³ C NMR spectrum of complex Ir4-H	83
Figure 4.1. Catalytic comparison in hydrogenation of benzaldehyde.....	88
Figure 4.2. Catalyst recycling studies in hydrogenation of benzaldehyde.....	90

Figure 4.3. Correlations between thermodynamic hydricity of metal hydride complexes and reaction yield of transfer hydrogenation by metal chloride complexes.	94
Figure 4.4. ¹ H NMR spectra in hydrolysis studies of Ir complexes.....	96
Figure 4.5. Kinetic plots from the reaction of benzaldehyde with iridium complex and sodium formate.	97
Figure 4.6. Initial rate comparison between different catalysts in transfer hydrogenation of benzaldehyde at various temperatures.....	98
Figure 4.7. UV-Vis kinetic studies of iridium hydride formation.	99
Figure 4.8. UV-Vis kinetic studies of hydride transfer reaction.....	100
Figure 4.9. Temperature dependence studies of iridium complexes.....	101
Figure A4.1. Cyclic voltammograms of complexes 2 , 8 , 10 , and 11	124
Figure A4.2. Hydride exchange study between complexes 1a and 1b-H in D ₂ O.	125
Figure A4.3. Hydride exchange study between complexes 1a and 1b-H in D ₂ O:CH ₃ OH (1:1).	125
Figure A4.4. Hydride exchange study between complexes Ir4-H and Ru6	127
Figure A4.5. Hydride exchange study between complexes Ir16-H and Ru6	128
Figure A4.6. Hydride exchange study between complexes Ir18-H and Ru6	129
Figure A4.7. Hydride exchange study between complexes Ir19-H and Ru6	130
Figure A4.8. Hydride exchange study between complexes Ir17-H and Ir2	131
Figure A4.9. Hydride exchange study between complexes Ir20 and Ir4-H	132
Figure A4.10. ¹ H NMR spectra of complex Ir2-H₂O in the presence of NaCl.	133
Figure A4.11. ¹ H NMR spectra of complex Ir4-H₂O in the presence of NaCl.	134
Figure A4.12. Reactions of iridium complexes with sodium formate (UV-vis).....	135
Figure A4.13. Kinetic plots for the reaction of Ir complexes with sodium formate.....	136
Figure A4.14. Reactions of iridium-hydride complexes with benzaldehyde (UV-vis).	137
Figure A4.15. Kinetic plots for the reaction of Ir-H complexes with benzaldehyde.....	138
Figure A4.16. Kinetic plots for the reaction of benzaldehyde with complex Ir4	140
Figure A4.17. Temperature dependence studies of the reaction of benzaldehyde with complex Ir4 and sodium formate.	141
Figure A4.18. Temperature dependence studies of the reaction of benzaldehyde with complex Ir18 and sodium formate.	142
Figure A4.19. Temperature dependence studies of the reaction of benzaldehyde with complex Ir17 and sodium formate.	143

Figure A4.20. Temperature dependence studies of the reaction of benzaldehyde with complex Ir20 and sodium formate.	144
Figure 5.1. Iridium accumulation in cells	151
Figure 5.2. IC ₅₀ of iridium complexes in NIH 3T3 cell lines.	153
Figure 5.3. IC ₅₀ of iridium complexes in SH-SY5Y cell lines.	153
Figure 5.4. IC ₅₀ of Iridium complexes in NIH 3T3 cell line with and without sodium formate addition.	154
Figure 5.5. IC ₅₀ of aldehydes, alcohol and aldehyde scavengers.	156
Figure 5.6. Compare iridium complexes and aldehyde scavengers in rescue NIH 3T3 cells from toxic aldehydes.	1588
Figure 5.7. Iridium complexes in rescue NIH 3T3 cells from acrolein.	159
Figure 5.8. Compare iridium complexes and aldehyde scavengers in rescue SH-SY5Y cells from toxic aldehydes.	161
Figure A5.1. IC ₅₀ plots of Iridium complexes in SH-SY5Y cell line.	175
Figure 6.1. Iridium accumulation in zebrafish.....	179
Figure 6.2. Toxicity of iridium complexes in zebrafish.....	181
Figure 6.3. Toxicity of acrolein and its alcohol products in zebrafish.....	182
Figure 6.4. Effect of Ir SIMCats on zebrafish exposed to acrolein.	183

LIST OF SCHEMES

Scheme 1.1. Possible applications of SIMCats	3
Scheme 1.2. Depiction of the different types of reported SIMCat-promoted reactions.....	6
Scheme 1.3. Ruthenium-catalyzed allylcarbamate cleavage studied by Meggers and co-workers.....	12
Scheme 1.4. Catalytic reduction of protons, dioxygen, quinones, ketones, and aldehydes by iridium complexes using NADH as a reductant	15
Scheme 1.5. Evaluation of various organoiridium complexes in facilitating the transfer hydrogenation between NADH and benzaldehydes.	16
Scheme 1.6. Transfer hydrogenation carried out in the live mammalian cells and its application in the detoxification of cytotoxic aldehydes	17
Scheme 1.7. Some promising reactions that might be suitable for further SIMCat-promoted chemistry development.....	20
Scheme 2.1. Proposed Mechanism for Alcohol Dehydrogenation by Ir3	34
Scheme 2.2. Proposed interconversion mechanism of symmetric six-membered ring substrates.....	37
Scheme 2.3. Proposed interconversion mechanism of asymmetric six-membered ring substrates.....	37
Scheme 2.4. Interconversion of cortisol.....	43
Scheme 3.1. Transfer Hydrogenation by Iridium Complexes.....	62
Scheme 4.1. Synthesis of Ir, Ru, and Rh complexes.....	87
Scheme 4.2. Thermodynamic hydricity calculations.	91
Scheme 4.3. Elementary steps in transfer hydrogenation by Cp*Ir complexes.	95
Scheme 5.1. Proposed aldehyde detoxification pathway of Ir complexes inside cells ..	147
Scheme 5.2. In vitro hydrogenation of toxic aldehyde.....	149
Scheme 5.3. Procedure for determining iridium accumulation inside cells.	150
Scheme 5.4. Procedure for determining toxicity of iridium complexes.....	152
Scheme 5.5. Procedure for determining toxicity of aldehydes and other compounds ...	155
Scheme 5.6. Procedure for aldehyde detoxification in cells	157
Scheme 6.1. Procedure for determining toxicity of iridium complexes in zebrafish.	180
Scheme 6.2. Procedure for aldehyde detoxification by Ir complexes in zebrafish.	183

LIST OF TABLES

Table 2.1. Alcohol Dehydrogenation Study.....	36
Table 2.2. Reaction Conditions Tested for Benzyl Alcohol Dehydrogenation.....	40
Table 3.1. Hydrogenation of Aldehydes and Ketones Using Ir4 /Formate	60
Table 3.2. Hydrogenation of Aldehydes and Ketones Using Ir4 /NADH.....	61
Table 4.1. Comparison of Calculated Hydricity of Ir2-H in Different Solvents.....	92
Table 4.2. Summary of Calculated Hydricities of Iridium-Hydride Complexes	92
Table 4.3. Summary of Calculated Hydricities of Complex Ir17-H	92
Table 4.4. Summary of Activation Parameters of Tested Iridium Catalysts.....	102
Table A4.1. Calculated Rate Constants from Kinetic Data.....	139
Table A5.1 Accumulation of Iridium in NIH 3T3 Cells	172
Table A5.2 Accumulation of Iridium in SH-SY5Y Cells	174
Table 6.1. Iridium Accumulation in Zebrafish.....	179

LIST OF ABBREVIATIONS

Bu	butyl
Calc	calculation
Cp*	pentamethylcyclopentadienyl
CV	cyclic voltammetry
d	doublet
DCM	dichloromethane
DMEM	Dulbecco's Modified Eagle Media
DMSO	dimethyl sulfoxide
dpf	day post fertilization
equiv.	equivalent
ESI	electrospray ionization
Et	ethyl
FBS	fetal bovine serum
FT-IR	fourier-transform infrared spectroscopy
GC-MS	gas chromatography–mass spectrometry
GSH	glutathione
h	hour
HEPES	(4-(2-hydroxyethyl)-1-piperazineethanesulfonic acid)
hpf	hour post fertilization
HRMS	high resolution mass spectrometry
IC50	half maximal inhibitory concentration
ICP-MS	inductively coupled plasma-mass spectrometry
IR	infrared (spectroscopy)
Ir	iridium
<i>J</i>	coupling constant
LC50	half maximal lethal concentration
m	multiplet or milli
<i>m/z</i>	mass to charge ratio
Me	methyl
min	minute
mL	milli liter
mM	milli molar
NAD ⁺	nicotinamide adenine dinucleotide, oxidized form
NADH	nicotinamide adenine dinucleotide, reduced form
ng	nano gram
NMR	nuclear magnetic resonance

PBS	phosphate buffer saline
Ph	phenyl
Py	pyridine
q	quartet
r_i	initial rate
ROS	reactive oxygen species
s	singlet or second
SAR	structure-activity relationship
SIMCat	small-molecule intracellular metal catalyst
t	triplet
Tosyl	p-toluenesulfonyl
V	volt
μM	micro molar

Chapter 1.
Small-Molecule Intracellular Metal Catalysts (SIMCats)
for Biological Studies

Portions of this work have been previously published.

Reproduced with permission from Ngo, A. H.; Bose, S.; Do, L. H. *Chem.–Eur. J.*, **2018**, *24*, 10584-10594. DOI: 10.1002/chem.201800504. (*Ngo and Bose contributed equally*).

Copyright 2017 WILEY-VCH Verlag GmbH & Co.

1.1. Introduction

Biological enzymes, with their extraordinary ability to recognize and transform complex molecules, have long fascinated chemists. They have been used in diverse applications ranging from enantioselective drug synthesis¹⁻³ to cascade reaction processes.⁴⁻⁶ Due to advances in site-directed mutagenesis⁷⁻⁸ and directed evolution⁹⁻¹¹ techniques, chemists can even engineer enzymes with user-defined substrate specificity and reactivity.

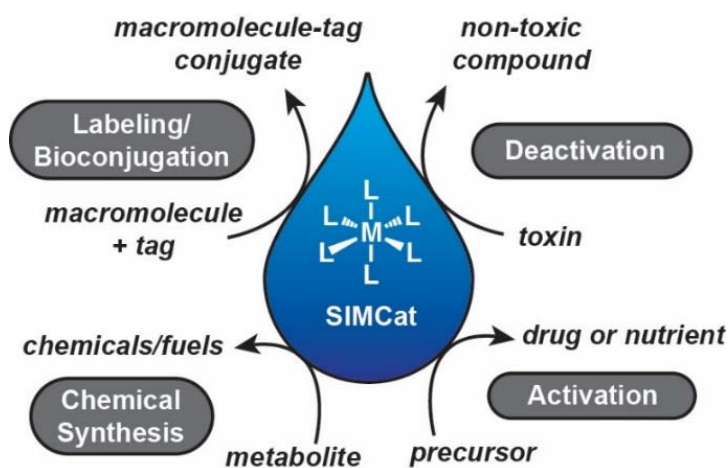
One of the most well-known examples of the fusion of chemistry with enzymology is artificial metalloenzymes, or protein complexes with synthetic metal active sites.¹²⁻¹⁶ Although these artificial protein hybrids can achieve functions that are new to nature,¹⁷ they have some potential drawbacks such as the cost to scale up, their difficulty in handling and storage, and their inability to be encoded in all living systems.

Using small-molecule metal compounds to mimic natural enzymes is an attractive approach to achieve new bioorthogonal chemistry.¹⁸⁻¹⁹ Unlike the metal centers in artificial metalloenzymes that are shielded, unprotected metal species are easily inhibited by biological nucleophiles such as glutathione (GSH),²⁰ thiol-containing proteins, or nucleobases, which have limited their application to *ex vivo* studies (i.e. in reaction flasks or test tubes). Despite this challenge, some successes in applying small-molecule metal compounds in living hosts have been reported.²¹

In this dissertation, the acronym SIMCat (small-molecule intracellular metal catalyst) will be used to define non-toxic low molecular weight metal catalysts that are active inside biological systems.²² This terminology can help to differentiate SIMCats from

macromolecular (e.g. enzymes, metalloenzymes, DNAszymes, and ribozymes) and heterogeneous catalysts (e.g. nanozymes²³⁻²⁴) studied in biological context.

As illustrated in Scheme 1.1, SIMCats can be employed in various applications. They can be applied to mediate bioconjugation reactions, in which molecular probes or other functional groups are covalently attached to biomolecules. Although non-metal based methods are commonly used in labeling studies, SIMCat-promoted reactions can offer expanded bioorthogonal capabilities.²⁵⁻²⁶ SIMCats can also be useful in chemical synthesis to manufacture chemicals and fuels in vivo from naturally occurring metabolites as synthons. Finally, SIMCats might be effective as therapeutic agents, such as by catalytically converting non-toxic precursor molecules to biologically active compounds or alternatively, by neutralizing chemical toxins to non-hazardous substances.¹⁸



Scheme 1.1. Possible applications of SIMCats

1.2 Challenges in SIMCat-Promoted Chemistry

SIMCat-promoted chemistry is an exciting research frontier because transition metal catalysts have been largely overlooked in the life sciences. Similar to conventional synthetic catalysts, the ideal SIMCat should be inexpensive, easy to use, and promote reactions that are fast, efficient, and selective (Figure 1.1). To be economical and environmental friendly, it should also be recyclable. Moreover, SIMCats must be biocompatible, which means that they must also be non-toxic, air and water stable, tolerant of biological nucleophiles, have good cellular retention, and are active under physiological conditions (i.e. in water, under air, at neutral pH and mild temperature).²⁷ These stringent requirements make designing novel SIMCats extremely challenging.

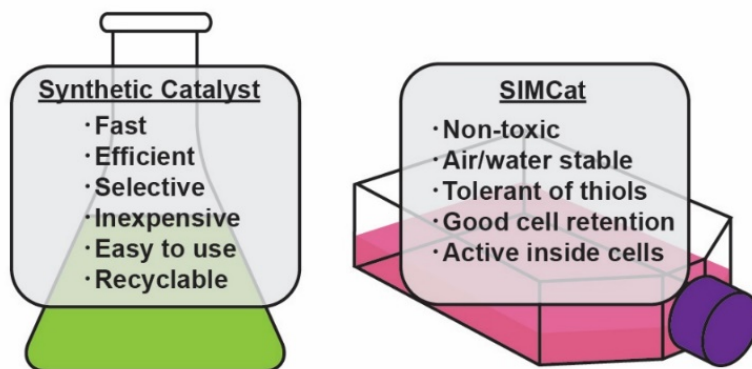


Figure 1.1. Ideal properties of synthetic catalysts and SIMCats

A variety of strategies have been used to enhance the performance of intracellular catalysts. For example, the biocompatibility of metal complexes can be enhanced by encapsulating them in protective matrices using protein scaffolds, polymers/dendrimers, or molecular cages.¹² Another approach is to reduce the intracellular concentrations of

potential catalyst inhibitors, such as treatment of cells with diamide,²⁰ buthionine sulfoximine (BSO), or *N*-ethylmaleimide (NEM)²⁸ to reduce GSH.

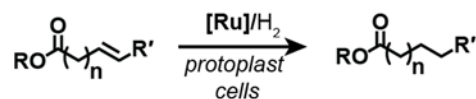
A common challenge in designing SIMCats is that it is difficult to predict their cytotoxicity, biodistribution, and retention time inside the cell. However, these parameters are often tunable. The IC₅₀ values (the 50 % growth inhibition concentration) of some metal complexes in mammalian cells were reported to be greater than 500 μM²⁹ and have been found to correlate with their lipophilicity.³⁰ Modification of a metal complex's ligand periphery can significantly enhance both its biocompatibility and catalytic activity.³¹ A variety of established targeting strategies could be used to direct metal complexes to specific biological organs or cellular compartments.³² As we will demonstrate, an iterative design process is often required to optimize SIMCats for intracellular applications.

1.3 Achievements of SIMCat-Promoted Chemistry

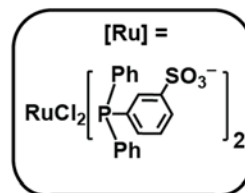
1.3.1. A Brief History

Studies of inorganic complexes in biology mainly focus on their medicinal properties.³³ They have been successfully applied as enzyme inhibitors,³⁴⁻³⁵ photodynamic therapy agents,³⁶ and carbon monoxide-releasing molecules (CORMs).³⁷ These applications utilize metal complex's unique three-dimensional structures, redox activities, and facile ligand exchange abilities, respectively. In comparison, the catalytic properties of these metal complexes in the biological systems have been nearly unexplored. To date, only a limited number of metal-catalyzed reactions can be considered biocompatible (Scheme 1.2).

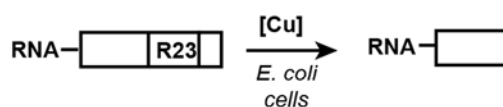
A) Hydrogenation



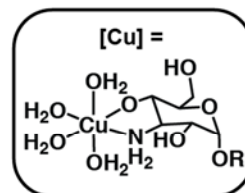
Vigh/Joó/Cséplő, 1985 (Ref. 38)



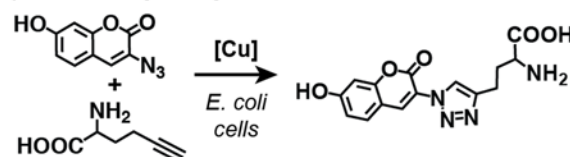
B) Hydrolysis/Oxidative Cleavage



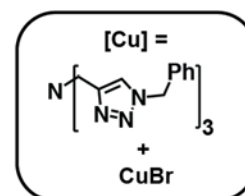
Cowan, 2002 (Ref. 47)



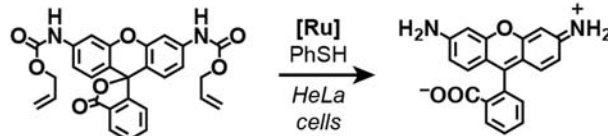
C) Azide-Alkyne Cycloaddition



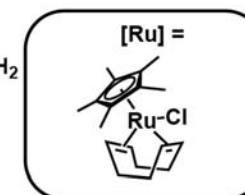
Tirrell, 2005 (Ref. 51)



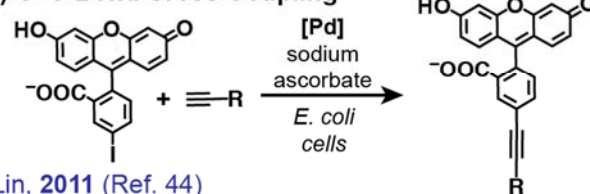
D) Allylcarbamate Cleavage



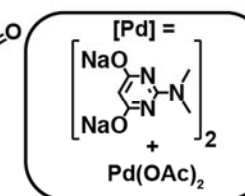
Meggers, 2006 (Ref. 43)



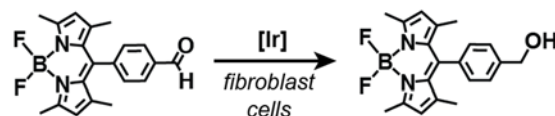
E) C-C Bond Cross Coupling



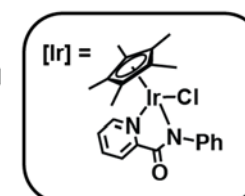
Lin, 2011 (Ref. 44)



F) Transfer Hydrogenation



Do, 2017 (Ref. 46)



Scheme 1.2. Depiction of the different types of reported SIMCat-promoted reactions.

One of the earliest examples of using SIMCats in living cells was reported in 1985 by Vigh, Joó, and Cséplö (Scheme 1.2A).³⁸ In this study, a ruthenium triarylphosphine chloride complex was shown to catalyze the hydrogenation of C-C double bonds in unsaturated fatty acids using hydrogen gas. This method was employed to study membrane fluidity in regulatory processes by modulating the microviscosity of intact plant cells. However, the protoplasts showed extensive cell damage after exposure to the ruthenium catalyst and hydrogen for 1 h. Detailed mechanistic studies of this biorthogonal hydrogenation chemistry, which may help to understand how the water-soluble ruthenium complex can react with the double bonds buried inside the interior of the membrane bilayer, has not yet been reported.

Research on SIMCats has grown since the 2000s. Breakthrough advances were achieved in the development of SIMCats for hydrolysis/oxidative cleavage,³⁹⁻⁴⁰ azide-alkyne cycloaddition,⁴¹⁻⁴² allylcarbamate cleavage,⁴³ C-C bond cross coupling,⁴⁴ and transfer hydrogenation.⁴⁵⁻⁴⁶ All of these reactions were performed inside living cells using soluble metal catalysts. Some of these SIMCats were well-defined metal complexes whereas others were generated in situ by combining free ligands with metal salts. The utilization of SIMCat-promoted reactions furnished new chemical tools for researchers working in the life sciences. In 2002, Cowan and co-workers showed that *E. coli* bacteria could be treated with copper aminoglycoside complexes to induce cleavage of specific RNA sequences (Scheme 1.2B).⁴⁷ The mechanism of ribonucleic acid splitting most likely involves copper-mediated hydrolysis and/or oxidation. This discovery could have important implications on antibiotics or antiviral therapeutic studies. In another example, Lin and co-workers used palladium aminopyrimidine complexes to perform Sonogashira

C-C bond cross-coupling reactions in *E. coli* (Scheme 1.2E).⁴⁴ They successfully tagged a homo-propargylglycine-encoded ubiquitin protein with a fluorescein dye. This SIMCat-promoted chemistry will expand the range of organic functional groups that could be utilized in bioconjugation, a useful strategy for studying protein dynamics in cellular systems.

1.3.2. Copper-Catalyzed Azide-Alkyne Cycloaddition (CuAAC)

In 2002, the regioselective synthesis of 1,4-disubstituted triazoles from organic azides and alkynes using copper (I) catalysts was independently reported by the research groups of Fokin/Sharpless⁴¹ and Meldal⁴² (Figure 1.2A). This discovery impacted many areas of scientific research, including chemical synthesis, drug development, and materials science.⁴⁸ CuAAC was successfully utilized in chemical biology, such as in the labeling of intact bacterial cells,⁴⁹ and profiling enzyme activity in whole proteasomes.⁵⁰ In 2005, CuAAC reactions were performed inside living cells for the first time by two different groups. Tirrell and co-workers were able to track the synthesis of a model protein barstar containing unnatural alkynyl amino acids in auxotrophic *E. coli* by tagging it with coumarin azides using a CuAAC ligation method (Scheme 1.2C).⁵¹ Similarly, Schultz and co-workers used CuAAC to conjugate propargyloxyphenylalanine, which was site selectively incorporated into intracellular proteins, with dansyl or fluorescein azide probes.⁵² This copper-based SIMCats-promoted reaction quickly gained popularity because it is fast, robust, and biorthogonal.

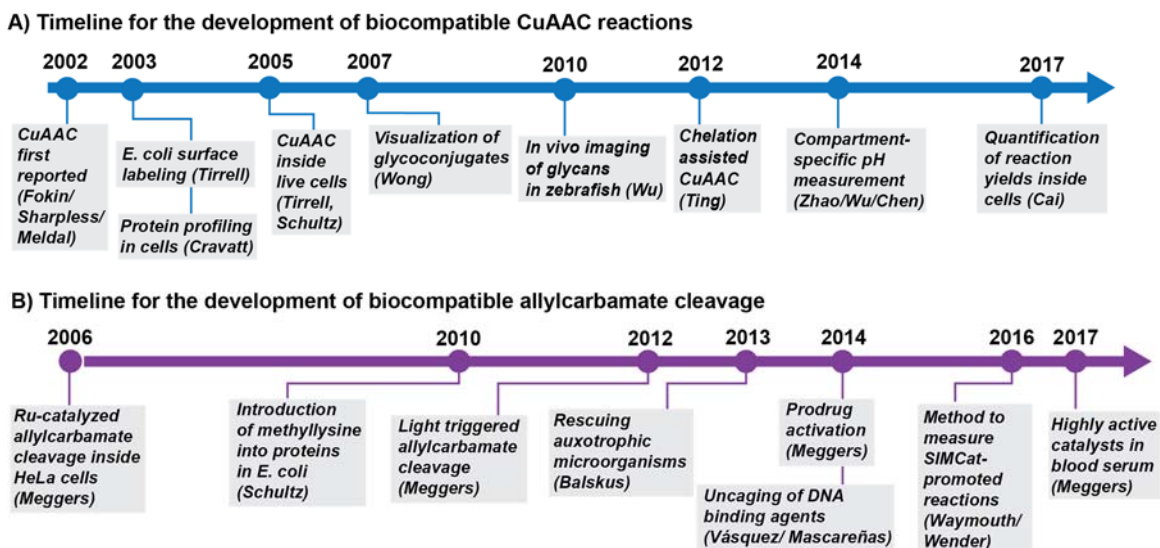


Figure 1.2. Timelines for the development of biocompatible reactions: A) copper azide-alkyne cycloaddition (CuAAC), and B) ruthenium-catalyzed allylcarbamate cleavage.

To reduce the potential cytotoxic effects of copper ions, many researchers used copper complexes that are stabilized by multidentate ligands. In 2007, Wong and co-workers reported that fucose and sialic analogs containing terminal alkynes could be fused with cellular glycans using copper tris(triazole)amine (Ligand 1, Figure 1.3) as the CuAAC catalyst.⁵³ Because aberrant glycosylation has been closely linked to cancer, this work is important for the identification of glycan-related biomarkers and targets for therapeutic intervention. However, due to the toxicity of the copper complexes, the CuAAC reactions in this work had to be performed on fixed rather than live cells. A significant advance in the development of more biocompatible copper complexes was made in 2010 by Wu and co-workers.³¹ From a library of 14 tris(triazole)amine ligand derivatives, they found that a bulky sulfonate variant (Ligand 2, Figure 1.3) provided Cu catalysts that achieved the ideal balance between reactivity and solubility. Wu's group was able to use this copper complex to fluorescently label alkyne-bearing guanosine diphosphate (GDP)-fucose inside zebrafish

embryos. Moreover, the emissive fucosylated glycans in the enveloping layer of zebrafish could be visualized in real time by confocal microscopy. A similar copper complex was successfully employed in the intracellular conjugation of an environment-sensitive fluorophore to an acid-stress chaperone protein called HdeA by Zhao/Wu/Chen and co-workers.⁵⁴ This HdeA-probe hybrid can be applied to measure pH in both the periplasm and cytoplasm of *E. coli*. These two findings demonstrate clearly the power of ligand design in the development of SIMCat-promoted chemistry.

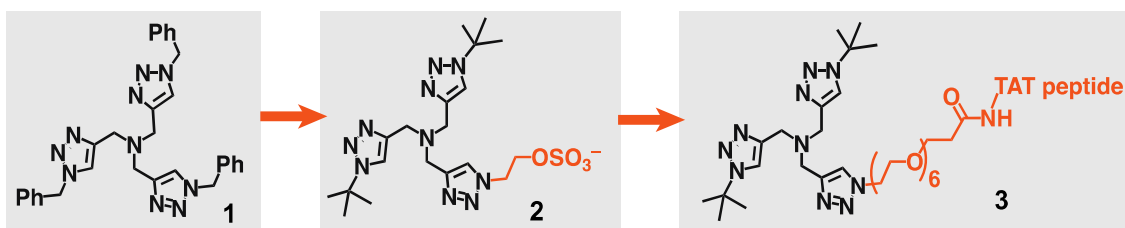


Figure 1.3. Evolution of tris(triazole)amine ligands used in CuAAC reactions.

An alternative approach to improve the cell compatibility and catalytic activity of copper complexes is to utilize metal chelating azide substrates. In 2012, Ting and co-workers showed that chelating substrates enhanced the cell labelling efficiency of CuAAC reactions up to 25-fold compared to that of non-chelating substrates.⁵⁵ Importantly, this substrate chelation ability enable relatively low concentrations (10-100 μM) of copper to be used for intracellular studies.

Recently, Cai and co-workers reported a method employing mass spectrometry to quantify the product yields in biological CuAAC reactions, and using those results to compare the catalytic performances between a variety of copper complexes.²⁸ They discovered that attachment of a cell-penetrating peptide into tris(triazole)amine (Ligand 3,

Figure 1.3) can increase the uptake of copper complexes in human OVCAR5 cancer cells up to 15-fold compared to that for conventional ligands. This study also found that high levels of glutathione were the main reason for the low catalytic activity (~ 0.8% yield) of CuAAC reactions inside cells.

1.3.3. Allylcarbamate Cleavage

Along with CuAAC, allylcarbamate cleavage is one of the most well-known bioorthogonal reactions used today. In 2006, Meggers and coworker reported the application of soluble organometallic ruthenium complexes in uncaging allylcarbamate substrates (Scheme 1.2D).⁴³ Using a Ru(Cp*)(COD)(Cl) complex (**Ru1**, Cp* = pentamethylcyclopentadienyl anion, COD = 1,5-cyclooctadiene) and thiophenol in aqueous solvent under air, they can convert compounds containing allylcarbamate groups to the corresponding amines in excellent yields. In HeLa cells, the conversion of the caged fluorophore to the free rhodamine by **Ru1** led to significant fluorescence enhancement within the cellular cytoplasm (Chart 1.2B). Interestingly, the presence of thiols promoted rather than inhibited the ruthenium SIMCat in this allylcarbamate cleavage reaction. A photo-activatable ruthenium catalyst for intracellular chemistry was also reported.⁵⁶

Although **Ru1** showed a fast initial rate, it was deactivated quickly (<30 min).⁴³ In searching for better catalysts, Meggers' group utilized a water-soluble allylcarbamate probe (**4**) that allowed them to monitor reactions in water by fluorescence spectroscopy. Initial catalyst screening studies indicated that cationic Ru(Cp)(2-quinolinecarboxylate)(allyl) (Cp = cyclopentadienyl anion) complexes exhibited more favorable reactivity compared to that of **Ru1**, with ruthenium 4-(dimethylamino)-2-

convenient way to introduce nucleophilic amino acids into proteins by previously masking potentially reactive side chains. Balskus and co-workers, in 2013, were also successful in applying **Ru1** to rescue *E. coli* mutants that cannot biosynthesize the essential nutrient *p*-aminobenzoic acid (PABA).⁶⁰ The auxotrophic bacteria were able to survive if the bacteria growth media were supplemented with allylcarbamoyl protected-PABA and **Ru1**, which generated free PABA in solution. In 2014, Vázquez/Mascareñas and co-workers exploited selective allylcarbamate cleavage reactions in developing a strategy to uncage DNA intercalators.⁶¹ The allylcarbamoyl protected DNA binding agents could be activated inside mammalian cells by **Ru1** and thiophenol. **Ru1** can also be attached to organelle-targeting units to direct it toward the mitochondria, where it could do selective chemistry.⁶² Waymouth/Wender and co-workers have also created a bioluminescent method to evaluate the efficiency of metal-catalyzed reactions in living systems using biocompatible allylcarbamate cleavage.⁶³ As more active generations of ruthenium SIMCats are developed, such as **Ru3**,⁵⁸ SIMCat-promoted chemistry will have ever greater utility in the life sciences.

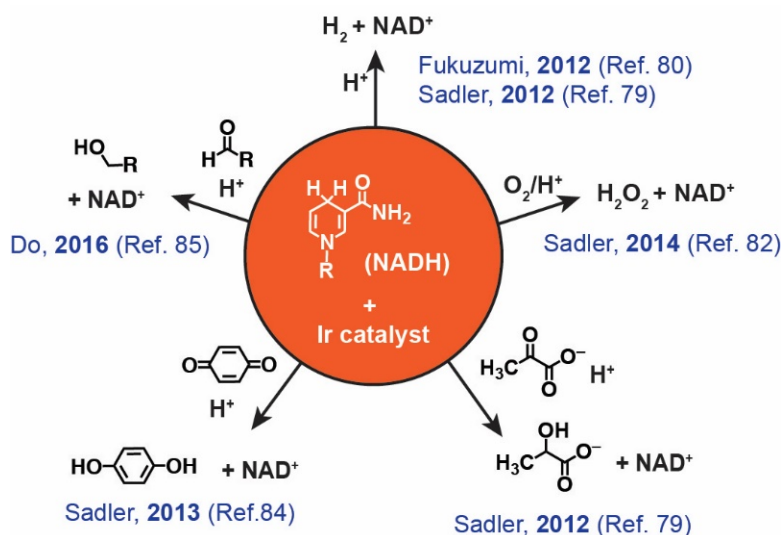
Although nanoparticles containing either palladium⁶⁴⁻⁶⁶ or gold⁶⁷⁻⁶⁸ have been used widely to uncage molecules inside cells, soluble catalysts based on these metals are rare. A unique example of homogeneous palladium-carbene complexes was reported in 2017 by Bradley and co-workers.⁶⁹ This system, which employed a cell penetrating peptide to enhance the cellular uptake of the palladium complex, is catalytically active inside prostate cancer cells.

1.3.4. Transfer Hydrogenation

Transfer hydrogenation catalysis, a process involving the shuttling of a hydride from a donor to an acceptor, has been reported over 100 years ago.⁷⁰⁻⁷¹ The most well-studied homogeneous transfer hydrogenation catalysts in aqueous media are based on ruthenium,⁷² rhodium,⁷³⁻⁷⁵ and iridium. For example, in 1999, Ogo/Watanabe and co-worker demonstrated that $\text{Ir}(\text{Cp}^*)(\text{H}_2\text{O})_3^{2+}$ could catalyze the conversion of aldehydes and ketones to alcohols using formate in acidic water.⁷⁶ Xiao and co-workers later found that $\text{Ir}(\text{Cp}^*)(\text{Ts-en})(\text{Cl})$ (Ts-en = *N*-(*p*-tosyl)ethylenediamine) could also promote similar reactions at pH 7.0.⁷⁷

Due to their biological importance, endogenous biomolecules are particularly attractive reactants in SIMCat-promoted chemistry. For examples, since nicotinamide adenine dinucleotide (NAD^+ = oxidized form, NADH = reduced form) is essential to all living organisms, it is ubiquitous in all living systems. Therefore, synthetic processes that could exploit these natural cofactors as oxidants or reductants provide a direct way to influence cellular growth and metabolism. As early as 1988, Steckhan and co-workers showed the first example in reducing NAD^+ by a synthetic metal catalyst. In this aqueous reaction, $\text{Rh}(\text{Cp}^*)(2,2'\text{-bipyridine})(\text{H}_2\text{O})_2^{2+}$ (**Rh1**) could mediate the transfer of a hydride equivalent from formate to NAD^+ in a 1,4-regioselective manner to yield NADH .⁷⁸ Excitingly, NADH could also be employed as a hydride donor in the reverse process. In 2012, the research groups of Sadler⁷⁹ and Fukuzumi⁸⁰ both reported independently that organoiridium catalysts could mediate hydride transfer from NADH to H^+ to yield NAD^+ and hydrogen gas. Mechanistic studies have demonstrated that both NADH and formate reacts with organoiridium complexes to generate iridium-hydride species that are capable

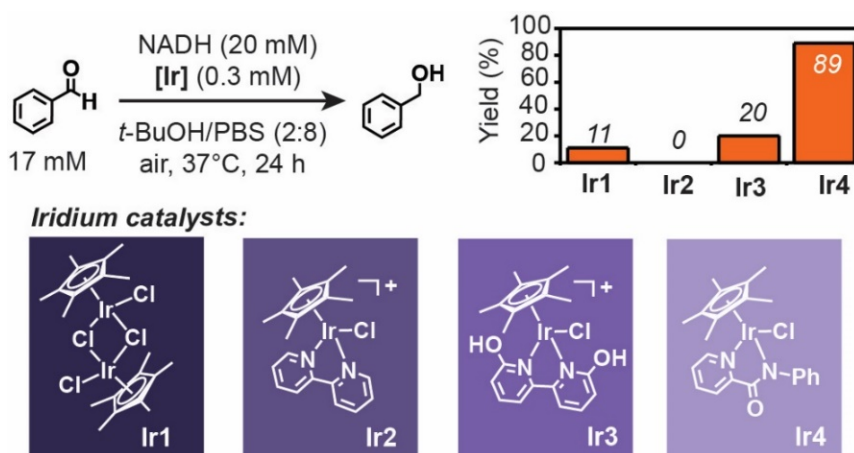
of transferring its hydride to protons,⁸¹ dioxygen,⁸²⁻⁸³ or organic electrophiles⁸⁴⁻⁸⁵ (Scheme 1.4). This chemistry is extraordinarily versatile, as demonstrated by its applications such as in bio-catalytic cascade processes (Ward and co-workers)⁸⁶⁻⁸⁷ or methods for reductive alkylation of proteins (Francis and coworker).⁸⁸



Scheme 1.4. Catalytic reduction of protons, dioxygen, quinones, ketones, and aldehydes by iridium complexes using NADH as a reductant. The reactions were all carried out in aqueous solutions.

Transfer hydrogenation is an attractive target for further SIMCat-promoted chemistry development. Although transfer hydrogenation can be performed by natural enzymes such as dehydrogenases,⁸⁹ synthetic transfer hydrogenation catalysts might be useful for bioorthogonal applications *in vivo*. In 2014, Komatsu/Ariga and co-workers used $\text{Ir}(\text{Cp}^*)(1,10\text{-phenanthroline})(\text{H}_2\text{O})^{2+}$ complexes to catalyze the reduction of a fluorescein-quinone conjugate using intracellular NAD(P)H inside living HeLa cells.⁴⁵ This study motivated us to develop synthetic catalysts that could transfer hydrides from NADH to organic carbonyl compounds rather than redox reagents inside cells.⁸⁵ Under biologically

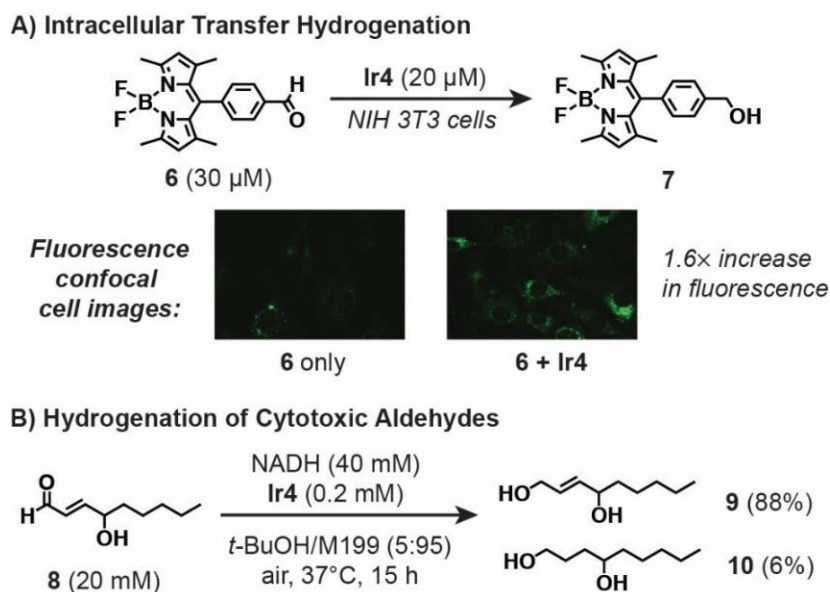
relevant reaction conditions, Ir(Cp*)(2,2'-bipyridine)(Cl)⁺ (**Ir2**) complex was completely inactive in promoting the conversion of benzaldehyde to benzyl alcohol using NADH (Scheme 1.5), whereas the half-sandwich precursor [Ir(Cp*)(Cl)₂]₂ (**Ir1**) and the hydroxylated variant Ir(Cp*)(6,6'-dihydroxy-2,2'-bipyridine)(Cl)⁺ (**Ir3**)⁹⁰⁻⁹¹ gave only modest yields. Surprisingly, Ir(Cp*)(*N*-phenyl-2-pyridinecarboxamidate)Cl (**Ir4**) afforded a remarkable 89% yield.⁸⁵ We also discovered that the iridium-hydride species generated from **Ir4**/NADH was capable of reducing aldehydes, whereas the iridium-hydride species generated from **Ir2**/NADH was not. This example nicely illustrates again the critical importance of supporting ligands in modulating the reactivity of inorganic catalysts.



Scheme 1.5. Evaluation of various organoiridium complexes in facilitating the transfer hydrogenation between NADH and benzaldehydes.

Next, we investigated whether **Ir4** is a competent catalyst inside living cells (Scheme 1.6A).⁴⁶ We chose a bodipy-aldehyde (**6**) substrate as an intracellular reaction probe to enable real time reaction monitoring. Compound **6** is dimly emissive in its aldehyde form, but gives off a strong fluorescence signal when reduced to **7**. In NIH 3T3 mouse fibroblast cells pre-incubated with **6**, cells treated with **Ir4** showed 1.6-fold increase

in fluorescence compared to that of untreated controls. The fluorescence images, which showed signals in the interior of the cells, suggested that the **Ir4** SIMCat-promoted reaction occurred within the cytoplasm. These exciting results indicate that organoiridium complexes could be integrated with living cells to do reductive chemistry on organic aldehydes.



Scheme 1.6. Transfer hydrogenation carried out in the live mammalian cells (A) and its application in the detoxification of cytotoxic aldehydes (B).

Our laboratory is particularly interested in applying SIMCats as novel therapeutics. Sadler and co-workers previously showed that piano stool ruthenium and iridium complexes could be utilized to modify the redox balance of mammalian cells.^{30, 92} They have recently reported that osmium complexes could be used to enantioselectively convert pyruvate to D-lactate inside cancer cells.⁹³ Our group was able to exploit the transfer hydrogenation ability of non-toxic organoiridium compounds to selectively chemosensitize cancer cells toward platinum anti-cancer drugs.²⁹ We also explored the possibility of

applying compound **Ir4** for detoxification of cytotoxic aldehydes, such as acrolein,⁹⁴ malondialdehyde, and 4-hydroxynonenal (**8**).⁹⁵ **Ir4** can reduce cytotoxic **8** to the less toxic compounds **9** and **10** with greater than 90% yield in cell culture media (Scheme 1.6B).⁸⁵ This detoxification strategy is currently under investigation in live cells and model organisms.

1.4. The Future of SIMCat-Promoted Chemistry

There are two main avenues for research on SIMCats: 1) the creation of new types of SIMCats; and 2) the invention of novel technologies based on established bioorthogonal capabilities. We have identified several major classes of metal-catalyzed reactions that are attractive for future biocompatible reaction discovery. One of the most promising reactions is olefin metathesis (Scheme 1.7A), a transformation that involves the cleavage of C–C double bonds followed by reassembly to generate products with new C–C double bonds.⁹⁶ Olefin metathesis reactions include cross metathesis, ring-opening metathesis polymerization (ROMP), and ring-closing metathesis (RCM). There are many creative applications of olefin metathesis in chemical biology, such as the synthesis of cyclic peptides, construction of polysaccharide mimics, or site selective modification of protein residues.⁹⁷

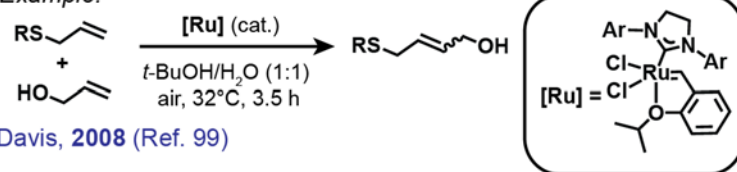
The above achievements were made possible by metal catalysts that have high tolerance of strong sigma donors such as amines and thiols and good water solubility. For example, in 2006 Grubbs and co-workers introduced polyethylene glycol (PEG) chains to a carbene ligand to get ruthenium complexes that are highly active for cross-metathesis in water at 45°C.⁹⁸ Davis and co-workers provided further catalyst improvements with

ruthenium complexes that could be used in open air and were not inhibited by thioether functionalities.⁹⁹ Ruthenium catalysts have even been embedded into proteins to produce “artificial metatases”.¹⁰⁰ Recently, Mitchel and co-workers reported the first example of an intracellular metathesis reaction.¹⁰¹ Using a Hoveyda-Grubbs second generation Ru catalyst bearing a BODIPY substituent, they were able to synthesize two profluorescent probes for the detection of ethylene. In live green algae cells, these dimly emissive ruthenium-BODIPY complexes react quickly with ethylene gas to release the strongly fluorescent BODIPY compound in 15 min. Since olefin metathesis is a versatile reaction with many useful applications, we expect that the chemical biology community will have significant interest in this type of SIMCat-promoted chemistry.

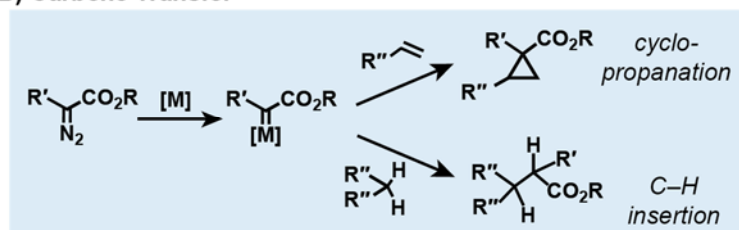
A) Olefin Metathesis



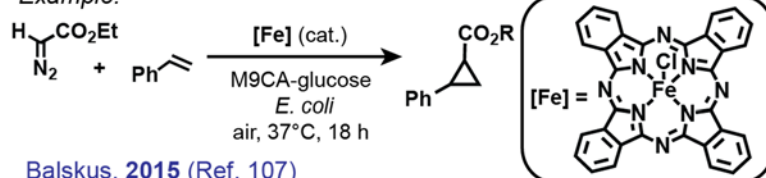
Example:



B) Carbene Transfer



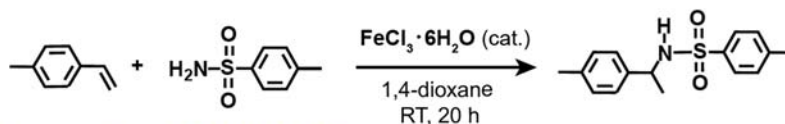
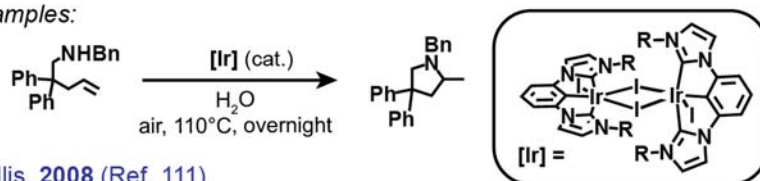
Example:



C) Hydrofunctionalization



Examples:



Scheme 1.7. Some promising reactions that might be suitable for further SIMCat-promoted chemistry development: A) olefin metathesis, B) carbene transfer, and C) hydrofunctionalization.

Another potential organometallic reaction that could be further explored in SIMCat-promoted chemistry is carbene transfer (Scheme 1.7B).¹⁰²⁻¹⁰³ This reaction requires first the generation of metal-carbene species through reaction of diazoester compounds with various metal precursors, followed by insertion of the carbene into olefins (cyclopropanation) or heteroatom–hydrogen bonds (X–H insertion, where X = C, O, B, Si, etc.). This chemistry has enabled synthetic chemists to manipulate biological molecules in unprecedented ways. For example, Ball and co-workers have designed rhodium metallopeptides that are capable of site-specific functionalization of proteins¹⁰⁴ and antibodies¹⁰⁵ with fluorophores, affinity tags, and pharmacological agents. P450 enzymes have been successfully evolved in catalyzing carbene transfer to produce drug molecules with exquisite stereoselectivity by the research groups of Arnold^{10, 17} and Fasan.¹⁰⁶ In 2005, Balskus and coworker demonstrated the application of cyclopropanation catalysts with living microorganisms (Scheme 7B).¹⁰⁷ Ferric phthalocyanine complexes were found to promote efficiently carbene transfer to styrene in the *presence* of *E. coli*. Because styrene was produced directly from D-glucose by the engineered microbes, this is the first example to show that non-biological carbene-transfer reactivity could be coupled to cellular metabolism for small molecule production. The use of designer micelles was later reported to accelerate styrene accumulation by *E. coli* and enhance catalytic efficiency.¹⁰⁸ Although these reactions occurred extracellularly, biocompatible SIMCats for carbene transfer reactions seem to be well within our reach.

The third class of reactions that we believe will be a valuable addition to the SIMCat-promoted chemistry toolbox is hydrofunctionalization catalysis (Scheme 7C).¹⁰⁹⁻

¹¹⁰ The functionalization of alkenes or alkynes by E–Nuc species (E = H, BR₂, etc.; Nuc =

halogen, CN, CHO, OH, CO, COOR, NR₂, etc.) is a popular method used in organic synthesis and industrial processes. In this reaction, unsymmetrical alkenes/alkynes can undergo either Markovnikov (Nuc adds to more substituted carbon) or anti-Markovnikov (Nuc adds to less substituted carbon), by regioselective transition metal catalysts. Despite the many achievements in hydrofunctionalization chemistry (i.e. hydroamination, hydroalkoxylation, hydration, etc.), its *in vivo* studies have been largely unexplored. However, there are many examples in which the reaction conditions employed suggest that SIMCat-assisted hydrofunctionalization is certainly achievable. For example, Hollis and co-workers used iridium and rhodium pincer complexes to catalyze the cyclization of linear amino olefins to pyrrolidines in pure water and under air at 110°C.¹¹¹ In 2011, Campagne/Prim and co-workers reported iron(III) chloride salts promoted the intermolecular hydroamination of styrene derivatives using *p*-toluenesulfonamide in 1,4-dioxane at room temperature.¹¹² This reaction is notable because iron(III) is air stable and a biologically compatible metal ion. Although these catalytic systems at present could not be applied in living environments due to the need for high temperature or organic solvents, we expect that biocompatible catalysis could be achieved through reaction optimization and/or catalyst modifications.

The development of SIMCat-promoted chemistry can be viewed as complementary to that of enzymatic chemistry, which includes efforts on evolving natural enzymes as well as creating *de novo* enzymes to achieve novel functions. Unlike macromolecular catalysts, SIMCats have no active site pockets for substrate recognition/binding and cannot stabilize unusual transition states. However, the small size of SIMCats offers distinct advantages over macromolecules, such as the ability to cross cellular membranes via passive transport,

ease of catalyst tuning and scale-up, and simplicity of use. We have discovered that ligand design and optimization play key roles in the engineering of SIMCats. A longstanding challenge in the field is being able to quantify catalyst efficiencies in cellular studies, since the relative catalyst activities observed in the test tube might not necessarily be replicated inside living cells. Other factors such as catalyst uptake, cellular localization, and inhibition might also need to be considered and evaluated. Perhaps the application of ratiometric substrate probes that could provide real time readouts of the reaction progress might aid in this effort.¹¹³

The future of SIMCat-promoted chemistry is full of possibilities and is certainly by no means restricted to the transformations that we have highlighted.¹¹⁴ It might be feasible to utilize SIMCats to repair DNA damage by correcting point mutations,¹¹⁵ promote cellular growth by replacing dysfunctional enzymes, or fight infections via novel mechanisms of action. Advancements in SIMCat-promoted intracellular chemistry will allow scientists to confront new research frontiers at the interface between chemistry and biology.

1.5. References

1. Patel, R. N., Biocatalysis for Synthesis of Pharmaceuticals. *Bioorganic & Medicinal Chemistry* **2018**, *26* (7), 1252-1274.
2. Truppo, M. D., Biocatalysis in the Pharmaceutical Industry: The Need for Speed. *ACS Medicinal Chemistry Letters* **2017**, *8* (5), 476-480.
3. Hönig, M.; Sondermann, P.; Turner, N. J.; Carreira, E. M., Enantioselective Chemo- and Biocatalysis: Partners in Retrosynthesis. *Angewandte Chemie International Edition* **2017**, *56* (31), 8942-8973.
4. Schrittwieser, J. H.; Velikogne, S.; Hall, M.; Kroutil, W., Artificial Biocatalytic Linear Cascades for Preparation of Organic Molecules. *Chemical Reviews* **2018**, *118* (1), 270-348.

5. Zhang, Y.; Hess, H., Toward Rational Design of High-efficiency Enzyme Cascades. *ACS Catalysis* **2017**, *7* (9), 6018-6027.
6. Mayer, S. F.; Kroutil, W.; Faber, K., Enzyme-initiated Domino (Cascade) Reactions. *Chemical Society Reviews* **2001**, *30* (6), 332-339.
7. Wright, T. H.; Vallée, M. R. J.; Davis, B. G., From Chemical Mutagenesis to Post-Expression Mutagenesis: A 50 Year Odyssey. *Angewandte Chemie International Edition* **2016**, *55* (20), 5896-5903.
8. Bachman, J., Chapter Nineteen - Site-Directed Mutagenesis. In *Methods in Enzymology*, Lorsch, J., Ed. Academic Press: **2013**, *529*, 241-248.
9. Wang, J.-b.; Li, G.; Reetz, M. T., Enzymatic Site-Selectivity Enabled by Structure-Guided Directed Evolution. *Chemical Communications* **2017**, *53* (28), 3916-3928.
10. Arnold, F. H., Directed Evolution: Bringing New Chemistry to Life. *Angewandte Chemie International Edition* **2017**, *56*, 2-8.
11. Packer, M. S.; Liu, D. R., Methods for the Directed Evolution of Proteins. *Nature Reviews. Genetics* **2015**, *16* (7), 379-394.
12. Schwizer, F.; Okamoto, Y.; Heinisch, T.; Gu, Y.; Pellizzoni, M. M.; Lebrun, V.; Reuter, R.; Köhler, V.; Lewis, J. C.; Ward, T. R., Artificial Metalloenzymes: Reaction Scope and Optimization Strategies. *Chemical Reviews* **2018**, *118* (1), 142-231.
13. Natri, F.; Chino, M.; Maglio, O.; Bhagi-Damodaran, A.; Lu, Y.; Lombardi, A., Design and Engineering of Artificial Oxygen-Activating Metalloenzymes. *Chemical Society Reviews* **2016**, *45* (18), 5020-5054.
14. Yu, F.; Cangelosi, V. M.; Zastrow, M. L.; Tegoni, M.; Plegaria, J. S.; Tebo, A. G.; Mocny, C. S.; Ruckthong, L.; Qayyum, H.; Pecoraro, V. L., Protein Design: Toward Functional Metalloenzymes. *Chemical Reviews* **2014**, *114* (7), 3495-3578.
15. Song, W. J.; Tezcan, F. A., A Designed Supramolecular Protein Assembly with In Vivo Enzymatic Activity. *Science* **2014**, *346* (6216), 1525-1528.
16. Ward, T. R., Artificial Metalloenzymes Based on the Biotin–Avidin Technology: Enantioselective Catalysis and Beyond. *Accounts of Chemical Research* **2011**, *44* (1), 47-57.
17. Hammer, S. C.; Kubik, G.; Watkins, E.; Huang, S.; Minges, H.; Arnold, F. H., Anti-Markovnikov Alkene Oxidation by Metal-Oxo–Mediated Enzyme Catalysis. *Science* **2017**, *358* (6360), 215-218.
18. Soldevila-Barreda, J. J.; Sadler, P. J., Approaches to the Design of Catalytic Metallodrugs. *Current Opinion in Chemical Biology* **2015**, *25*, 172-183.
19. Sasmal, P. K.; Streu, C. N.; Meggers, E., Metal Complex Catalysis in Living Biological Systems. *Chemical Communications* **2013**, *49* (16), 1581-1587.

20. Wilson, Y. M.; Dürrenberger, M.; Nogueira, E. S.; Ward, T. R., Neutralizing the Detrimental Effect of Glutathione on Precious Metal Catalysts. *Journal of the American Chemical Society* **2014**, *136* (25), 8928-8932.
21. Rebelein, J. G.; Ward, T. R., In Vivo Catalyzed New-To-Nature Reactions. *Current Opinion in Biotechnology* **2018**, *53*, 106-114.
22. Ngo, A. H.; Bose, S.; Do, L. H., Intracellular Chemistry: Integrating Molecular Inorganic Catalysts with Living Systems. *Chemistry – A European Journal* **2018**, *24* (42), 10584-10594.
23. Zhou, Y.; Liu, B.; Yang, R.; Liu, J., Filling in the Gaps between Nanozymes and Enzymes: Challenges and Opportunities. *Bioconjugate Chemistry* **2017**, *28* (12), 2903-2909.
24. Wei, H.; Wang, E., Nanomaterials with Enzyme-Like Characteristics (Nanozymes): Next-Generation Artificial Enzymes. *Chemical Society Reviews* **2013**, *42* (14), 6060-6093.
25. Patterson, D. M.; Nazarova, L. A.; Prescher, J. A., Finding the Right (Bioorthogonal) Chemistry. *ACS Chemical Biology* **2014**, *9* (3), 592-605.
26. Sletten, E. M.; Bertozzi, C. R., Bioorthogonal Chemistry: Fishing for Selectivity in a Sea of Functionality. *Angewandte Chemie International Edition* **2009**, *48* (38), 6974-6998.
27. Hartwig, J. F., *Organotransition Metal Chemistry*. University Science Books: Mill Valley, California, **2010**.
28. Li, S.; Wang, L.; Yu, F.; Zhu, Z.; Shobaki, D.; Chen, H.; Wang, M.; Wang, J.; Qin, G.; Erasquin, U. J.; Ren, L.; Wang, Y.; Cai, C., Copper-Catalyzed Click Reaction on/in Live Cells. *Chemical Science* **2017**, *8* (3), 2107-2114.
29. Yang, L.; Bose, S.; Ngo, A. H.; Do, L. H., Innocent But Deadly: Nontoxic Organoiridium Catalysts Promote Selective Cancer Cell Death. *ChemMedChem* **2017**, *12* (4), 292-299.
30. Liu, Z.; Sadler, P. J., Organoiridium Complexes: Anticancer Agents and Catalysts. *Accounts of Chemical Research* **2014**, *47* (4), 1174-1185.
31. Soriano del Amo, D.; Wang, W.; Jiang, H.; Besanceney, C.; Yan, A. C.; Levy, M.; Liu, Y.; Marlow, F. L.; Wu, P., Biocompatible Copper(I) Catalysts for in Vivo Imaging of Glycans. *Journal of the American Chemical Society* **2010**, *132* (47), 16893-16899.
32. Qiu, K.; Chen, Y.; Rees, T. W.; Ji, L.; Chao, H., Organelle-Targeting Metal Complexes: from Molecular Design to Bio-Applications. *Coordination Chemistry Reviews* **2017**, ASAP.
33. Bradford, S. S.; Cowan, J. A., From Traditional Drug Design to Catalytic Metallodrugs: A Brief History of the Use of Metals in Medicine. *Metallodrugs* **2014**, *1*, 10-23.

34. Kilpin, K. J.; Dyson, P. J., Enzyme Inhibition by Metal Complexes: Concepts, Strategies and Applications. *Chemical Science* **2013**, *4* (4), 1410-1419.
35. Gasser, G.; Metzler-Nolte, N., Metal Compounds as Enzyme Inhibitors. In *Bioinorganic Medicinal Chemistry*, Wiley-VCH Verlag GmbH & Co. KGaA: 2011; pp 351-382.
36. White, J. K.; Schmehl, R. H.; Turro, C., An Overview of Photosubstitution Reactions of Ru(II) Imine Complexes and Their Application in Photobiology and Photodynamic Therapy. *Inorganica Chimica Acta* **2017**, *454* (Supplement C), 7-20.
37. Chakraborty, I.; Carrington, S. J.; Mascharak, P. K., Design Strategies to Improve the Sensitivity of Photoactive Metal Carbonyl Complexes (photoCORMs) to Visible Light and Their Potential as CO-Donors to Biological Targets. *Accounts of Chemical Research* **2014**, *47* (8), 2603-2611.
38. Vigh, L.; Joó, F.; Cséplő, Á., Modulation of Membrane Fluidity in Living Protoplasts of *Nicotiana Plumbaginifolia* by Catalytic Hydrogenation. *European Journal of Biochemistry* **1985**, *146* (2), 241-244.
39. Yu, Z.; Cowan, J. A., Catalytic Metallodrugs: Substrate-Selective Metal Catalysts as Therapeutics. *Chemistry – A European Journal* **2017**, *23*, 14113-14127.
40. Jeon, J. W.; Son, S. J.; Yoo, C. E.; Hong, I. S.; Song, J. B.; Suh, J., Protein-Cleaving Catalyst Selective for Protein Substrate. *Organic Letters* **2002**, *4* (23), 4155-4158.
41. Rostovtsev, V. V.; Green, L. G.; Fokin, V. V.; Sharpless, K. B., A Stepwise Huisgen Cycloaddition Process: Copper(I)-Catalyzed Regioselective “Ligation” of Azides and Terminal Alkynes. *Angewandte Chemie International Edition* **2002**, *41* (14), 2596-2599.
42. Tornøe, C. W.; Christensen, C.; Meldal, M., Peptidotriazoles on Solid Phase: [1,2,3]-Triazoles by Regiospecific Copper(I)-Catalyzed 1,3-Dipolar Cycloadditions of Terminal Alkynes to Azides. *The Journal of Organic Chemistry* **2002**, *67* (9), 3057-3064.
43. Streu, C.; Meggers, E., Ruthenium-Induced Allylcarbamate Cleavage in Living Cells. *Angew. Chem. Int. Ed.* **2006**, *45* (34), 5645-5648.
44. Li, N.; Lim, R. K. V.; Edwardraja, S.; Lin, Q., Copper-Free Sonogashira Cross-Coupling for Functionalization of Alkyne-Encoded Proteins in Aqueous Medium and in Bacterial Cells. *Journal of the American Chemical Society* **2011**, *133* (39), 15316-15319.
45. Komatsu, H.; Shindo, Y.; Oka, K.; Hill, J. P.; Ariga, K., Ubiquinone-Rhodol (UQ-Rh) for Fluorescence Imaging of NAD(P)H through Intracellular Activation. *Angew. Chem. Int. Ed.* **2014**, *53* (15), 3993-3995.
46. Bose, S.; Ngo, A. H.; Do, L. H., Intracellular Transfer Hydrogenation Mediated by Unprotected Organoiridium Catalysts. *Journal of the American Chemical Society* **2017**, *139* (26), 8792-8795.

47. Chen, C.-A.; Cowan, J. A., In Vivo Cleavage of a Target RNA by Copper Kanamycin A. Direct Observation by a Fluorescence Assay. *Chemical Communications* **2002**, (3), 196-197.
48. Meldal, M.; Tornøe, C. W., Cu-Catalyzed Azide–Alkyne Cycloaddition. *Chemical Reviews* **2008**, *108* (8), 2952-3015.
49. Link, A. J.; Tirrell, D. A., Cell Surface Labeling of Escherichia coli via Copper(I)-Catalyzed [3+2] Cycloaddition. *Journal of the American Chemical Society* **2003**, *125* (37), 11164-11165.
50. Speers, A. E.; Adam, G. C.; Cravatt, B. F., Activity-Based Protein Profiling in Vivo Using a Copper(I)-Catalyzed Azide-Alkyne [3 + 2] Cycloaddition. *Journal of the American Chemical Society* **2003**, *125* (16), 4686-4687.
51. Beatty, K. E.; Xie, F.; Wang, Q.; Tirrell, D. A., Selective Dye-Labeling of Newly Synthesized Proteins in Bacterial Cells. *Journal of the American Chemical Society* **2005**, *127* (41), 14150-14151.
52. Deiters, A.; Schultz, P. G., In Vivo Incorporation of an Alkyne into Proteins in Escherichia Coli. *Bioorganic & Medicinal Chemistry Letters* **2005**, *15* (5), 1521-1524.
53. Hsu, T.-L.; Hanson, S. R.; Kishikawa, K.; Wang, S.-K.; Sawa, M.; Wong, C.-H., Alkynyl Sugar Analogs for The Labeling and Visualization of Glycoconjugates in Cells. *Proceedings of the National Academy of Sciences* **2007**, *104* (8), 2614-2619.
54. Yang, M.; Jalloh, A. S.; Wei, W.; Zhao, J.; Wu, P.; Chen, P. R., Biocompatible Click Chemistry Enabled Compartment-Specific pH Measurement Inside E. coli. *Nature Communications* **2014**, *5*, 4981.
55. Uttamapinant, C.; Tangpeerachaikul, A.; Grecian, S.; Clarke, S.; Singh, U.; Slade, P.; Gee, K. R.; Ting, A. Y., Fast, Cell-Compatible Click Chemistry with Copper-Chelating Azides for Biomolecular Labeling. *Angewandte Chemie International Edition* **2012**, *51* (24), 5852-5856.
56. Sasmal, P. K.; Carregal-Romero, S.; Parak, W. J.; Meggers, E., Light-Triggered Ruthenium-Catalyzed Allylcarbamate Cleavage in Biological Environments. *Organometallics* **2012**, *31* (16), 5968-5970.
57. Völker, T.; Dempwolff, F.; Graumann, P. L.; Meggers, E., Progress Towards Bioorthogonal Catalysis with Organometallic Compounds. *Angew. Chem. Int. Ed.* **2014**, *53* (39), 10536-10540.
58. Völker, T.; Meggers, E., Chemical Activation in Blood Serum and Human Cell Culture: Improved Ruthenium Complex for Catalytic Uncaging of Alloc-Protected Amines. *ChemBioChem* **2017**, *18* (12), 1083-1086.
59. Ai, H.-w.; Lee, J. W.; Schultz, P. G., A Method to Site-Specifically Introduce Methyllysine into Proteins in E. coli. *Chemical Communications* **2010**, *46* (30), 5506-5508.

60. Lee, Y.; Umeano, A.; Balskus, E. P., Rescuing Auxotrophic Microorganisms with Nonenzymatic Chemistry. *Angew. Chem. Int. Ed.* **2013**, *52* (45), 11800-11803.
61. Sánchez, M. I.; Penas, C.; Vázquez, M. E.; Mascareñas, J. L., Metal-Catalyzed Uncaging of DNA-Binding Agents in Living Cells. *Chem. Sci.* **2014**, *5* (5), 1901-1907.
62. Tomás-Gamasa, M.; Martínez-Calvo, M.; Couceiro, J. R.; Mascareñas, J. L., Transition Metal Catalysis in the Mitochondria of Living Cells. *Nature Communications* **2016**, *7*, 12538.
63. Hsu, H.-T.; Trantow, B. M.; Waymouth, R. M.; Wender, P. A., Bioorthogonal Catalysis: A General Method To Evaluate Metal-Catalyzed Reactions in Real Time in Living Systems Using a Cellular Luciferase Reporter System. *Bioconjugate Chemistry* **2016**, *27* (2), 376-382.
64. Miller, M. A.; Askevold, B.; Mikula, H.; Kohler, R. H.; Pirovich, D.; Weissleder, R., Nano-Palladium is a Cellular Catalyst for In Vivo Chemistry. *Nature Communications* **2017**, *8*, 15906.
65. Yusop, R. M.; Unciti-Broceta, A.; Johansson, E. M. V.; Sánchez-Martín, R. M.; Bradley, M., Palladium-Mediated Intracellular Chemistry. *Nature Chemistry* **2011**, *3* (3), 239-243.
66. Weiss, J. T.; Dawson, J. C.; Macleod, K. G.; Rybski, W.; Fraser, C.; Torres-Sánchez, C.; Patton, E. E.; Bradley, M.; Carragher, N. O.; Unciti-Broceta, A., Extracellular Palladium-Catalysed Dealkylation of 5-Fluoro-1-Propargyl-Uracil as a Bioorthogonally Activated Prodrug Approach. *Nature Communication* **2014**, *5*, 3277.
67. Pérez-López, A. M.; Rubio-Ruiz, B.; Sebastián, V.; Hamilton, L.; Adam, C.; Bray, T. L.; Irusta, S.; Brennan, P. M.; Lloyd-Jones, G. C.; Sieger, D.; Santamaría, J.; Unciti-Broceta, A., Gold-Triggered Uncaging Chemistry in Living Systems. *Angewandte Chemie International Edition* **2017**, *56* (41), 12548-12552.
68. Tonga, G. Y.; Jeong, Y.; Duncan, B.; Mizuhara, T.; Mout, R.; Das, R.; Kim, S. T.; Yeh, Y.-C.; Yan, B.; Hou, S.; Rotello, V. M., Supramolecular Regulation of Bioorthogonal Catalysis in Cells Using Nanoparticle-Embedded Transition Metal Catalysts. *Nature Chemistry* **2015**, *7*, 597-603.
69. Indrigo, E.; Clavadetscher, J.; Chankeshwara, S. V.; Megia-Fernandez, A.; Lilienkamp, A.; Bradley, M., Intracellular Delivery of a Catalytic Organometallic Complex. *Chemical Communications* **2017**, *53* (50), 6712-6715.
70. Dobereiner, G. E.; Crabtree, R. H., Dehydrogenation as a Substrate-Activating Strategy in Homogeneous Transition-Metal Catalysis. *Chemical Reviews* **2010**, *110* (2), 681-703.
71. Wang, D.; Astruc, D., The Golden Age of Transfer Hydrogenation. *Chem. Rev.* **2015**, *115* (13), 6621-6686.

72. Robertson, A.; Matsumoto, T.; Ogo, S., The Development of Aqueous Transfer Hydrogenation Catalysts. *Dalton Transactions* **2011**, 40 (40), 10304-10310.
73. Leiva, C.; Lo, H. C.; Fish, R. H., Aqueous Organometallic Chemistry. 3. Catalytic Hydride Transfer Reactions with Ketones and Aldehydes Using [Cp*Rh(bpy)(H₂O)](OTf)₂ as the Precatalyst and Sodium Formate as the Hydride Source: Kinetic and Activation Parameters, and the Significance of Steric and Electronic Effects. *Journal of Organometallic Chemistry* **2010**, 695 (2), 145-150.
74. Lo, H. C.; Fish, R. H., Biomimetic NAD⁺ Models for Tandem Cofactor Regeneration, Horse Liver Alcohol Dehydrogenase Recognition of 1,4-NADH Derivatives, and Chiral Synthesis. *Angewandte Chemie International Edition* **2002**, 41 (3), 478-481.
75. Lo, H. C.; Leiva, C.; Buriez, O.; Kerr, J. B.; Olmstead, M. M.; Fish, R. H., Bioorganometallic Chemistry. 13. Regioselective Reduction of NAD⁺ Models, 1-Benzylnicotinamide Triflate and β -Nicotinamide Ribose-5'-methyl Phosphate, with in Situ Generated [Cp*Rh(Bpy)H]⁺: Structure–Activity Relationships, Kinetics, and Mechanistic Aspects in the Formation of the 1,4-NADH Derivatives. *Inorganic Chemistry* **2001**, 40 (26), 6705-6716.
76. Ogo, S.; Makihara, N.; Watanabe, Y., pH-Dependent Transfer Hydrogenation of Water-Soluble Carbonyl Compounds with [Cp*IrIII(H₂O)₃]₂⁺ (Cp* = η^5 -C₅Me₅) as a Catalyst Precursor and HCOONa as a Hydrogen Donor in Water. *Organometallics* **1999**, 18 (26), 5470-5474.
77. Wu, X.; Liu, J.; Li, X.; Zanotti-Gerosa, A.; Hancock, F.; Vinci, D.; Ruan, J.; Xiao, J., On Water and in Air: Fast and Highly Chemoselective Transfer Hydrogenation of Aldehydes with Iridium Catalysts. *Angewandte Chemie International Edition* **2006**, 45 (40), 6718-6722.
78. Ruppert, R.; Herrmann, S.; Steckhan, E., Very Efficient Reduction of NAD(P)⁺ with Formate Catalysed by Cationic Rhodium Complexes. *Journal of the Chemical Society, Chemical Communications* **1988**, (17), 1150-1151.
79. Betanzos-Lara, S.; Liu, Z.; Habtemariam, A.; Pizarro, A. M.; Qamar, B.; Sadler, P. J., Organometallic Ruthenium and Iridium Transfer-Hydrogenation Catalysts Using Coenzyme NADH as a Cofactor. *Angewandte Chemie International Edition* **2012**, 51 (16), 3897-3900.
80. Maenaka, Y.; Suenobu, T.; Fukuzumi, S., Efficient Catalytic Interconversion Between NADH and NAD⁺ Accompanied by Generation and Consumption of Hydrogen with a Water-Soluble Iridium Complex at Ambient Pressure and Temperature. *Journal of the American Chemical Society* **2012**, 134 (1), 367-374.
81. Pitman, C. L.; Miller, A. J. M., Molecular Photoelectrocatalysts for Visible Light-Driven Hydrogen Evolution from Neutral Water. *ACS Catalysis* **2014**, 4 (8), 2727-2733.
82. Liu, Z.; Romero-Canelón, I.; Qamar, B.; Hearn, J. M.; Habtemariam, A.; Barry, N. P. E.; Pizarro, A. M.; Clarkson, G. J.; Sadler, P. J., The Potent Oxidant Anticancer

- Activity of Organoiridium Catalysts. *Angewandte Chemie International Edition* **2014**, 53 (15), 3941-3946.
83. Heiden, Z. M.; Rauchfuss, T. B., Homogeneous Catalytic Reduction of Dioxygen Using Transfer Hydrogenation Catalysts. *Journal of the American Chemical Society* **2007**, 129 (46), 14303-14310.
 84. Liu, Z.; Deeth, R. J.; Butler, J. S.; Habtemariam, A.; Newton, M. E.; Sadler, P. J., Reduction of Quinones by NADH Catalyzed by Organoiridium Complexes. *Angewandte Chemie International Edition* **2013**, 52 (15), 4194-4197.
 85. Ngo, A. H.; Ibañez, M.; Do, L. H., Catalytic Hydrogenation of Cytotoxic Aldehydes Using Nicotinamide Adenine Dinucleotide (NADH) in Cell Growth Media. *ACS Catalysis* **2016**, 6 (4), 2637-2641.
 86. Köhler, V.; Wilson, Y. M.; Dürrenberger, M.; Ghislieri, D.; Churakova, E.; Quinto, T.; Knörr, L.; Häussinger, D.; Hollmann, F.; Turner, N. J.; Ward, T. R., Synthetic Cascades are Enabled by Combining Biocatalysts with Artificial Metalloenzymes. *Nature Chemistry* **2013**, 5 (2), 93-99.
 87. Okamoto, Y.; Köhler, V.; Ward, T. R., An NAD(P)H-Dependent Artificial Transfer Hydrogenase for Multienzymatic Cascades. *Journal of the American Chemical Society* **2016**, 138 (18), 5781-5784.
 88. McFarland, J. M.; Francis, M. B., Reductive Alkylation of Proteins Using Iridium Catalyzed Transfer Hydrogenation. *Journal of the American Chemical Society* **2005**, 127 (39), 13490-13491.
 89. Nealon, C. M.; Musa, M. M.; Patel, J. M.; Phillips, R. S., Controlling Substrate Specificity and Stereospecificity of Alcohol Dehydrogenases. *ACS Catalysis* **2015**, 5 (4), 2100-2114.
 90. Kawahara, R.; Fujita, K.-i.; Yamaguchi, R., Dehydrogenative Oxidation of Alcohols in Aqueous Media Using Water-Soluble and Reusable Cp*Ir Catalysts Bearing a Functional Bipyridine Ligand. *Journal of the American Chemical Society* **2012**, 134 (8), 3643-3646.
 91. Fujita, K.-i.; Ito, W.; Yamaguchi, R., Dehydrogenative Lactonization of Diols in Aqueous Media Catalyzed by a Water-Soluble Iridium Complex Bearing a Functional Bipyridine Ligand. *ChemCatChem* **2014**, 6 (1), 109-112.
 92. Soldevila-Barreda, J. J.; Romero-Canelón, I.; Habtemariam, A.; Sadler, P. J., Transfer Hydrogenation Catalysis in Cells as a New Approach to Anticancer Drug Design. *Nature Communication* **2015**, 6, 6582.
 93. Coverdale, J. P. C.; Romero-Canelón, I.; Sanchez-Cano, C.; Clarkson, G. J.; Habtemariam, A.; Wills, M.; Sadler, P. J., Asymmetric transfer hydrogenation by synthetic catalysts in cancer cells. *Nature Chemistry* **2018**, ASAP.
 94. Nam, D. T.; Arseneault, M.; Murthy, V.; Ramassamy, C., Potential Role of Acrolein in Neurodegeneration and in Alzheimers Disease. *Current Molecular Pharmacology* **2010**, 3 (2), 66-78.

95. Dalleau, S.; Baradat, M.; Guéraud, F.; Huc, L., Cell Death and Diseases Related to Oxidative Stress: 4-Hydroxynonenal (HNE) in the Balance. *Cell Death Differ.* **2013**, *20* (12), 1615-1630.
96. Astruc, D., The Metathesis Reactions: From a Historical Perspective to Recent Developments. *New Journal of Chemistry* **2005**, *29* (1), 42-56.
97. Binder, J. B.; Raines, R. T., Olefin Metathesis for Chemical Biology. *Current Opinion in Chemical Biology* **2008**, *12* (6), 767-773.
98. Hong, S. H.; Grubbs, R. H., Highly Active Water-Soluble Olefin Metathesis Catalyst. *Journal of the American Chemical Society* **2006**, *128* (11), 3508-3509.
99. Lin, Y. A.; Chalker, J. M.; Floyd, N.; Bernardes, G. J. L.; Davis, B. G., Allyl Sulfides Are Privileged Substrates in Aqueous Cross-Metathesis: Application to Site-Selective Protein Modification. *Journal of the American Chemical Society* **2008**, *130* (30), 9642-9643.
100. Sauer, D. F.; Gotzen, S.; Okuda, J., Metatases: Artificial Metalloproteins for Olefin Metathesis. *Organic & Biomolecular Chemistry* **2016**, *14* (39), 9174-9183.
101. Toussaint, S. N. W.; Calkins, R. T.; Lee, S.; Michel, B. W., Olefin Metathesis-Based Fluorescent Probes for the Selective Detection of Ethylene in Live Cells. *Journal of the American Chemical Society* **2018**, *140* (41), 13151-13155.
102. Deng, Y.; Qiu, H.; Srinivas, H. D.; Doyle, M. P., Chiral Dirhodium(II) Catalysts for Selective Metal Carbene Reactions. *Current Organic Chemistry* **2016**, *20*, 61-81.
103. Zhang, X. P.; Cui, X., Asymmetric C–H Functionalization by Transition Metal-Catalyzed Carbene Transfer Reactions. *Comprehensive Organic Synthesis* **2014**, *7*, 86-120.
104. Popp, B. V.; Ball, Z. T., Structure-Selective Modification of Aromatic Side Chains with Dirhodium Metallopeptide Catalysts. *Journal of the American Chemical Society* **2010**, *132* (19), 6660-6662.
105. Ohata, J.; Ball, Z. T., A Hexa-rhodium Metallopeptide Catalyst for Site-Specific Functionalization of Natural Antibodies. *Journal of the American Chemical Society* **2017**, *139* (36), 12617-12622.
106. Bajaj, P.; Sreenilayam, G.; Tyagi, V.; Fasan, R., Gram-Scale Synthesis of Chiral Cyclopropane-Containing Drugs and Drug Precursors with Engineered Myoglobin Catalysts Featuring Complementary Stereoselectivity. *Angewandte Chemie International Edition* **2016**, *55* (52), 16110-16114.
107. Wallace, S.; Balskus, E. P., Interfacing Microbial Styrene Production with a Biocompatible Cyclopropanation Reaction. *Angewandte Chemie International Edition* **2015**, *54* (24), 7106-7109.
108. Wallace, S.; Balskus, E. P., Designer Micelles Accelerate Flux Through Engineered Metabolism in *E. coli* and Support Biocompatible Chemistry. *Angewandte Chemie International Edition* **2016**, *55* (20), 6023-6027.

109. Beller, M.; Seayad, J.; Tillack, A.; Jiao, H., Catalytic Markovnikov and anti-Markovnikov Functionalization of Alkenes and Alkynes: Recent Developments and Trends. *Angewandte Chemie International Edition* **2004**, *43* (26), 3368-3398.
110. Crossley, S. W. M.; Obradors, C.; Martinez, R. M.; Shenvi, R. A., Mn-, Fe-, and Co-Catalyzed Radical Hydrofunctionalizations of Olefins. *Chemical Reviews* **2016**, *116* (15), 8912-9000.
111. Bauer, E. B.; Andavan, G. T. S.; Hollis, T. K.; Rubio, R. J.; Cho, J.; Kuchenbeiser, G. R.; Helgert, T. R.; Letko, C. S.; Tham, F. S., Air- and Water-Stable Catalysts for Hydroamination/Cyclization. Synthesis and Application of CCC–NHC Pincer Complexes of Rh and Ir. *Organic Letters* **2008**, *10* (6), 1175-1178.
112. Zotto, C. D.; Michaux, J.; Zarate-Ruiz, A.; Gayon, E.; Virieux, D.; Campagne, J.-M.; Terrasson, V.; Pieters, G.; Gaucher, A.; Prim, D., FeCl₃-Catalyzed Addition of Nitrogen and 1,3-Dicarbonyl Nucleophiles to Olefins. *Journal of Organometallic Chemistry* **2011**, *696* (1), 296-304.
113. Lee, M. H.; Kim, J. S.; Sessler, J. L., Small Molecule-Based Ratiometric Fluorescence Probes for Cations, Anions, and Biomolecules. *Chemical Society Reviews* **2015**, *44* (13), 4185-4191.
114. Tsubokura, K.; Vong, K. K. H.; Pradipta, A. R.; Ogura, A.; Urano, S.; Tahara, T.; Nozaki, S.; Onoe, H.; Nakao, Y.; Sibgatullina, R.; Kurbangalieva, A.; Watanabe, Y.; Tanaka, K., In Vivo Gold Complex Catalysis within Live Mice. *Angewandte Chemie International Edition* **2017**, *56* (13), 3579-3584.
115. Gaudelli, N. M.; Komor, A. C.; Rees, H. A.; Packer, M. S.; Badran, A. H.; Bryson, D. I.; Liu, D. R., Programmable Base Editing of A•T to G•C in Genomic DNA without DNA Cleavage. *Nature* **2017**, *551*, 464.

Chapter 2.

Iridium Complexes for Aqueous Alcohol Dehydrogenation

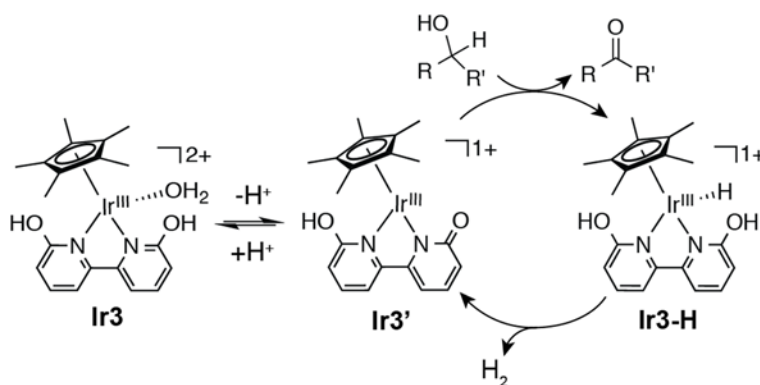
Portions of this work have been previously published.

Reproduced with permission from Ngo, A. H.; Adams, M. J.; Do, L. H. *Organometallics*, **2014**, 33, 6742-6745. DOI: DOI: 10.1021/om5010258.

Copyright 2014 American Chemical Society.

2.1 Introduction

Transition metal-hydrides are important intermediates in many catalytic organometallic transformations. Formation of these hydride species allows the efficient shuttling of nucleophilic hydrides derived from primary and secondary alcohols or other hydride sources to electrophilic carbonyl groups (transfer hydrogenation) or to protons to generate hydrogen gas (acceptorless dehydrogenation).¹⁻² Many hydrogenation/dehydrogenation systems based on metal ions such as Ru,³⁻⁶ Rh,⁷⁻⁸ Ir,⁹⁻¹¹ Fe,¹²⁻¹⁷ and Co¹⁸ have been reported, with various applications ranging from enantioselective chemical synthesis⁵ to facile hydrogen release from liquid fuels.¹⁹⁻²¹



Scheme 2.1. Proposed Mechanism for Alcohol Dehydrogenation by **Ir3**.

In order to develop atom economical methods to elaborate complex biomolecules, we were fascinated by alcohol dehydrogenation catalysts that require neither sacrificial hydride acceptors nor base additives (Scheme 2.1).² Typically, oxidation of benzylic and secondary alcohols occurs more readily than primary alcohols due to their lower oxidation potentials. However, during the course of our studies we discovered a pentamethylcyclopentadienyl (Cp*) iridium(III) complex²²⁻²⁷ that is unreactive toward

benzylic/aliphatic alcohols but reactive toward allylic alcohols. Such chemoselectivity is rare and to the best of our knowledge, has only been achieved using catalyst systems that employ stoichiometric oxidants.²⁸⁻²⁹ In this chapter, I will describe the unusual alcohol dehydrogenation chemistry of an organometallic iridium catalyst³⁰ and demonstrate its utility in the selective interconversion of glucocorticoids,³¹ an important class of naturally occurring steroids.

2.2 Catalytic Activity Check and Substrate Scope Study

In 2012, Yamaguchi and co-workers reported that [Cp*Ir(6,6'-dihydroxy-2,2'-bipyridine)(H₂O)]²⁺ (**Ir3**) can convert benzylic and secondary alcohols to aldehydes and ketones, respectively, in aqueous media under reflux.²⁴ This transformation is a potential bioorthogonal reaction for converting alcohols to carbonyls in living systems if it can work under mild conditions.

With biocatalytic orientation, we synthesized **Ir3** and tested it with different types of alcohol under biological relevant conditions. Under our reaction conditions, however, we did not get any carbonyl products with neither benzylic (entries 1-4, Table 2.1) nor saturated aliphatic alcohols (entries 5-7). When we expanded the scope of our substrate studies, we discovered that our iridium catalyst (**Ir3**, 2 mol %) can oxidize cyclic α,β -unsaturated alcohols to their corresponding enones under air in *tert*-butanol/water (1:9), at 40°C with yields ranging from modest to excellent (entries 8-11). The reversible isomerization of the starting substrate was observed for compounds containing six-membered rings (Schemes 2.2 and 2.3).³²⁻³⁴ However, dehydrogenation to the enone is favored in the absence of added hydrogen; in fact, nearly quantitative yield of 3-

methylcyclohex-2-en-1-one was obtained from reaction of **Ir3** with 3-methylcyclohex-2-en-1-ol after 24 h (entry 9).

Table 2.1. Alcohol Dehydrogenation Study^a

$$\text{R}-\text{CH}(\text{OH})-\text{CH}_2-\text{R}' \xrightarrow[\text{40}^\circ\text{C, air, 24 h}]{\text{Ir3 (2 mol \%), t-BuOH/H}_2\text{O (1:9)}} \text{R}-\text{C}(=\text{O})-\text{CH}_2-\text{R}' + \text{H}_2$$

alcohol aldehyde or ketone

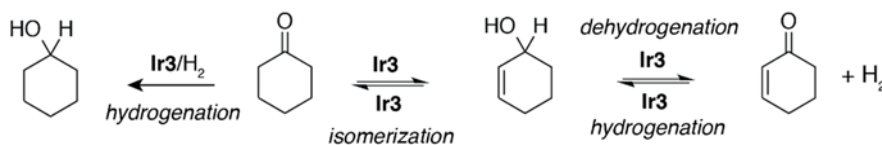
Entry	Product	Conversion,% ^b	Yield,% ^b	Entry	Product	Conversion,% ^b	Yield,% ^b
1		0	0	8		79	46 ^c
2		0	0	9		99	95
3		0	0	10		63	35 ^c
4		0	0	11		17	12
5		0	0	12		99	0 ^d
6		0	0	13		13 ^e	13 ^e
7		0	0	14		9 ^e	9 ^e

^aAlcohol (0.50 mmol), Ir3 catalyst (1.0 μmol), t-BuOH/H₂O (1:9, 1.0 mL), sealed reaction vial under air.
^bDetermined by GC. ^cAdditional side products were obtained. ^dAn intractable solid was isolated. ^eDetermined by NMR spectroscopy.

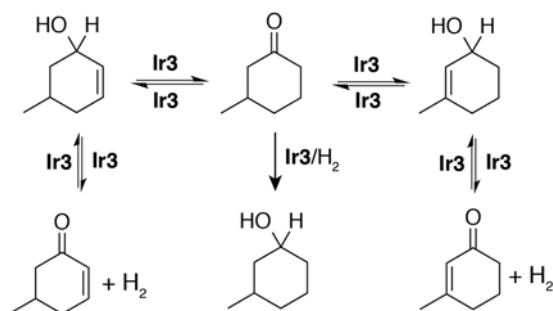
The seven-membered ring cyclohep-2-en-1-ol can be dehydrogenated but not as efficiently as six-membered ring substrates, as indicated by its low conversion and yield (entry 11). The five-membered ring 3-methylcyclopent-2-en-1-ol was fully consumed after 24 h but no expected product (3-methylcyclopent-2-en-1-one) was detected by GC analysis (entry 12); instead, a significant amounts of an intractable solid was found in this reaction.

Surprisingly, linear allylic alcohols were found to react poorly in the presence of **Ir3** at 40°C (entries 13-14), with yields only up to ~10% of the corresponding enone as quantified by ¹H NMR spectroscopy and gas chromatography. Acyclic enones have been shown to form strong *s-cis* adducts to transition metal complexes,³⁵⁻³⁶ which may result in catalyst inhibition by blocking substrate coordination sites at the metal center. In contrast, cyclic enones have *s-trans* geometric configurations and thus, cannot bind to transition metal ions as tightly as the *s-cis* form. Nevertheless, the unusual reactivity of **Ir3** toward *cyclic* allylic alcohols over a variety of other alcohols makes it an unusually chemoselective oxidation catalyst.

Scheme 2.2. Proposed interconversion mechanism of symmetric six-membered ring substrates.



Scheme 2.3. Proposed interconversion mechanism of asymmetric six-membered ring substrates.



The representative GC plots from alcohol dehydrogenation studies are shown in Figure 2.1, and the ¹³C NMR spectra to compare the product from reaction of cyclohex-2-en-1-ol/**Ir3** to those of authentic standards are shown in Figure 2.2.

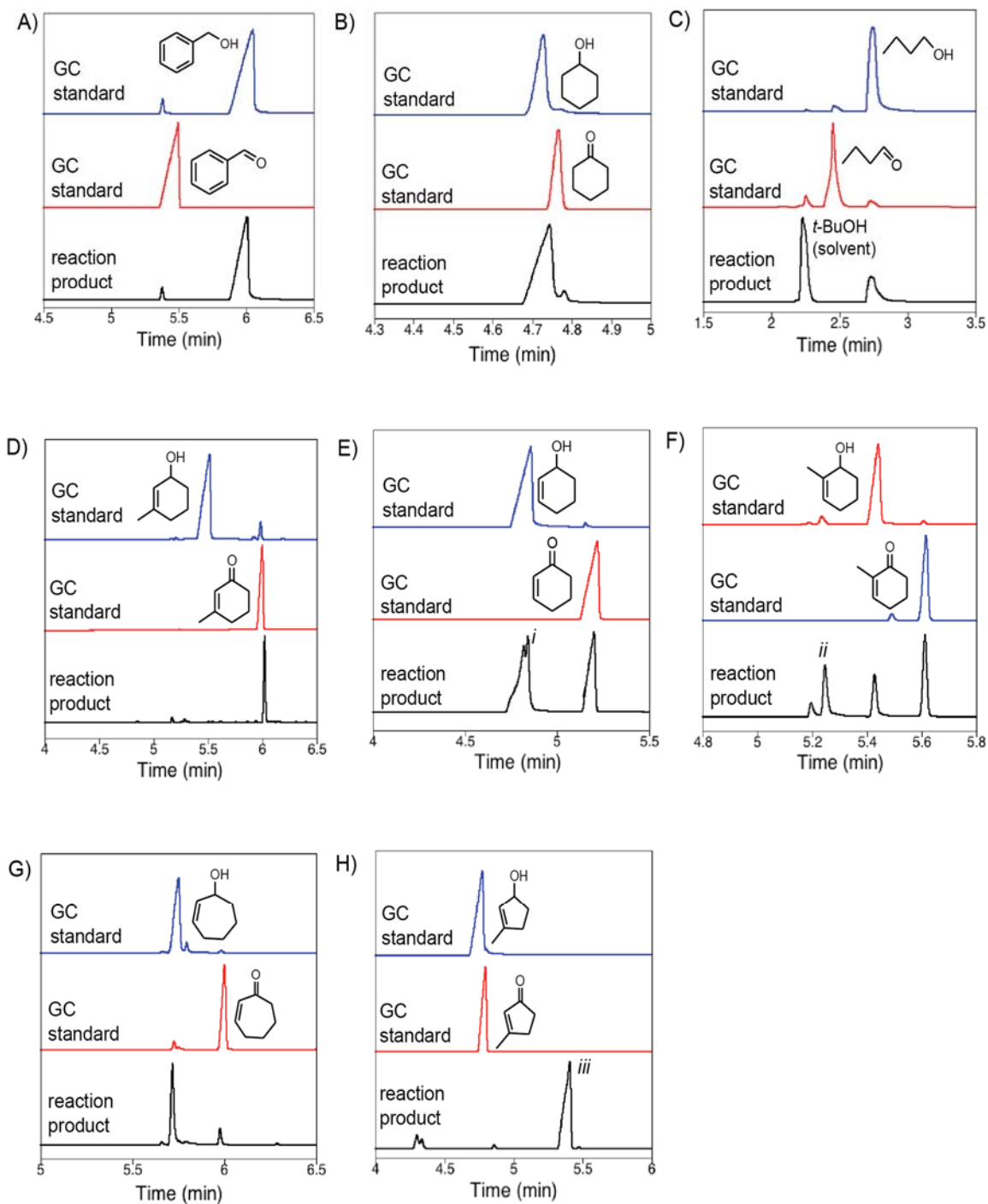


Figure 2.1. Representative GC plots from alcohol dehydrogenation studies. Notes: i. Cyclohex-2-en-1-ol, cyclohexanone, and cyclohexanol appear at similar retention times in the GC. Due to this ambiguity, identities of the products were verified by NMR spectroscopy. ii. Products resulting from isomerization. iii. This GC trace shows the soluble minor products of the reaction. The major product is a solid intractable material.

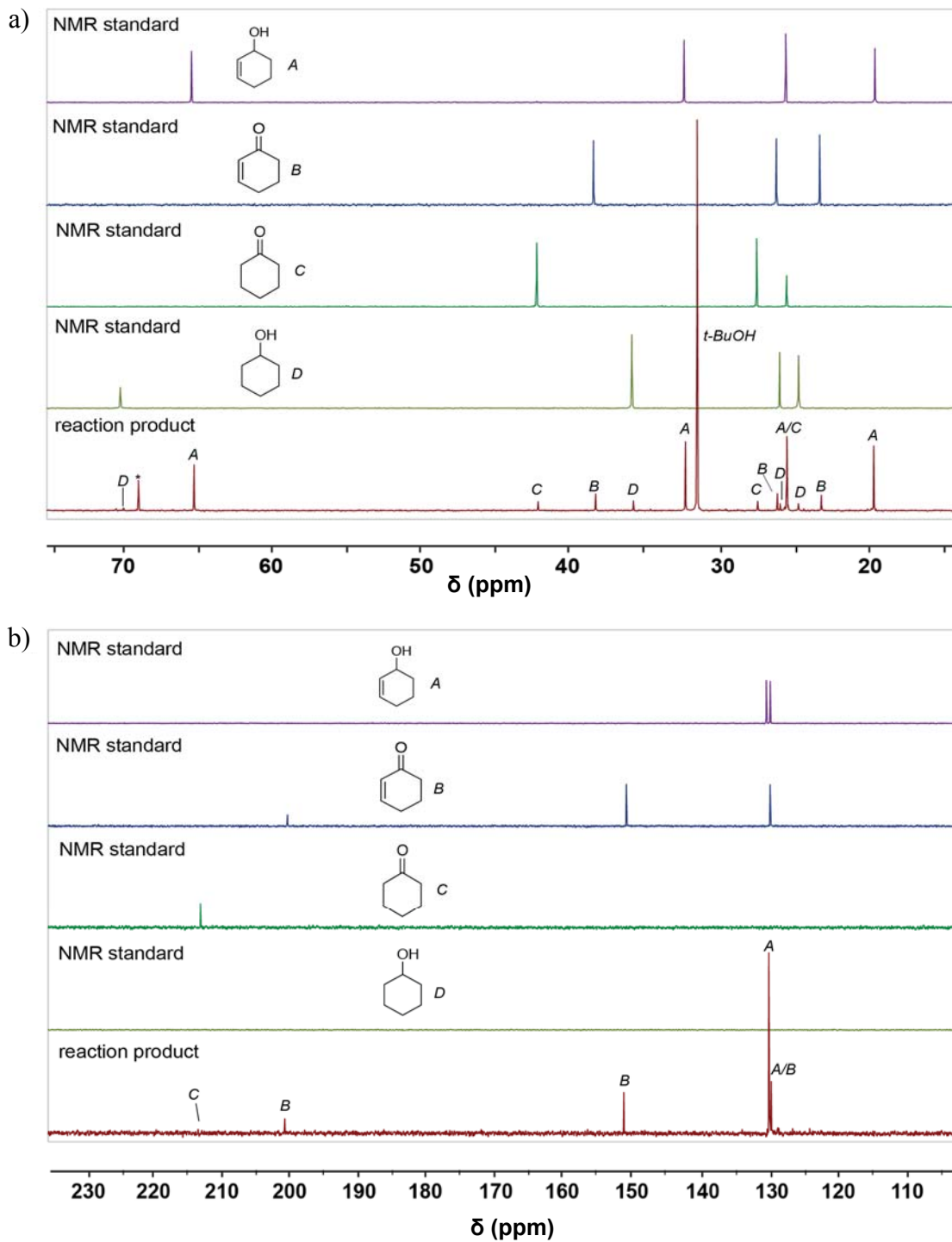
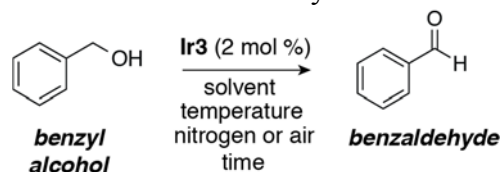


Figure 2.2. ¹³C NMR spectral (CDCl₃, 125 MHz) comparison of the product from reaction of cyclohex-2-en-1-ol/**Ir3** to those of authentic standards. The top (a) and bottom (b) plots show spectral ranges from 17-75 ppm and 100-230 ppm, respectively. The signal marked with (*) has been assigned to the presence of an impurity.

We also tried other reaction conditions for benzyl alcohol dehydrogenation. Reactions with different sources of water at acidic, neutral, and basic pH were tested at 100°C, either under air or under nitrogen, but no benzaldehyde product was observed (Table 2.2, entries 1-8). Even at 110°C, our reaction gave only trace amounts of product (entry 9). In our effort to understand what led to the different results in our study and the reported one, we contacted Yamaguchi group. With instruction from Prof. Fujita, we tested dehydrogenation of benzyl alcohol again with the oil bath set to 130°C (reaction was under reflux and the actual temperature inside the reaction flask was 120°C). As shown in entry 10, this reaction condition gave 87% yield, which was similar with the reported results.²⁴

Table 2.2. Reaction Conditions Tested for Benzyl Alcohol Dehydrogenation



Entry	Solvent	Temperature (°C)	Nitrogen or air	Time (h)	Conversion % ^a	Yield % ^a
1	ACS reagent grade water	100	air	20	0	0
2	ACS reagent grade water	100	nitrogen	24	0	0
3	pH 3.75, acetic acid buffer	100	nitrogen	36	0	0
4	pH 6.75, sodium phosphate buffer	100	nitrogen	36	0	0
5	pH 10.0, sodium borate buffer	100	nitrogen	36	0	0
6	Tap water (University of Houston)	100	nitrogen	20	0	0
7	Deionized water (University of Houston)	100	nitrogen	20	0	0
8	<i>t</i> -butanol/water (1:9)	80	air	38	0	0
9	ACS reagent grade water	110	air	20	~5	trace
10	ACS reagent grade water	120 ^b	air	20	90	87

^aDetermined by GC analysis; ^bReflux with a water cooling condenser.

2.3 Mechanistic Studies

Mechanistic studies were performed to explain the reactivity of **Ir3**. Yamaguchi and co-workers proposed that acceptorless dehydrogenation proceeds through the following mechanism: 1) metal binding to 1° or 2° alkoxide, 2) β -H elimination to form the corresponding aldehyde or ketone, and 3) catalyst regeneration via protonation of the resulting metal-hydride species to yield H₂ (Scheme 2.1).⁶

In our study, the formation of iridium hydride species **Ir3-H** was observed when 15 equiv. of 3-methylcyclohex-2-en-1-ol was added to a solution of **Ir3** in D₂O and heated at 90°C (Figure 2.3). After heating for several minutes, the solution rapidly changed from yellow to orange ($\lambda_{\text{shoulder}} = \sim 450$ nm). The reaction mixture showed a peak at -17.7 ppm in its ¹H NMR spectrum, which is similar to the reported for an iridium hydride species.⁹ This peak was *not* observed in the absence of cyclohexenol or when benzyl alcohol was used as the hydride donor. The reaction byproduct, hydrogen gas, was detected by gas chromatography with a thermal conductivity detector (GC-TCD) (Figure 2.4).

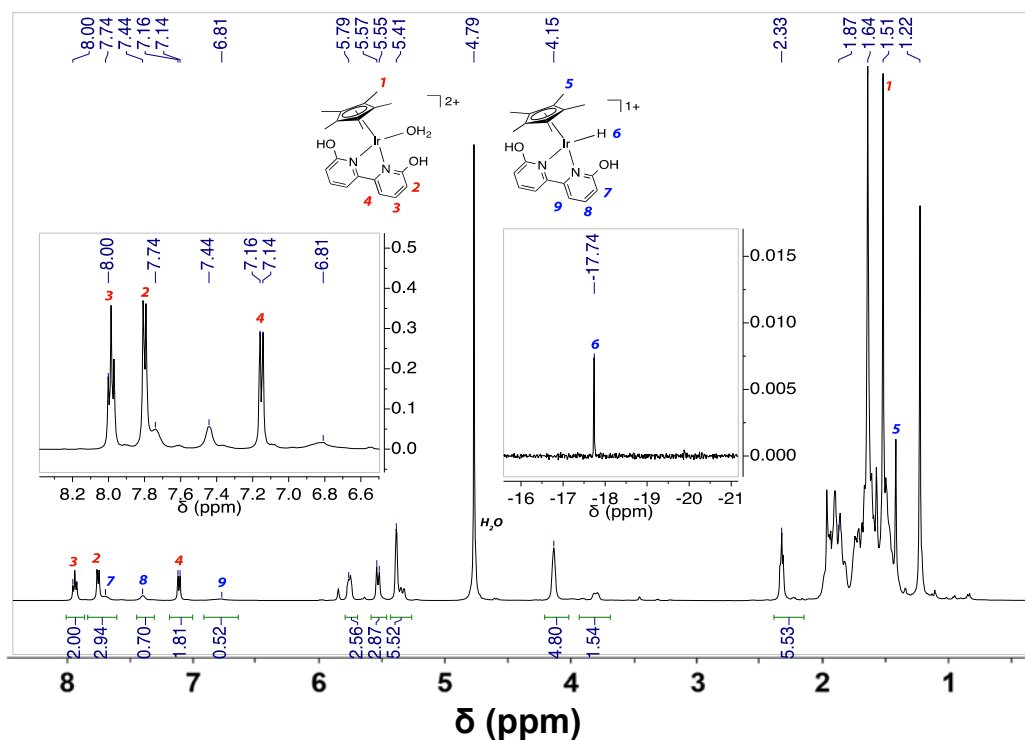


Figure 2.3. ^1H NMR spectrum (D₂O, 500 MHz) of reaction of **Ir3** (3 mM) with 3-methylcyclohex-2-en-1-ol (45 mM).

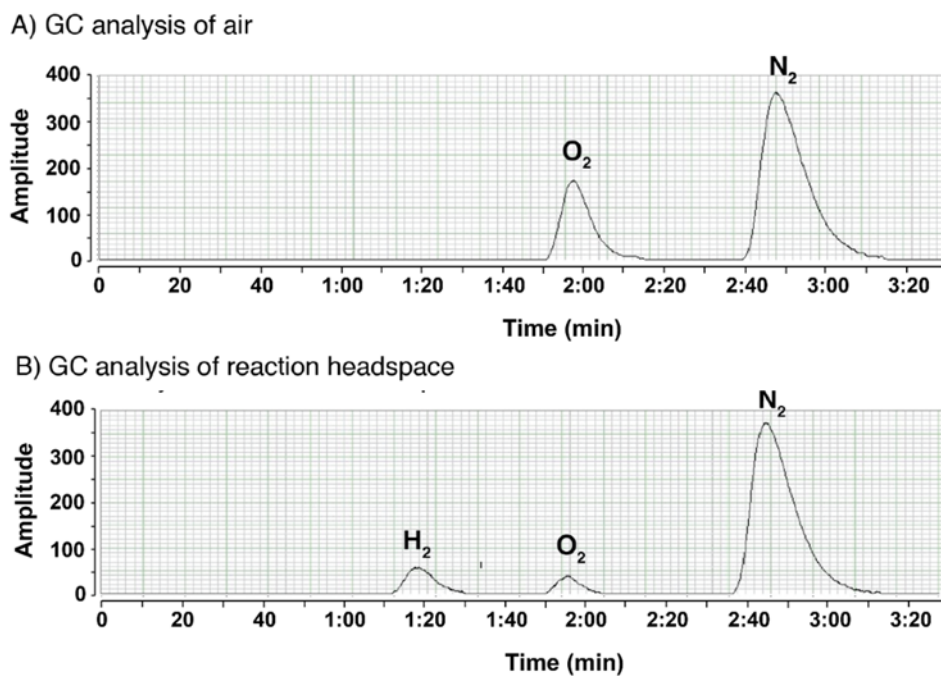
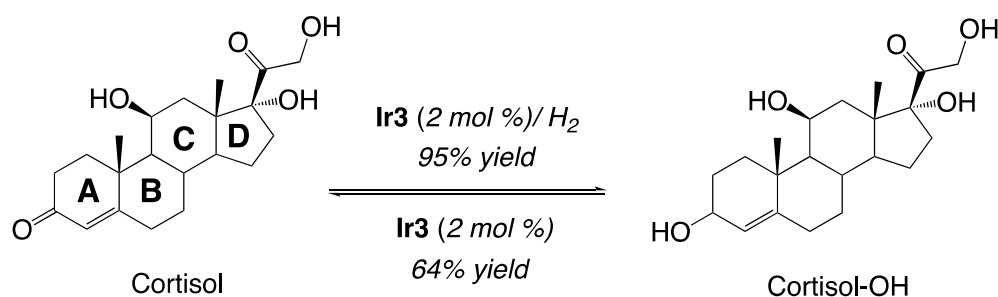


Figure 2.4. GC-TCD traces obtained from analysis of A) 100 μL of air (as background control) and B) 100 μL of headspace from reaction of 2 mol % **Ir3** and 3-methylcyclohex-2-en-1-ol in tert-butanol/water (1:9) after ~16 h.

Further investigations showed that **Ir3** is also an active catalyst for the reversed reaction, hydrogenation of aldehydes/ketones, at 25°C under 1 atm of hydrogen gas. A variety of carbonyl-containing compounds, including benzaldehydes, acetophenone, aliphatic aldehydes/ketones, and enones, were successfully reduced to their alcohols with up to 99% yield.

Interestingly, we found that **Ir3** can catalyze efficiently both the oxidation of cortisol-OH and reduction of cortisol under the appropriate reaction conditions. The hydride transfer reactions are highly selective for ring A of cortisol, despite the presence of other alcohol and carbonyl functionalities in rings C and D (Scheme 2.4).



Scheme 2.4. Interconversion of cortisol.

2.4 Conclusion

We have identified an air- and water-compatible iridium (III) catalyst that is highly efficient at both oxidation of cyclic allylic alcohols and reduction of aldehydes/ketones under appropriate reaction conditions. The formation of an iridium-hydride intermediate during catalysis was observed by spectroscopy, and detection of H₂ as a reaction byproduct supports an acceptorless alcohol dehydrogenation mechanism. This chemistry allows easy access to several glucocorticoid derivatives, which may be useful in studies of steroid metabolism^{31,37} or as possible chemotherapeutics³⁸⁻⁴⁰ and drug conjugates.⁴¹⁻⁴³

2.5 Experimental

Materials and Methods Commercial reagents and solvents were used as received without further purification. The iridium catalyst $[\text{Cp}^*\text{Ir}(6,6'\text{-dihydroxy-2,2'\text{-bipyridine})(\text{H}_2\text{O})](\text{SO}_3\text{CF}_3)_2$ (**Ir3**) was prepared according to a literature procedure.²⁴ ACS reagent grade water was obtained from Mallinckrodt and hydrogen was obtained from Matheson Tri-Gas.

Physical Methods NMR spectra were recorded on either JOEL ECA-400P or ECA-500 spectrometers. Gas chromatographic (GC) analyses were performing using an Agilent 7820E spectrometer equipped with both a 5977A extractor mass spectral detector (MSD) and a flame ionization detector (FID). For GC-MS analysis, an Agilent HP-5MS capillary column (0.25 mm x 0.25 μm x 25 m) was used with the following method: start at 60°C, hold for 3 min, increase temperature at a rate of 30°C/min up to 200°C and then 40°C/min to 275°C; column flow rate is 1 mL/min. For GC-FID analysis, a Zebtron ZB-5MS capillary column (0.25 mm x 0.25 μm x 25 m) was used with the following method: start at 60°C, hold for 3 min, increase temperature at a rate of 40°C/min up to 150°C and then 30°C/min to 250°C; column flow rate is 1 mL/min. All substrate quantification measurements were conducted by integrating peaks in their GC-FID chromatograms and corrected based on their experimental GC response factors; biphenyl or 1,3,5-trimethylbenzene were used as internal standards. Gas samples were analyzed using a GOW-MAC gas chromatography instrument equipped with a thermal conductivity detector (TCD).

General Dehydrogenation Procedure The alcohol (0.50 mmol) was dissolved in 1.0 mL of *t*-BuOH/H₂O (1:9) in 1 dram vials with a small stir bar. Solid **Ir3** (1.0 μmol , 2 mol %)

was added and the vials were sealed in order to prevent evaporation of volatile substrates. The resulting yellow mixture was stirred at 40°C for 24 h. No additional effort was taken to remove air from inside the reaction vials. When the reaction was complete, the reaction mixture was diluted with 4.0 mL of *i*-PrOH and then combined with biphenyl or 1,3,5-trimethylbenzene (~0.3 mmol) as an internal standard. A 1.0 mL aliquot of this solution was transferred to a GC vial and then analyzed by gas chromatography. The identities of the products were further confirmed using NMR spectroscopy.

2.6 References

1. Dobereiner, G. E.; Crabtree, R. H., Dehydrogenation as a Substrate-Activating Strategy in Homogeneous Transition-Metal Catalysis. *Chemical Reviews* **2009**, *110* (2), 681-703.
2. Gunanathan, C.; Milstein, D., Applications of Acceptorless Dehydrogenation and Related Transformations in Chemical Synthesis. *Science* **2013**, *341* (6143), 1229712.
3. Haack, K.-J.; Hashiguchi, S.; Fujii, A.; Ikariya, T.; Noyori, R., The Catalyst Precursor, Catalyst, and Intermediate in the RuII-Promoted Asymmetric Hydrogen Transfer between Alcohols and Ketones. *Angewandte Chemie International Edition* **1997**, *36* (3), 285-288.
4. Dobson, A.; Robinson, S. D., Complexes of the Platinum Metals. 7. Homogeneous Ruthenium and Osmium Catalysts for the Dehydrogenation of Primary and Secondary Alcohols. *Inorganic Chemistry* **1977**, *16* (1), 137-142.
5. Noyori, R.; Ohkuma, T., Asymmetric Catalysis by Architectural and Functional Molecular Engineering: Practical Chemo- and Stereoselective Hydrogenation of Ketones. *Angewandte Chemie International Edition* **2001**, *40* (1), 40-73.
6. Nielson, M.; Kammer, A.; Cozzula, D.; Junge, H.; Gladiali, S.; Beller, M., Efficient Hydrogen Production from Alcohols under Mild Reaction Conditions. *Angewandte Chemie International Edition* **2011**, *50* (41), 9593–9597.
7. Brewster, T. P.; Miller, A. J. M.; Heinekey, D. M.; Goldberg, K. I., Hydrogenation of Carboxylic Acids Catalyzed by Half-Sandwich Complexes of Iridium and Rhodium. *Journal of the American Chemical Society* **2013**, *135* (43), 16022-16025.
8. Blacker, A. J.; Clot, E.; Duckett, S. B.; Eisenstein, O.; Grace, J.; Nova, A.; Perutz, R. N.; Taylor, D. J.; Whitwood, A. C., Synthesis and Structure of "16-electron"

- Rhodium(iii) Catalysts for Transfer Hydrogenation of a Cyclic Imine: Mechanistic Implications. *Chemical Communications* **2009**, (44), 6801-6803.
9. Tang, W.; Johnston, S.; Iggo, J. A.; Berry, N. G.; Phelan, M.; Lian, L.; Bacsá, J.; Xiao, J., Cooperative Catalysis through Noncovalent Interactions. *Angewandte Chemie International Edition* **2013**, *52* (6), 1668-1672.
 10. Royer, A. M.; Rauchfuss, T. B.; Gray, D. L., Organoiridium Pyridonates and Their Role in the Dehydrogenation of Alcohols. *Organometallics* **2010**, *29* (24), 6763-6768.
 11. Wu, X.; Liu, J.; Li, X.; Zanotti-Gerosa, A.; Hancock, F.; Vinci, D.; Ruan, J.; Xiao, J., On Water and in Air: Fast and Highly Chemoselective Transfer Hydrogenation of Aldehydes with Iridium Catalysts. *Angewandte Chemie International Edition* **2006**, *45* (40), 6718-6722.
 12. Song, H.; Kang, B.; Hong, S. H., Fe-Catalyzed Acceptorless Dehydrogenation of Secondary Benzylic Alcohols. *ACS Catalysis* **2014**, 2889-2895.
 13. Bielinski, E. A.; Lagaditis, P. O.; Zhang, Y.; Mercado, B. Q.; Würtele, C.; Bernskoetter, W. H.; Hazari, N.; Schneider, S., Lewis Acid-Assisted Formic Acid Dehydrogenation Using a Pincer-Supported Iron Catalyst. *Journal of the American Chemical Society* **2014**, *136* (29), 10234-10237.
 14. Zell, T.; Ben-David, Y.; Milstein, D., Unprecedented Iron-Catalyzed Ester Hydrogenation. Mild, Selective, and Efficient Hydrogenation of Trifluoroacetic Esters to Alcohols Catalyzed by an Iron Pincer Complex. *Angewandte Chemie International Edition* **2014**, *53*, 4685-4689.
 15. Moyer, S. A.; Funk, T. W., Air-stable iron catalyst for the Oppenauer-type oxidation of alcohols. *Tetrahedron Letters* **2010**, 5430-5433.
 16. Quintard, A.; Rodriguez, J., Iron Cyclopentadienone Complexes: Discovery, Properties, and Catalytic Reactivity *Angewandte Chemie International Edition* **2014**, *53*, 4044-4055.
 17. Chakraborty, S.; Brennessel, W. W.; Jones, W. J., A Molecular Iron Catalyst for the Acceptorless Dehydrogenation and Hydrogenation of N-Heterocycles. *Journal of the American Chemical Society* **2014**, *136* (24), 8564-8567.
 18. Zhang, G.; Vasudevan, K. V.; Scott, B. L.; Hanson, S. K., Understanding the Mechanisms of Cobalt-Catalyzed Hydrogenation and Dehydrogenation Reactions. *Journal of the American Chemical Society* **2013**, *135* (23), 8668-8681.
 19. Johnson, T. C.; Morris, D. J.; Wills, M., Hydrogen Generation from Formic Acid and Alcohols using Homogeneous Catalysts. *Chemical Society Reviews* **2010**, *39*, 81-88.
 20. Nielson, M.; Alberico, E.; Baumann, W.; Drexler, H.-J.; Junge, H.; Gladiali, S., Low-temperature Aqueous-phase Methanol Dehydrogenation to Hydrogen and Carbon Dioxide. *Nature* **2013**, *495*, 85-90.
 21. Brewster, T. P.; Ou, W. C.; Tran, J. C.; Goldberg, K. I.; Hanson, S. K.; Cundari, T. R.; Heinekey, D. M., Iridium, Rhodium, and Ruthenium Catalysts for the “Aldehyde-Water Shift” Reaction. *ACS Catalysis* **2014**, *4* (9), 3034-3038.

22. Kawahara, R.; Fujita, K.-i.; Yamaguchi, R., Cooperative Catalysis by Iridium Complexes with a Bipyridonate Ligand: Versatile Dehydrogenative Oxidation of Alcohols and Reversible Dehydrogenation–Hydrogenation between 2-Propanol and Acetone. *Angewandte Chemie International Edition* **2012**, *51* (51), 12790-12794.
23. Fujita, K.-i.; Tanaka, Y.; Kobayashi, M.; Yamaguchi, R., Homogeneous Perdehydrogenation and Perhydrogenation of Fused Bicyclic N-Heterocycles Catalyzed by Iridium Complexes Bearing a Functional Bipyridonate Ligand. *Journal of the American Chemical Society* **2014**, *136* (13), 4829-4832.
24. Kawahara, R.; Fujita, K.-i.; Yamaguchi, R., Dehydrogenative Oxidation of Alcohols in Aqueous Media Using Water-Soluble and Reusable Cp*Ir Catalysts Bearing a Functional Bipyridine Ligand. *Journal of the American Chemical Society* **2012**, *134* (8), 3643-3646.
25. Zeng, G.; Sakaki, S.; Fujita, K.-i.; Sano, H.; Yamaguchi, R., Efficient Catalyst for Acceptorless Alcohol Dehydrogenation: Interplay of Theoretical and Experimental Studies. *ACS Catalysis* **2014**, *4* (3), 1010-1020.
26. Fujita, K.-i.; Ito, W.; Yamaguchi, R., Dehydrogenative Lactonization of Diols in Aqueous Media Catalyzed by a Water-Soluble Iridium Complex Bearing a Functional Bipyridine Ligand. *ChemCatChem* **2014**, *6* (1), 109-112.
27. DePasquale, J.; Nieto, I.; Reuther, L. E.; Herbst-Gervasoni, C. J.; Paul, J. J.; Mochalin, V.; Zeller, M.; Thomas, C. M.; Addison, A. W.; Papish, E. T., Iridium Dihydroxybipyridine Complexes Show That Ligand Deprotonation Dramatically Speeds Rates of Catalytic Water Oxidation. *Inorganic Chemistry* **2013**, *52* (16), 9175-9183.
28. Shen, S.-S.; Kartika, V.; Tan, Y. S.; Webster, R. D.; Narasaka, K., Selective Aerobic Oxidation of Allylic and Benzylic Alcohols Catalyzed by N-hydroxyindole and Copper(I) Chloride. *Tetrahedron Letters* **2012**, *53* (8), 986-990.
29. Cosner, C. C.; Cabrera, P. J.; Byrd, K. M.; Thomas, A. M. A.; Helquist, P., Selective Oxidation of Benzylic and Allylic Alcohols Using Mn(OAc)₃/Catalytic 2,3-Dichloro-5,6-dicyano-1,4-benzoquinone. *Organic Letters* **2011**, *13* (8), 2071-2073.
30. Ngo, A. H.; Adams, M. J.; Do, L. H., Selective Acceptorless Dehydrogenation and Hydrogenation by Iridium Catalysts Enabling Facile Interconversion of Glucocorticoids. *Organometallics* **2014**, *33* (23), 6742-6745.
31. Okihara, R.; Mitamura, K.; Hasegawa, M.; Mori, M.; Muto, A.; Kakiyama, G.; Ogawa, S.; Iida, T.; Shimada, M.; Mano, N.; Ikegawa, S., Potential Corticoid Metabolites: Chemical Synthesis of 3- and 21-Monosulfates and Their Double-Conjugates of Tetrahydrocorticosteroids in the 5 α - and 5 β -Series. *Chemical and Pharmaceutical Bulletin* **2010**, *58* (3), 344-353.
32. Mantilli, L.; Mazet, C., Iridium-catalyzed Isomerization of Primary Allylic Alcohols under Mild Reaction Conditions. *Tetrahedron Letters* **2009**, *50* (28), 4141-4144.

33. Bouziane, A.; Carboni, B.; Bruneau, C.; Carreaux, F.; Renaud, J.-L., Pentamethylcyclopentadienyl Ruthenium: an Efficient Catalyst for the Redox Isomerization of Functionalized Allylic Alcohols into Carbonyl Compounds. *Tetrahedron* **2008**, *64* (51), 11745-11750.
34. Cadierno, V.; García-Garrido, S. E.; Gimeno, J.; Varela-Álvarez, A.; Sordo, J. A., Bis(allyl)-Ruthenium(IV) Complexes as Highly Efficient Catalysts for the Redox Isomerization of Allylic Alcohols into Carbonyl Compounds in Organic and Aqueous Media: Scope, Limitations, and Theoretical Analysis of the Mechanism. *Journal of the American Chemical Society* **2006**, *128* (4), 1360-1370.
35. Kanaya, S.; Imai, Y.; Komine, N.; Hirano, M.; Komiya, S., Dehydrogenative Formation of a (η^4 -Enone)ruthenium(0) Complex as a Key Intermediate in the Catalytic Isomerization of Allylic Alcohol to Ketone. *Organometallics* **2005**, *24* (6), 1059-1061.
36. Daugulis, O.; Brookhart, M., Decarbonylation of Aryl Ketones Mediated by Bulky Cyclopentadienylrhodium Bis(ethylene) Complexes. *Organometallics* **2003**, *23* (3), 527-534.
37. Yazdi, M. T.; Arabi, H.; Faramarzi, M. A.; Ghasemi, Y.; Amini, M.; Shokravi, S.; Mohseni, F. A., Biotransformation of Hydrocortisone by a Natural Isolate of *Nostoc muscorum*. *Phytochemistry* **2004**, *65* (15), 2205-2209.
38. Bansal, R.; Acharya, P. C., Man-Made Cytotoxic Steroids: Exemplary Agents for Cancer Therapy. *Chemical Reviews* **2014**, *114* (14), 6986-7005.
39. Pokhrel, M.; Ma, E., Synthesis and Screening of Aromatase Inhibitory Activity of Substituted C19 Steroidal 17-Oxime Analogs. *Molecules* **2011**, *16* (12), 9868-9885.
40. Varela, C.; Tavares da Silva, E. J.; Amaral, C.; Correia da Silva, G.; Baptista, T.; Alcaro, S.; Costa, G.; Carvalho, R. A.; Teixeira, N. A. A.; Roleira, F. M. F., New Structure-Activity Relationships of A- and D-Ring Modified Steroidal Aromatase Inhibitors: Design, Synthesis, and Biochemical Evaluation. *Journal of Medicinal Chemistry* **2012**, *55* (8), 3992-4002.
41. Huxley, M.; Sanchez-Cano, C.; Browning, M. J.; Navarro-Ranninger, C.; Quiroga, A. G.; Rodger, A.; Hannon, M. J., An Androgenic Steroid Delivery Vector that Imparts Activity to a Non-conventional Platinum(ii) Metallo-drug. *Dalton Transactions* **2010**, *39* (47), 11353-11364.
42. Sanchez-Cano, C.; Huxley, M.; Ducani, C.; Hamad, A. E.; Browning, M. J.; Navarro-Ranninger, C.; Quiroga, A. G.; Rodger, A.; Hannon, M. J., Conjugation of Testosterone Modifies the Interaction of Mono-functional Cationic Platinum(ii) Complexes with DNA, Causing Significant Alterations to the DNA Helix. *Dalton Transactions* **2010**, *39* (47), 11365-11374.
43. Levine, P. M.; Garabedian, M. J.; Kirshenbaum, K., Targeting the Androgen Receptor with Steroid Conjugates. *Journal of Medicinal Chemistry* **2014**, *57* (20), 8224-8237.

Chapter 3. Iridium Complexes for Aldehyde Hydrogenation in Cell Culture Media

This work have been previously published.

Reproduced with permission from Ngo, A. H.; Ibañez, M.; Do, L. H. *ACS Catalysis*,
2016, *6*, 2637–2641. DOI: 10.1021/acscatal.6b00395.

Copyright 2016 American Chemical Society.

3.1 Introduction

The development of synthetic catalysts that can interface with biological systems is an emerging frontier in chemical biology. They can be applied directly inside living organisms or indirectly in the reaction flasks.¹⁻² Achieving intracellular catalysis is more difficult to attain because the catalysts must be operate within heterogeneous environments. In recent years, remarkable progress has been made in expanding our toolbox of biocompatible metal-catalyzed transformations, which include alkene hydrogenation,³⁻⁶ azide-alkyne cycloaddition,⁷⁻⁸ carbamate cleavage,⁹⁻¹⁶ and C–C bond cross-coupling.¹⁷⁻²⁰ These achievements have made possible new research avenues to be pursued, such as the design of novel catalytic drugs^{2, 21-23} or the creation of new biosynthetic methods.

Transition metal-mediated transfer hydrogenations are versatile methods to convert carbonyl to alcohol groups or vice versa.²⁴ Some iridium complexes have even been shown to be active transfer hydrogenation catalysts in the presence of both air and water.²⁵⁻³⁰ For example, Sadler and co-workers reported the use of an organometallic Ir complex to promote hydride transfer from the natural cofactor nicotinamide adenine dinucleotide (NADH) to pyruvate in methanol/water (1:9) under air;³¹ however, the iridium complex used in this study was not employed in catalytic amounts and the reactions were performed in the absence of common biological components and salts, which are often catalyst inhibitors.

This chapter will demonstrate the use of pentamethylcyclopentadienyl (Cp*) iridium pyridinecarboxamidate complexes in catalytic hydride transfer from NADH or sodium formate to aldehydes in pH 7.4 phosphate buffered saline (PBS) or cell growth media at 37 °C and in the presence of various biomolecules and metal ions.³² Additional

experiments were performed to understand the mechanistic activity of the iridium catalysts. The application of iridium complexes in reducing cytotoxic aldehyde 4-hydroxynon-2-enal under physiologically relevant reaction conditions was also described.

3.2 Synthesis of Iridium Complexes and Catalytic Activity Study

In our study, a total of 12 pentamethylcyclopentadienyl (Cp*) iridium and 1 ruthenium complexes were synthesized and tested in *catalytic* hydride transfer from NADH or sodium formate to organic acceptors under biologically relevant conditions (Chart 3.1).

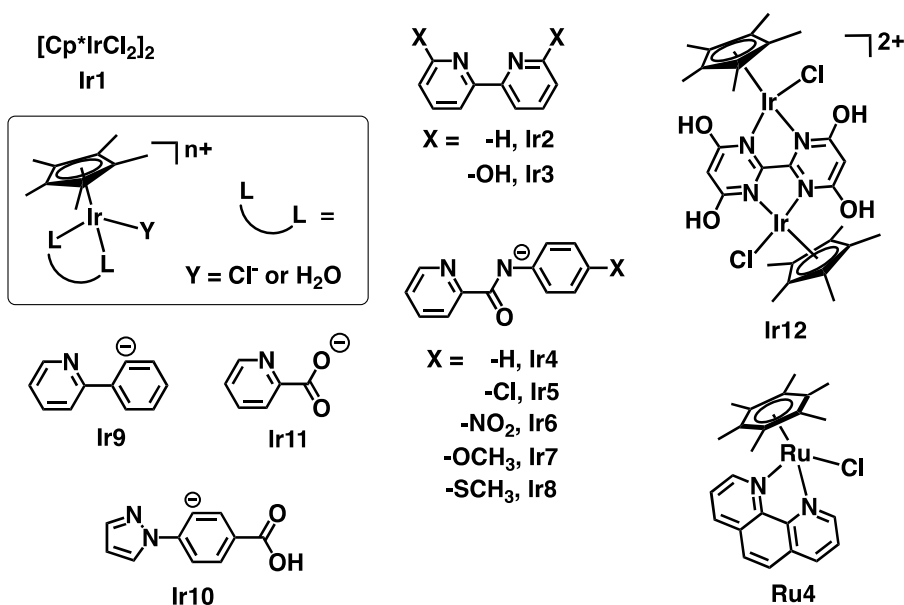


Chart 3.1. Ir and Ru complexes tested in this study.

We first evaluated the competency of the iridium complexes in converting benzaldehyde to benzyl alcohol using NADH as the hydride donor.³³ As shown in Figure 3.1.A, reaction of benzaldehyde (1.0 equiv.) and NADH (1.2 equiv.) in *tert*-butanol and phosphate buffered saline (PBS) (2:8) for 24 h at 37 °C gave no benzyl alcohol when complexes $[Cp^*Ir(2,2'\text{-bipyridine})(H_2O)](SO_3CF_3)_2$ (**Ir2**),³⁴ $[Cp^*Ir(2\text{-phenylpyridine})Cl]$

(**Ir9**),³⁵ [Cp*Ir(4-(1-pyrazoyl)benzoic acid)Cl] (**Ir10**),²⁸ or monoruthenium [Ru(hexamethylbenzene)(phenanthroline)Cl]Cl (**Ru4**)³⁶ were tested as catalysts (2 mol%, Chart 1). The [Cp*Ir(6,6'-dihydroxy-2,2'-bipyridine)(H₂O)](SO₃CF₃)₂ (**Ir3**),³⁷ [Cp*Ir(2,6-dicarboxypyridine)Cl] (**Ir11**)³⁸, and diiridium [Cp*₂Ir₂Cl₂(4,4',6,6'-tetrahydroxybipyrimidine)]Cl₂ (**Ir12**)³⁹ complexes were also found to be poor catalysts (≤ 20% yield). To our surprise, when [Cp*Ir(*N*-phenyl-2-pyridinecarboxamidate)Cl] (**Ir4**)⁴⁰ was used instead, benzyl alcohol was obtained in ~89% yield. Derivatives of **Ir4**, containing either electron-withdrawing (e.g. chloro in **Ir5** and nitro in **Ir6**) or electron-donating groups (e.g. methoxy in **Ir7** and methylthio in **Ir8**) on the phenyl ring of the pyridinecarboxamidate ligand were also highly efficient catalysts (81–91% yield). In comparison, the [Cp*IrCl₂]₂ (**Ir1**) complex and IrCl₃ salt afforded only ~11% and ~0% of benzyl alcohol, respectively. Similar results were obtained when sodium formate was used as the hydride donor instead of NADH (Figure A3.1.B).

Ir4 was shown to be a robust catalyst since it could be recycled at least five times with minimal lost in activity (Figure 3.2). Reaction optimization studies revealed that using greater amounts of the hydride donors NADH or sodium formate led to higher yields in much less time (96% yield after 1 h with 5 equiv. of formate, and 100% yield after 24 h with 5 equiv. of NADH). Reactions using NADH required longer time than those using sodium formate, which suggests that iridium-hydride (Ir-H) formation from the dehydrogenation of NADH by **Ir4** occurs more slowly than with formate (Figures 3.3 and 3.4).

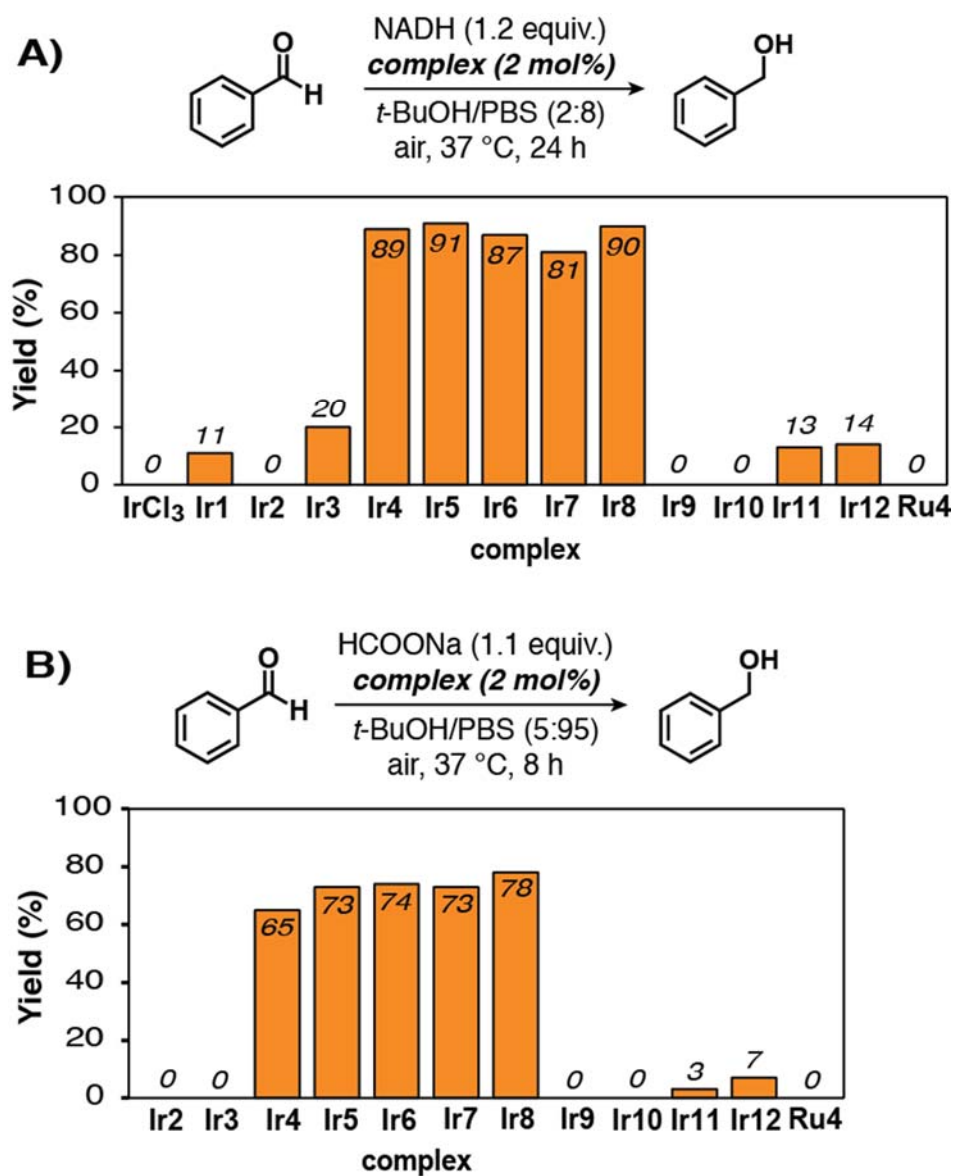


Figure 3.1. Catalytic comparison in hydrogenation of benzaldehyde. Reaction conditions: A) benzaldehyde (0.05 mmol), NADH (0.06 mmol), metal complex or salt (1.0 μmol), *t*-BuOH/PBS (2:8, 3 mL), 37 $^\circ\text{C}$, 24 h. B) benzaldehyde (0.015 mmol), sodium formate (0.017 mmol), metal complex or salt (0.3 μmol), *t*-BuOH/PBS (5:95, 3 mL), 37 $^\circ\text{C}$, 8 h. Yields were determined by GC using biphenyl as internal standard.

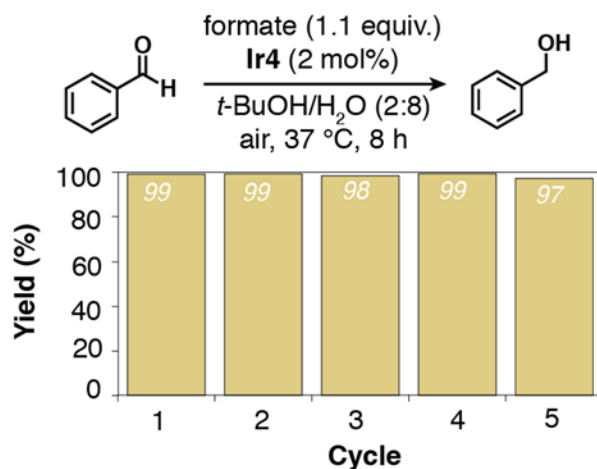


Figure 3.2. Recyclability study of **Ir4** in the hydrogenation of benzaldehyde. Reaction conditions: benzaldehyde (2.0 mmol), sodium formate (2.2 mmol), **Ir4** (0.04 mmol), *t*-BuOH/H₂O (2:8, 100 mL), 37 °C, 8 h. Biphenyl (80 mg, 0.52 mmol) was added as an internal standard for GC analysis. After each reaction cycle, the products were analyzed by GC. The volatiles were then removed by vacuum and more benzaldehyde (2.0 mmol), formate (2.2 mmol), and solvent were added for subsequent rounds of hydrogenation.

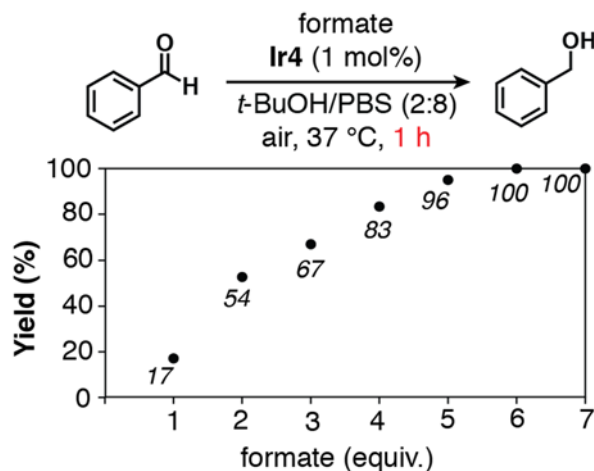


Figure 3.3. Effect of formate equivalence on the hydrogenation efficiency of **Ir4**. Reaction conditions: benzaldehyde (0.03 mmol), sodium formate (0.03–0.21 mmol), **Ir4** (0.30 μmol), *t*-BuOH/PBS (2:8, 3 mL), 37 °C, 1 h.

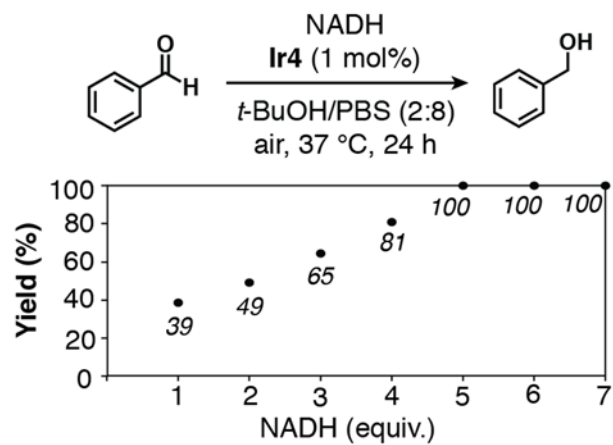


Figure 3.4. Effect of NADH equivalence on the hydrogenation efficiency of **Ir4**. Reaction conditions: benzaldehyde (0.03 mmol), NADH (0.03–0.21 mmol), **Ir4** (0.30 μ mol), *t*-BuOH/PBS (2:8, 3 mL), 37 °C, 24 h.

3.3 Aldehyde Hydrogenation Study under Biological Conditions

To evaluate the tolerance of **Ir4** toward common biomolecules, such as amino acids, nucleobases, carbohydrates, and organic cofactors, the reduction of benzaldehyde by **Ir4**/NADH was investigated in the presence of various additives (Figure 3.5).

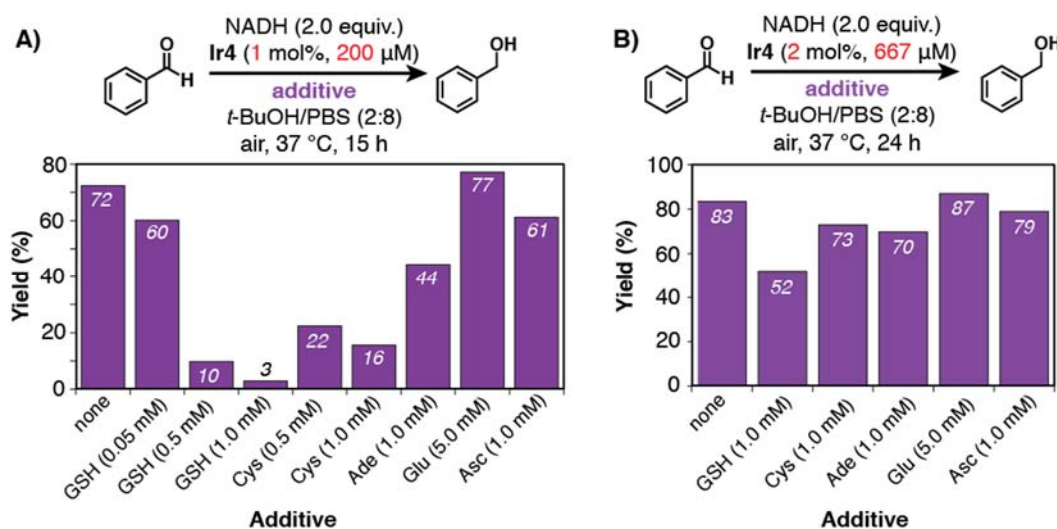


Figure 3.5. Hydrogenation of benzaldehyde by **Ir4**/NADH in the presence of biologically relevant additives. Reaction conditions: A) benzaldehyde (0.06 mmol), NADH (0.12 mmol), **Ir4** (0.6 μmol), t-BuOH/PBS (2:8, 3 mL), 37 °C, 15 h. B) benzaldehyde (0.1 mmol), NADH (0.2 mmol), **Ir4** (2.0 μmol), t-BuOH/PBS (2:8, 3 mL), 37 °C, 24 h. Yields were determined by GC using biphenyl as internal standard. Abbreviations: GSH = glutathione, Cys = cysteine, Ade = adenine, Glu = glucose, Asc = ascorbic acid.

When using 1 mol% of **Ir4** at 200 μM concentration (Figure 3.5.A), good yield of benzyl alcohol was obtained in the presence of glucose (Glu, 5.0 mM, 77% yield) and ascorbic acid (Asc, 1.0 mM, 61%), but modest yields for the nitrogenous base adenine (Ade, 1.0 mM, 44%). The presence of thiol-containing additives has the greatest inhibitory effect on **Ir4**. At 0.05 mM of glutathione (GSH), ~60% of benzyl alcohol was obtained, whereas at 1.0 mM of GSH only ~3% of benzyl alcohol was obtained. The amino acid cysteine (Cys, 1.0 mM) also had a similar effect as GSH on **Ir4**, giving only ~16% of

product. Cystine (the disulfide form of cysteine) does not exhibit any catalyst inhibitory effect whereas *N*-acetyl cysteine showed moderate catalyst inhibition but to a lesser degree compared to cysteine. We found that increasing the iridium catalyst loading to 2 mol% at a concentration of 667 μM (Figure 3.5.B) led to good conversions of benzaldehyde to benzyl alcohol (up to 73%) even in the presence of GSH (1.0 mM) or Cys (1.0 mM). The sensitivity of metal catalysts toward thiols and nucleobases is typically attributed to metal coordination inhibition.^{21, 41} Ward and co-workers have shown that precious metal catalysts can be shielded from the detrimental effects of cellular components by attaching the catalyst to a protein scaffold and/or using thiol neutralizing chemical reagents. Similar strategies could be employed to enable the use of iridium catalysts under high concentrations (> 0.5 mM) of biological nucleophiles.

When **Ir4** was tested in cell culture media, such as RPMI-1640 or M199, we observed decreased catalytic activity compared to that in PBS. Under the same reaction conditions, reduction of benzaldehyde by **Ir4** and NADH gave 42% yield in M199, and 49% yield in RPMI-1640 compared to 91% yield in PBS (Figure 3.6). The decreased catalytic activity may come from the catalyst poisoning effects of sulfur- and nitrogen-containing nucleophiles present in cell growth media. Although the catalytic activity of **Ir4** was reduced in cell culture media compared to in PBS, it is still remarkable in comparison to other

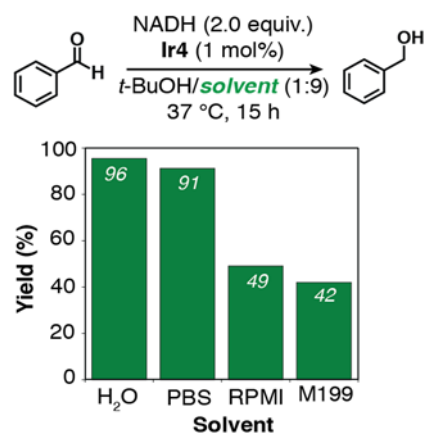


Figure 3.6. Effect of solvent on the hydrogenation of benzaldehyde by **Ir4**/NADH. Reaction conditions: benzaldehyde (0.05 mmol), NADH (0.10 mmol), **Ir4** (0.50 μmol), t-BuOH/solvent (1:9, 3 mL), 37 °C, 15 h.

transition metal catalysts that have been tested in cell culture media or cell lysate (e.g. 14% conversion with a Ru complex¹⁹, 21% conversion with Pd nanoparticles⁴).

In the absence of **Ir4**, the addition of metal salts containing either transition metals (Cr^{2+} , Mn^{2+} , Fe^{2+} , Co^{2+} , Ni^{2+} , Cu^{2+} , Zn^{2+}) or alkali/alkaline earth metals (Na^+ , K^+ , Mg^{2+} , Ca^{2+}) to the reaction mixture did not produce any transfer hydrogenation products (Figure 3.7). Although it has been reported previously that Mg^{2+} could be used to promote hydride transfer from nicotinamide analogues to ketones,⁴² these reactions were conducted in acetonitrile rather than in aqueous media. Our results suggest that transfer hydrogenation between NADH and aldehydes could be carried out selectively by **Ir4** rather than by biological metal ions, which suggest that the iridium complexes could be used for bioorthogonal reactions.

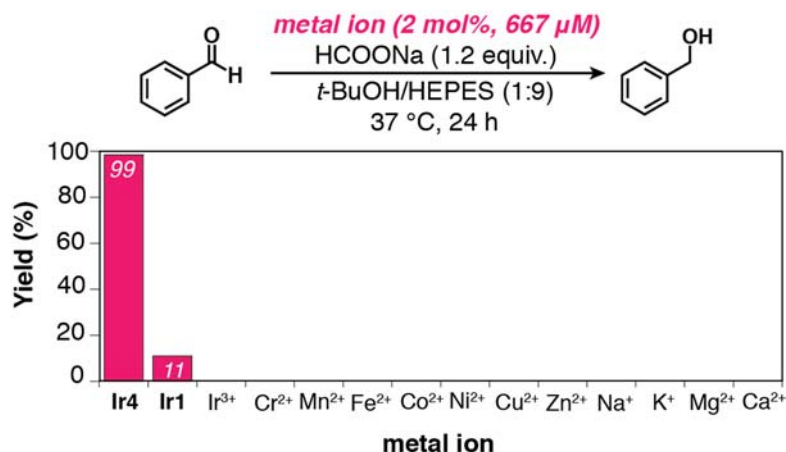
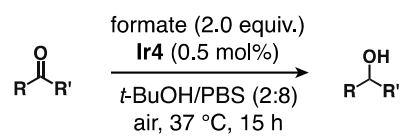
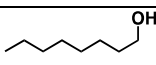
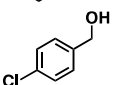
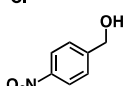
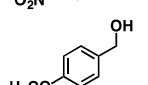
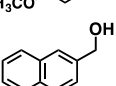
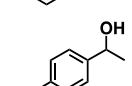
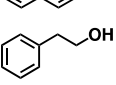
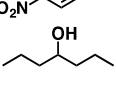
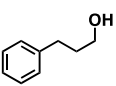


Figure 3.7. Reaction of benzaldehyde/sodium formate in the presence of various metal ions. Reactions catalyzed by the iridium complexes [Cp*Ir(N-phenyl-2-pyridinecarboxamidate)Cl] (**Ir4**) and [Cp*IrCl₂]₂ (**Ir1**) are shown for comparison. Reaction conditions: benzaldehyde (0.10 mmol), sodium formate (0.12 mmol), metal salt (2.0 μmol), t-BuOH/solvent (2:8, 3 mL), 37 °C, 24 h. The reaction with FeCl₂ was performed in the absence of air.

3.4 Substrate Scope Studies

To investigate the substrate scope of catalytic transfer hydrogenation by the Cp*Ir pyridinecarboxamidate complexes, we set up reactions with an aldehyde or ketone (1.0 equiv.), formate (2.0 equiv.), and 0.5 mol% of **Ir4** in *t*-BuOH/PBS (2:8 or 4:6) at 37 °C for 15 h (Table 3.1). Benzaldehyde and its derivatives (entries 1–4) were reduced to their corresponding benzyl alcohols in excellent yields (> 90%). The modest conversion of 2-naphthaldehyde to 2-naphthol (~35% yield, entry 5) has been attributed to its poor solubility in *t*-BuOH/PBS since we observed significant white solid precipitation as the reaction progressed. Aliphatic aldehydes (entries 6–10) were reduced to primary alcohols with moderate to good yields (~54–97%). Ketone-containing compounds are poor substrates. Neither acetophenone (entry 11) nor 4-heptanone (entry 13) was converted to its corresponding alcohol. Only the electron-deficient ketone 4'-nitroacetophenone (entry 12) was reduced but in low yield (~11%). These studies clearly indicate that there is a preference of the iridium-hydride (**Ir-H**) species, generated from **Ir4**/formate, to react with aldehydes over ketones. Similar results were obtained when NADH was used instead of formate as the hydride source (Table 3.2).

Table 3.1. Hydrogenation of Aldehydes and Ketones Using **Ir4**/Formate^a

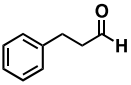
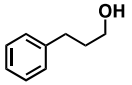
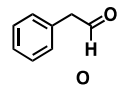
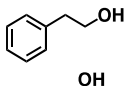
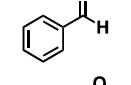
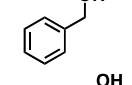
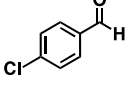
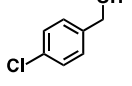
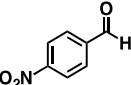
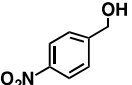
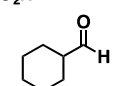
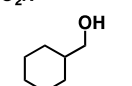
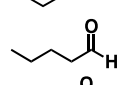
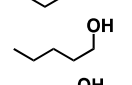
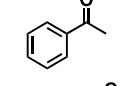
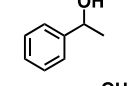
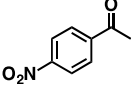
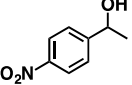
					
Entry	Product	Yield ^b (%)	Entry	Product	Yield ^b (%)
1		93 (87 ^d)	8		54
2 ^c		99 (93 ^d)	9		58
3 ^c		96 (92 ^d)	10		85
4		91 (84 ^d)	11		0
5 ^c		35 (30 ^d)	12 ^c		11
6		97	13		0
7		90			

^aConditions: aldehyde or ketone (0.06 mmol), formate (0.12 mmol), **Ir4** (0.3 μmol), *t*-BuOH/PBS (2:8, 3.0 mL), 37 °C, 15 h. ^bYields were determined by GC analysis relative to an internal standard. Averaged from duplicate runs. See Fig. A.3.1 (Appendix) for the GC analyses. ^cTo improve substrate solubility, solutions containing *t*BuOH/PBS (4:6) were used as solvent. ^dIsolated yield.

Table 3.2. Hydrogenation of Aldehydes and Ketones Using **Ir4**/NADH^a

$$\text{R}-\overset{\text{O}}{\parallel}{\text{C}}-\text{R}' \xrightarrow[\text{air, 37 }^\circ\text{C, 24 h}]{\text{NADH (1.2 equiv.)}, \text{Ir4 (2 mol\%)} } \text{R}-\underset{\text{OH}}{\text{C}}-\text{R}'$$

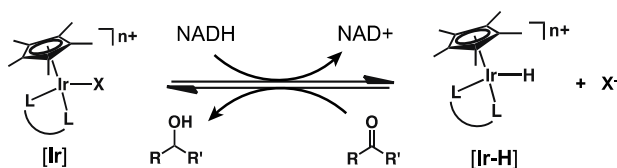
t-BuOH/PBS (2:8)

Entry	Substrate	Product	Yield (%) ^b
1			69
2			65
3			88
4 ^c			96
5 ^c			98
6			37
7			58
8			0
9 ^c			9

^aConditions: aldehyde or ketone (0.05 mmol), NADH (0.06 mmol), **Ir4** (1.0 μmol), *t*-BuOH/PBS (2:8, 3.0 mL), 37 °C, 24 h. ^bYields were determined by GC analysis relative to an internal standard. Averaged from duplicate runs. ^cTo improve substrate solubility, solutions containing *t*-BuOH/PBS (3:7) were used as solvent.

3.5 Mechanistic Studies

Transfer hydrogenation catalysis is believed to occur through a two steps mechanism. First, the metal catalyst reacts with a hydride donor to form a metal-hydride species. The hydride in the M-H intermediate is subsequently delivered to an organic acceptor or is protonated to give H₂.²⁴ To determine whether the differences in reactivity between the various complexes tested in Chart 1 is due to either the formation of iridium-hydride (**Ir-H**) species from NADH or hydride transfer from **Ir-H** to benzaldehyde, we carried out NMR spectroscopic studies (Scheme 1).



Scheme 3.1. Transfer Hydrogenation by Iridium Complexes

Ir2, **Ir4**, and **Ir9** were selected as representative examples of complexes that have neutral *N,N*-, anionic *N,N*-, and anionic *C,N*-bidentate donors respectively for further studies. Each iridium complex (1.0 equiv.) was combined with NADH (2.0 equiv.) in a deoxygenated mixture of *t*-BuOH/D₂O (7:3) or THF/D₂O (7:3) and then sealed inside a J-Young tube. After 15 h at 37 °C, the ¹H NMR spectra of all three samples showed peaks corresponding to the presence of new **Ir-H** species. The hydride signals for [Cp*Ir(2,2'-bipyridine)H]⁺ (**Ir2-H**),⁴³ [Cp*Ir(2-phenylpyridine)H] (**Ir9-H**),⁴⁴ and [Cp*Ir(*N*-phenyl-2-pyridinecarboxamidate)H] (**Ir4-H**) were observed at -11.5 (*t*-BuOH/D₂O), -15.3 (THF/D₂O), and -11.3 ppm (*t*-BuOH/D₂O) in their ¹H NMR spectra (Figure 3.8), respectively. Their assignments were confirmed by comparison to the spectra of authentic samples of the corresponding **Ir-H** complexes.

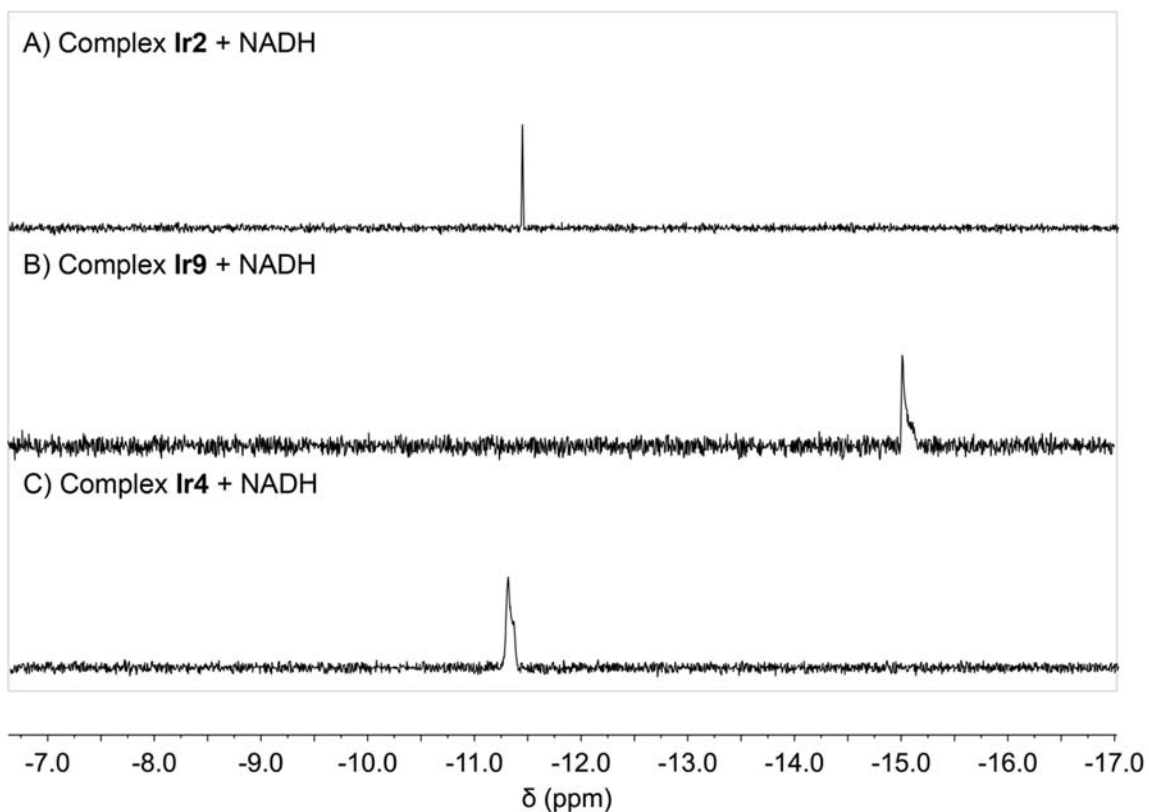


Figure 3.8. ^1H NMR spectra (500 MHz, D_2O) obtained from the reaction of the iridium complexes with NADH (1:2) in $t\text{-BuOH}:\text{D}_2\text{O}$ (3:7) (for **Ir2** and **Ir4**) or $\text{THF}:\text{D}_2\text{O}$ (3:7) (for **Ir9**) at $37\text{ }^\circ\text{C}$ for 15 h. Only the NMR spectral regions where the hydride signals appear are shown. The signals at -11.5, -15.3, and -11.3 ppm match the hydride peaks for independently prepared samples of **Ir2-H**, **Ir9-H**, and **Ir4-H**, respectively.

Since **Ir2**, **Ir4**, and **Ir9** can all generate Ir-H species from NADH, the differences in their reactivity are most likely due to their hydride transfer abilities. To test this possibility, we investigated the reactions between independently prepared iridium-hydride complexes and benzaldehyde. When either **Ir2-H** or **Ir9-H** (1.0 equiv.) was mixed with benzaldehyde (1.0 equiv.) in a deoxygenated solution of CD_3OD and allowed to react for 20 h at $37\text{ }^\circ\text{C}$, no hydride transfer took place as determined by ^1H NMR spectroscopy (Figures A3.5 and A3.6 in Appendix).⁴³ However, when **Ir4-H** was tested under the same reaction conditions, after 15 h, benzaldehyde was converted quantitatively to benzyl

alcohol, as indicated by both NMR spectroscopic (Figures 3.9 and A3.7) and gas chromatographic analyses of the reaction products (Figures A3.2 and A3.3). These results are consistent with the observation above that **Ir4** is a much more efficient hydride transfer catalyst than **Ir2** and **Ir9** (Figure 3.1).

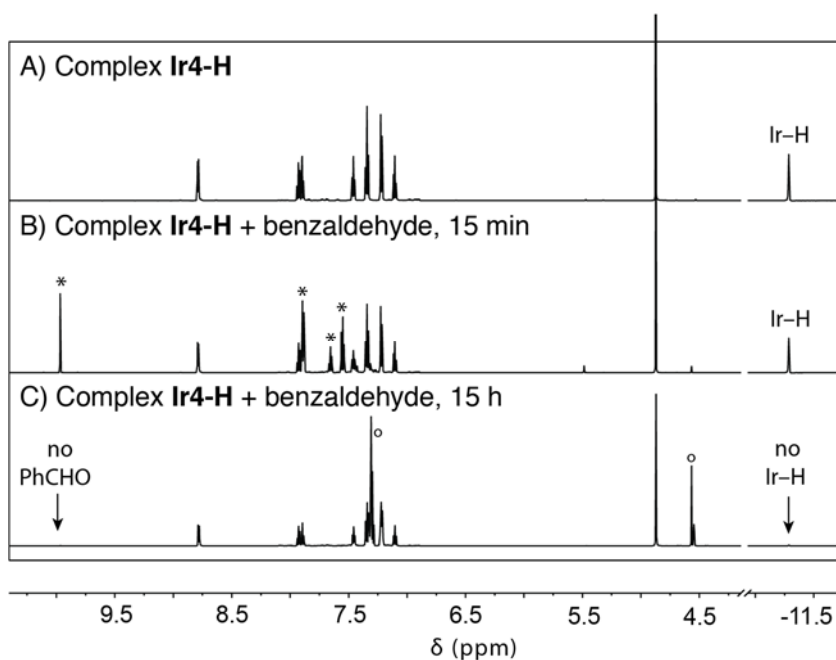


Figure 3.9. ¹H NMR spectra (CD₃OD, 500 MHz) of A) complex **Ir4-H**, B) complex **Ir4-H** + benzaldehyde, 15 min, and C) complex **Ir4-H** + benzaldehyde, 15 h. Peaks corresponding to benzaldehyde (*) and benzyl alcohol (o) are labeled accordingly in the spectra.

3.6 Hydrogenation of Cytotoxic Aldehyde

Catalytic transfer hydrogenation by the Cp*Ir pyridinecarboxamidate complexes might be potentially useful in reducing cytotoxic aldehydes in vivo. Low molecular weight α,β -unsaturated aldehydes produced from lipid peroxidation, such as acrolein⁴⁵ and 4-hydroxynon-2-enal,⁴⁶⁻⁴⁷ have been found to be associated with many metabolic diseases, neurodegenerative disorders, and cancers due to their reactive unsaturated aldehyde

groups. Although enzymes such as glutathione *s*-transferase, aldose reductase, and aldehyde dehydrogenase can metabolize cytotoxic aldehydes endogenously, patients with certain diseases typically exhibit low levels of these enzymes.⁴⁷

Based on our results above, we posit that our iridium complexes can be good candidates as enzyme mimics for aldehyde detoxification. Because the naturally occurring cofactor NADH can be employed as a hydride source, intracellular transfer hydrogenation would not require any external co-additives. To determine the feasibility of such an approach, we evaluated the reaction of 4-hydroxynon-2-enal (**8**, 1 equiv.) with NADH (2.0 equiv.) using **Ir4** (1 mol%) in *t*-BuOH/M199 (5:95) at 37 °C (Figure 3.10). After 15 h, ~94% of **8** was converted to 4-hydroxynon-2-en-1-ol (**9**, 88%) and 4-hydroxynonan-1-ol (**10**, 6%). Increasing the reaction time (> 24 h) led to higher ratios of **10:9**, which suggests that hydrogenation occurs at the aldehyde group prior to hydrogenation of the double bond. Similar results were obtained when *t*-BuOH/RPMI-1640 was used as solvent, while *t*-BuOH/PBS gave higher ratios of **10:9** (23:76). The high efficiency of this reaction in cell growth media suggests that **Ir4** is an excellent candidate for further studies inside live cells, which is the focus of our future work.

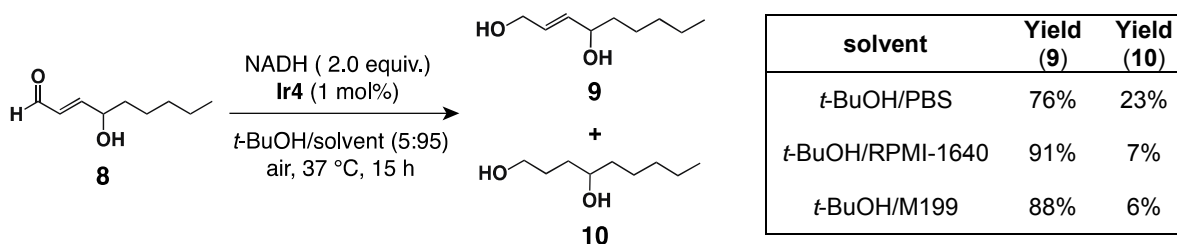


Figure 3.10. Hydrogenation of 4-hydroxynon-2-enal by **Ir4**/NADH. Reaction conditions: 4-hydroxynon-2-enal (0.05 mmol), NADH (0.10 mmol), **Ir4** (0.5 μmol), *t*-BuOH/solvent (5:95, 3.0 mL), 37 °C, 15 h. Yields were determined by GC using an internal standard (Figure A.3.6).

3.7 Conclusion

In summary, our investigations revealed that Cp*Ir pyridinecarboxamidate complexes are capable of mediating catalytic hydride transfer from either NADH or formate to aldehydes in PBS buffer and cell culture media. The iridium catalysts are tolerant of up to moderate concentrations of biological nucleophiles, including thiols such as glutathione and cysteine. Stoichiometric hydride transfer studies showed that iridium hydride species derived from **Ir4** are more efficient hydride donors compared to other structurally similar Cp*Ir complexes. These iridium complexes can be exploited further in intracellular transfer hydrogenation catalysis for applications such as the catalytic detoxification of disease-causing agents.

3.8 Experimental

General. Commercial reagents were used as received without further purification. All air- and water-sensitive manipulations were performed using standard Schlenk techniques or under a nitrogen atmosphere using a glovebox. Anhydrous solvents were obtained from an Innovative Technology solvent drying system saturated with Argon. The iridium complexes [Cp*Ir(2,2'-bipyridine)(H₂O)](SO₃CF₃)₂ (**1a**),³⁴ [Cp*Ir(6,6'-dihydroxy-2,2'-bipyridine)(H₂O)](SO₃CF₃)₂ (**1b**),^{26, 37} [Cp*Ir(2-phenylpyridine)Cl] (**2**),³⁵ [Cp*Ir(4-(1-pyrazoyl)benzoic acid)Cl] (**3**),^{28, 48} [Cp*Ir(2,6-dicarboxypyridine)Cl] (**4**),³⁸ [Cp*Ir(*N*-phenyl-2-pyridinecarboxamidate)Cl] (**5a**),⁴⁰ [Cp*₂Ir₂Cl₂(4,4',6,6'-tetrahydroxybipyrimidine)]Cl₂ (**6**)³⁹ and [Cp*IrCl₂]₂ (**8**)⁴⁹ and ruthenium complex [Ru(hexamethylbenzene)(phenanthroline)Cl]Cl (**7**)³⁶ were prepared according to literature procedures. The iridium-hydride complex [Cp*Ir(2-phenylpyridine)H] (**2-H**) was prepared

as described previously.⁴⁴ The compound 4-hydroxynon-2-enal was synthesized as reported.⁵⁰

Physical Methods. NMR spectra were acquired using JOEL spectrometers (ECA-400, 500, or 600 MHz) and referenced using residual solvent peaks. IR spectra were measured using a Thermo Nicolet Avatar FT-IR spectrometer. High-resolution mass spectra were obtained from the mass spectral facility at the University of Texas at Austin. Gas chromatography-mass spectrometry was performed using an Agilent 7890 GC/5977A MSD instrument equipped with an HP-5MS capillary column.

Synthesis

*Preparation of [Cp*Ir(N-(4-chlorophenyl)-2-pyridinecarboxamide)Cl] (Ir5).* In a Schlenk flask, 20 mL of ethanol was purged with nitrogen for about 15 min. Solid [Cp*IrCl₂]₂ (0.15 mmol, 1.0 equiv.) and *N*-(4-chlorophenyl)-2-pyridinecarboxamide (0.32 mmol, 2.1 equiv.) were added and stirred for 15 min at 80 °C. The reaction mixture was then treated with ammonium hexafluorophosphate (0.68 mmol, 4.5 equiv.) and stirring was continued overnight at 80°C. The ethanol solvent was removed by rotatory evaporation to yield a yellow-orange solid, which was then redissolved in 20 mL of dichloromethane and washed with water (3 x 20 mL). The organic phase was separated, dried over sodium sulfate, filtered, and then evaporated to dryness. The crude product was purified by layering pentane over a solution of the compound in dichloromethane. Yield (116 mg, 65%). ¹H NMR (CDCl₃, 500 MHz): 8.57 (d, *J* = 10 Hz, 1H), 8.14 (d, *J* = 10 Hz, 1H), 7.92 (td, *J* = 10 Hz, 1H), 7.62 (dt, *J* = 10 Hz, 2H), 7.49 (td, *J* = 5 Hz, 1H), 7.26 (dt, *J* = 10 Hz, 2H), 1.40 (s, 15H). ¹³C NMR (CDCl₃, 125 MHz): 168.6, 155.4, 149.7, 146.8, 138.8, 129.4, 128.4,

128.2, 127.6, 126.6, 86.7, 8.6. IR: $\nu = 684, 767, 825, 807, 1010, 1029, 1084, 1291, 1354, 1481, 1566, 1583, 1597, \text{ and } 1622 \text{ cm}^{-1}$. Mp: 284 °C (decomp.). HRMS–ESI(+): Calc for $\text{IrC}_{22}\text{H}_{23}\text{Cl}_2\text{N}_2\text{O}$ $[\text{M}+\text{H}]^+ = 595.0876$, found 595.0870.

*Preparation of [Cp*Ir(N-(4-nitrophenyl)-2-pyridinecarboxamidate)Cl] (Ir6).* The same procedure was used as described for the synthesis of **Ir5** except that the ligand *N*-(4-nitrophenyl)-2-pyridinecarboxamide was used instead of *N*-(4-chlorophenyl)-2-pyridinecarboxamide. Yield: 73%. ^1H NMR (CDCl_3 , 500 MHz): 8.59 (d, $J = 5$ Hz, 1H), 8.18 (dt, $J = 10$ Hz, 2H), 8.14 (dd, $J = 10$ Hz, 1H), 7.96 (td, $J = 10$ Hz, 1H), 7.90 (dt, $J = 5$ Hz, 2H), 7.55 (td, $J = 10$ Hz, 1H), 1.40 (s, 15H). ^{13}C NMR (CDCl_3 , 125 MHz): 168.6, 155.1, 154.7, 150.0, 143.7, 139.1, 128.1, 127.6, 126.8, 124.0, 86.9, 8.7. IR: $\nu = 684, 717, 756, 853, 864, 1105, 1258, 1290, 1358, 1486, 1567, 1598, \text{ and } 1623 \text{ cm}^{-1}$. Mp: 309 °C (decomp.). HRMS–ESI(+): Calc for $\text{IrC}_{22}\text{H}_{23}\text{ClN}_3\text{O}_3$ $[\text{M}+\text{H}]^+ = 606.1122$, found 606.1118.

*Preparation of [Cp*Ir(N-(4-methoxyphenyl)-2-pyridinecarboxamidate)Cl] (Ir7).* The same procedure was used as described for the synthesis of **Ir5** except that the ligand *N*-(4-methoxyphenyl)-2-pyridinecarboxamide was used instead of *N*-(4-chlorophenyl)-2-pyridinecarboxamide. Yield: 67%. ^1H NMR (CDCl_3 , 500 MHz): 8.55 (d, $J = 5$ Hz, 1H), 8.14 (d, $J = 5$ Hz, 1H), 7.90 (td, $J = 10$ Hz, 1H), 7.57 (dt, $J = 10$ Hz, 2H), 7.47 (td, $J = 10$ Hz, 1H), 6.86 (dt, $J = 10$ Hz, 2H), 3.80 (s, 3H), 1.41 (s, 15H). ^{13}C NMR (CDCl_3 , 125 MHz): 168.8, 156.4, 155.9, 149.6, 141.4, 138.6, 127.8, 127.3, 126.5, 113.4, 86.7, 8.6. IR: $\nu = 685, 730, 761, 805, 1030, 1239, 1285, 1373, 1442, 1503, 1564, 1575, 1585, \text{ and } 1618 \text{ cm}^{-1}$. Mp: 249 °C (decomp.). HRMS–ESI(+): Calc for $\text{IrC}_{23}\text{H}_{26}\text{ClN}_2\text{O}_2$ $[\text{M}+\text{H}]^+ = 591.1377$, found 591.1379.

*Preparation of [Cp*Ir(N-(4-methylthiophenyl)-2-pyridinecarboxamidate)Cl] (Ir8).* The same procedure was used as described for the synthesis of **Ir5** except that the ligand *N*-(4-methylthiophenyl)-2-pyridinecarboxamide was used instead of *N*-(4-chlorophenyl)-2-pyridinecarboxamide. Yield: 61%. ¹H NMR (CDCl₃, 500 MHz): 8.56 (d, *J* = 5 Hz, 1H), 8.14 (dd, *J* = 5 Hz, 1H), 7.91 (td, *J* = 5 Hz, 1H), 7.60 (d, *J* = 5 Hz, 2H), 7.48 (td, *J* = 5 Hz, 1H), 7.25 (d, *J* = 5 Hz, 2H), 2.47 (s, 3H), 1.40 (s, 15H). ¹³C NMR (CDCl₃, 125 MHz): 168.6, 155.7, 149.7, 146.0, 138.7, 133.1, 127.6, 127.5, 127.4, 126.6, 86.7, 8.6. IR: 1565, 1578, 1595, and 1620 cm⁻¹. IR: ν = 698, 725, 760, 809, 830, 1029, 1287, 1329, 1372, 1485, 1565, 1578, 1595, 1620 cm⁻¹. Mp: 254 °C (decomp.). HRMS–ESI(+): Calc for IrC₂₃H₂₆ClN₂OS [M+H]⁺ = 607.1147, found 607.1148.

*Preparation of [Cp*Ir(2,2'-bipyridine)H](PF₆) (Ir2-H).* This synthesis was adapted from a literature procedure.⁵¹ Inside the glovebox, complex **Ir2** (80 mg, 0.1 mmol) was dissolved in 3.0 mL of methanol. A 3.0 mL aqueous solution of NaBH₄ (38 mg, 1.0 mmol) was added slowly dropwise. After 2 h, a 0.5 mL saturated aqueous solution of KPF₆ was added to the reaction mixture, which resulted in the instantaneous formation of a yellow precipitate. The solid was isolated by filtration and then washed with water and dried overnight (47 mg, 74%). NMR spectroscopic characterization of the product matches those measured previously for **1a-H**.^{43, 52}

*Preparation of [Cp*Ir(N-phenyl-2-pyridinecarboxamidate)H] (Ir4-H).* Inside the glovebox, complex **Ir4** (112 mg, 0.20 mmol) was dissolved in 5.0 mL of methanol. A 5.0 mL aqueous solution of NaBH₄ (76 mg, 2.0 mmol) was added slowly dropwise. After 8 h, the solution was concentrated under vacuum to about 5.0 mL, which led to the formation

of a large amount of an orange precipitate. The solid was isolated by filtration, washed with water, and then dried overnight (80 mg, 75%). ¹H NMR (CD₃OD, 500 MHz): 8.79 (d, *J* = 5 Hz, 1H), 7.92 (m, 2H), 7.46 (t, *J* = 5 Hz, 1H), 7.35 (t, *J* = 10 Hz, 2H), 7.22 (d, *J* = 5 Hz, 2H), 7.11 (t, *J* = 10 Hz, 1H), 1.54 (s, 15H), -11.28 (s, 1H, Ir-H); ¹³C NMR (CD₃OD, 125 MHz): 169.8, 156.2, 153.3, 150.0, 137.8, 129.4, 128.0, 127.9, 126.8, 125.6, 89.5, 9.5; IR: ν = 1565, 1595, and 1615 cm⁻¹. IR: ν = 684, 704, 807, 956, 1031, 1379, 1447, 1489, 1551, 1568, 1583, 2027 cm⁻¹.

Hydrogenation Studies

General procedure for transfer hydrogenation (GC yield). The appropriate volumes of the following stock solutions were combined in a 20 mL scintillation vial: carbonyl compound (aldehyde or ketone), hydride donor (sodium formate or NADH), and catalyst (or metal salt). The mixture was then diluted with the desired solvent. The reaction vial was tightly sealed with a screw cap and allowed to proceed at 37 °C. After an allotted amount of time, biphenyl (0.7 equiv relative to the aldehyde/ketone) was added and the reaction mixture was further diluted with isopropanol (~4 times the total volume of the reaction solvent). The solution was then filtered through a pipette plug containing celite and the sample was analyzed by GC. This general procedure was used for the screening of catalysts, metal salts, biological additives, solvents, and substrates.

General procedure for transfer hydrogenation (isolated yield). In a 500 mL round bottom flask, complex **Ir4** (20 μ mol) was dissolved in 40 mL of *t*-BuOH, followed by the addition of an aldehyde (4.0 mmol), sodium formate (8.0 mmol), and PBS solution (160 mL). The reaction flask was sealed with a rubber septum and the reaction mixture was stirred at 37°C.

After 15 h, 100 mL of water was added and the reaction product was extracted into dichloromethane. The organic phase was separated, dried over Na₂SO₄, and then evaporated under vacuum. The crude material was purified by silica gel column chromatography. The final product was weighed and analyzed for purity by NMR spectroscopy.

General procedure for hydride formation study. Inside the glovebox, complex **Ir2**, **Ir4**, or **Ir9** (0.01 mmol) was dissolved in 0.7 mL of *t*-BuOH or THF and then mixed with an aqueous solution of NADH (0.02 mmol) in 0.3 mL of D₂O. The reaction mixture was filtered through a pipette filter to remove any undissolved particulates and then transferred to a J Young NMR tube. The NMR tube was sealed with a Teflon screw cap and then taken outside of the glovebox and heated at 37°C. The NMR spectra of the samples were collected after 15 min and 15 h.

General procedure for hydride transfer study. Inside the glovebox, complex **Ir2-H**, **Ir4-H**, or **Ir9-H** (0.01 mmol) was dissolved in 0.6 mL of D₂O or CD₃OD and then combined with 0.1 mL of a 0.1 M solution of benzaldehyde (0.01 mmol, D₂O or CD₃OD). The mixture was further diluted by the addition of 0.3 mL of solvent. The solution was filtered through a pipette plug to remove any undissolved particulates and transferred to a J Young NMR tube. The NMR tube was sealed with a Teflon screw cap and taken outside of the glovebox to heat at 37°C. The NMR spectra of the samples were recorded after 15 h.

3.9 References

1. Völker, T.; Meggers, E., Transition-metal-mediated Uncaging in Living Human Cells - an Emerging Alternative to Photolabile Protecting Groups. *Current Opinion in Chemical Biology* **2015**, *25*, 48-54.
2. Soldevila-Barreda, J. J.; Sadler, P. J., Approaches to the Design of Catalytic Metallodrugs. *Current Opinion in Chemical Biology* **2015**, *25*, 172-183.
3. Vigh, L.; Joó, F.; Cséplő, Á., Modulation of Membrane Fluidity in Living Protoplasts of *Nicotiana Plumbaginifolia* by Catalytic Hydrogenation. *European Journal of Biochemistry* **1985**, *146* (2), 241-244.
4. Vigh, L.; Horváth, I.; Joó, F.; Thompson, J., Guy A., The Hydrogenation of Phospholipid-Bound Unsaturated Fatty Acids by a Homogeneous, Water-Soluble, Palladium Catalyst. *Biochimica et Biophysica Acta* **1987**, *921*, 167-174.
5. Joó, F.; Balogh, N.; Horváth, L.; Filep, G.; Horváth, I.; Vigh, L., Complex Hydrogenation/Oxidation Reactions of the Water-soluble Hydrogenation Catalyst Palladium Di (Sodium Alizarinmonosulfonate) and Details of Homogeneous Hydrogenation of Lipids in Isolated Biomembranes and Living Cells. *Analytical Biochemistry* **1991**, *194* (1), 34-40.
6. Sirasani, G.; Tong, L.; Balskus, E. P., A Biocompatible Alkene Hydrogenation Merges Organic Synthesis with Microbial Metabolism. *Angewandte Chemie International Edition* **2014**, *53* (30), 7785-7788.
7. Jiang, H.; Zheng, T.; Lopez-Aguilar, A.; Feng, L.; Kopp, F.; Marlow, F. L.; Wu, P., Monitoring Dynamic Glycosylation in Vivo Using Supersensitive Click Chemistry. *Bioconjugate Chemistry* **2014**, *25* (4), 698-706.
8. Li, S.; Wang, L.; Yu, F.; Zhu, Z.; Shobaki, D.; Chen, H.; Wang, M.; Wang, J.; Qin, G.; Erasquin, U. J.; Ren, L.; Wang, Y.; Cai, C., Copper-Catalyzed Click Reaction on/in Live Cells. *Chemical Science* **2017**, *8* (3), 2107-2114.
9. Streu, C.; Meggers, E., Ruthenium-Induced Allylcarbamate Cleavage in Living Cells. *Angewandte Chemie International Edition* **2006**, *45* (34), 5645-5648.
10. Sasmal, P. K.; Carregal-Romero, S.; Parak, W. J.; Meggers, E., Light-Triggered Ruthenium-Catalyzed Allylcarbamate Cleavage in Biological Environments. *Organometallics* **2012**, *31* (16), 5968-5970.
11. Lee, Y.; Umeano, A.; Balskus, E. P., Rescuing Auxotrophic Microorganisms with Nonenzymatic Chemistry. *Angewandte Chemie International Edition* **2013**, *52* (45), 11800-11803.
12. Völker, T.; Dempwolff, F.; Graumann, P. L.; Meggers, E., Progress towards Bioorthogonal Catalysis with Organometallic Compounds. *Angewandte Chemie International Edition* **2014**, *53* (39), 10536-10540.

13. Sanchez, M. I.; Penas, C.; Vazquez, M. E.; Mascarenas, J. L., Metal-catalyzed Uncaging of DNA-binding Agents in Living Cells. *Chemical Science* **2014**, *5* (5), 1901-1907.
14. Li, J.; Yu, J.; Zhao, J.; Wang, J.; Zheng, S.; Lin, S.; Chen, L.; Yang, M.; Jia, S.; Zhang, X.; Chen, P. R., Palladium-triggered Deprotection Chemistry for Protein Activation in Living Cells. *Nature Chemistry* **2014**, *6* (4), 352-361.
15. Weiss, J. T.; Dawson, J. C.; Macleod, K. G.; Rybski, W.; Fraser, C.; Torres-Sánchez, C.; Patton, E. E.; Bradley, M.; Carragher, N. O.; Unciti-Broceta, A., Extracellular Palladium-catalysed Dealkylation of 5-fluoro-1-propargyl-uracil as a Bioorthogonally Activated Prodrug Approach. *Nature Communication* **2014**, *5*, 3277.
16. Hsu, H.-T.; Trantow, B. M.; Waymouth, R. M.; Wender, P. A., Bioorthogonal Catalysis: A General Method To Evaluate Metal-Catalyzed Reactions in Real Time in Living Systems Using a Cellular Luciferase Reporter System. *Bioconjugate Chemistry* **2015**, *27* (2), 376-382.
17. Yusop, R. M.; Unciti-Broceta, A.; Johansson, E. M. V.; Sánchez-Martín, R. M.; Bradley, M., Palladium-mediated Intracellular Chemistry. *Nature Chemistry* **2011**, *3* (3), 239-243.
18. Li, N.; Lim, R. K. V.; Edwardraja, S.; Lin, Q., Copper-Free Sonogashira Cross-Coupling for Functionalization of Alkyne-Encoded Proteins in Aqueous Medium and in Bacterial Cells. *Journal of the American Chemical Society* **2011**, *133* (39), 15316-15319.
19. Spicer, C. D.; Triemer, T.; Davis, B. G., Palladium-Mediated Cell-Surface Labeling. *Journal of the American Chemical Society* **2012**, *134* (2), 800-803.
20. Li, J.; Lin, S.; Wang, J.; Jia, S.; Yang, M.; Hao, Z.; Zhang, X.; Chen, P. R., Ligand-Free Palladium-Mediated Site-Specific Protein Labeling Inside Gram-Negative Bacterial Pathogens. *Journal of the American Chemical Society* **2013**, *135* (19), 7330-7338.
21. Liu, Z.; Romero-Canelón, I.; Qamar, B.; Hearn, J. M.; Habtemariam, A.; Barry, N. P. E.; Pizarro, A. M.; Clarkson, G. J.; Sadler, P. J., The Potent Oxidant Anticancer Activity of Organoiridium Catalysts. *Angewandte Chemie International Edition* **2014**, *53* (15), 3941-3946.
22. Liu, Z.; Sadler, P. J., Organoiridium Complexes: Anticancer Agents and Catalysts. *Accounts of Chemical Research* **2014**, *47* (4), 1174-1185.
23. Soldevila-Barreda, J. J.; Romero-Canelón, I.; Habtemariam, A.; Sadler, P. J., Transfer Hydrogenation Catalysis in Cells as a New Approach to Anticancer Drug Design. *Nature Communication* **2015**, *6*, 6582.
24. Wang, D.; Astruc, D., The Golden Age of Transfer Hydrogenation. *Chemical Reviews* **2015**, *115* (13), 6621-6686.

25. Letko, C. S.; Heiden, Z. M.; Rauchfuss, T. B., Activation and Deactivation of Cp*Ir(TsDPEN) Hydrogenation Catalysts in Water. *European Journal of Inorganic Chemistry* **2009**, (33), 4927-4930.
26. Kawahara, R.; Fujita, K.-i.; Yamaguchi, R., Dehydrogenative Oxidation of Alcohols in Aqueous Media Using Water-Soluble and Reusable Cp*Ir Catalysts Bearing a Functional Bipyridine Ligand. *Journal of the American Chemical Society* **2012**, *134* (8), 3643-3646.
27. Maenaka, Y.; Suenobu, T.; Fukuzumi, S., Efficient Catalytic Interconversion between NADH and NAD⁺ Accompanied by Generation and Consumption of Hydrogen with a Water-Soluble Iridium Complex at Ambient Pressure and Temperature. *Journal of the American Chemical Society* **2012**, *134* (1), 367-374.
28. Maenaka, Y.; Suenobu, T.; Fukuzumi, S., Hydrogen Evolution from Aliphatic Alcohols and 1,4-Selective Hydrogenation of NAD⁺ Catalyzed by a [C,N] and a [C,C] Cyclometalated Organoiridium Complex at Room Temperature in Water. *Journal of the American Chemical Society* **2012**, *134* (22), 9417-9427.
29. Liu, Z.; Deeth, R. J.; Butler, J. S.; Habtemariam, A.; Newton, M. E.; Sadler, P. J., Reduction of Quinones by NADH Catalyzed by Organoiridium Complexes. *Angewandte Chemie International Edition* **2013**, *52* (15), 4194-4197.
30. Fujita, K.-i.; Ito, W.; Yamaguchi, R., Dehydrogenative Lactonization of Diols in Aqueous Media Catalyzed by a Water-Soluble Iridium Complex Bearing a Functional Bipyridine Ligand. *ChemCatChem* **2014**, *6* (1), 109-112.
31. Betanzos-Lara, S.; Liu, Z.; Habtemariam, A.; Pizarro, A. M.; Qamar, B.; Sadler, P. J., Organometallic Ruthenium and Iridium Transfer-Hydrogenation Catalysts Using Coenzyme NADH as a Cofactor. *Angewandte Chemie International Edition* **2012**, *51* (16), 3897-3900.
32. Ngo, A. H.; Ibañez, M.; Do, L. H., Catalytic Hydrogenation of Cytotoxic Aldehydes Using Nicotinamide Adenine Dinucleotide (NADH) in Cell Growth Media. *ACS Catalysis* **2016**, *6* (4), 2637-2641.
33. Wu, X.; Liu, J.; Li, X.; Zanotti-Gerosa, A.; Hancock, F.; Vinci, D.; Ruan, J.; Xiao, J., On Water and in Air: Fast and Highly Chemoselective Transfer Hydrogenation of Aldehydes with Iridium Catalysts. *Angewandte Chemie International Edition* **2006**, *45* (40), 6718-6722.
34. Youinou, M.-T.; Ziesel, R., Synthesis and Molecular Structure of a New Family of Iridium(III) and Rhodium(III) Complexes: $[(\eta^5\text{-Me}_5\text{C}_5)\text{Ir}(\text{LL})\text{X}]^+$ and $[(\eta^5\text{-Me}_5\text{C}_5)\text{Rh}(\text{LL})\text{Cl}]^+$; LL = 2,2'-bipyridine or 1,10-phenanthroline; X = Cl or H. Single Crystal Structures of $[(\eta^5\text{-Me}_5\text{C}_5)\text{Ir}(\text{bpy})\text{Cl}]\text{Cl}$ and $[(\eta^5\text{-Me}_5\text{C}_5)\text{Rh}(\text{phen})\text{Cl}]\text{ClO}_4$. *Journal of Organometallic Chemistry* **1989**, *363* (1-2), 197-208.
35. Li, L.; Brennessel, W. W.; Jones, W. D., An Efficient Low-Temperature Route to Polycyclic Isoquinoline Salt Synthesis via C-H Activation with $[\text{Cp}^*\text{MCl}_2]_2$ (M = Rh, Ir). *Journal of the American Chemical Society* **2008**, *130* (37), 12414-12419.

36. Canivet, J.; Karmazin-Brelot, L.; Süß-Fink, G., Cationic Arene Ruthenium Complexes Containing Chelating 1,10-phenanthroline Ligands. *Journal of Organometallic Chemistry* **2005**, *690* (13), 3202-3211.
37. DePasquale, J.; Nieto, I.; Reuther, L. E.; Herbst-Gervasoni, C. J.; Paul, J. J.; Mochalin, V.; Zeller, M.; Thomas, C. M.; Addison, A. W.; Papish, E. T., Iridium Dihydroxybipyridine Complexes Show That Ligand Deprotonation Dramatically Speeds Rates of Catalytic Water Oxidation. *Inorganic Chemistry* **2013**, *52* (16), 9175-9183.
38. Bucci, A.; Savini, A.; Rocchigiani, L.; Zuccaccia, C.; Rizzato, S.; Albinati, A.; Llobet, A.; Macchioni, A., Organometallic Iridium Catalysts Based on Pyridinecarboxylate Ligands for the Oxidative Splitting of Water. *Organometallics* **2012**, *31* (23), 8071-8074.
39. Hull, J. F.; Himeda, Y.; Wang, W.-H.; Hashiguchi, B.; Periana, R.; Szalda, D. J.; Muckerman, J. T.; Fujita, E., Reversible Hydrogen Storage Using CO₂ and a Proton-Switchable Iridium Catalyst in Aqueous Media under Mild Temperatures and Pressures. *Nature Chemistry* **2012**, *4* (5), 383-388.
40. Almodares, Z.; Lucas, S. J.; Crossley, B. D.; Basri, A. M.; Pask, C. M.; Hebden, A. J.; Phillips, R. M.; McGowan, P. C., Rhodium, Iridium, and Ruthenium Half-Sandwich Picolinamide Complexes as Anticancer Agents. *Inorganic Chemistry* **2014**, *53* (2), 727-736.
41. Wilson, Y. M.; Dürrenberger, M.; Nogueira, E. S.; Ward, T. R., Neutralizing the Detrimental Effect of Glutathione on Precious Metal Catalysts. *Journal of the American Chemical Society* **2014**, *136* (25), 8928-8932.
42. Zehani, S.; Lin, J.; Gelbard, G., Reductions with NADH Models ii: Asymmetric Induction with Sugar Substituted Hantzsch Esters or with Chiral Lewis Acids. *Tetrahedron* **1989**, *45* (3), 733-740.
43. Abura, T.; Ogo, S.; Watanabe, Y.; Fukuzumi, S., Isolation and Crystal Structure of a Water-Soluble Iridium Hydride: A Robust and Highly Active Catalyst for Acid-Catalyzed Transfer Hydrogenations of Carbonyl Compounds in Acidic Media. *Journal of the American Chemical Society* **2003**, *125* (14), 4149-4154.
44. Hu, Y.; Li, L.; Shaw, A. P.; Norton, J. R.; Sattler, W.; Rong, Y., Synthesis, Electrochemistry, and Reactivity of New Iridium(III) and Rhodium(III) Hydrides. *Organometallics* **2012**, *31* (14), 5058-5064.
45. Dang Thanh, N.; Madeleine, A.; Ven, M.; Charles, R., Potential Role of Acrolein in Neurodegeneration and in Alzheimers Disease. *Current Molecular Pharmacology* **2010**, *3* (2), 66-78.
46. Bradley, M. A.; Xiong-Fister, S.; Markesbery, W. R.; Lovell, M. A., Elevated 4-Hydroxyhexenal in Alzheimer's Disease (AD) Progression. *Neurobiology of Aging* **2012**, *33* (6), 1034-1044.

47. Dalleau, S.; Baradat, M.; Gueraud, F.; Huc, L., Cell Death and Diseases Related to Oxidative Stress: 4-Hydroxynonenal (HNE) in the Balance. *Cell Death Differentiation* **2013**, *20* (12), 1615-1630.
48. Maenaka, Y.; Suenobu, T.; Fukuzumi, S., Catalytic Interconversion between Hydrogen and Formic Acid at Ambient Temperature and Pressure. *Energy and Environmental Science* **2012**, *5* (6), 7360-7367.
49. Kang, J. W.; Moseley, K.; Maitlis, P. M., Pentamethylcyclopentadienylrhodium and -iridium Halides. I. Synthesis and properties. *Journal of the American Chemical Society* **1969**, *91* (22), 5970-5977.
50. Gardner, H. W.; Bartelt, R. J.; Weisleder, D., A Facile Synthesis of 4-hydroxy-2(E)-nonenal. *Lipids* **1992**, *27* (9), 686-689.
51. Konno, H.; Kobayashi, A.; Sakamoto, K.; Fagalde, F.; Katz, N. E.; Saitoh, H.; Ishitani, O., Synthesis and Properties of $[\text{Ru}(\text{tpy})(4,4'\text{-X}_2\text{bpy})\text{H}]^+$ (tpy=2,2':6',2''-terpyridine, bpy=2,2'-bipyridine, X=H and MeO), and their reactions with CO₂. *Inorganica Chimica Acta* **2000**, *299* (2), 155-163.
52. Barrett, S. M.; Pitman, C. L.; Walden, A. G.; Miller, A. J. M., Photoswitchable Hydride Transfer from Iridium to 1-Methylnicotinamide Rationalized by Thermochemical Cycles. *Journal of the American Chemical Society* **2014**, *136* (42), 14718-14721.

Chapter 3 Appendix

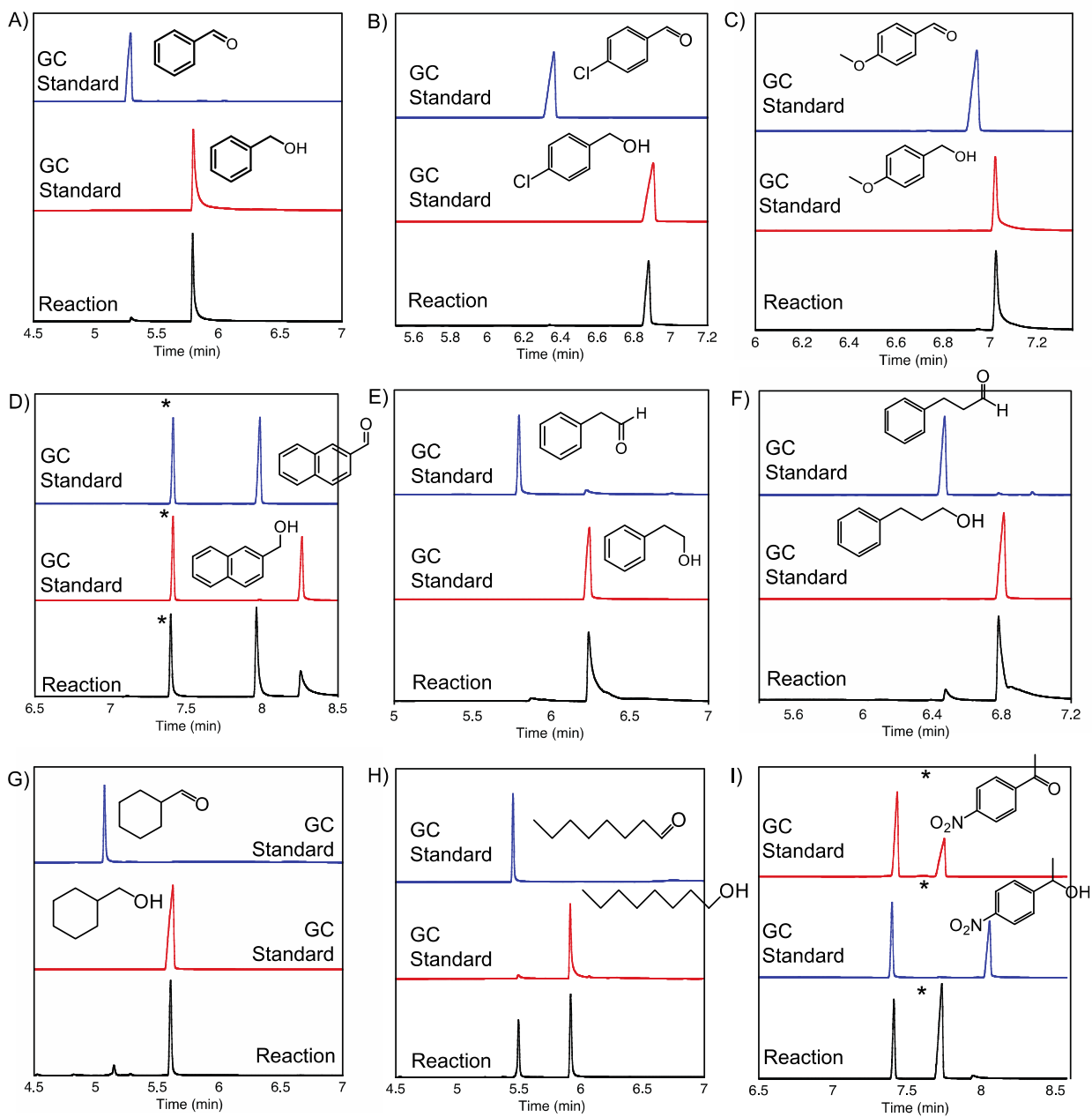


Figure A3.1. Representative GC plots from the hydride transfer studies. See Table 1 for the reaction yields. The peaks at ~7.4 min that are marked with an asterisk (*) come from the internal standard biphenyl.

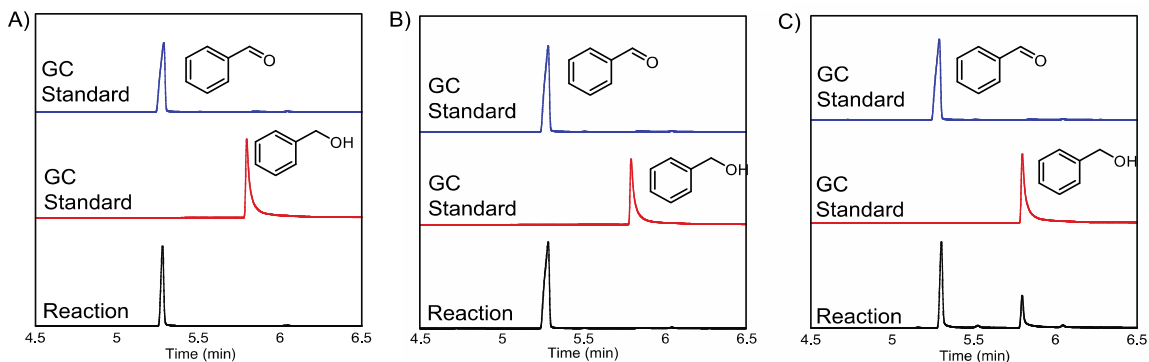


Figure A3.2. GC traces from the reaction of iridium-hydride complexes with benzaldehyde in D_2O . The plots show the GC analysis from the reaction of benzaldehyde and A) **Ir2-H**, B), **Ir9-H**, and C) **Ir4-H**.

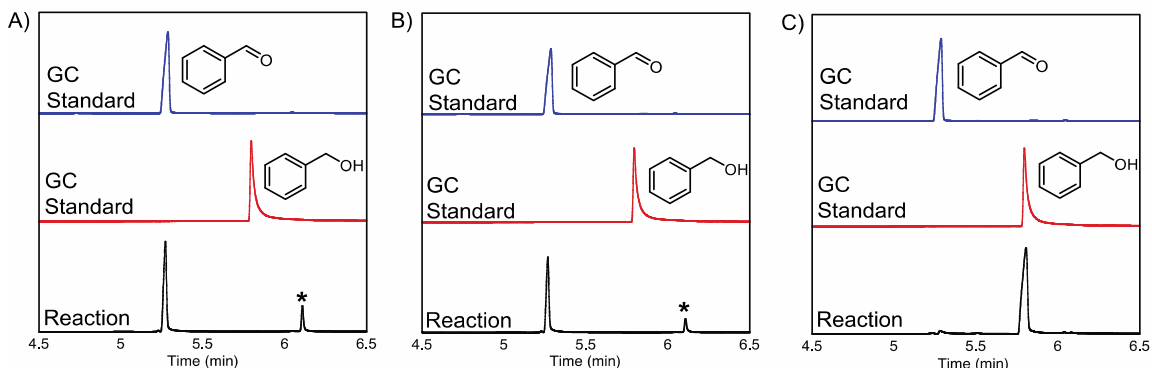


Figure A3.3. GC traces from the reaction of iridium-hydride complexes with benzaldehyde in CD_3OD . The plots show the GC analysis from the reaction of benzaldehyde and A) **Ir2-H**, B), **Ir9-H**, and C) **Ir4-H**. The peaks at ~6.1 min marked with as asterisk (*) arise from an unidentified compound in the product mixture, possibly benzaldehyde methyl hydroxy hemiacetal.

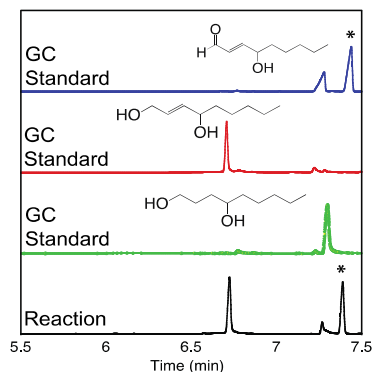


Figure A3.4. GC plot from the reaction of 4-hydroxynon-2-enal (0.06 mmol), NADH (0.12 mmol), and **Ir4** (0.6 μ mol) in t -BuOH/M199 (5:95, 3.0 mL) at 37 $^{\circ}C$ for 15 h. The peaks marked with an asterisk (*) are biphenyl, the GC internal standard.

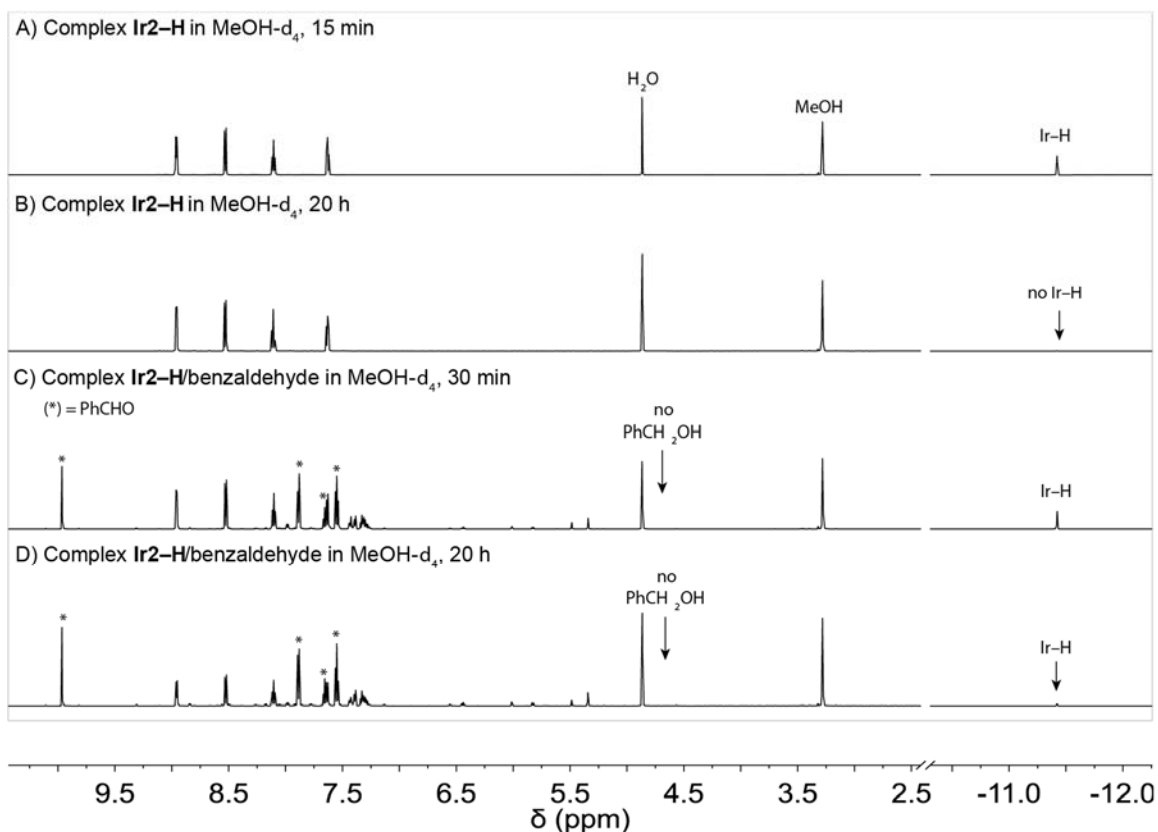


Figure A3.5. ^1H NMR spectra (CD_3OD , 600 MHz) of the iridium-hydride complex $[\text{Cp}^*\text{Ir}(2,2'\text{-bipyridine})\text{H}]$ (**Ir2-H**, $10\ \mu\text{M}$) in the absence (A = 15 min and B = 20 h) and presence (C = 30 min and D = 20 h) of benzaldehyde ($10\ \mu\text{M}$). No hydride transfer from **Ir2-H** to benzaldehyde to yield benzyl alcohol was observed at $37\ ^\circ\text{C}$ after 20 h. The absence of benzyl alcohol was confirmed by GC analysis (see Figure A3.3.A). Complex **Ir2-H** appears to decompose completely after 20 h whether benzaldehyde was present or not. Peaks corresponding to benzaldehyde are marked with (*). In Part B, the disappearance of the Ir-H signal at $-11.5\ \text{ppm}$ in the ^1H NMR spectrum may be due to H/D exchange with the CD_3OD solvent to yield Ir-D species; however, we were unable to detect any signals corresponding to Ir-D in its ^2H NMR spectrum.

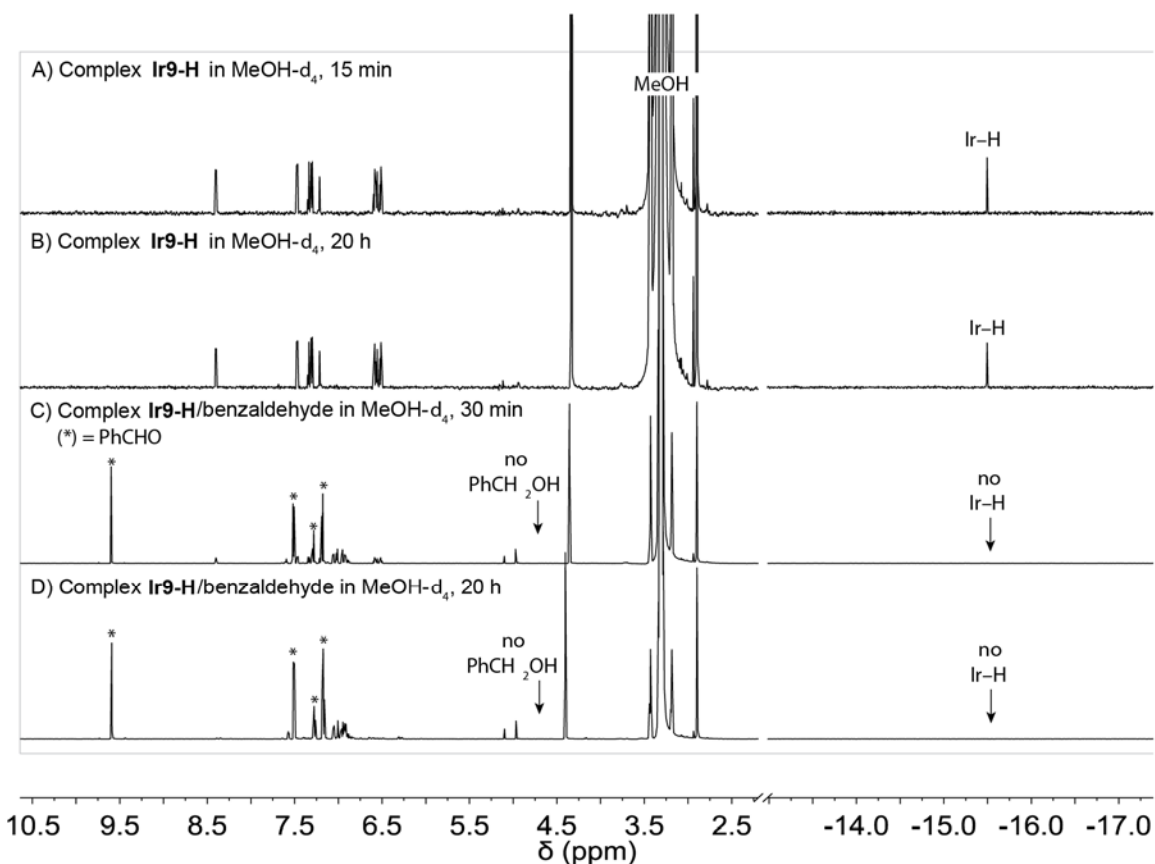


Figure A3.6. ^1H NMR spectra (CD_3OD , 600 MHz) of the iridium-hydride complex $[\text{Cp}^*\text{Ir}(\text{2-phenylpyridine})\text{H}]$ (**Ir9-H**, 10 μM) in the absence (A = 15 min and B = 20 h) and presence (C = 30 min and D = 20 h) of benzaldehyde (10 μM). No hydride transfer from **Ir9-H** to benzaldehyde to yield benzyl alcohol was observed at 37 $^\circ\text{C}$ after 20 h. The absence of benzyl alcohol was confirmed by GC analysis (see Figure A3.3.B). The **Ir9-H** complex appears to be stable over a period of 20 h in the absence of benzaldehyde (compare the NMR spectrum in A vs. in B) but decomposes when benzaldehyde is present (compare the NMR spectrum in A vs. in C/D). Peaks corresponding to benzaldehyde are marked with (*).

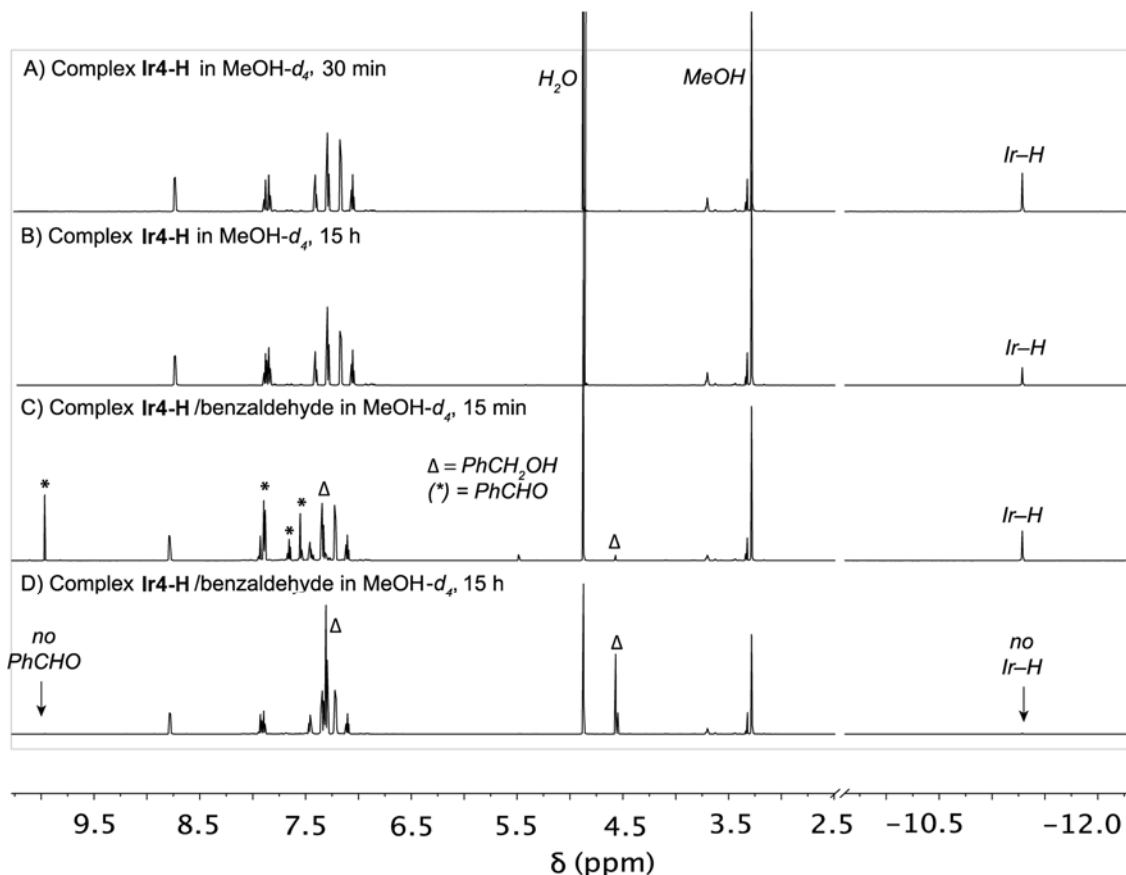


Figure A.3.7. ^1H NMR spectra (CD_3OD , 600 MHz) of the iridium-hydride complex $[\text{Cp}^*\text{Ir}(\text{N-phenyl-2-pyridinecarboxamidate})\text{H}]$ (**Ir4-H**, 10 μM) in the absence (A = 15 min and B = 15 h) and presence (C = 15 min and D = 15 h) of benzaldehyde (10 μM). After 15 h at 37 $^\circ\text{C}$ (part D), transfer hydrogenation is complete as indicated by the disappearance of signals corresponding to benzaldehyde and **Ir4-H** and the appearance of signals for benzyl alcohol. The quantitative formation of benzyl alcohol was confirmed by GC analysis (see Figure A3.3.C). Peaks corresponding to benzaldehyde are marked with (*), whereas those corresponding to benzyl alcohol are marked with (Δ).

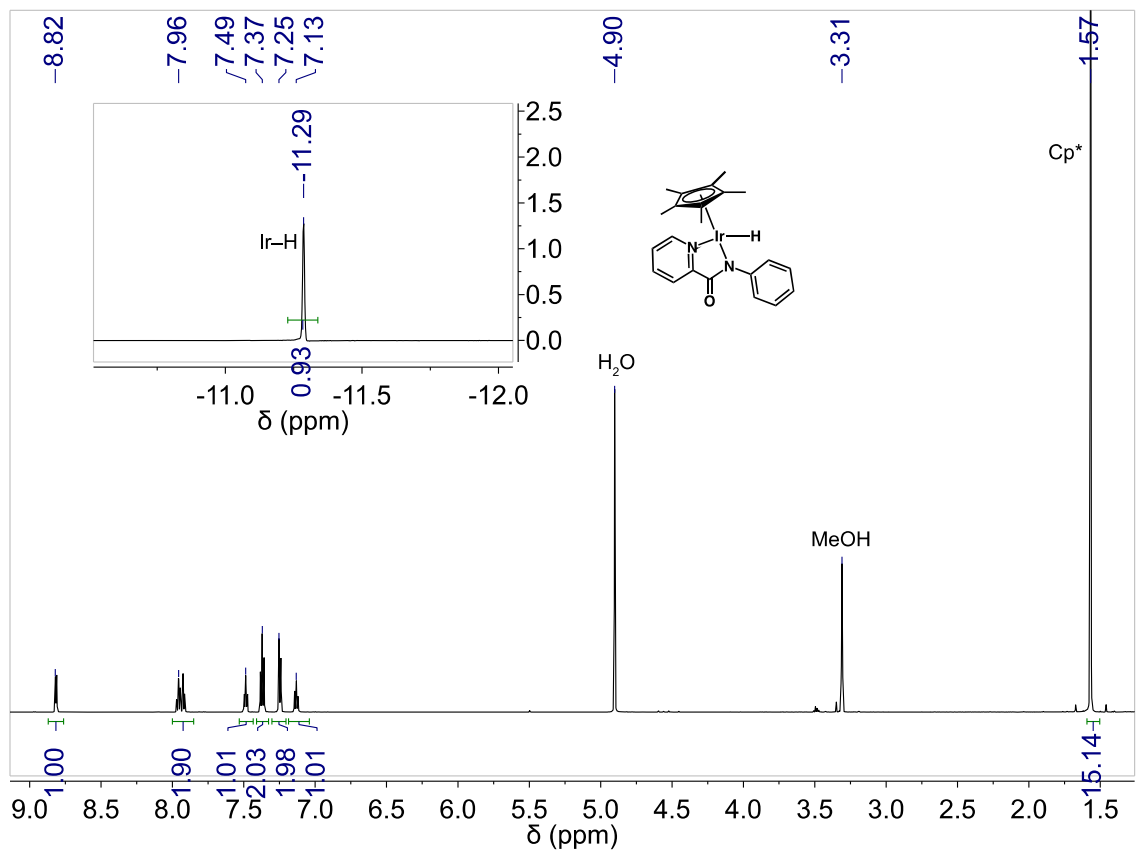


Figure A3.8. ^1H NMR spectrum (CD_3OD , 500 MHz) of complex **Ir4-H**.

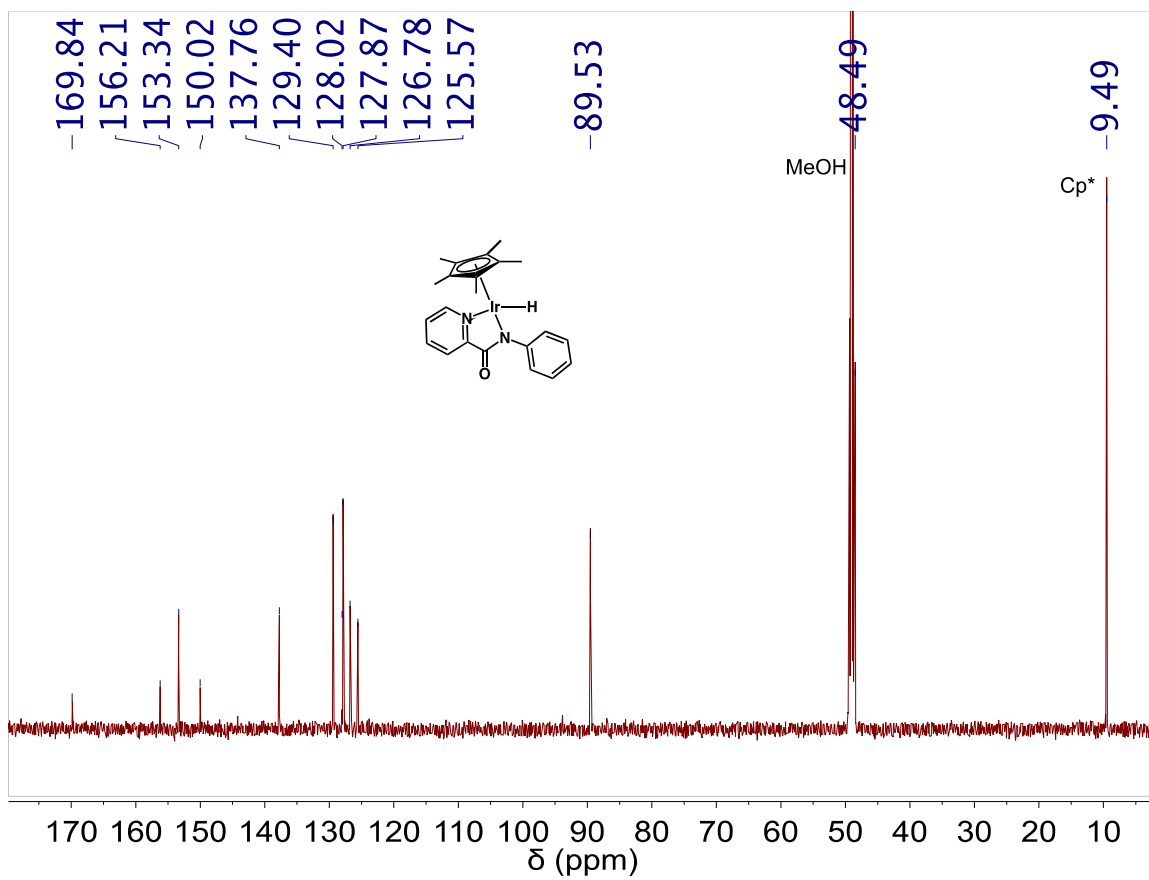


Figure A3.9. ^{13}C NMR spectrum (CD_3OD , 125 MHz) of complex **Ir4-H**.

Chapter 4.

Optimization of Iridium Transfer Hydrogenation Catalysts

Guided by Structure-Activity Relationship Studies

4.1 Introduction

Transfer hydrogenation catalysis¹ is an important process in chemical synthesis,²⁻¹¹ energy conversion,¹²⁻¹⁴ and hydrogen storage.¹⁵ It has recently been shown to have potential therapeutic applications, such as anticancer drug design,¹⁶⁻¹⁹ protein modification,²⁰⁻²¹ genetic engineering,²² and aldehyde detoxification.²³ Our group and others have demonstrated intracellular transfer hydrogenation reactions using small-molecule intracellular metal catalyst (SIMCats),²⁴ which utilize nicotinamide adenine dinucleotide (NADH) inside cells as the hydride source.²⁵⁻²⁸ To develop more advanced SIMCats, such as adding targeting groups or changing lipophilicity and cytotoxicity, it would be useful to know which catalyst components could be modified without affecting their catalytic activity.

In this chapter, we describe the structure-activity relationship (SAR) studies of pentamethylcyclopentadienyl iridium(III) (Cp*Ir) complexes bearing 2-pyridinecarboxamidate ligands in aqueous transfer hydrogenation. These studies will allow us to explain the reactivity diversity between structurally different complexes and to design more robust transfer hydrogenation catalysts in future work.

4.2 Structural Modifications and Catalyst Activity Comparison

Our previous work showed that $[\text{Cp}^*\text{Ir}(\text{N-phenyl-2-pyridinecarboxamidate})\text{Cl}]$ (**Ir4**) was a more active catalyst than other structurally similar Ir and Ru complexes in transfer hydrogenation.²³ To perform our structure-activity relationship (SAR) studies, we prepared a series of Ir derivatives and related Ru, and Rh complexes (Chart 4.1).

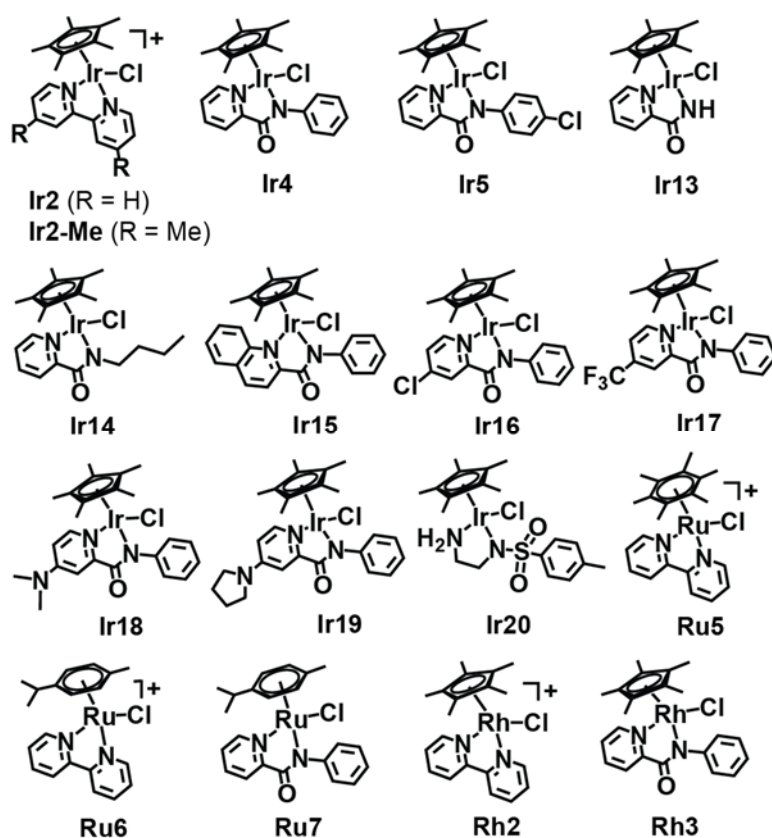


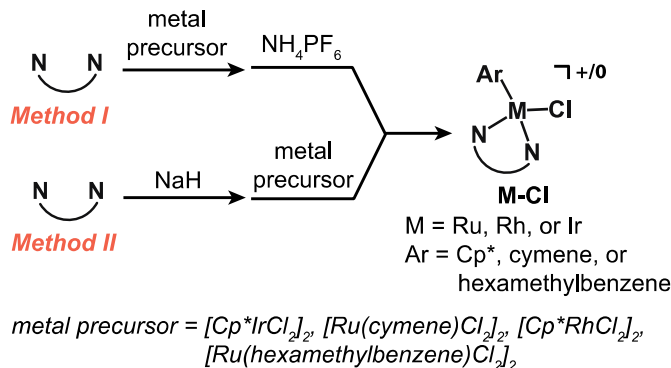
Chart 4.1. Ir, Ru, and Rh complexes tested in this study.

The metal chloride complexes were synthesized from a bidentate ligand and the corresponding metal precursor ($[\text{Cp}^*\text{IrCl}_2]_2$), $[\text{Ru}(\text{cymene})\text{Cl}_2]_2$, $[\text{Ru}(\text{C}_6\text{Me}_6)\text{Cl}_2]_2$, or $[\text{Cp}^*\text{RhCl}_2]_2$), either by A) refluxing in ethanol with the presence of ammonium

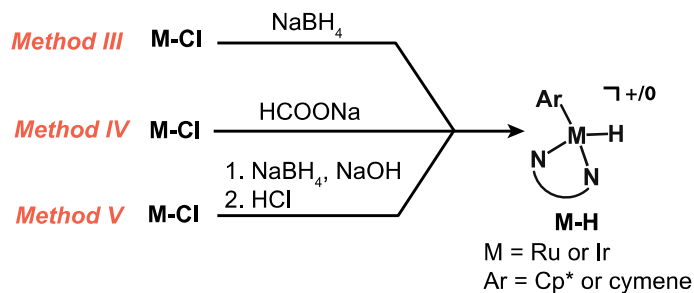
hexafluorophosphate; B) treatment with sodium hydride in anhydrous tetrahydrofuran (THF) at room temperature. The pure complexes were obtained in 70-90% yields after purification (Scheme 4.1A).

The metal hydride complexes were synthesized (70-90% yields) by treating the metal chlorides with sodium formate or sodium boron hydride. Alternatively, the metal chloride should be reduced using sodium boron hydride under basic condition and then protonated to the hydride complexes by a solution of HCl in Et₂O (Scheme 4.1B).

A) Synthesis of Half-Sandwich Metal Complexes



B) Synthesis of Half-Sandwich Metal-Hydride Complexes



Scheme 4.1. Synthesis of Ir, Ru, and Rh complexes.

Next, we evaluated the transfer hydrogenation activity of these Ir/Ru/Rh complexes in the conversion of benzaldehyde to benzyl alcohol. As shown in Figure 4.1, the reaction of benzaldehyde (1.0 equiv.) and sodium formate (3.0 equiv.) in *tert*-butanol and phosphate buffered saline (PBS) (1:9) for 1 h at 37°C gave no benzyl alcohol when complexes [Cp*Ir(2,2'-bipyridine)(Cl)](Cl) (**Ir2**), [(hexamethylbenzene)Ru(2,2'-bipyridine)(Cl)](Cl) (**Ru5**), [(cymene)Ru(2,2'-bipyridine)(Cl)](Cl) (**Ru6**), [Cp*Rh(2,2'-bipyridine)(Cl)](Cl) (**Rh2**) were tested as catalysts (0.5 mol%). To our surprise, [(cymene)Ru(*N*-phenyl-2-pyridinecarboxamidate)(Cl)](Cl) (**Ru7**), and [Cp*Rh(*N*-phenyl-2-pyridinecarboxamidate)(Cl)] (**Rh3**) also gave no benzyl alcohol under the same conditions, while [Cp*Ir(*N*-phenyl-2-pyridinecarboxamidate)Cl] (**Ir4**)²³ afforded 45% benzyl alcohol product. Derivatives of **Ir4** with a hydrogen in place of the phenyl group (**Ir13**), gave low yield (~19%). If the phenyl group was substituted by an electron-donating group (n-butyl in **Ir14**), the yield increased to 73%.

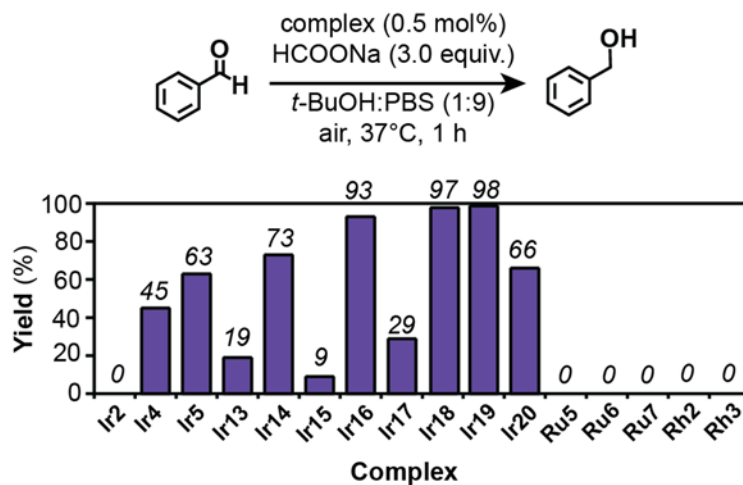


Figure 4.1. Catalytic comparison in hydrogenation of benzaldehyde. Reaction conditions: benzaldehyde (18 μ mol), HCOONa (54 μ mol), metal complex (0.09 μ mol), *t*-BuOH/PBS (1:9, 3 mL), 37 °C, 1 h. Yields were determined by GC using biphenyl as internal standard.

When the pyridine group was replaced by a more bulky group (quinoline in **Ir15**), the catalytic activity of the Ir complex decreased significantly (~9%), possibly due to the poor solubility of the iridium complex in aqueous medium. Addition of a substituent on the phenyl ring (chloro in **Ir5**) gave 63% yield, whereas addition of para substituents on the pyridine ring (e.g. chloro in **Ir16**, dimethylamino in **Ir18**, and pyrrolidine in **Ir19**) increased the yield to greater than 90%. These results suggest that having electron donating groups on the pyridine ring has a greater electronic effect on the catalysts than having them on the phenyl ring. If an electron withdrawing group was used as a substituent on the pyridine ring (e.g. trifluoromethyl in **Ir17**), however, the yield decreased to 29%. In comparison, a well-studied [Cp*Ir(*p*-toluenesulfonylethylenediamine)Cl] (**Ir20**)²⁹ complex gave 66% benzyl alcohol product.

Cyclic voltammetry measurements showed that **Ir4**, **Ir17**, **Ir18**, and **Ir20** are electronically different. Data recorded at 0.1 V/s in dichloromethane with 0.1 M N(Bu)₄PF₆ as supporting electrolyte revealed that the oxidation potentials of these complexes range from 0.47 V (**Ir20**) to 0.56 V (**Ir18**) vs. Fc/Fc* (Figure A4.1 in Appendix). The oxidation potentials of these complexes in PBS with scan rate 0.1 V/s are -1.08 V (**Ir18**), -0.95 V (**Ir4**), and -0.87 V (**Ir17**) vs. NHE. The reduction potentials of these complexes in PBS are -0.02 V (**Ir18**), 0.02 V (**Ir4**), 0.14 V (**Ir17**), and 0.82 V (**Ir20**) vs. NHE. CV diagram of **Ir20** did not show reduction potential.

Ir18 and **Ir19** were not only the more active catalysts, but they were also the most chemically stable since they could be recycled at least five times with minimal loss in activity (Figure 4.2). In contrast, both **Ir17** and **Ir20** showed significant reduction in

catalytic activity after only the second round of catalyst recycling (~30% yield for **Ir17** and ~20% yield for **Ir20**). **Ir20** was completely inactive after cycle #5.

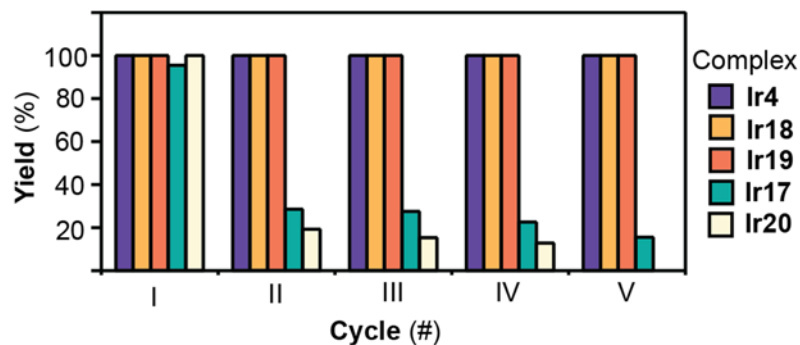
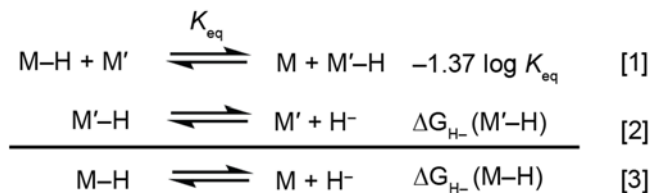


Figure 4.2. Catalyst recycling studies in hydrogenation of benzaldehyde. Reaction conditions: benzaldehyde (1.0 mmol), sodium formate (2.0 mmol), metal complex (0.02 mmol), t-BuOH/PBS (2:8, 20 mL), 37 °C, 8 h. Phenol or biphenyl (0.64 mmol) was added as a GC internal standard. After each reaction cycle, the products were analyzed by GC. The volatiles were then removed by vacuum and more benzaldehyde (1.0 mmol), formate (2.0 mmol), and solvent were added for subsequent rounds of hydrogenation.

4.3 Thermodynamic Hydricity Measurement

Metal hydrides are important intermediates in many chemical processes, including in transfer hydrogenation.^{1, 30} The term *hydricity*, which was first used in the literature in 1992 to describe the donor ability of a metal hydride, provides an experimentally measurable parameter to help predict the reactivity of such species.³¹⁻³² Thermodynamic hydricity describes the change in free energy ($\Delta G^{\circ}_{H^-}$) associated with the release of a hydride anion (H^-) from a hydride donor.³² Metal-hydride species with more negative $\Delta G^{\circ}_{H^-}$ values have greater hydride donor capabilities. Modeling after the work from the Miller group, which showed that the aqueous hydricity of metal catalysts can be tuned by their supporting ligands,³²⁻³³ we determined the hydricity of several Ir hydride complexes using the hydride transfer method (Scheme 4.2).

In the hydride transfer method, the hydricity of a metal hydride can be calculated from the equilibrium constant of the reaction between a hydride donor of unknown hydricity (M-H) and a referenced hydride acceptor (M'), where M'-H has a known hydricity value).³²



Scheme 4.2. Thermodynamic hydricity calculations.

As illustrated in Scheme 4.2, hydricity of M-H (equation 3) can be calculated from known values in equations 1 and 2. This hydride transfer method is a simple and straightforward method in measuring hydricity, but requires that the hydricity between M-H and M'-H differ by no more than 3 kcal/mol to obtain accurate measurements. Therefore, three hydride complexes with known hydricity, [Cp*Ir(2,2'-bipyridine)H]Cl (**Ir2-H**, $\Delta G^{\circ}_{\text{H}^-}(\text{Cl}) = 27$ kcal/mole), [Cp*Ir(4,4'-dimethyl-2,2'-bipyridine)H]Cl (**Ir2-Me-H**, $\Delta G^{\circ}_{\text{H}^-}(\text{Cl}) = 26.6$ kcal/mole), and [(cymene)Ru(2,2'-bipyridine)H](Cl) (**Ru6-H**, $\Delta G^{\circ}_{\text{H}^-}(\text{Cl}) = 22.3$ kcal/mole), were chosen as standard hydride complexes because their $\Delta G^{\circ}_{\text{H}^-}$ values are similar to those of our iridium complexes.

The hydride exchange reactions were performed in D₂O with either THF or methanol co-solvents to increase the solubility of the metal complexes. The NMR spectra of M + M'-H or M' + M-H were monitored over the course of several days and the equilibrium constants were calculated from these data. Although the $\Delta G^{\circ}_{\text{H}^-}$ of the standard metal-hydride were reported in water, our experiments showed that the differences in

hydricity measured in 100% D₂O vs. in mixtures of D₂O:Methanol (1:1) are not significant under our experimental conditions (Table 4.1).

Table 4.1. Comparison of Calculated Hydricity of **Ir2-H** in Different Solvents

Hydride Exchange Reaction	ΔG_{H^-} (kcal/mol)	
	D ₂ O ^a	D ₂ O ^a :MeOH (1:1)
Ir2 + Ir2-Me-H	26.3	26.1
	26.2	26.2
Ir2-H + Ir2-Me	26.2	26.2
	26.3	26.1
Average	26.2	26.1
Std. Dev.	0.06	0.06
Reported Hydricity ⁸	27.0	

^aD₂O solution contains NaP

Table 4.2. Summary of Calculated Hydricities of Iridium-Hydride Complexes

Hydride Exchange Reaction	ΔG_{H^-} (kcal/mol)			
	Ir4-H	Ir16-H	Ir18-H	Ir19-H
Ir-Cl + Ru6-H	24.20	23.43	21.30	21.35
	23.23	22.86	21.29	21.33
Ir-H + Ru6	22.40	20.42	21.33	21.34
	22.84	20.42	21.36	21.31
Average	23.17	21.78	21.32	21.33
Std. Dev.	0.66	1.38	0.03	0.01

Table 4.3. Summary of Calculated Hydricities of Complex **Ir17-H**

Hydride Exchange Reaction	ΔG_{H^-} (kcal/mol)
	Ir17-H
Ir17 + Ir2-H	28.52
	28.47
Ir17 + Ir2-Me-H	28.16
	28.06
Ir17-H + Ir2	28.53
	28.55
Ir17-H + Ir2-Me	28.24
	28.26
Average	28.35
Std. Dev.	0.18

To obtain accurate hydricity values, we carried out both the forward and backward hydride transfer reactions, i.e using referenced compounds in both the hydride and chloride forms (Figures A4.2-A4.8). The calculated $\Delta G^{\circ}_{\text{H}^-}$ for [Cp*Ir(*N*-phenyl-2-pyridinecarboxamidate)H] (**Ir4-H**) is 23.2 ± 0.7 kcal/mole, which is about 4 kcal/mole lower than that for **Ir2-H**, suggesting that **Ir4-H** is a stronger hydride donor than **Ir2-H**. The derivatives with electron donating substituents on the pyridine ring (**Ir16**, **Ir18**, and **Ir19**) have smaller $\Delta G^{\circ}_{\text{H}^-}$ values than that of **Ir4-H**, which also correlates with their greater catalytic activities (Tables 4.2 and Figure 4.1). Interestingly, complex **Ir17** bearing CF₃ electron withdrawing group, have a larger $\Delta G^{\circ}_{\text{H}^-}$ (28.4 ± 0.2 kcal/mole) and correspondingly, gave lower yield in transfer hydrogenation of benzaldehyde (29%) compared to complex **Ir4** (Tables 4.3 and Figure 4.1).

These results show that ligand electronics can have significant effects on metal-hydride donor abilities and consequently, their transfer hydrogenation activity. Our data clearly indicate that there is a strong link between the hydricity of Ir-H species and their observed reaction yields (Figure 4.3). The hydricity of the well-studied complex **Ir20** could not be determined because hydride transfer reaction was not clean (other species appeared and the main species decomposed slowly in aqueous solvent, see Figure A4.9).

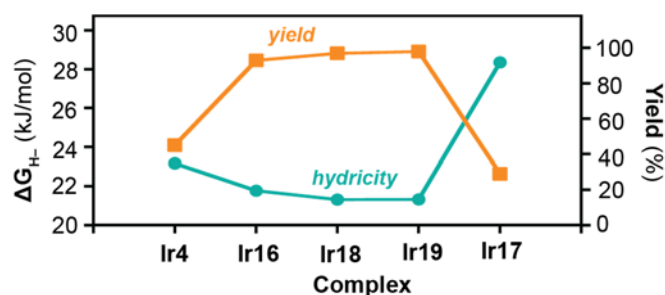
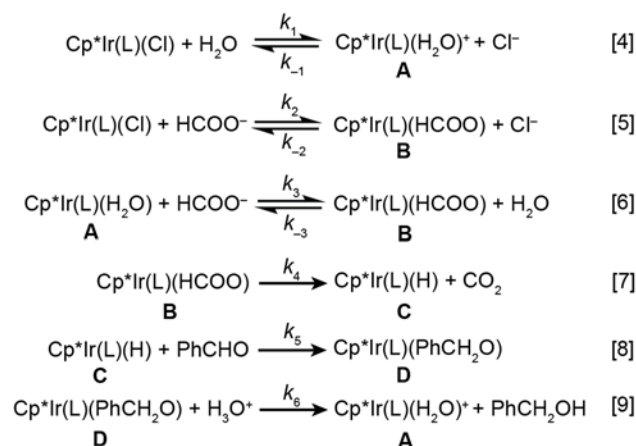


Figure 4.3. Correlations between thermodynamic hydricity of metal hydride complexes and reaction yield of transfer hydrogenation by metal chloride complexes.

It is important to note, however, that this relationship does not necessarily apply to other metal systems, since the ruthenium-hydride species **Ru7-H** is relatively hydridic ($\Delta G_{H^-}^{\circ} = 22.3$ kcal/mol),³³ but its parent catalyst **Ru** gave 0% yield in transfer hydrogenation (Figure 4.1).

4.4 Kinetic Studies

Transfer hydrogenation reactions, are proposed to occur through two main steps: 1) formation of metal-hydride complexes, and 2) hydride transfer from the metal-hydride intermediates to substrates. The detailed elementary sequence of this process is shown in Scheme 4.3. First, the metal-chloride complexes may undergo aquation to form metal-aqua complexes (equation 4). Formate anions may exchange with M-Cl or M-H₂O species to yield metal-formate species that could spontaneously convert to metal-hydrides and CO₂ (equation 5-7). The metal-hydride will then transfer H⁻ to the carbonyl substrate, giving back the M-H₂O complex along with a new alcohol product (equation 8-9).



Scheme 4.3. Elementary steps in transfer hydrogenation by Cp*Ir complexes.

To determine if aquation of the metal-hydride species occur, we performed halide abstraction experiment using several iridium complexes. First, authentic samples of Ir-H₂O complexes were synthesized by reacting Ir-Cl with silver salts in D₂O. Various amounts of sodium chloride were added to the Ir-H₂O solutions and their ¹H NMR spectra were recorded to determine whether a new species had formed. We observed that **Ir2** was stable in the aqua form with no change in its NMR spectra up to 100 mM of sodium chloride, whereas **Ir4** converted from the aqua to chloride form at ≥ 5 mM of sodium chloride (Figures 4.4, A4.10, and A4.11). Although it has been proposed that complexes with more labile ligands could react with hydride donors more readily and give more efficient catalysts,³⁴⁻³⁵ our results suggest that this is not always so since **Ir4** is a more active transfer hydrogenation catalyst than **Ir2** (Figure 4.1).

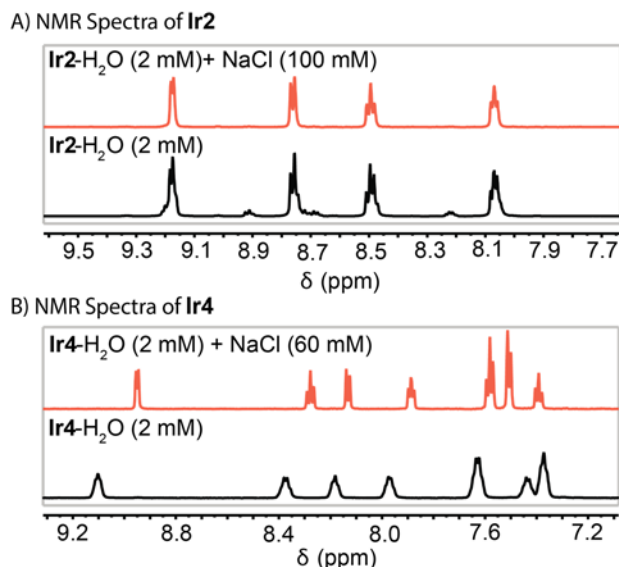


Figure 4.4. ¹H NMR (D₂O, 600 MHz) spectra in hydrolysis studies of Ir complexes.

To understand kinetic behavior of the catalysts, we performed kinetic studies of select catalysts using gas chromatography. First, the concentration dependence of the reaction components on the initial rate (r_i) was determined. Consistent with a report by Fish and co-workers,³⁶ reactions catalyzed by **Ir4** were found to be dependent on only the concentrations of sodium formate and catalyst, but not benzaldehyde (A-C, Figure 4.5). Therefore, the experimental rate-law for our reaction is:

$$\text{Reaction rate} = k_{cat} [\text{catalyst}] [\text{HCOONa}].$$

This rate law suggests that hydride formation is the rate limiting step in the transfer hydrogenation process. Interestingly, transfer hydrogenation reactions catalyzed by **Ir17** were found to be third order since they are dependent on the concentrations of sodium formate, catalyst, and substrate (D-F, Figure 4.5).

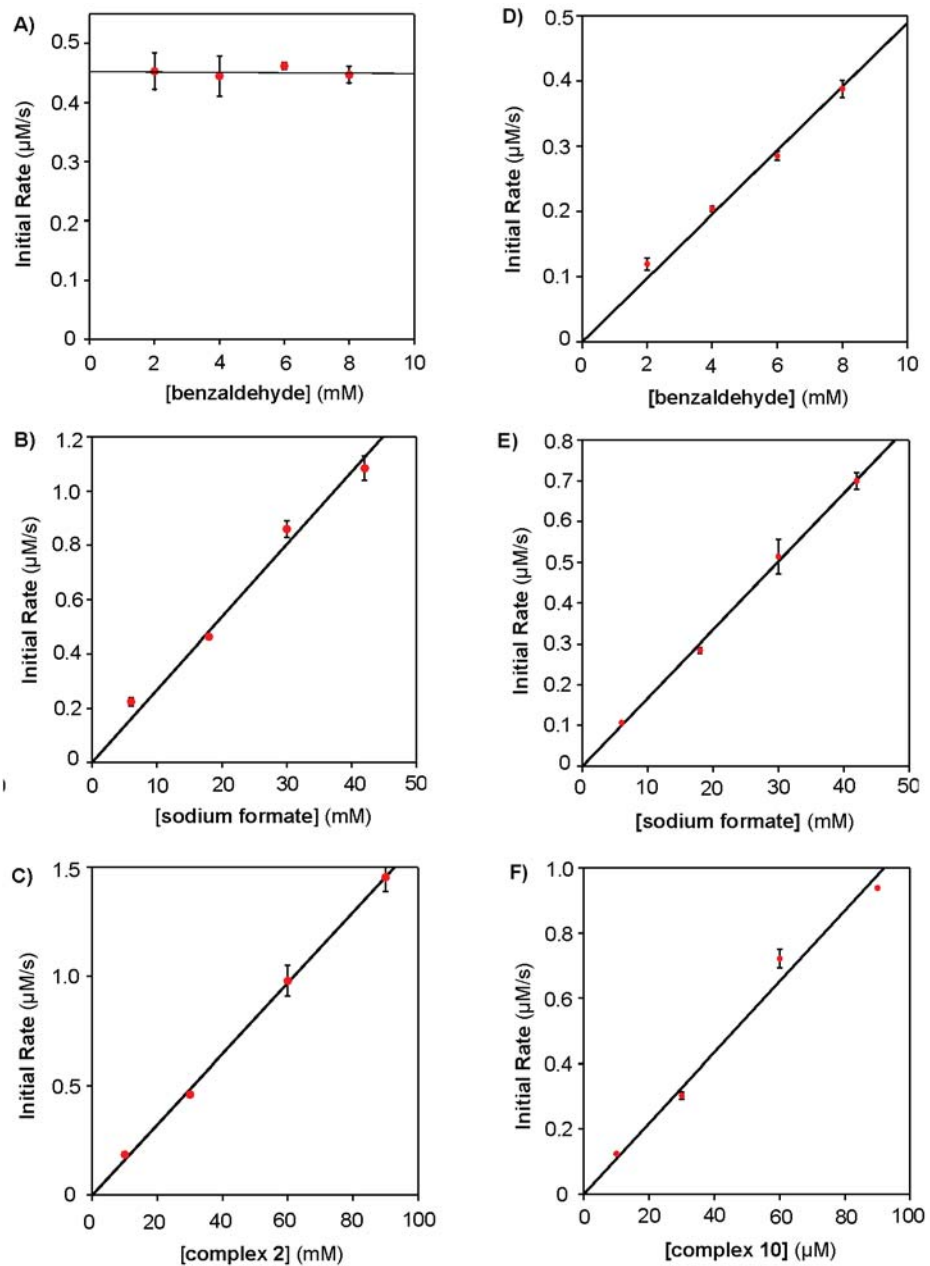


Figure 4.5. Kinetic plots from the reaction of benzaldehyde with iridium complex and sodium formate in tBuOH/PBS (1:9) at 37°C. A-C: complex **Ir4**; D-F: complex **Ir17**. These data show the dependence of the initial rate on the concentration of A) benzaldehyde (zero order), B) sodium formate (first order), C) **Ir4** (first order), D) benzaldehyde (first order), E) sodium formate (first order), F) **Ir17** (first order).

As shown in Figure 4.6, **Ir18** and **Ir20** are faster catalysts compared to **Ir4** and **Ir17** since they have higher initial rates from 20-50°C. All of the iridium catalysts showed strong dependence on temperature since their initial rates increase 2- to 3- folds for each 10°C increment. This result suggests that transfer hydrogenation reactions must be performed at physiological temperatures for biological relevance.

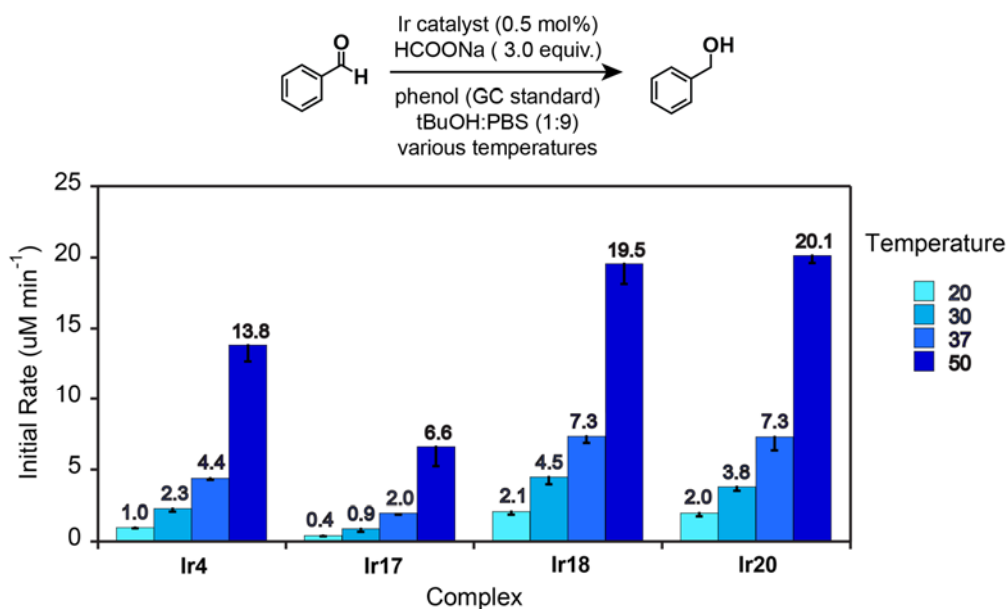
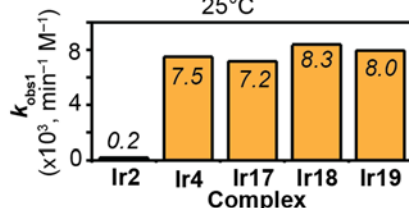
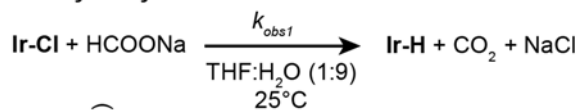


Figure 4.6. Initial rate comparison between different catalysts in transfer hydrogenation of benzaldehyde at various temperatures. Reaction conditions: benzaldehyde (6 mM), Ir catalyst (30 μM), sodium formate (18 mM) in t-BuOH/PBS (1:9). Yields were determined by GC using phenol as internal standard.

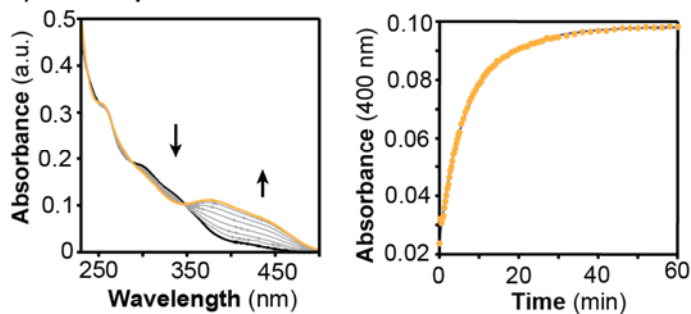
Next, we measured the hydride formation rate constants by UV-vis absorption spectroscopy. The Ir-Cl complexes were mixed with sodium formate and the spectral changes were recorded to observe the formation of Ir-H species. **Ir4**, **Ir17**, **Ir18** and **Ir20** showed similar k_{obs} for hydride formation (7.2 - $8.3 \times 10^3 \text{ min}^{-1}\text{M}^{-1}$), whereas that for **Ir2** was ~40 times lower (Figure 4.7). Since hydride formation is the rate determining step of

benzaldehyde transfer hydrogenation, these k_{obs1} correlate with the reaction yields, specifically that **Ir4**, **Ir17**, **Ir18** and **Ir20** are more efficient catalysts than **Ir2** (see more detail in Figures A4.12 and A4.13).

A) Summary of Hydride Formation Kinetic Data



B) UV-Vis Spectra of Ir4/HCOONa



C) UV-Vis Spectra of Ir18/HCOONa

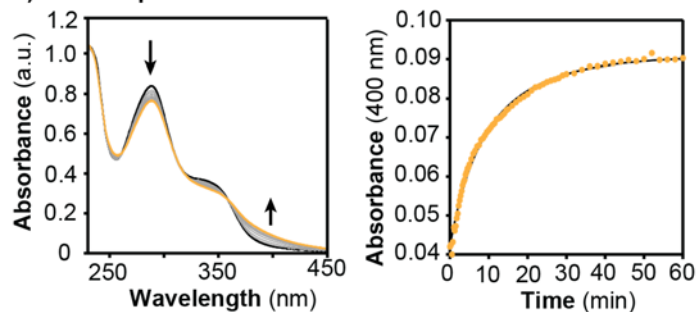
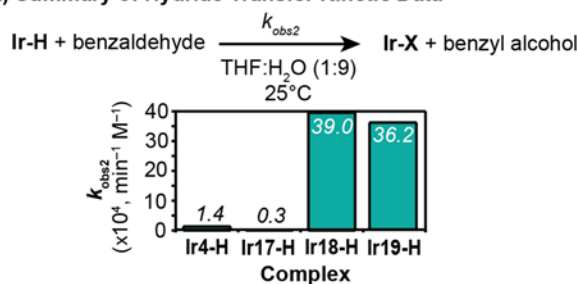


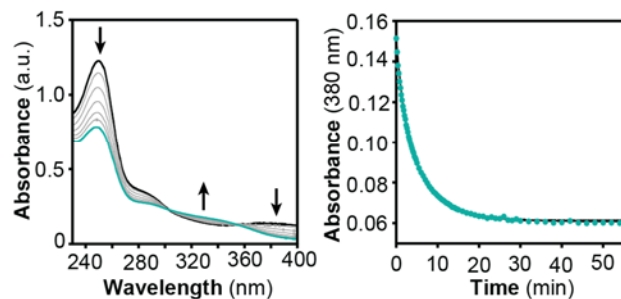
Figure 4.7. UV-Vis kinetic studies of iridium hydride formation. A) Comparison of hydride formation rate (k_{obs}) of iridium complexes; B) UV-Vis spectra of hydride formation reaction of **Ir4** (0.09 μmol) and sodium formate (0.18 μmol) in THF:H₂O (1:9, 3.0 mL); B) UV-Vis spectra of hydride formation reaction of **Ir18** (0.09 μmol) and sodium formate (0.18 μmol) in THF:H₂O (1:9, 3.0 mL) at 25°C.

We also observed dramatic rate differences in hydride transfer step (Figure 4.8). We found that **Ir2-H** did not react with benzaldehyde after 15 hours (UV-vis spectra showed only decomposition of **Ir2-H**). **Ir4-H** and **Ir17-H** were able to reduce benzaldehyde but at much slower rates compared to **Ir18** and **Ir20** (~40 times lower k_{obs2}). These kinetic data indicate that **Ir18** is the most efficient catalyst since it has the highest k_{obs1} and k_{obs2} rate constants (see more details in Figures A4.14 and A4.15).

A) Summary of Hydride Transfer Kinetic Data



B) UV-Vis Spectra of Ir4-H/Benzaldehyde



C) UV-Vis Spectra of Ir18-H/Benzaldehyde

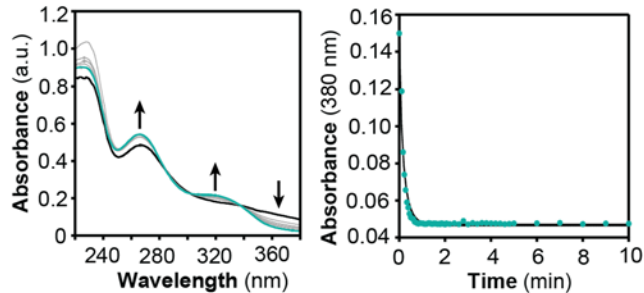


Figure 4.8. UV-Vis kinetic studies of hydride transfer reaction. A) Comparison of hydride transfer rate (k_{obs}) of iridium complexes; B) UV-Vis spectra of hydride transfer reaction of **Ir4-H** (0.09 μmol) and benzaldehyde (0.18 μmol) in THF:H₂O (1:9, 3.0 mL); B) UV-Vis spectra of hydride transfer reaction of **Ir18-H** (0.09 μmol) and benzaldehyde (0.18 μmol) in THF:H₂O (1:9, 3.0 mL) at 25°C.

4.5 Temperature Dependence of the Reaction Rate Studies

The temperature dependence (20–50°C) of the reaction rate was studied in PBS under air. These data allowed us to determine the activation energy (E_a) by using Arrhenius plots ($\ln k_{cat}$ vs. $1/T$), as well as enthalpy (ΔH^\ddagger) and entropy (ΔS^\ddagger) by using Eyring plots ($\ln k_{cat}/T$ vs. $1/T$). (Figures 4.9, A4.16–20).

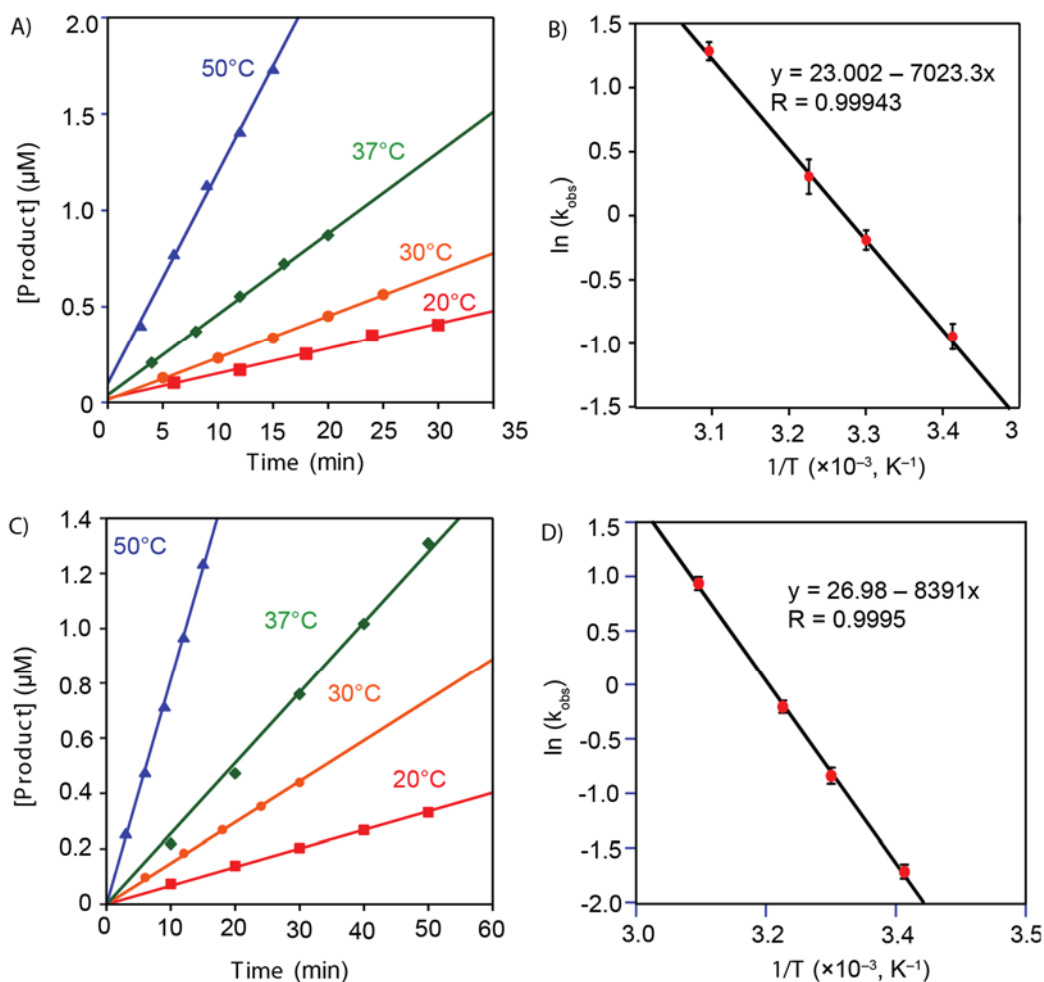


Figure 4.9. Temperature dependence studies of the reaction of benzaldehyde (6 mM) with iridium complex (30 μM) and sodium formate (18 mM) in t-BuOH/PBS (1:9). The data show: The change in the rates of product formation from 20–50°C of complex **Ir4** (A), and **Ir18** (C); Arrhenius plots showing the dependence of k_{obs} as a function of temperature of complex **Ir4** (B), and **Ir18** (D).

The experimentally-derived activation parameters are summarized in Table 4.4. Our results showed that more electron donating ligands make the iridium complexes stronger hydride donors, as well as lower the energy of activation of transfer hydrogenation (13.4 kcal/mol for **Ir18** with dimethyl amino substituent, 16.6 kcal/mol for **Ir4** with no substituent, and 19.0 kcal/mol for **Ir17** with trifluoromethyl substituent). In comparison, the well-studied catalyst **Ir20** showed similar E_a , and the rhodium complex **Rh2** showed higher activation energy (24 kcal/mol³⁶, reported by Fish and co-workers).

Table 4.4. Summary of Activation Parameters of Tested Iridium Catalysts

Complex	E_a (kcal/mol)	ΔS^\ddagger (kcal/mol·K)	ΔH^\ddagger (kcal/mol)	ΔG^\ddagger (25°C, (kcal/mol)
Ir4	16.6	0.04	16.0	4.1
Ir17	13.4	0.03	12.8	4.8
Ir18	19.0	0.05	18.4	3.7
Ir20	14.5	0.03	13.9	3.8

4.6 Conclusion

Using kinetic and thermodynamic measurements, we have investigated the structure-activity relationship (SAR) of the pentamethylcyclopentadienyl iridium(III) (Cp*Ir) complexes in aqueous transfer hydrogenation. As illustrated in Chart 4.2, we found that modifications of the pyridine ring have larger effects on the catalytic activity of the iridium complexes than the modifications of the N-amide substituent. More electron donating groups on the pyridine ring, such as in complexes **Ir18** and **Ir19**, can increase the hydride donor ability of the corresponding Ir-H complexes, and lower the activation energy associated with the transfer hydrogenation process. We have also discovered that the more electron-rich Ir complexes could be recycled multiple times with minimal loss in activity.

Our findings in this study could be useful in predicting the catalytic activity of Cp*Ir complexes and designing more efficient catalysts for transfer hydrogenation reactions. Future studies will focus on optimizing catalysts for better biocompatibility, such as enhancing their tolerance towards biological thiols, increasing their cellular uptake, and reducing their cytotoxicity.

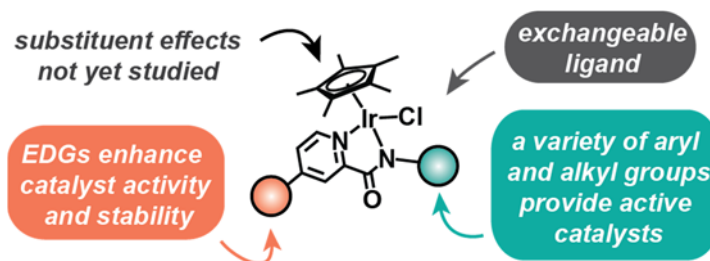


Chart 4.2. Summary of SAR study.

4.7 Experimental

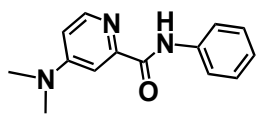
General. Commercial reagents were used as received without further purification. All air- and water-sensitive manipulations were performed using standard Schlenk techniques or under a nitrogen atmosphere inside a glovebox. NMR samples for hydride complexes and hydride exchange experiments were prepared inside the glovebox and then transferred to J-Young tubes before taken outside. Anhydrous solvents were obtained from an Innovative Technology solvent drying system saturated with Argon.

Physical Methods. NMR spectra were acquired using JEOL spectrometers (ECA-400, 500, and 600) at room temperature and referenced using residual solvent peaks. All ^{13}C NMR spectra were proton-decoupled. Gas chromatography-mass spectrometry (GC/GC-MS) was performed using an Agilent 7890 GC/5977A MSD instrument equipped with an HP-5MS capillary column. Cyclic voltammetry (CV) experiments were performed using a BAS Epsilon electroanalytical system. Ultraviolet-visible (UV) experiments were performed using an Agilent Cary 60 UV-Vis.

Synthesis

The iridium precursor $[\text{Cp}^*\text{IrCl}_2]_2$ (**Ir1**),³⁷ and iridium complexes $[\text{Cp}^*\text{Ir}(2,2'$ -bipyridine) $\text{Cl}]\text{Cl}$ (**Ir2**),³⁸ $[\text{Cp}^*\text{Ir}(N$ -phenyl-2-pyridinecarboxamidate) $\text{Cl}]\text{Cl}$ (**Ir4**),²³ $[\text{Cp}^*\text{Ir}(N$ -(4-chlorophenyl)-2-pyridinecarboxamidate) $\text{Cl}]\text{Cl}$ (**Ir5**),²³ [(hexamethylbenzene) Ru(2,2'-bipyridine) $\text{Cl}]\text{Cl}$ (**Ru5**),³⁹ [(cymene)Ru(2,2'-bipyridine) $\text{Cl}]\text{Cl}$ (**Ru6**),³⁹ $[\text{Cp}^*\text{Rh}(2,2'$ -bipyridine) $\text{Cl}]\text{Cl}$ (**Rh2**),⁴⁰ $[\text{Cp}^*\text{Ir}(2,2'$ -bipyridine) $\text{H}](\text{PF}_6)$ (**Ir2-H**),²³ and $[\text{Cp}^*\text{Ir}(N$ -phenyl-2-pyridinecarboxamidate) $\text{Cl}]\text{Cl}$ (**Ir4-H**)²³ were synthesized according to literature procedures.

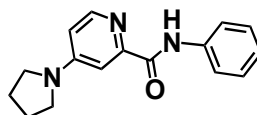
Preparation of N-phenyl-2-(4-dimethylaminopyridine)carboxamide. In a high-pressure



glass tube, 4-chloro-*N*-phenylpicolinamide (1.0 mmol) and dimethylamine (40% in water, 3.0 mL) were combined with 1.5 mL

of acetonitrile. The tube was sealed tightly with a Teflon screwcap, and stirred at 120°C overnight. After removing the solvent under vacuum, the resulting light yellow solid was crystallized from dichloromethane and pentane as a fluffy white powder (203 mg, 84% yield). ¹H NMR (CDCl₃, 500 MHz): 10.15 (s, 1H), 8.20 (d, *J* = 5.8 Hz, 1H), 7.77 (d, *J* = 8.0 Hz, 2H), 7.55 (s, 1H), 7.37 (t, *J* = 8.0 Hz, 2H), 7.12 (d, *J* = 7 Hz, 1H), 6.59 (dd, *J* = 5.8, 2.5 Hz, 1H), 3.09 (s, 6H). ¹³C NMR (CDCl₃, 126 MHz): 163.2, 155.5, 150.1, 148.1, 138.1, 129.1, 124.1, 119.7, 108.4, 105.3, 39.4 ppm.

Preparation of N-phenyl-2-(4-pyrrolidinylpyridine)carboxamide. In a high-pressure glass



tube, 4-chloro-*N*-phenylpicolinamide (1.0 mmol, 1 equiv.) and pyrrolidine (1.4 gr, 20 equiv.) were combined with 3.0 mL of

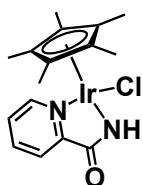
acetonitrile. This tube was sealed tightly, and stirred at 120°C overnight. After removing the solvent under vacuum, the resulting light yellow solid was crystallized from dichloromethane and pentane as a fluffy white powder (217 mg, 81% yield). ¹H NMR (CDCl₃, 400 MHz): 10.19 (s, 1H), 8.16 (d, *J* = 5.7 Hz, 1H), 7.78 (d, *J* = 7.9 Hz, 2H), 7.41 (d, *J* = 2.6 Hz, 1H), 7.37 (t, *J* = 7.9 Hz, 2H), 7.12 (t, *J* = 7.9 Hz, 1H), 6.47 (dd, *J* = 5.7, 2.6 Hz, 1H), 3.39 (t, *J* = 6.5 Hz, 4H), 2.11-1.99 (m, 4H). ¹³C NMR (CDCl₃, 126 MHz): 163.2, 152.9, 149.8, 147.9, 138.2, 129.1, 124.0, 119.6, 108.8, 105.7, 47.3, 25.4 ppm.

General Procedure for the Preparation of Iridium/Ruthenium/Rhodium Complexes

Method A: In a Schlenk flask, 20 mL of ethanol was purged with nitrogen for about 10 min. Solid Ir/Ru/Rh precursor (0.15 mmol, 1.0 equiv.) and the ligand (0.31 mmol, 2.05 equiv.) were added and stirred for 15 min at 80°C. The reaction mixture was treated with ammonium hexafluorophosphate (0.68 mmol, 4.5 equiv.) and stirred overnight at 80°C. The ethanol solvent was removed by rotary evaporation and then the solid residual was redissolved in 20 mL of dichloromethane and washed with water (3×20 mL). The organic phase was separated, dried over sodium sulfate, filtered, and then evaporated to dryness. The crude product was purified by crystallization using a solvent layering method.

Method B: In a round bottom flask, the ligand (0.31 mmol, 1.0 equiv.) was added into 20 mL of anhydrous THF and stirred for 10 min at RT. The reaction mixture was treated with sodium hydride (0.34 mmol, 1.1 equiv.), which then slowly turned milky white, and stirred for 2 h. Solid Ir/Ru/Rh precursor (0.15 mmol, 0.49 equiv.) was added and the reaction solution immediately turned an orange/red brown color. After stirring for 5 h at RT, the heterogeneous mixture was filtered to remove the precipitates. The filtrate was collected and evaporated to dryness. The crude product was purified by crystallization using a solvent layering method.

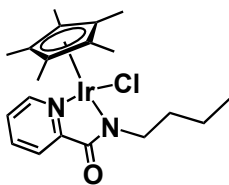
Preparation of [Cp*Ir(2-pyridinecarboxamidate)Cl] (Ir10). This complex was synthesized



using method A with [Cp*IrCl₂]₂ as precursor, and purified by crystallization using dichloromethane and pentane. The product was obtained as an orange-yellow solid in 79% yield. The characterization data for this material matched

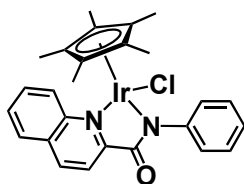
those reported previously.⁴¹

Preparation of [Cp*Ir(*N*-butyl-2-pyridinecarboxamidate)Cl] (**Ir11**). This complex was



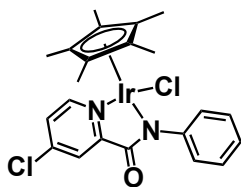
synthesized by method B with [Cp*IrCl₂]₂ as precursor, and purified by crystallization using THF and Et₂O. The product was obtained as an orange solid (72% yield). ¹H NMR (CDCl₃, 500 MHz): 8.50 (d, *J* = 5.7 Hz, 1H), 8.04 (d, *J* = 7.8 Hz, 1H), 7.85 (td, *J* = 7.8, 1.5 Hz, 1H), 7.40 (ddd, *J* = 7.8, 5.7, 1.5 Hz, 1H), 4.65-4.55 (m, 2H), 3.10-3.01 (m, 2H), 1.65 (s, 15H), 1.46-1.27 (m, 2H), 0.92 (t, *J* = 7.4 Hz, 3H) ppm. ¹³C NMR (CDCl₃, 126 MHz): 169.9, 156.0, 148.9, 138.4, 126.7, 126.0, 86.4, 50.1, 31.4, 21.0, 14.3, 8.9 ppm. FT-IR: 1613, 1584, 1563 (ν_{CO}) cm⁻¹. MP = 119–120°C. HRMS-ESI(+): Calc (C₂₀H₂₈ClIrN₂O) = 564.1496 [M+Na]⁺, Found = 564.1586.

Preparation of [Cp*Ir(*N*-phenyl-2-quinolinecarboxamidate)Cl] (**Ir12**). This complex was



synthesized by method A with [Cp*IrCl₂]₂ as precursor, and purified by crystallization using dichloromethane and pentane. The product was obtained as an orange solid (71% yield). ¹H NMR (CDCl₃, 500 MHz): 8.61 (d, *J* = 8.4 Hz, 1H), 8.31 (d, *J* = 8.4 Hz, 1H), 8.28 (d, *J* = 8.4 Hz, 1H), 7.97 (d, *J* = 7.5 Hz, 2H), 7.92 (d, *J* = 8.4 Hz, 1H), 7.84 (t, *J* = 7.2 Hz, 1H), 7.70 (t, *J* = 7.5 Hz, 1H), 7.29 (t, *J* = 7.5 Hz, 2H), 7.08 (t, *J* = 7.2 Hz, 1H), 1.44 (s, 15H) ppm. ¹³C NMR (CDCl₃, 126 MHz): 168.8, 157.5, 148.2, 145.2, 139.5, 130.9, 130.6, 129.9, 128.8, 128.7, 128.1, 127.0, 124.1, 122.6, 87.1, 8.6 ppm. FT-IR: 1621, 1588, 1536 (ν_{CO}) cm⁻¹. MP = 317–319°C (decomposed). HRMS-ESI(+): Calc (C₂₆H₂₆ClIrN₂O) = 634.1339 [M+Na]⁺, Found = 634.1458.

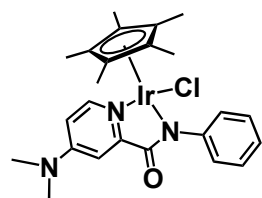
Preparation of [Cp*Ir(*N*-phenyl-2-(4-chloro-pyridine)carboxamidate)Cl] (**Ir17**). This



complex was synthesized by method A with [Cp*IrCl₂]₂ as precursor, and purified by crystallization using dichloromethane and pentane.

The product was obtained as a yellow solid (89% yield). ¹H NMR (CDCl₃, 500 MHz): 8.42 (d, *J* = 6.2 Hz, 1H), 8.13 (d, *J* = 2.4 Hz, 1H), 7.59 (dd, *J* = 8.4, 1.0 Hz, 2H), 7.47 (dd, *J* = 6.2, 2.4 Hz, 1H), 7.31 (t, *J* = 8.4 Hz, 2H), 7.10 (td, *J* = 8.4, 1.0 Hz, 1H), 1.39 (s, 15H) ppm. ¹³C NMR (CDCl₃, 126 MHz): 167.6, 157.1, 150.0, 148.0, 128.3, 127.8, 127.0, 126.9, 124.6, 86.8, 8.5 ppm. FT-IR: 1621, 1585, 1550 (ν_{CO}) cm⁻¹. MP = 295–297°C (decomposed). HRMS-ESI(+): Calc (C₂₂H₂₃Cl₂IrN₂O) = 618.0793 [M+Na]⁺, Found = 618.0887.

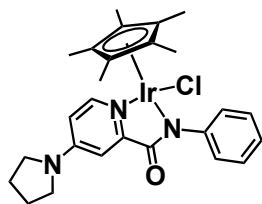
Preparation of [Cp*Ir(*N*-phenyl-2-(4-dimethylaminopyridine)carboxamidate)Cl] (**Ir18**).



This complex was synthesized by method B with [Cp*IrCl₂]₂ as the precursor, and was purified by crystallization using dichloromethane/pentane or silica gel column chromatography

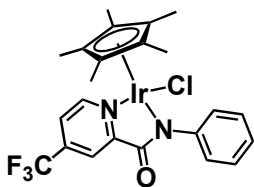
(ethyl acetate:methanol = 95:5). The product was obtained as a yellow solid (85% yield by crystallization, 88% yield by chromatography). ¹H NMR (CDCl₃, 500 MHz): 8.05 (d, *J* = 6.5 Hz, 1H), 7.63 (d, *J* = 8.0 Hz, 2H), 7.30 (dd, *J* = 4.8, 2.4 Hz, 2H), 7.28 (s, 1H), 7.04 (t, *J* = 8.0 Hz, 1H), 6.56 (dd, *J* = 6.5, 3.2 Hz, 1H), 3.11 (s, 6H), 1.37 (s, 15H) ppm. ¹³C NMR (CDCl₃, 126 MHz): 169.4, 155.2, 154.5, 148.6, 128.0, 127.2, 124.0, 109.4, 108.6, 85.8, 39.6, 8.6 ppm. FT-IR: 1629, 1603, 1585 (ν_{CO}) cm⁻¹. MP = 314–316°C (decomposed). HRMS-ESI(+): Calc (C₂₄H₂₉ClIrN₃O) = 627.1605 [M+Na]⁺, Found = 627.1701.

Preparation of [Cp*Ir(*N*-phenyl-2-(4-pyrrolidinylpyridine)carboxamidate)Cl] (**Ir19**). This



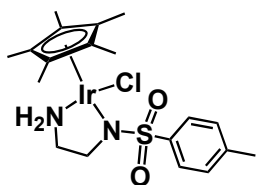
complex was synthesized by method B with [Cp*IrCl₂]₂ as precursor, and was purified by crystallization using dichloromethane and pentane. The product was obtained as a yellow solid (77% yield). ¹H NMR (CDCl₃, 500 MHz): 8.04 (d, *J* = 6.7 Hz, 1H), 7.65 (d, *J* = 6.7 Hz, 2H), 7.28 (t, *J* = 6.7 Hz, 2H), 7.18 (d, *J* = 2.9 Hz, 1H), 7.04 (t, *J* = 6.7 Hz, 1H), 6.45 (dd, *J* = 6.7, 2.9 Hz, 1H), 3.47-3.37 (m, 4H), 2.04 (dd, *J* = 7.9, 5.3 Hz, 4H), 1.37 (s, 15H) ppm. ¹³C NMR (CDCl₃, 126 MHz): 169.5, 154.3, 152.6, 148.8, 148.5, 128.0, 127.2, 124.0, 109.8, 109.1, 85.7, 47.6, 25.5, 8.6 ppm. FT-IR: 1630, 1604, 1583 (ν_{CO}) cm⁻¹. MP = 325–326°C (decomposed). HRMS-ESI(+): Calc (C₂₆H₃₁ClIrN₃O) = 653.1761 [M+Na]⁺, Found = 653.1876.

Preparation of [Cp*Ir(*N*-phenyl-2-(4-trifluoromethylpyridine)carboxamidate)Cl] (**Ir17**).



This complex was synthesized by method A with [Cp*IrCl₂]₂ as precursor, and was purified by crystallization using dichloromethane/pentane or silica gel column chromatography (ethyl acetate:methanol = 95:5). The product was obtained as an orange solid (77% yield by crystallization, 81% yield by chromatography). ¹H NMR (CDCl₃, 500 MHz): 8.72 (d, *J* = 5.8 Hz, 1H), 8.38 (s, 1H), 7.68 (dd, *J* = 5.8, 2.0 Hz, 1H), 7.59 (dd, *J* = 8.0, 1.1 Hz, 2H), 7.32 (t, *J* = 7.0 Hz, 2H), 7.11 (t, *J* = 8.0 Hz, 1H), 1.40 (s, 15H) ppm. ¹³C NMR (CDCl₃, 126 MHz): 167.5, 157.7, 150.6, 147.8, 128.4, 126.8, 124.8, 123.3, 122.9, 87.3, 86.4, 9.5, 8.6 ppm. ¹⁹F NMR (CDCl₃, 470 MHz): -64.7 ppm. FT-IR: 1632, 1604, 1589 (ν_{CO}) cm⁻¹. MP = 318–321°C (decomposed). HRMS-ESI(+): Calc (C₂₃H₂₃ClF₃IrN₂O) = 652.1056 [M+Na]⁺, Found = 652.1141.

Preparation of [Cp*Ir(*N*-tosylethylenediamine)Cl] (**Ir20**). This complex was synthesized



by method B with [Cp*IrCl₂]₂ as precursor, and was purified by

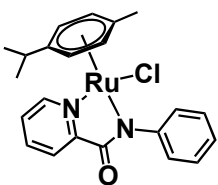
crystallization using methanol/diethyl ether or silica gel column

chromatography (ethyl acetate:methanol = 95:5). The product was

obtained as a yellow solid (81% yield by crystallization, 78% yield by chromatography).

The characterization data for this material matched those reported previously.⁴²

Preparation of [(*p*-cymene)Ru(*N*-phenyl-2-pyridinecarboxamidate)Cl] (**Ru6**). This



complex was synthesized by method B, with [Ru(cymene)Cl₂]₂ as

precursor, and purified by crystallization using

dichloromethane/diethyl ether or silica gel column chromatography

(ethyl acetate:methanol = 95:5). The product was obtained as a brown-orange solid (75%

yield by crystallization, 73% yield by chromatography). ¹H NMR (CD₃OD, 500 MHz):

9.25 (d, *J* = 5.5 Hz, 1H), 8.05 (t, *J* = 7.6 Hz, 1H), 7.91 (d, *J* = 7.6 Hz, 1H), 7.62 (t, *J* = 6.5

Hz, 2H), 7.56 (d, *J* = 7.6 Hz, 2H), 7.39 (t, *J* = 7.6 Hz, 2H), 7.20 (t, *J* = 7.6 Hz, 1H), 5.58

(d, *J* = 6.0 Hz, 1H), 5.37 (d, *J* = 6.0 Hz, 1H), 5.21 (d, *J* = 6.0 Hz, 1H), 4.82 (d, *J* = 6.0 Hz,

1H), 2.58-2.50 (m, 1H), 2.12 (s, 3H), 1.01 (dd, *J* = 6.8, 4.1 Hz, 6H) ppm. ¹³C NMR

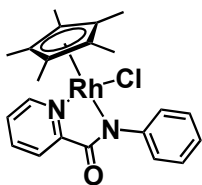
(CD₃OD, 126 MHz): 167.6, 155.2, 154.4, 151.7, 139.0, 128.3, 127.1, 125.9, 125.1, 124.8,

101.9, 100.7, 85.0, 83.9, 30.8, 21.2, 20.8, 17.6 ppm. FT-IR: 1614, 1593, 1581, 1564 (ν_{CO})

cm⁻¹. MP = 218–219°C (decomposed). HRMS-ESI(+): Calc (C₂₃H₂₆ClN₂ORu) = 491.0441

[M+Na]⁺, Found = 491.0560.

Preparation of [Cp*Rh(N-phenyl-2-pyridinecarboxamidate)Cl] (Rh3). This complex was



synthesized by method A, with [Cp*RhCl₂]₂ as precursor, and purified by washing with hexane and diethyl ether (no crystallization needed).

The product was obtained as a purple-brown solid (77% yield). ¹H NMR (CDCl₃, 500 MHz): 8.62 (d, *J* = 5.1 Hz, 1H), 8.15 (d, *J* = 7.6 Hz, 1H), 7.94 (t, *J* = 7.2 Hz, 1H), 7.74 (d, *J* = 7.6 Hz, 2H), 7.52 (td, *J* = 5.1, 2.0 Hz, 1H), 7.32 (t, *J* = 7.6 Hz, 2H), 7.08 (t, *J* = 7.2 Hz, 1H), 1.40 (s, 15H) ppm. ¹³C NMR (CDCl₃, 126 MHz): 166.6, 156.5, 149.5, 148.2, 138.9, 128.1, 127.2, 127.0, 126.1, 124.1, 94.7, 8.7 ppm. FT-IR: 1614, 1580, 1561 (ν_{CO}) cm⁻¹. MP = 267–269°C (decomposed). HRMS-ESI(+): Calc (C₂₂H₂₄ClN₂ORh) = 494.0608 [M+Na]⁺, Found = 494.0696.

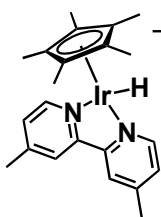
General Procedures for the Preparation of Iridium/Ruthenium Hydride Complexes

Method A. Inside the glovebox, the Ir(III) or Ru(II) chloride complex (0.2 mmol, 1.0 equiv.) was dissolved in 5.0 mL of methanol. A 2.5 mL aqueous solution containing NaBH₄ (2.0 mmol, 10 equiv.) was added dropwise. After 3 h, the solution was concentrated under vacuum to about 2.0 mL, which led to the formation of a large amount of precipitate. The solid was isolated by filtration, washed with water, and then dried overnight.

Method B. Inside the glovebox, the Ir(III) chloride complex (0.20 mmol, 1.0 equiv.) was dissolved in 5.0 mL of methanol. A 5.0 mL aqueous solution containing HCOONa (4.0 mmol, 20 equiv.) was added dropwise. After 8 h, the solution was concentrated under vacuum to about 4.0 mL, which led to the formation of a large amount of precipitate. The solid was isolated by filtration, washed with water, and then dried overnight.

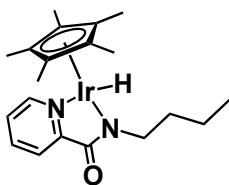
Method C. This two-step synthesis was adapted from a literature procedure.⁸ *Step 1:* Inside the glovebox, the Ir(III) or Ru(II) chloride complex (0.2 mmol, 1.0 equiv.) and excess NaBH₄ (2.0 mmol, 10 equiv.) were stirred in a 10.0 mL solution containing 1 M (or 5 M) NaOH. As the reaction proceeded, a very dark purple (almost black) solid had formed. After 4 h stirring, the solid was isolated by filtration, washed with water, collected in benzene, and evaporated to dryness. *Step 2:* Inside the glovebox, the Ir(I) or Ru(0) complex obtained in step 1 (0.10 mmol, 1.0 equiv.) was dissolved in 3.0 mL of diethyl ether. A solution of HCl in Et₂O (40 mM, 0.95 equiv.) was added dropwise to the dark purple solution, which led to the formation of a yellow precipitate. The solid was then isolated by filtration, washed with benzene, and then dried overnight.

Preparation of [Cp*Ir(4,4'-methyl-2,2'-bipyridine)H]Cl (**Ir1a-H**). This complex was



synthesized by method C with 5 M NaOH, and was obtained as a yellow solid (76% overall yield after 2 steps). The characterization data for this material matched those reported previously.⁸

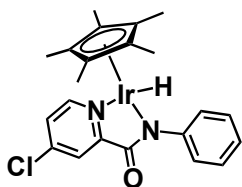
Preparation of [Cp*Ir(*N*-butyl-2-pyridinecarboxamidate)H] (**Ir5-H**). This complex was



synthesized by method A and was obtained as an orange-yellow solid (79% yield, a minor impurity could not be removed). ¹H NMR (CD₃OD, 500 MHz): 8.72 (d, *J* = 5.5 Hz, 1H), 7.87 (t, *J* = 7.8 Hz, 0H),

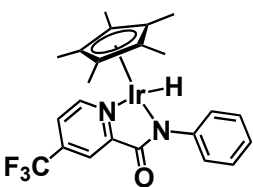
7.80 (d, *J* = 7.2 Hz, 1H), 7.38 (dd, *J* = 7.2, 5.5 Hz, 1H), 4.35-4.24 (m, 1H), 2.94-2.85 (m, 1H), 1.82 (s, 15H), 1.64-1.55 (m, 1H), 1.54-1.43 (m, 1H), 1.40-1.21 (m, 6H), 0.95 (t, *J* = 7.2 Hz, 3H), 0.88 (t, *J* = 7.2 Hz, 3H), -12.17 (s, 1H, Ir-H) ppm. ¹³C NMR (CD₃OD, 126 MHz): 170.1, 156.2, 152.5, 137.2, 127.0, 125.8, 89.1, 50.6, 32.7, 20.9, 14.3, 9.5 ppm.

Preparation of [Cp*Ir(*N*-phenyl-2-(4-chloropyridine)carboxamidate)H] (**Ir16-H**). This



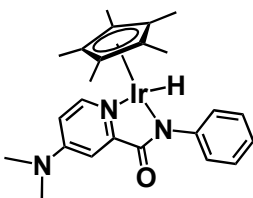
complex was synthesized by method A and was obtained as an orange-yellow solid (90% yield). ¹H NMR (CD₃CN, 600 MHz): 8.48 (d, *J* = 6.1 Hz, 1H), 7.72 (s, 1H), 7.29 (m, 1H), 7.16 (t, *J* = 7.5 Hz, 2H), 7.11 (d, *J* = 7.6 Hz, 2H), 6.92 (t, *J* = 7.2 Hz, 1H), 1.38 (s, 12H), -11.26 (s, 1H, Ir-H) ppm. ¹³C NMR (CD₃CN, 151 MHz): 168.9, 157.6, 154.0, 149.8, 145.6, 129.5, 128.2, 127.7, 127.0, 125.7, 89.7, 9.5 ppm.

Preparation of [Cp*Ir(*N*-phenyl-2-(4-trifluoromethylpyridine)carboxamidate)H] (**Ir17-**



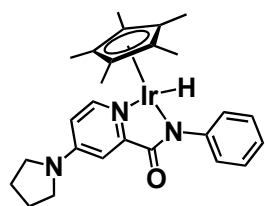
H). This complex was synthesized by method B and was obtained as a orange solid (79% yield). ¹H NMR (CD₃OD, 500 MHz): 9.06 (d, *J* = 5.9 Hz, 1H), 8.10 (s, 1H), 7.73 (d, *J* = 5.9, 1H), 7.37 (t, *J* = 7.6 Hz, 2H), 7.23 (d, *J* = 7.8 Hz, 2H), 7.14 (t, *J* = 7.5 Hz, 1H), 1.57 (s, 15H), -11.28 (s, 1H, Ir-H) ppm. ¹³C NMR (CD₃OD, 126 MHz): 167.6, 156.3, 153.2, 148.3, 128.2, 126.3, 124.5, 122.4, 121.2, 88.9, 67.5, 25.2, 8.1 ppm. ¹⁹F NMR (CD₃OD, 470 MHz): -66.2 ppm.

Preparation of [Cp*Ir(*N*-phenyl-2-(4-dimethylaminopyridine)carboxamidate)H] (**Ir18-H**).



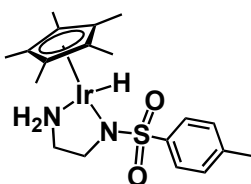
This complex was synthesized by method A and was obtained as a yellow solid (81% yield). ¹H NMR (CD₃OD, 500 MHz): 8.20 (d, *J* = 6.7 Hz, 1H), 7.33 (t, *J* = 7.6 Hz, 2H), 7.22 (d, *J* = 6.9 Hz, 2H), 7.17 (s, 1H), 7.08 (t, *J* = 7.2 Hz, 1H), 6.74 (dd, *J* = 6.8, 3.3 Hz, 1H), 3.33 (s, 1H), 3.12 (s, 6H), 2.67 (s, 1H), 1.52 (s, 12H), -11.30 (s, 1H, Ir-H) ppm. ¹³C NMR (CD₃OD, 126 MHz): 170.2, 155.7, 155.2, 151.8, 150.22, 129.1, 127.8, 125.1, 109.8, 108.9, 88.3, 39.3, 9.5 ppm.

Preparation of [Cp*Ir(*N*-phenyl-2-(4-pyrrolidinylpyridine)carboxamidate)H] (Ir19-H).



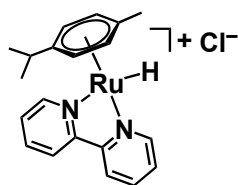
This complex was synthesized by method A and as obtained as a yellow solid (76% yield). ¹H NMR (CD₃OD, 500 MHz): 8.16 (d, *J* = 6.6 Hz, 1H), 7.34 (dd, *J* = 10.8, 4.5 Hz, 2H), 7.22 (d, *J* = 7.4 Hz, 2H), 7.09 (dd, *J* = 10.8, 4.5 Hz, 1H), 7.03 (d, *J* = 3.0 Hz, 1H), 6.59 (dd, *J* = 6.6, 3.0 Hz, 1H), 3.45 (t, *J* = 6.5 Hz, 4H), 2.09-2.03 (m, 4H), 1.54 (s, 15H), -11.28 (s, 1H, Ir-H) ppm. ¹³C NMR (CD₃OD, 126 MHz): 170.4, 155.2, 153.2, 151.9, 150.4, 129.2, 128.0, 125.2, 110.4, 109.5, 88.5, 26.4, 25.3, 9.6 ppm.

Preparation of [Cp*Ir(*N*-tosylethylenediamine)H] (Ir20-H). This complex was



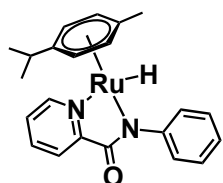
synthesized by method B and was obtained as a dark yellow sticky solid (76% yield, a minor impurity could not be removed). ¹H NMR (CD₃OD, 500 MHz): 7.66 (d, *J* = 8.3 Hz, 2H), 7.18 (d, *J* = 7.7 Hz, 2H), 2.61 (m, 1H), 2.43 (m, 1H), 2.33 (s, 3H), 2.24 (m, 1H), 2.15 (m, 1H), 1.82 (s, 15H), -11.45 (s, 1H, Ir-H) ppm.

Preparation of [(cymene)Ru(2,2'-bipyridine)H](Cl) (Ru5-H). This complex was



synthesized by method C with 1 M NaOH, and was obtained as a yellow solid (70% overall yield after 2 steps). The characterization data for this material matched those reported previously.⁶

Preparation of [(cymene)Ru(*N*-phenyl-2-pyridinecarboxamidate)H](Cl) (Ru6-H). This



complex was synthesized by method A with only 1.5 equiv. of NaBH₄. Product was obtained as a dark brown-orange sticky solid (80% yield, not pure). ¹H NMR (D₂O, 500 MHz): 10.18 (d, *J* = 5.1 Hz, 1H), 9.34

(t, $J = 7.7$ Hz, 1H), 9.27 (d, $J = 7.7$ Hz, 1H), 8.81 (t, $J = 6.8$ Hz, 1H), 8.76 (t, $J = 7.7$ Hz, 2H), 8.62 – 8.49 (m, 3H), 6.53 (d, $J = 5.9$ Hz, 1H), 6.44 (d, $J = 5.8$ Hz, 1H), 6.23 (d, $J = 6.0$ Hz, 1H), 6.08 (d, $J = 6.0$ Hz, 1H), 3.80 (m, 1H), 3.51 (s, 3H), 2.52 (dd, $J = 19.2, 6.8$ Hz, 6H), -4.40 (s, 1H, Ir–H) ppm.

Procedure for Transfer Hydrogenation/Product Quantification

The following reagents from individually prepared stock solutions were combined in a 20 mL scintillation vial: benzaldehyde (18 μ mol), HCOONa (54 μ mol), and metal complex (0.09 μ mol). The mixture was diluted with *t*-BuOH/PBS (1:9) to give a total volume of 3.0 mL. The vial was then tightly sealed with a screw cap and the reaction was allowed to proceed at 37 °C. After 1 h, biphenyl (12 μ mol) was added as an internal standard and the reaction mixture was further diluted with isopropanol (12 mL). The solution was then filtered through a pipette plug containing celite and Na₂SO₄ before the sample was analyzed by GC.

Procedure for Hydride Exchange Studies

Inside the glovebox, a Ir or Ru chloride complex (0.01 mmol) was dissolved in 0.4 mL of THF and then mixed with an aqueous solution of another Ir or Ru hydride complex (0.01 mmol) in 0.4 mL of D₂O with NaP_i buffer (32.9 mg NaH₂PO₄ + 37.1 mg Na₂HPO₄ + 5.0 mL D₂O). The reaction mixture was filtered through a pipette plug to remove any undissolved particulates and then transferred to a J Young NMR tube. The NMR tube was sealed with a Teflon screw cap and then taken outside of the glovebox for spectral measurements. The NMR spectra of all samples were collected right after mixing (0 h), and then every 2, 5, 8, 24, 28, 32, and 48 h.

Hydricity Calculation

Equilibrium Constant (K_{eq}) Calculation: K_{eq} was calculated using the equation ($[\text{product \#1}] \times [\text{product \#2}] / ([\text{starting material \#1}] \times [\text{starting material \#2}])$). The relative concentrations of all four compounds were determined by integrating their respective signals in the ^1H NMR spectra of the reaction between starting material #1 and #2. The equilibrium constants were calculated at different reaction times (2–48 h) and the average K_{eq} was determined from various time points (3–5) after the hydride exchange process had reached equilibrium.

Hydricity (ΔG_{H^-}) Calculation: The free energy terms ΔG_{H^-} were calculated using the average K_{eq} values determined. A literature method was used for these calculations.³³

Procedure for Catalyst Stability Studies

The Ir-Cl complex (0.01 μmol) was dissolved in CDCl_3 (0.5 mL) or THF: D_2O (1:1, 0.5 mL), filtered to remove insoluble particles, and then transferred to an NMR tube. The ^1H NMR spectra were recorded at different time points and compared to determine whether the iridium complexes had undergone any changes in solution over time.

Procedure for Hydrolysis Studies

The Ir-Cl complex (1.0 μmol) was combined with AgOTf (1.0 μmol) in $\text{CD}_3\text{OD}:\text{D}_2\text{O}$ (1:4, 0.5 mL). The mixture was stirred for 5 min and then filtered to remove a white precipitate. The light yellow filtrate was recorded by ^1H NMR spectroscopy (D_2O , 600 MHz, 1000 scans). This solution was treated with 0.5–50 equiv. of aqueous NaCl relative to the iridium complex (1–100 mM concentration of salt, respectively) and the spectral changes were measured accordingly (D_2O , 600 MHz, 800 scans).

Procedure for Catalyst Recycling Studies

The appropriate volumes of stock solutions containing the following reagents were combined in a 100 mL round bottom flask: benzaldehyde (1.0 mmol), sodium formate (2.0 mmol), and catalyst (0.02 mmol) in 20 mL of *t*-BuOH/H₂O (2:8). The flask was sealed with a rubber septum, and vented with a needle inserted into the septum. The reaction was stirred at 37 °C for 8 h. Phenol (60 mg, 0.64 mmol) was added into the reaction mixture as an internal standard for GC analysis. After the completion of each reaction cycle, the products were analyzed by gas chromatography. The volatiles were then removed by vacuum and additional amounts of benzaldehyde (1.0 mmol, sodium formate (2.0 mmol), and solvent were added for subsequent rounds of transfer hydrogenation.

Procedure for Kinetic Studies by GC

The appropriate volumes of stock solutions containing the following reagents were combined in a reaction flask: benzaldehyde, HCOONa, metal complex, and phenol (as a GC internal standard). The mixture was then diluted with *t*-BuOH/PBS (1:9) to a total volume of 30 mL to obtain the desired concentrations. The flask was sealed with a rubber septum, and vented with a needle inserted into the septum. The reaction was allowed to proceed at the desired temperature. At different time points, aliquots containing 3.0 mL of the reaction mixture were removed via syringe for GC analysis. The fractions collected were extracted into ethyl acetate, filtered through a pipette plug containing silica gel and sodium sulfate to remove the catalyst and water, respectively, and then analyzed by GC.

Procedure for Hydride Formation Studies by UV-vis Absorption Spectroscopy

Inside the glovebox, 50 μL of a stock solution containing the Ir-Cl complex (0.09 μmol , 1.8 mM) and 2.9 mL of THF:H₂O (1:9) were added to a quartz cuvette. The cuvette was sealed with a septum screw cap and then brought outside of the glovebox to be measured by UV-Vis absorption spectroscopy. A 50 μL stock solution of HCOONa (0.18 μmol , 2.0 equiv.) was then injected into the cuvette and the reaction was stirred at 25°C while the spectral changes were recorded at periodic intervals.

Procedure for Hydride Transfer Studies by UV-vis Absorption Spectroscopy

Inside the glovebox, 50 μL of a stock solution containing the Ir-H complex (0.09 μmol , 1.8 mM) and 2.9 mL of THF:H₂O (1:9) were added to a quartz cuvette. The cuvette was sealed with a septum screw cap and then brought outside of the glovebox to be measured by UV-Vis absorption spectroscopy. A 50 μL stock solution of benzaldehyde (0.18 μmol , 2.0 equiv.) was then injected into the cuvette and the reaction was stirred at 25°C while the spectral changes were recorded at periodic intervals.

Reaction Rate Calculation from UV-vis Absorption Spectroscopic Kinetic Experiments

The UV-vis absorption spectroscopic data were fit to a bimolecular reaction rate law ($v = k[A][B]$)⁴³ using the following equation:

$$Y_t = \frac{Y_\infty + \left[Y_0 \left(1 - \frac{[A]_0}{[B]_0} \right) - Y_\infty \right] e^{-k\Delta t}}{1 - \frac{[A]_0}{[B]_0} e^{-k\Delta t}}$$

where $[A]_0$ = initial concentration of reactant A, $[B]_0$ = initial concentration of reactant B, Y_0 = initial absorbance, Y_t = absorbance at time t , Y_∞ = absorbance at infinite time, k = kinetic rate constant, and $\Delta_0 = [B]_0 - [A]_0$. The reaction rate constants k was determined from the average values from two independent experiments.

4.8 References

1. Wang, D.; Astruc, D., The Golden Age of Transfer Hydrogenation. *Chemical Reviews* **2015**, *115* (13), 6621-6686.
2. Albrecht, M.; Crabtree, R. H.; Mata, J.; Peris, E., Chelating bis-carbene rhodium(iii) complexes in transfer hydrogenation of ketones and imines. *Chemical Communications* **2002**, (1), 32-33.
3. Dani, P.; Karlen, T.; Gossage, R. A.; Gladiali, S.; van Koten, G., Hydrogen-Transfer Catalysis with Pincer-Aryl Ruthenium(II) Complexes. *Angewandte Chemie International Edition* **2000**, *39* (4), 743-745.
4. Fu, S.; Chen, N.-Y.; Liu, X.; Shao, Z.; Luo, S.-P.; Liu, Q., Ligand-Controlled Cobalt-Catalyzed Transfer Hydrogenation of Alkynes: Stereodivergent Synthesis of Z- and E-Alkenes. *Journal of the American Chemical Society* **2016**, *138* (27), 8588-8594.
5. Hashiguchi, S.; Fujii, A.; Takehara, J.; Ikariya, T.; Noyori, R., Asymmetric Transfer Hydrogenation of Aromatic Ketones Catalyzed by Chiral Ruthenium(II) Complexes. *Journal of the American Chemical Society* **1995**, *117* (28), 7562-7563.
6. Kang, S.; Han, J.; Lee, E. S.; Choi, E. B.; Lee, H.-K., Enantioselective Synthesis of Cyclic Sulfamides by Using Chiral Rhodium-Catalyzed Asymmetric Transfer Hydrogenation. *Organic Letters* **2010**, *12* (18), 4184-4187.
7. Li, F.; Ma, J.; Wang, N., α -Alkylation of Ketones with Primary Alcohols Catalyzed by a Cp*Ir Complex Bearing a Functional Bipyridonate Ligand. *The Journal of Organic Chemistry* **2014**, *79* (21), 10447-10455.
8. Ogo, S.; Makihara, N.; Kaneko, Y.; Watanabe, Y., pH-Dependent Transfer Hydrogenation, Reductive Amination, and Dehalogenation of Water-Soluble Carbonyl Compounds and Alkyl Halides Promoted by Cp*Ir Complexes. *Organometallics* **2001**, *20* (23), 4903-4910.
9. Shibahara, F.; Bower, J. F.; Krische, M. J., Diene Hydroacylation from the Alcohol or Aldehyde Oxidation Level via Ruthenium-Catalyzed C-C Bond-Forming Transfer Hydrogenation: Synthesis of β,γ -Unsaturated Ketones. *Journal of the American Chemical Society* **2008**, *130* (43), 14120-14122.
10. Wang, Y.; Huang, Z.; Leng, X.; Zhu, H.; Liu, G.; Huang, Z., Transfer Hydrogenation of Alkenes Using Ethanol Catalyzed by a NCP Pincer Iridium Complex: Scope and Mechanism. *Journal of the American Chemical Society* **2018**, *140* (12), 4417-4429.
11. Yamada, I.; Noyori, R., Asymmetric Transfer Hydrogenation of Benzaldehydes. *Organic Letters* **2000**, *2* (22), 3425-3427.
12. Hull, J. F.; Himeda, Y.; Wang, W.-H.; Hashiguchi, B.; Periana, R.; Szalda, D. J.; Muckerman, J. T.; Fujita, E., Reversible hydrogen storage using CO₂ and a proton-switchable iridium catalyst in aqueous media under mild temperatures and pressures. *Nature Chemistry* **2012**, *4*, 383.

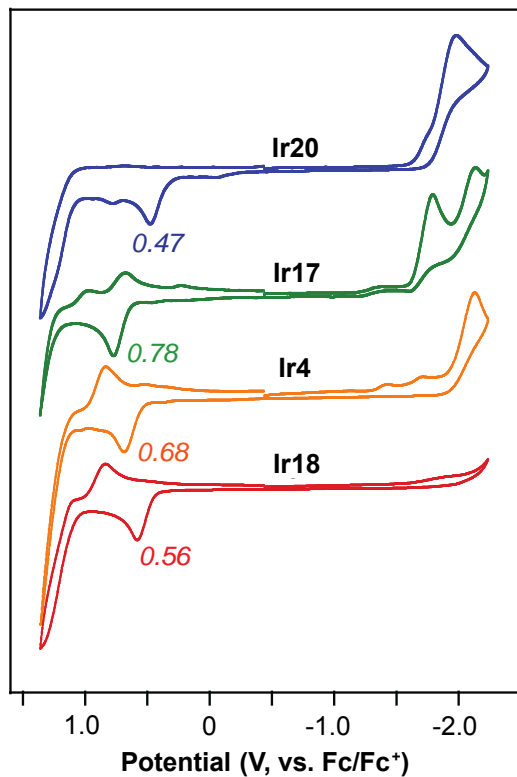
13. Wang, L.; Ertem, M. Z.; Murata, K.; Muckerman, J. T.; Fujita, E.; Himeda, Y., Highly Efficient and Selective Methanol Production from Paraformaldehyde and Water at Room Temperature. *ACS Catalysis* **2018**, *8* (6), 5233-5239.
14. Zhang, J.; Chen, J., Selective Transfer Hydrogenation of Biomass-Based Furfural and 5-Hydroxymethylfurfural over Hydrotalcite-Derived Copper Catalysts Using Methanol as a Hydrogen Donor. *ACS Sustainable Chemistry & Engineering* **2017**, *5* (7), 5982-5993.
15. Wang, L.; Ertem, M. Z.; Kanega, R.; Murata, K.; Szalda, D. J.; Muckerman, J. T.; Fujita, E.; Himeda, Y., Additive-Free Ruthenium-Catalyzed Hydrogen Production from Aqueous Formaldehyde with High Efficiency and Selectivity. *ACS Catalysis* **2018**, *8* (9), 8600-8605.
16. Soldevila-Barreda, J. J.; Romero-Canelón, I.; Habtemariam, A.; Sadler, P. J., Transfer hydrogenation catalysis in cells as a new approach to anticancer drug design. *Nature Communications* **2015**, *6*, 6582.
17. Chen, F.; Romero-Canelón, I.; Soldevila-Barreda, J. J.; Song, J.-I.; Coverdale, J. P. C.; Clarkson, G. J.; Kasparkova, J.; Habtemariam, A.; Wills, M.; Brabec, V.; Sadler, P. J., Transfer Hydrogenation and Antiproliferative Activity of Tethered Half-Sandwich Organoruthenium Catalysts. *Organometallics* **2018**, *37* (10), 1555-1566.
18. Coverdale, J. P. C.; Romero-Canelón, I.; Sanchez-Cano, C.; Clarkson, G. J.; Habtemariam, A.; Wills, M.; Sadler, P. J., Asymmetric transfer hydrogenation by synthetic catalysts in cancer cells. *Nature Chemistry* **2018**, *10*, 347.
19. Li, J.; Guo, L.; Tian, Z.; Zhang, S.; Xu, Z.; Han, Y.; Li, R.; Li, Y.; Liu, Z., Half-Sandwich Iridium and Ruthenium Complexes: Effective Tracking in Cells and Anticancer Studies. *Inorganic Chemistry* **2018**.
20. McFarland, J. M.; Francis, M. B., Reductive Alkylation of Proteins Using Iridium Catalyzed Transfer Hydrogenation. *Journal of the American Chemical Society* **2005**, *127* (39), 13490-13491.
21. Monnard, F. W.; Nogueira, E. S.; Heinisch, T.; Schirmer, T.; Ward, T. R., Human carbonic anhydrase II as host protein for the creation of artificial metalloenzymes: the asymmetric transfer hydrogenation of imines. *Chemical Science* **2013**, *4* (8), 3269-3274.
22. Zhao, J.; Rebelein, J. G.; Mallin, H.; Trindler, C.; Pellizzoni, M. M.; Ward, T. R., Genetic Engineering of an Artificial Metalloenzyme for Transfer Hydrogenation of a Self-Immolative Substrate in *Escherichia coli*'s Periplasm. *Journal of the American Chemical Society* **2018**.
23. Ngo, A. H.; Ibañez, M.; Do, L. H., Catalytic Hydrogenation of Cytotoxic Aldehydes Using Nicotinamide Adenine Dinucleotide (NADH) in Cell Growth Media. *ACS Catalysis* **2016**, *6* (4), 2637-2641.

24. Ngo, A. H.; Bose, S.; Do, L. H., Intracellular Chemistry: Integrating Molecular Inorganic Catalysts with Living Systems. *Chemistry – A European Journal* **2018**, *24* (42), 10584-10594.
25. Betanzos-Lara, S.; Liu, Z.; Habtemariam, A.; Pizarro, A. M.; Qamar, B.; Sadler, P. J., Organometallic Ruthenium and Iridium Transfer-Hydrogenation Catalysts Using Coenzyme NADH as a Cofactor. *Angewandte Chemie International Edition* **2012**, *51* (16), 3897-3900.
26. Maenaka, Y.; Suenobu, T.; Fukuzumi, S., Efficient Catalytic Interconversion between NADH and NAD⁺ Accompanied by Generation and Consumption of Hydrogen with a Water-Soluble Iridium Complex at Ambient Pressure and Temperature. *Journal of the American Chemical Society* **2012**, *134* (1), 367-374.
27. Liu, Z.; Romero-Canelón, I.; Qamar, B.; Hearn, J. M.; Habtemariam, A.; Barry, N. P. E.; Pizarro, A. M.; Clarkson, G. J.; Sadler, P. J., The Potent Oxidant Anticancer Activity of Organoiridium Catalysts. *Angewandte Chemie International Edition* **2014**, *53* (15), 3941-3946.
28. Bose, S.; Ngo, A. H.; Do, L. H., Intracellular Transfer Hydrogenation Mediated by Unprotected Organoiridium Catalysts. *Journal of the American Chemical Society* **2017**, *139* (26), 8792-8795.
29. Wu, X.; Liu, J.; Li, X.; Zanotti-Gerosa, A.; Hancock, F.; Vinci, D.; Ruan, J.; Xiao, J., On Water and in Air: Fast and Highly Chemoselective Transfer Hydrogenation of Aldehydes with Iridium Catalysts. *Angewandte Chemie International Edition* **2006**, *45* (40), 6718-6722.
30. Noyori, R.; Hashiguchi, S., Asymmetric Transfer Hydrogenation Catalyzed by Chiral Ruthenium Complexes. *Accounts of Chemical Research* **1997**, *30* (2), 97-102.
31. Dedieu, A., Transition Metal Hydrides. *VCH Publishers: New York* **1992**.
32. Wiedner, E. S.; Chambers, M. B.; Pitman, C. L.; Bullock, R. M.; Miller, A. J. M.; Appel, A. M., Thermodynamic Hydricity of Transition Metal Hydrides. *Chemical Reviews* **2016**, *116* (15), 8655-8692.
33. Pitman, C. L.; Breton, K. R.; Miller, A. J. M., Aqueous Hydricity of Late Metal Catalysts as a Continuum Tuned by Ligands and the Medium. *Journal of the American Chemical Society* **2016**, *138* (7), 2252-2260.
34. Du, Q.; Guo, L.; Tian, M.; Ge, X.; Yang, Y.; Jian, X.; Xu, Z.; Tian, Z.; Liu, Z., Potent Half-Sandwich Iridium(III) and Ruthenium(II) Anticancer Complexes Containing a P⁺O-Chelated Ligand. *Organometallics* **2018**, *37* (17), 2880-2889.
35. Liu, Z.; Habtemariam, A.; Pizarro, A. M.; Fletcher, S. A.; Kisova, A.; Vrana, O.; Salassa, L.; Bruijninx, P. C. A.; Clarkson, G. J.; Brabec, V.; Sadler, P. J., Organometallic Half-Sandwich Iridium Anticancer Complexes. *Journal of Medicinal Chemistry* **2011**, *54* (8), 3011-3026.
36. Leiva, C.; Christine Lo, H.; Fish, R. H., Aqueous organometallic chemistry. 3. Catalytic hydride transfer reactions with ketones and aldehydes using

- [Cp*Rh(bpy)(H₂O)](OTf)₂ as the precatalyst and sodium formate as the hydride source: Kinetic and activation parameters, and the significance of steric and electronic effects. *Journal of Organometallic Chemistry* **2010**, 695 (2), 145-150.
37. Kang, J. W.; Moseley, K.; Maitlis, P. M., Pentamethylcyclopentadienylrhodium and -iridium halides. I. Synthesis and properties. *Journal of the American Chemical Society* **1969**, 91 (22), 5970-5977.
 38. Youinou, M.-T.; Ziessel, R., Synthesis and molecular structure of a new family of iridium-(III) and rhodium(III) complexes: [(η⁵-Me₅C₅)Ir(LL)X]⁺ and [(η⁵-Me₅C₅)Rh(LL)Cl]⁺; LL = 2,2'-bipyridine or 1,10-phenanthroline; X = Cl or H. Single crystal structures of [(η⁵-Me₅C₅)Ir(bpy)Cl]Cl and [(η⁵-Me₅C₅)Rh(phen)Cl]ClO₄. *Journal of Organometallic Chemistry* **1989**, 363 (1), 197-208.
 39. Dadci, L.; Elias, H.; Frey, U.; Hoernig, A.; Koelle, U.; Merbach, A. E.; Paulus, H.; Schneider, J. S., π-Arene Aqua Complexes of Cobalt, Rhodium, Iridium, and Ruthenium: Preparation, Structure, and Kinetics of Water Exchange and Water Substitution. *Inorganic Chemistry* **1995**, 34 (1), 306-315.
 40. Steckhan, E.; Herrmann, S.; Ruppert, R.; Dietz, E.; Frede, M.; Spika, E., Analytical study of a series of substituted (2,2'-bipyridyl)(pentamethylcyclopentadienyl)rhodium and -iridium complexes with regard to their effectiveness as redox catalysts for the indirect electrochemical and chemical reduction of NAD(P)⁺. *Organometallics* **1991**, 10 (5), 1568-1577.
 41. Bucci, A.; Dunn, S.; Bellachioma, G.; Menendez Rodriguez, G.; Zuccaccia, C.; Nervi, C.; Macchioni, A., A Single Organoiridium Complex Generating Highly Active Catalysts for both Water Oxidation and NAD⁺/NADH Transformations. *ACS Catalysis* **2017**, 7 (11), 7788-7796.
 42. Heiden, Z. M.; Gorecki, B. J.; Rauchfuss, T. B., Lewis Base Adducts Derived from Transfer Hydrogenation Catalysts: Scope and Selectivity. *Organometallics* **2008**, 27 (7), 1542-1549.
 43. Espenson, J. H., Chemical Kinetics and Reaction Mechanisms. *McGraw-Hill Education* **2002**, second edition.

Chapter 4 Appendix

A) CV in Dichloromethane



B) CV in PBS Buffer

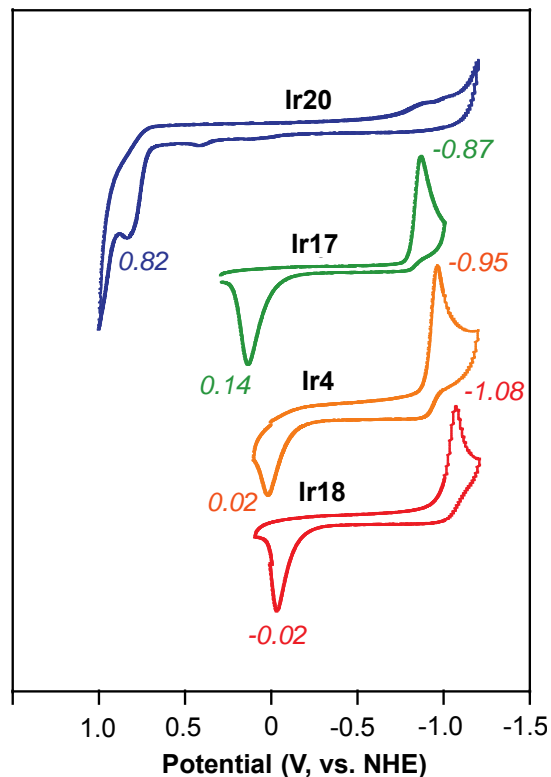


Figure A4.1. Cyclic voltammograms of complexes **2**, **8**, **10**, and **11**. A) Data recorded at 0.1 V/s in CH₂Cl₂ with 0.1 M N(Bu)₄PF₆ as supporting electrolyte, a glassy carbon working electrode, an Ag/AgCl reference electrode, and a Pt wire as the auxiliary electrode, with ferrocene as the external standard. B) CV recorded at 0.1 V/s in phosphate buffer saline (PBS) 0.1 M, a glassy carbon working electrode, an Ag/AgCl reference electrode, and a Pt wire as the auxiliary electrode. Potentials are referenced to NHE.

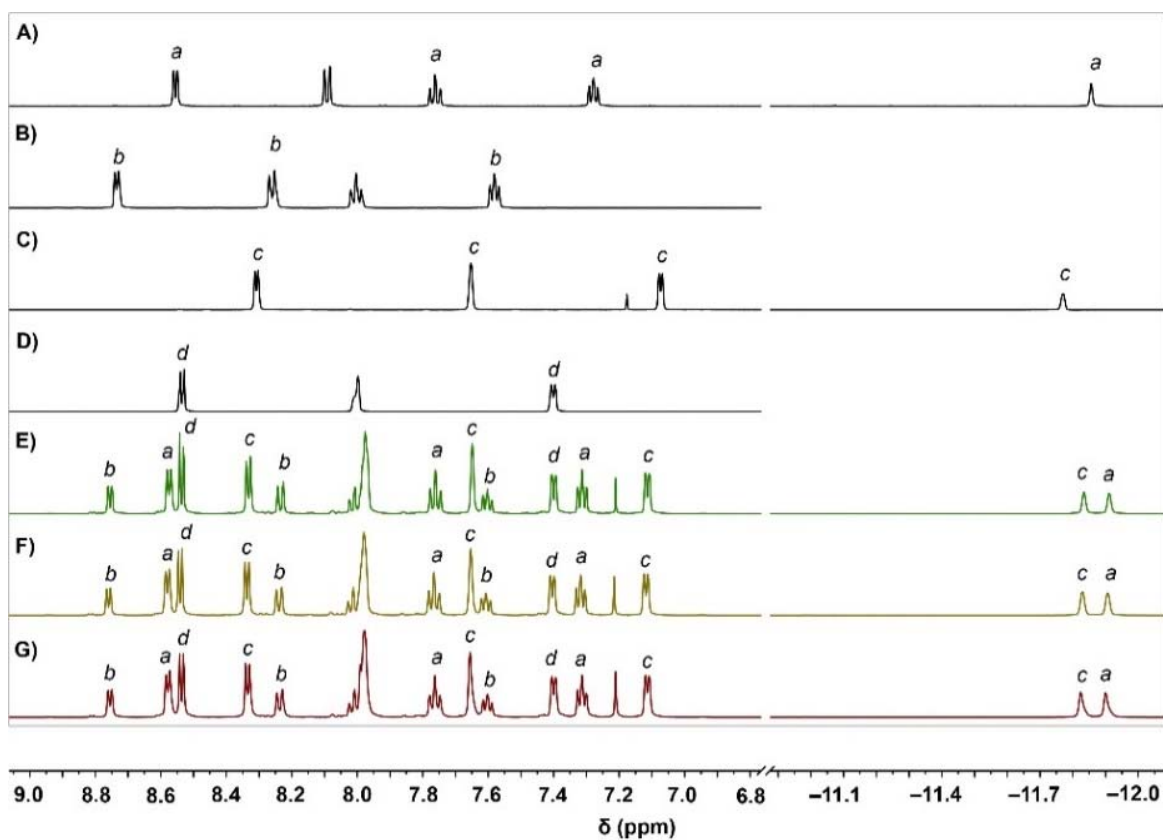


Figure A4.2. Hydride exchange study between complexes **1a** and **1b-H** in D₂O. The ¹H NMR spectra (600 MHz, CD₃OD) shown are as follows: A) complex **1a-H**; B) complex **1a**; C) complex **1b-H**; D) complex **1b**; E) reaction between **1b-H** and **1a** after 23 h; F) reaction between **1b-H** and **1a** after 4 h; and G) reaction between **1b-H** and **1a** immediately after mixing. The italicized lowercase letters above indicate which compounds the peaks are assigned to.

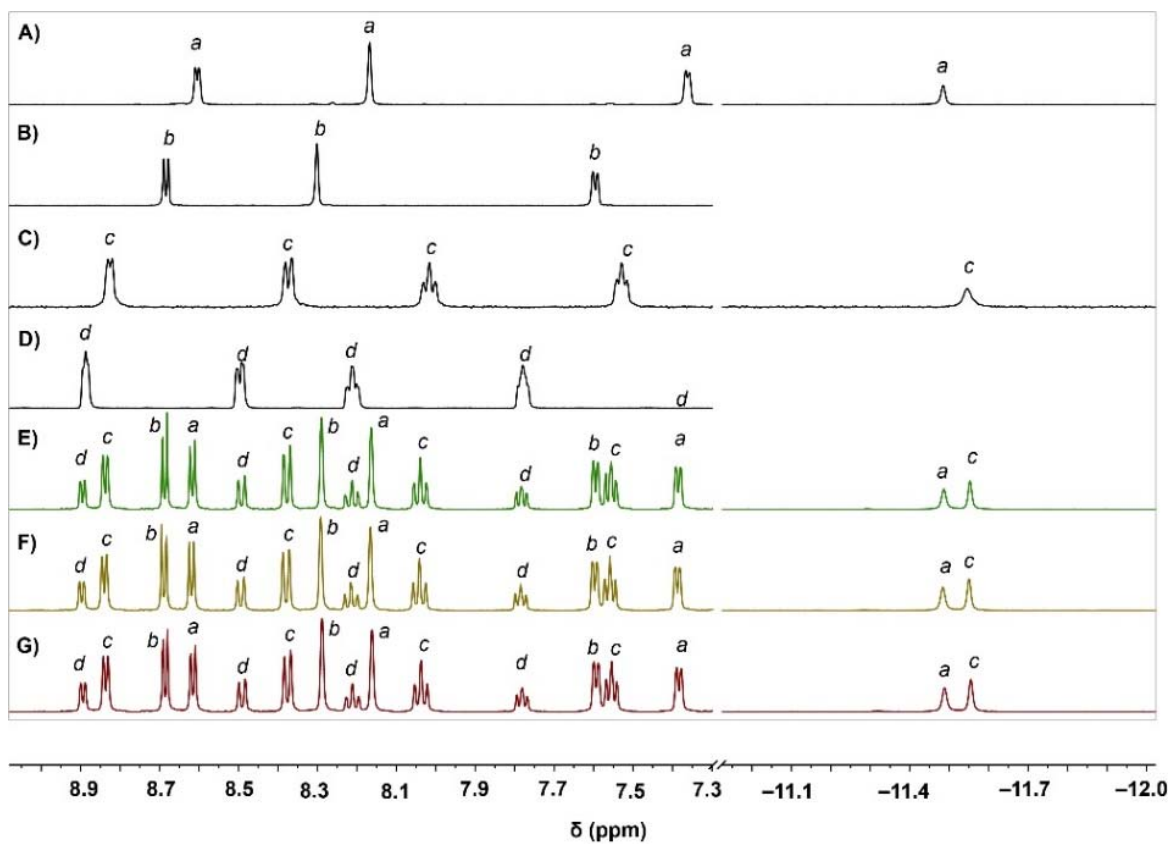


Figure A4.3. Hydride exchange study between complexes **1a** and **1b-H** in $D_2O:CH_3OH$ (1:1). The 1H NMR spectra (600 MHz, CD_3OD) shown are as follows: A) complex **Ir2-Me-H**; B) complex **Ir2-Me**; C) complex **Ir2-H**; D) complex **Ir2**; E) reaction between **Ir2-Me-H** and **Ir2** after 24 h; F) reaction between **Ir2-Me-H** and **Ir2** after 5 h; and G) reaction between **Ir2-Me-H** and **Ir2** immediately after mixing. The italicized lowercase letters above indicate which compounds the peaks are assigned to.

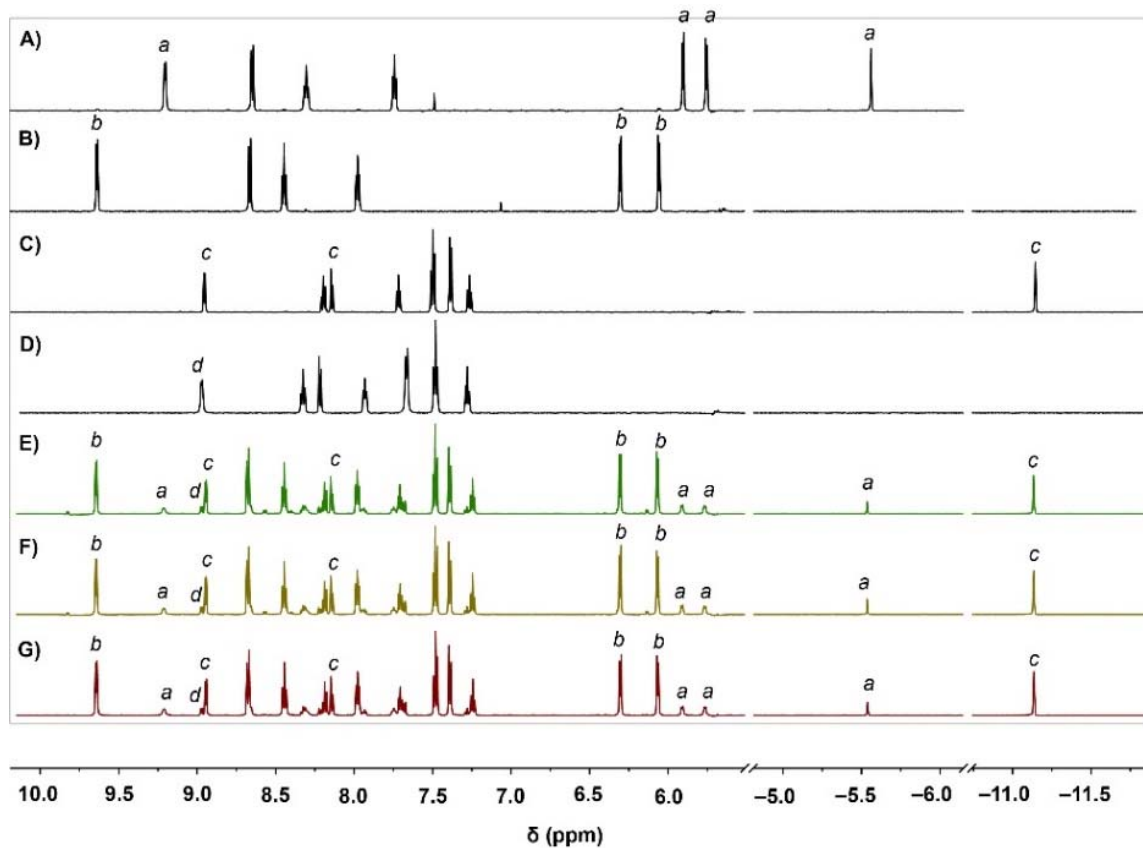


Figure A4.4. Hydride exchange study between complexes **Ir4-H** and **Ru6** in $D_2O:THF$ (1:1). The 1H NMR spectra (600 MHz, CD_3OD) shown are as follows: A) complex **Ru6-H**; B) complex **Ru6**; C) complex **Ir4-H**; D) complex **Ir4**; E) reaction between **Ru6-H** and **Ir4** after 25 h; F) reaction between **Ru6-H** and **Ir4** after 6 h; and G) reaction between **Ru6-H** and **Ir4** immediately after mixing. The italicized lowercase letters above indicate which compounds the peaks are assigned to.

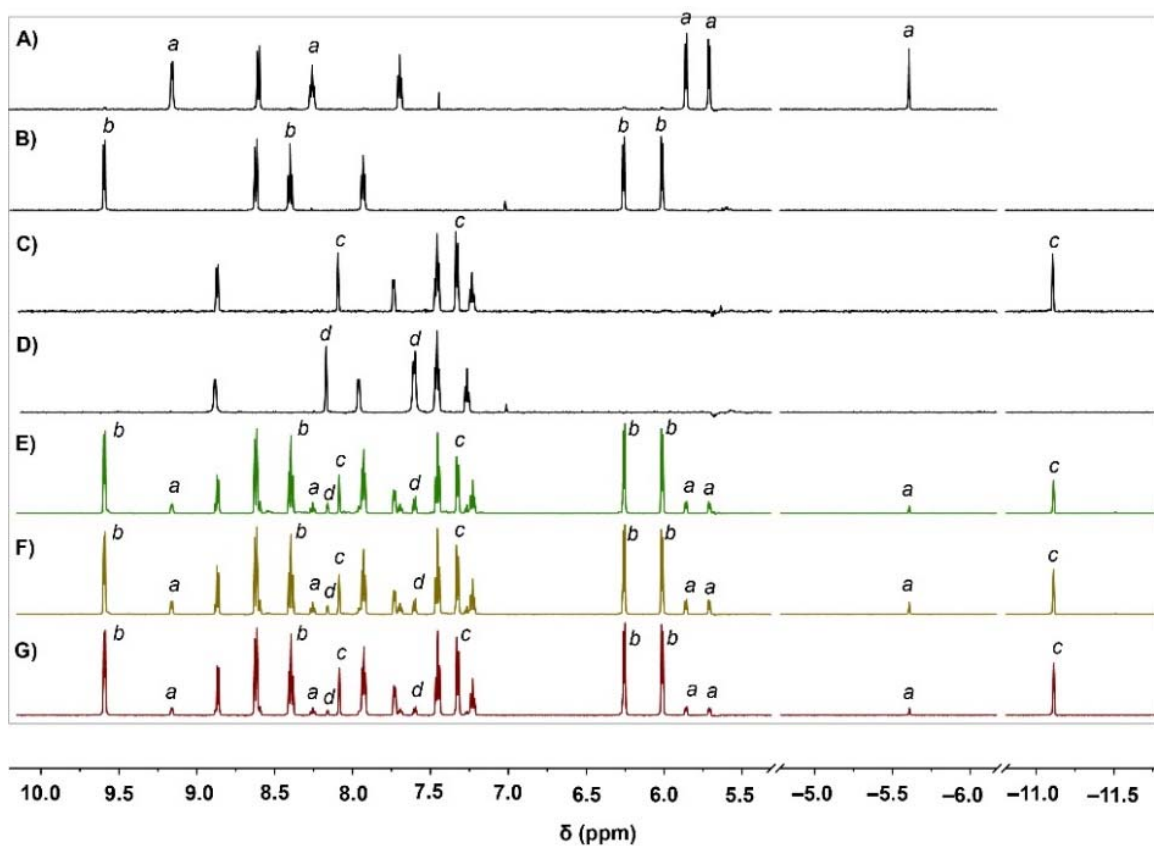


Figure A4.5. Hydride exchange study between complexes **Ir16-H** and **Ru6** in $D_2O:THF$ (1:1). The 1H NMR spectra (600 MHz, CD_3OD) shown are as follows: A) complex **Ru6-H**; B) complex **Ru6**; C) complex **Ir16-H**; D) complex **Ir16**; E) reaction between **Ir16-H** and **Ru6** after 26 h; F) reaction between **Ir16-H** and **Ru6** after 8 h; and G) reaction between **Ir16-H** and **Ru6** immediately after mixing. The italicized lowercase letters above indicate which compounds the peaks are assigned to.

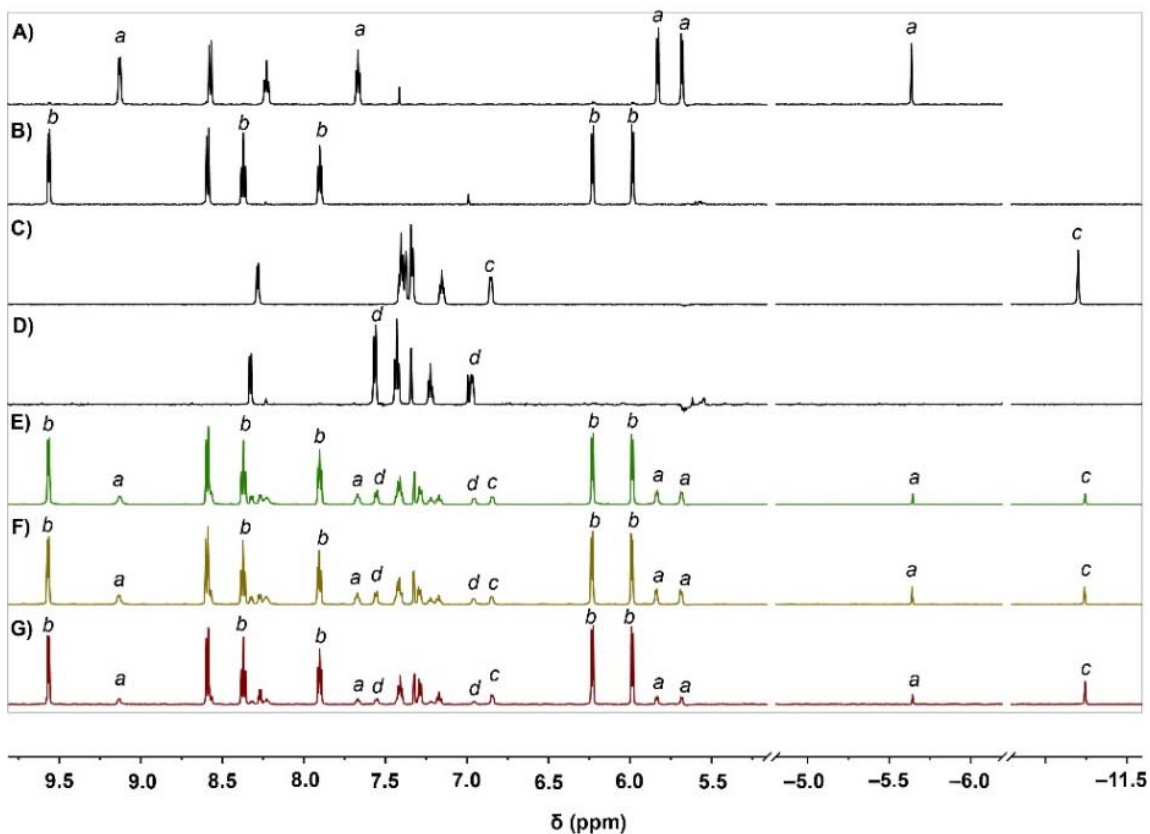


Figure A4.6. Hydride exchange study between complexes **Ir18-H** and **Ru6** in $D_2O:THF$ (1:1). The 1H NMR spectra (600 MHz, CD_3OD) shown are as follows: A) complex **Ru6-H**; B) complex **Ru6**; C) complex **Ir18-H**; D) complex **Ir18**; E) reaction between **Ir18-H** and **Ru6** after 25 h; F) reaction between **Ir18-H** and **Ru6** after 7 h; and G) reaction between **Ir18-H** and **Ru6** immediately after mixing. The italicized lowercase letters above indicate which compounds the peaks are assigned to.

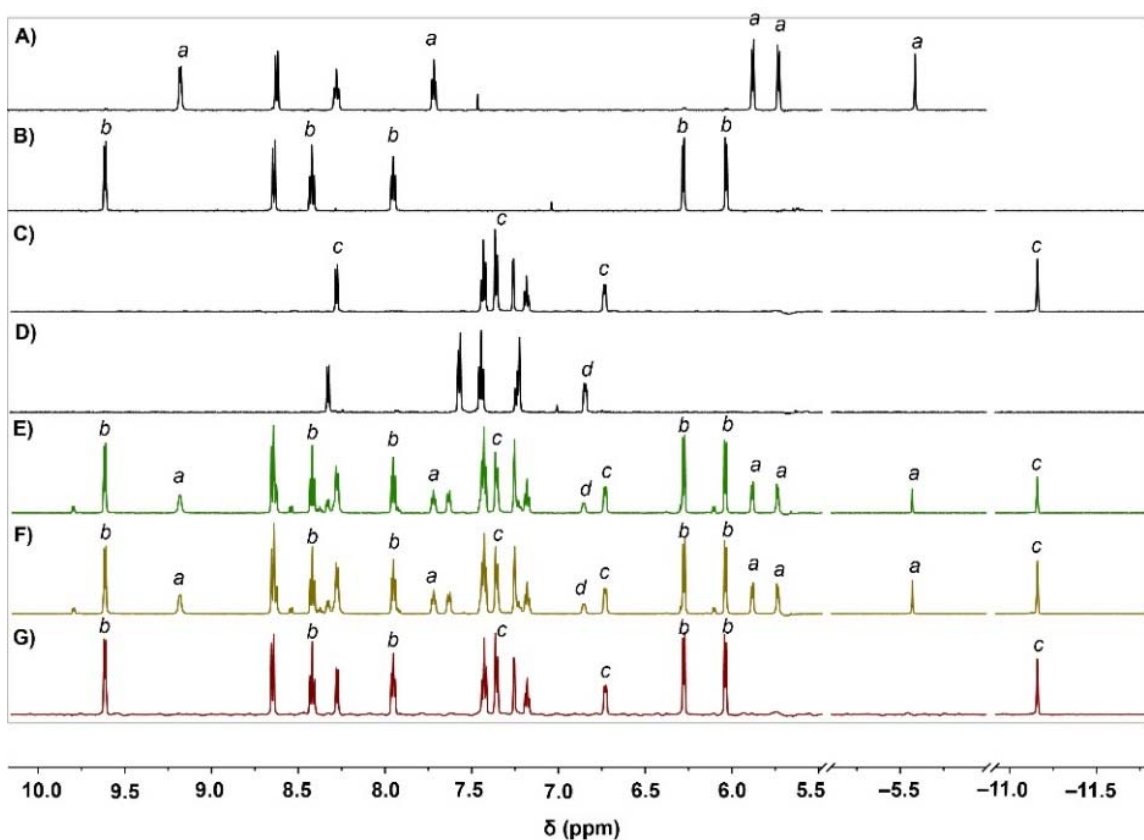


Figure A4.7. Hydride exchange study between complexes **Ir19-H** and **Ru6** in D₂O:THF (1:1). The ¹H NMR spectra (600 MHz, CD₃OD) shown are as follows: A) complex **Ru6-H**; B) complex **Ru6**; C) complex **Ir19-H**; D) complex **Ir19**; E) reaction between **Ir19-H** and **Ru6** after 24 h; F) reaction between **Ir19-H** and **Ru6** after 6 h; and G) reaction between **Ir19-H** and **Ru6** immediately after mixing. The italicized lowercase letters above indicate which compounds the peaks are assigned to.

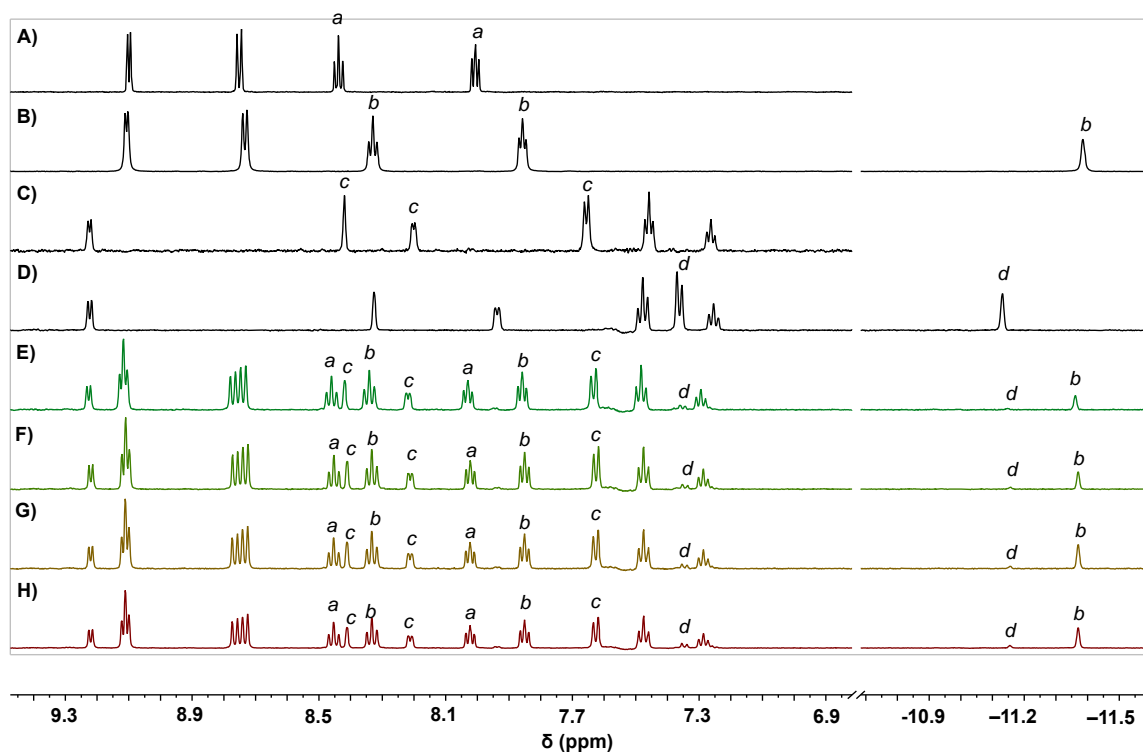


Figure A4.8. Hydride exchange study between complexes **Ir17-H** and **Ir2** in $D_2O:THF$ (1:1). The 1H NMR spectra (600 MHz, CD_3OD) shown are as follows: A) complex **Ir2**; B) complex **Ir2-H**; C) complex **Ir17**; D) complex **Ir17-H**; E) reaction between **Ir17-H** and **Ir2** after 24 h; F) reaction between **Ir17-H** and **Ir2** after 6 h; G) reaction between **Ir17-H** and **Ir2** after 2 h; and H) reaction between **Ir17-H** and **Ir2** immediately after mixing.

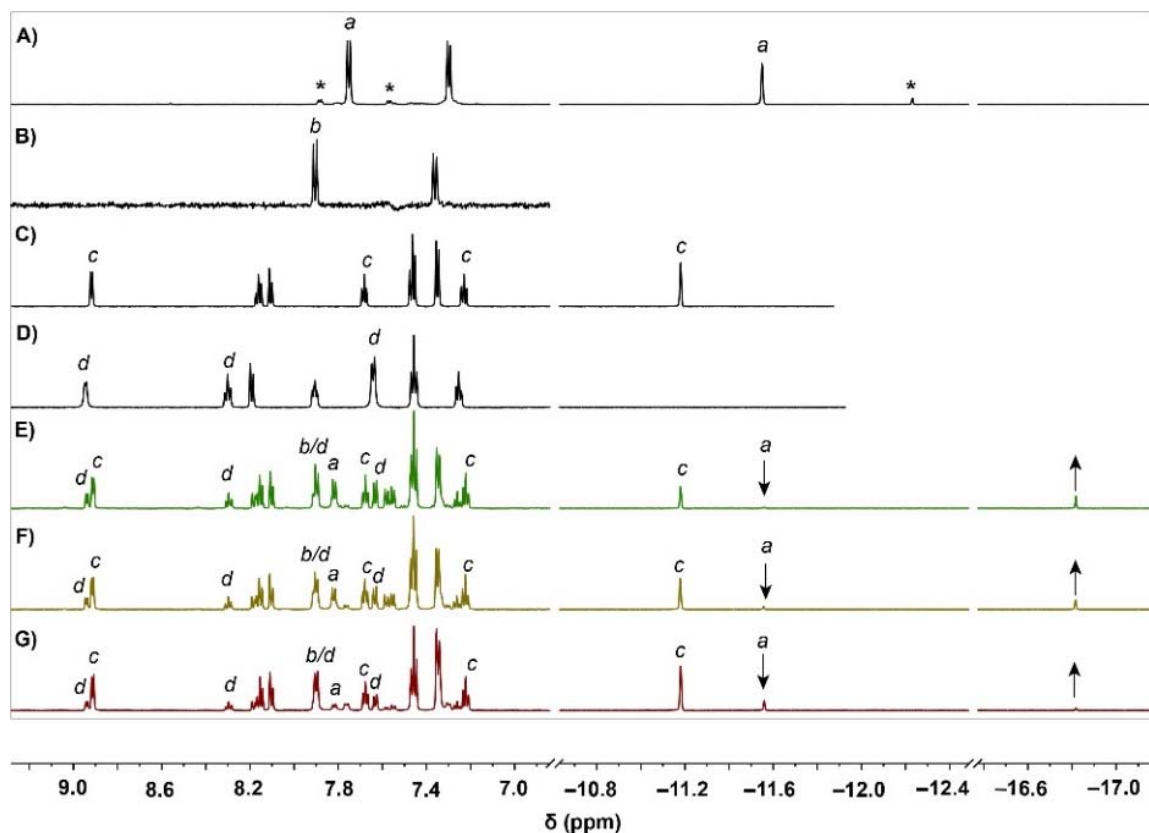


Figure A4.9. Hydride exchange study between complexes **Ir20** and **Ir4-H** in $D_2O:THF$ (1:1). The 1H NMR spectra (600 MHz, CD_3OD) shown are as follows: A) complex **Ir20-H**; B) complex **Ir20**; C) complex **Ir4-H**; D) complex **Ir4**; E) reaction between **Ir4-H** and **Ir20** after 24 h; F) reaction between **Ir4-H** and **Ir20** after 8 h; and G) reaction between **Ir4-H** and **Ir20** immediately after mixing. The italicized lowercase letters above indicate which compounds the peaks are assigned to. The peaks marked with an asterisk (*) in spectrum A has been assigned to a second Ir-H species of unknown identity. In spectra E–G, the peak at -16.8 ppm increases whereas the peak at -11.5 ppm decreases over time.

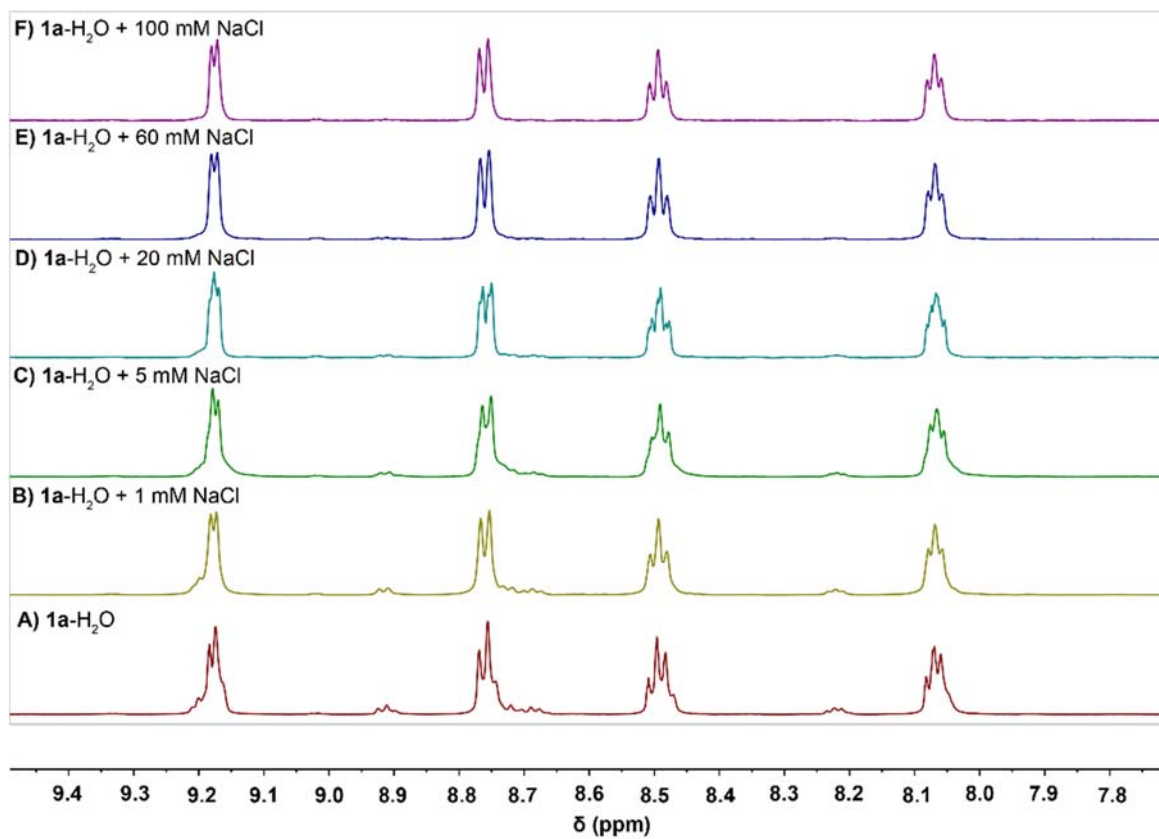


Figure A4.10. ^1H NMR spectra (600 MHz, D₂O) of complex **Ir2**-H₂O (2 mM) in the presence of various concentrations of NaCl.

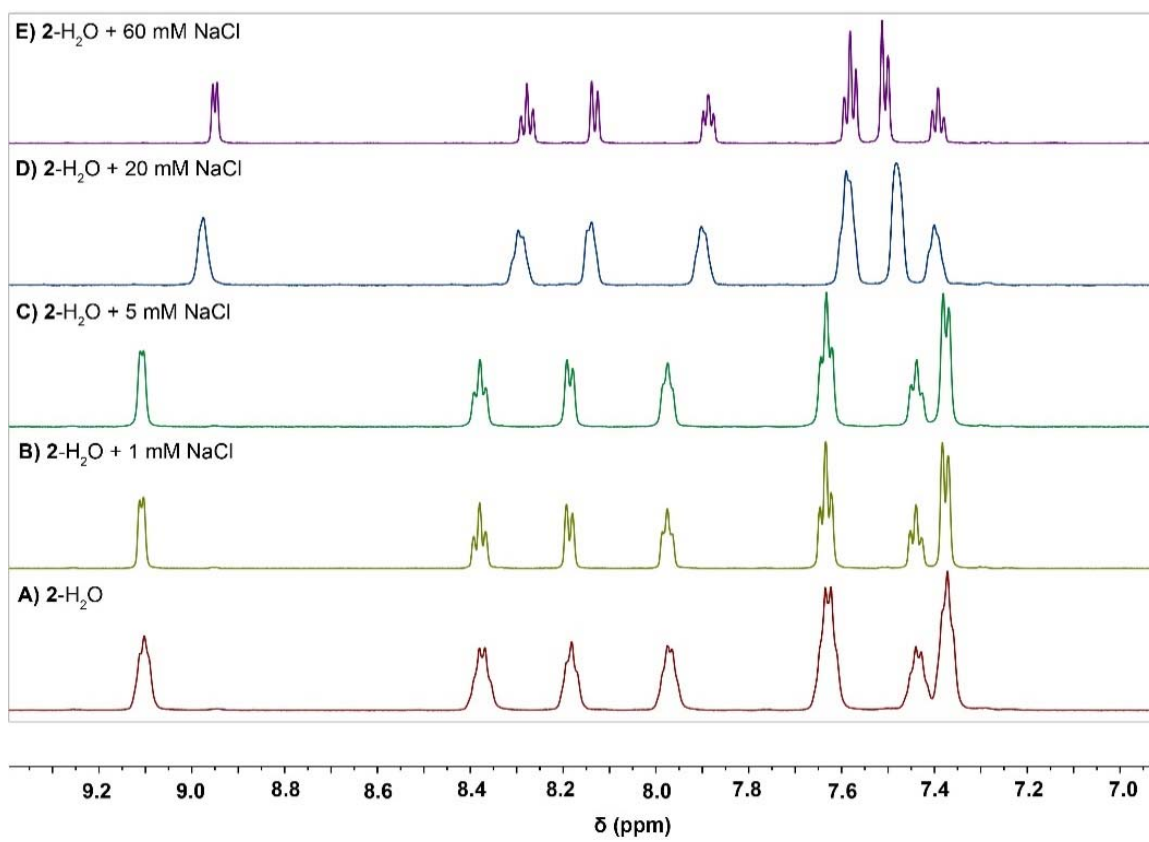


Figure A4.11. ¹H NMR spectra (600 MHz, D₂O) of complex **Ir4**-H₂O (2 mM) in the presence of various concentrations of NaCl.

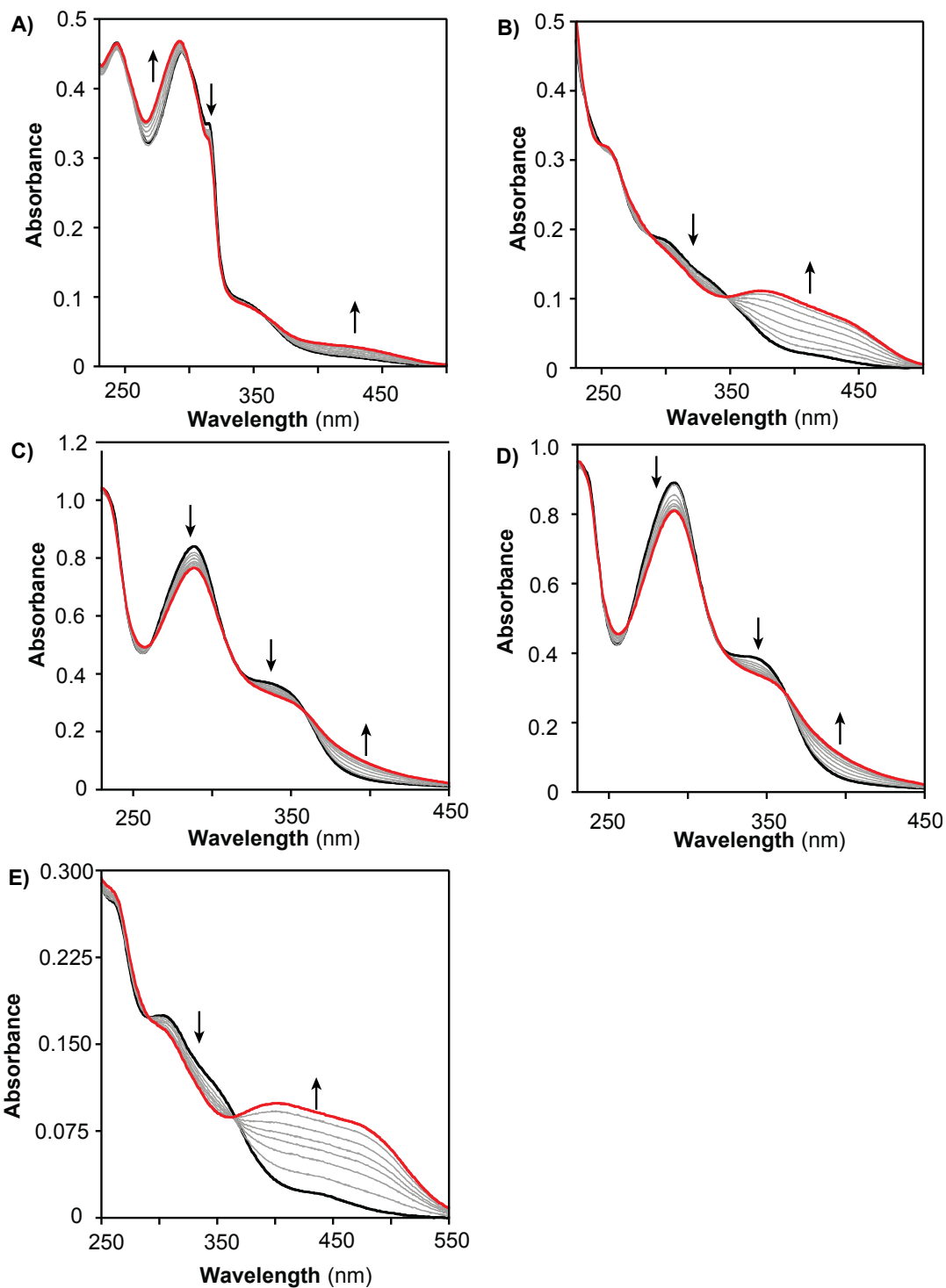


Figure A4.12. Reactions of iridium complexes (30 μM) with sodium formate (60 μM) in THF:H₂O (1:9) at 25°C. The data show the UV-vis absorbance spectra of A) complex **Ir2**; B) complex **Ir4**; C) complex **Ir18**; D) complex **Ir19**; and E) complex **Ir17** after mixing with sodium formate. The black trace is the initial spectrum and the red trace is the final spectrum.

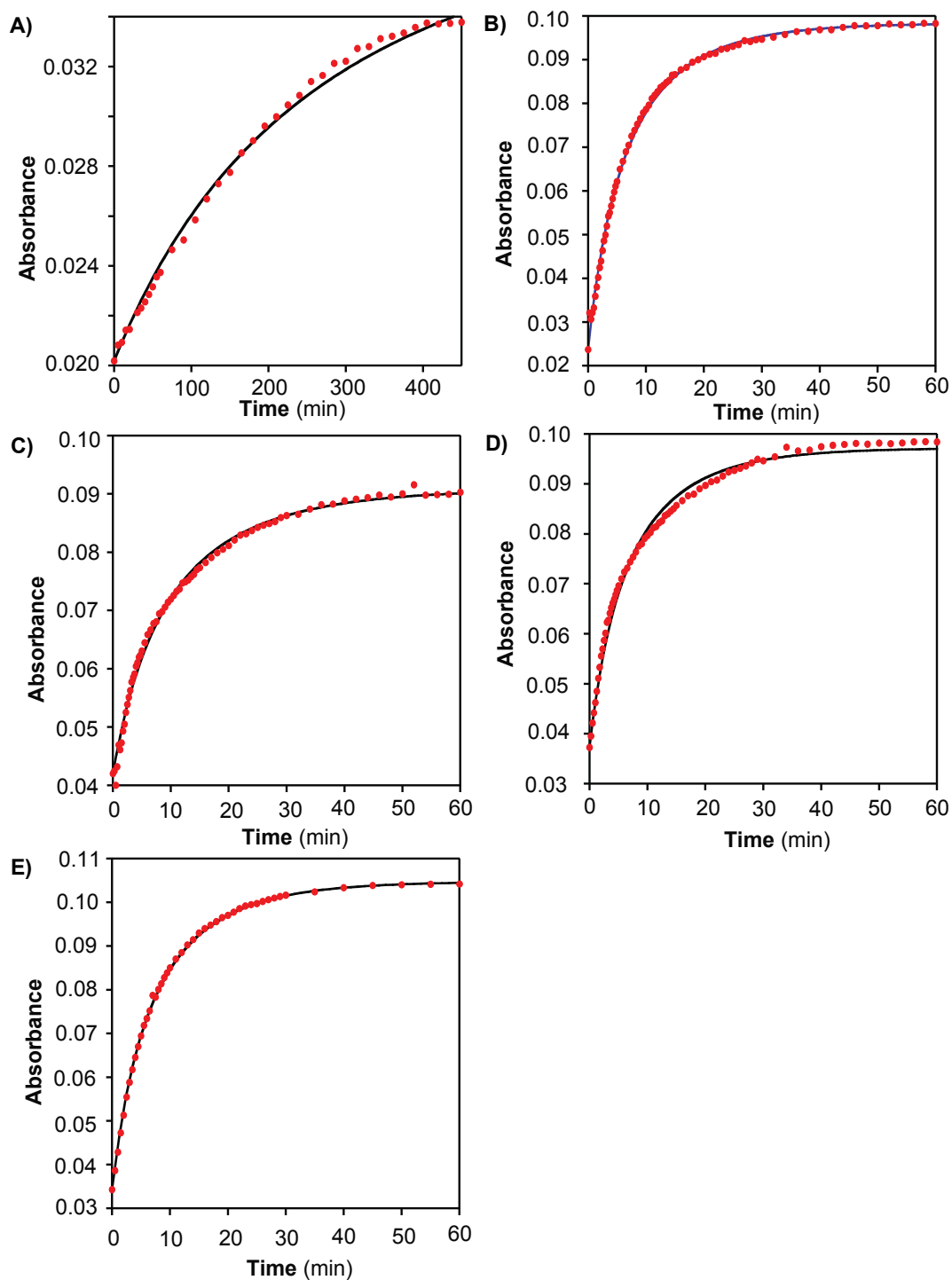


Figure A4.13. Kinetic plots for the reaction of iridium complexes (30 μM) with sodium formate (60 μM) in THF:H₂O (1:9) at 25°C. The data show the UV-Vis spectra at $\lambda = 400$ nm of A) complex **Ir2**; B) complex **Ir4**; C) complex **Ir18**; D) complex **Ir19**; and E) complex **Ir17**. The raw data are shown as red dots and the black lines are the curve fits.

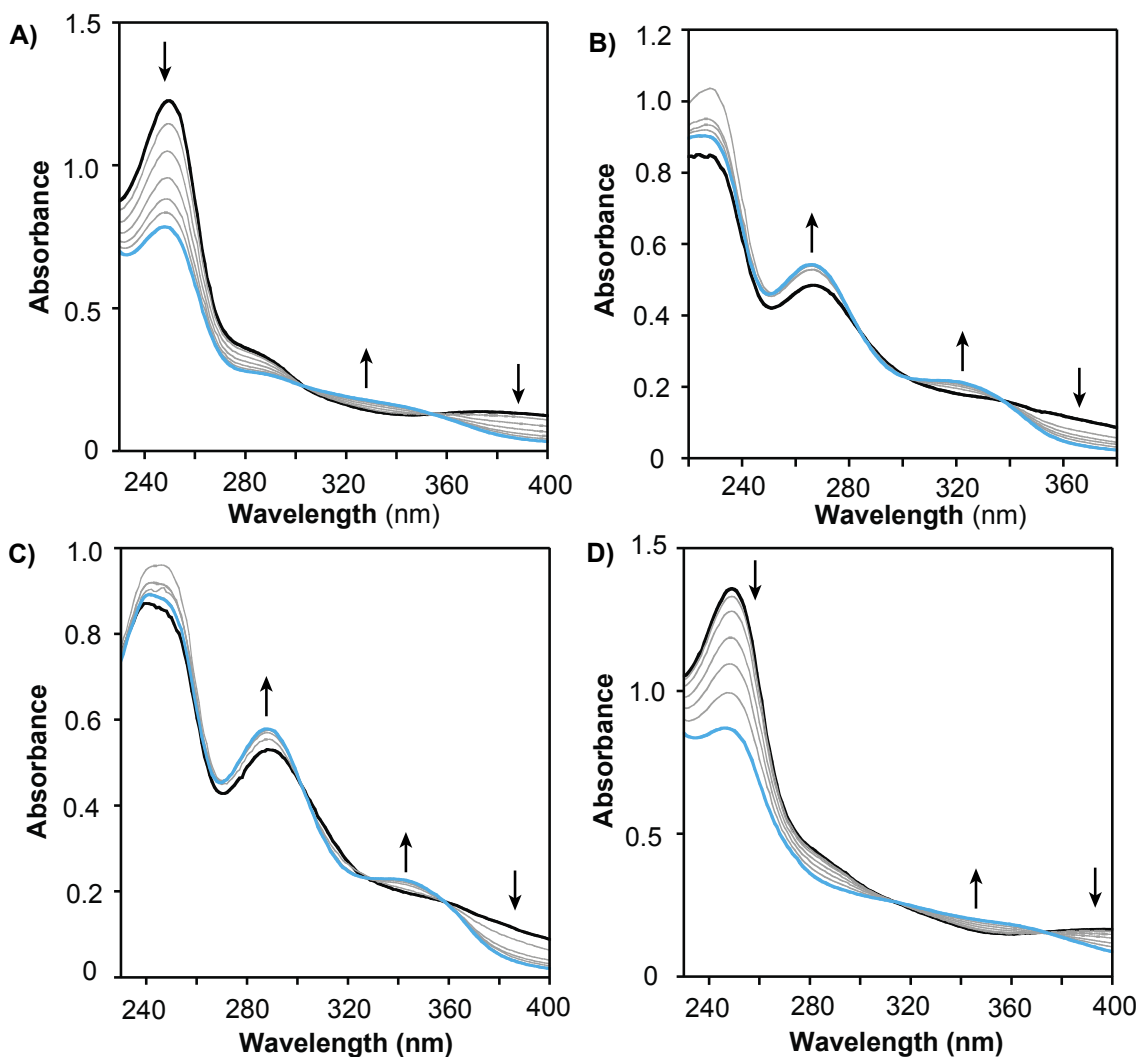


Figure A4.14. Reactions of iridium-hydride complexes (30 μM) with benzaldehyde (60 μM) in THF:H₂O (1:9) at 25°C. The data show the UV-Vis spectra of A) complex **Ir4-H**; B) complex **Ir18-H**; C) complex **Ir19-H**; and D) complex **Ir17-H** after mixing with the substrate. The black trace is the initial spectrum and the light blue trace is the final spectrum.

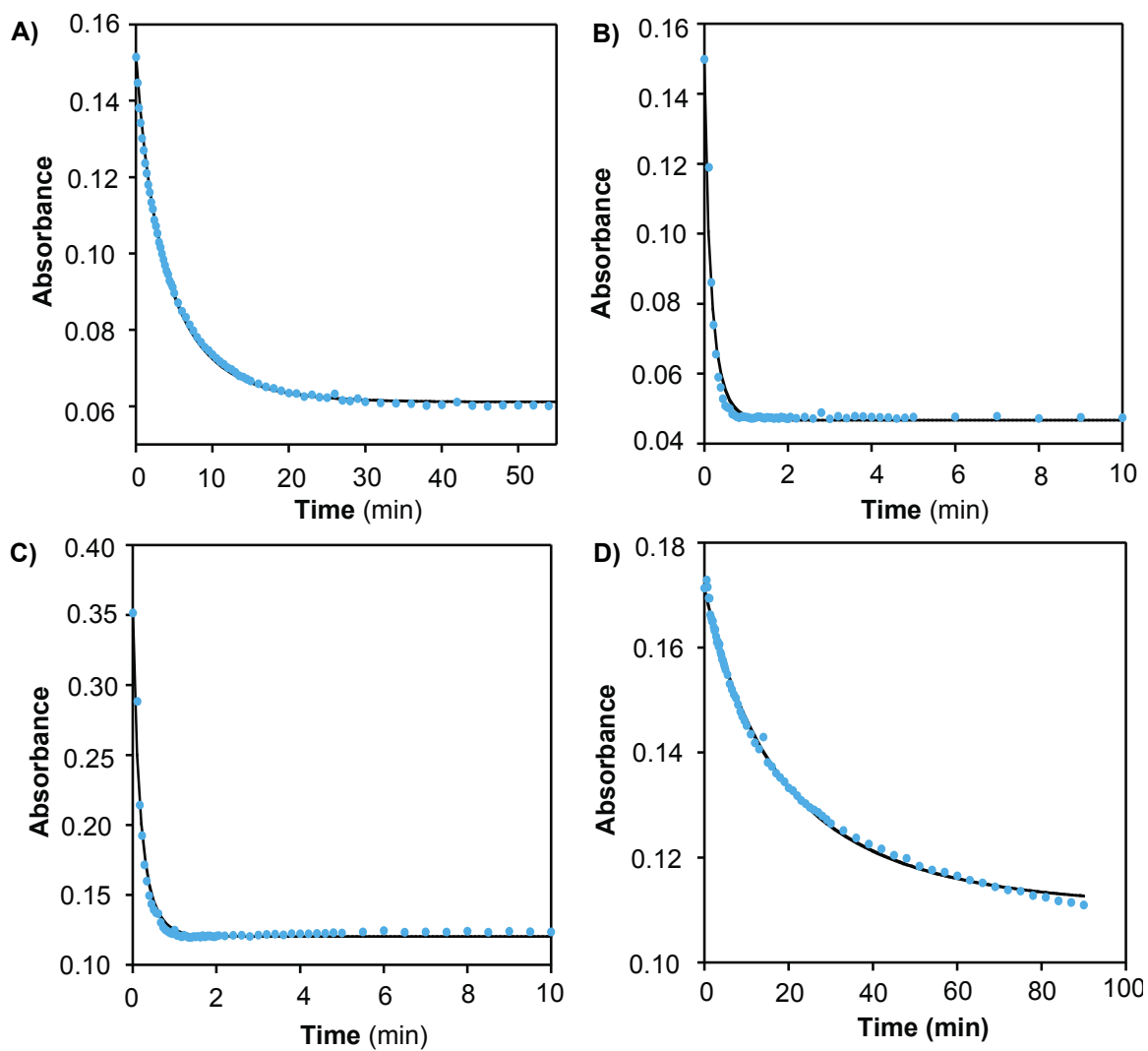
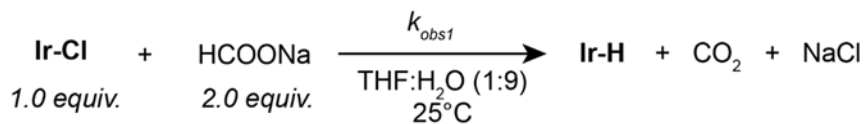


Figure A4.15. Kinetic plots for the reaction of iridium-hydride complexes (30 μM) with benzaldehyde (60 μM) in THF:H₂O (1:9) at 25°C. The data show the UV-Vis spectra at $\lambda = 380$ nm of A) complex **Ir4-H**; B) complex **Ir18-H**; C) complex **Ir19-H**; and D) complex **Ir17-H**. The raw data are shown as light blue dots and the black lines are the curve fits.

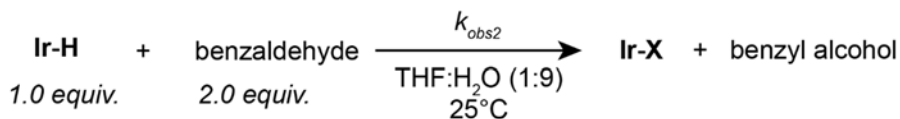
Table A4.1. Calculated Rate Constants from Kinetic Data

A) Hydride Formation Reactions



k_{obs1} (min ⁻¹ M ⁻¹)										
Complex	Ir4		Ir18		Ir19		Ir17		Ir2	
	<i>k</i>	<i>R</i>	<i>k</i>	<i>R</i>	<i>k</i>	<i>R</i>	<i>k</i>	<i>R</i>	<i>k</i>	<i>R</i>
Run 1	6490	0.992	8840	0.989	7393	0.997	8135	0.999	219	0.996
Run 2	8512	0.999	7843	0.998	8530	0.996	6187	0.998	210	0.997
Average	7501		8342		7962		7161		215	
SD	1011		499		569		974		5	

B) Hydride Transfer Reactions



k_{obs2} (min ⁻¹ M ⁻¹)										
Complex	Ir4-H		Ir18-H		Ir19-H		Ir17-H			
	<i>k</i>	<i>R</i>	<i>k</i>	<i>R</i>	<i>k</i>	<i>R</i>	<i>k</i>	<i>R</i>	<i>k</i>	<i>R</i>
Run 1	14931	0.999	406390	0.971	358810	0.977	3201	0.993		
Run 2	12088	0.995	372820	0.982	365460	0.969	3033	0.998		
Average	13510		389605		362135		3117			
SD	1422		16785		3325		84			

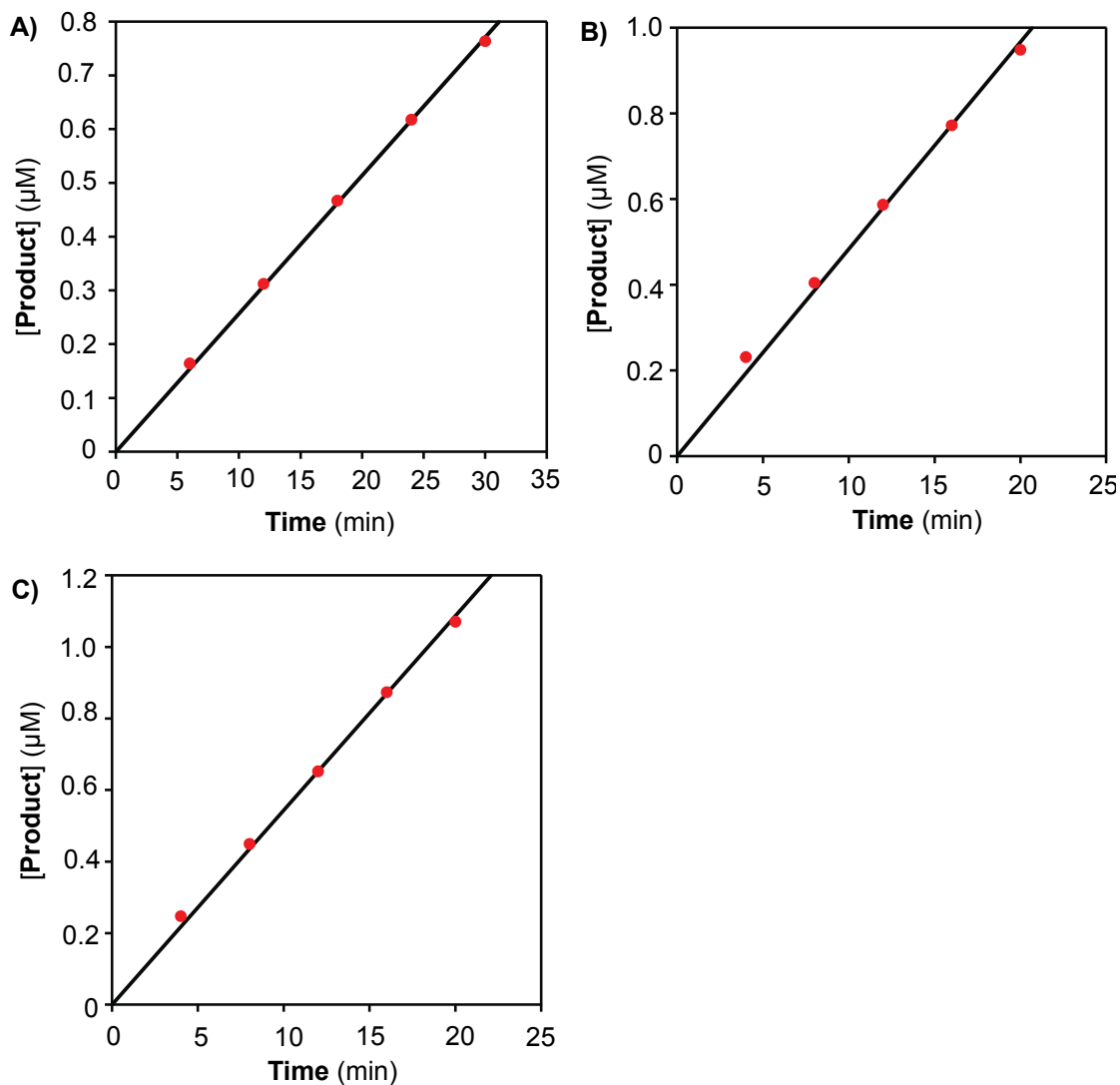


Figure A4.16. Representative kinetic plots from the reaction of benzaldehyde with complex **Ir4** and sodium formate in tBuOH/PBS (1:9) at 37°C. The concentrations used were as follows: A) benzaldehyde (6 mM), **Ir4** (30 μM), sodium formate (18 mM); B) benzaldehyde (6 mM), **Ir4** (30 μM), sodium formate (30 mM); and C) benzaldehyde (6 mM), **Ir4** (60 μM), sodium formate (18 mM). The times points from 0 to 25 or 30 min (red dots) were fit to a linear line (black) and the slopes were taken as the initial rate.

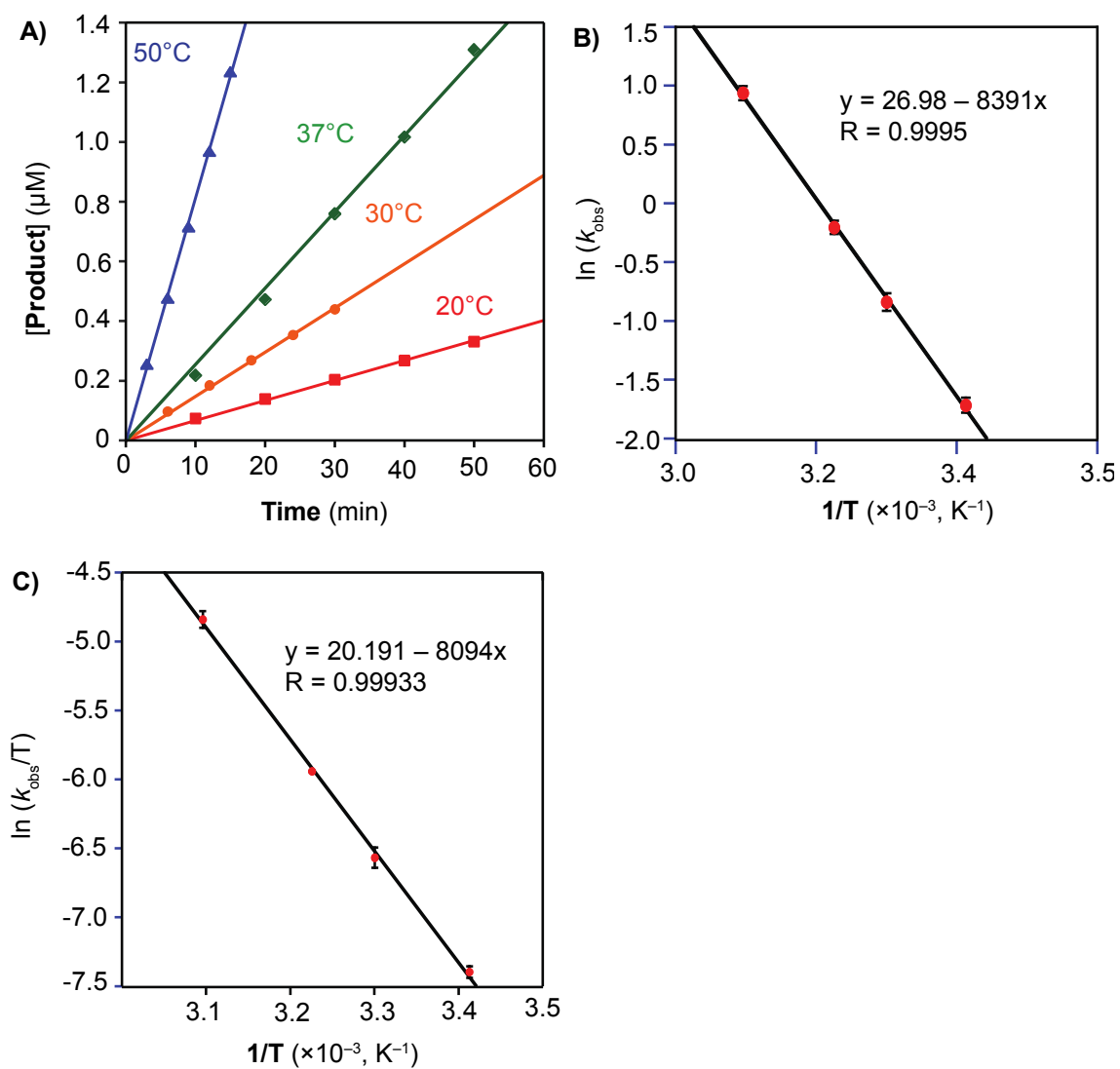


Figure A4.17. Temperature dependence studies of the reaction of benzaldehyde (6 mM) with complex **Ir4** (30 μM) and sodium formate (18 mM) in t-BuOH/PBS (1:9). The data show A) the change in the rates of product formation from 20–50°C; B) Arrhenius plot showing the dependence of k_{obs} as a function of temperature; and C) Eyring plot showing the dependence of k_{obs} as a function of temperature.

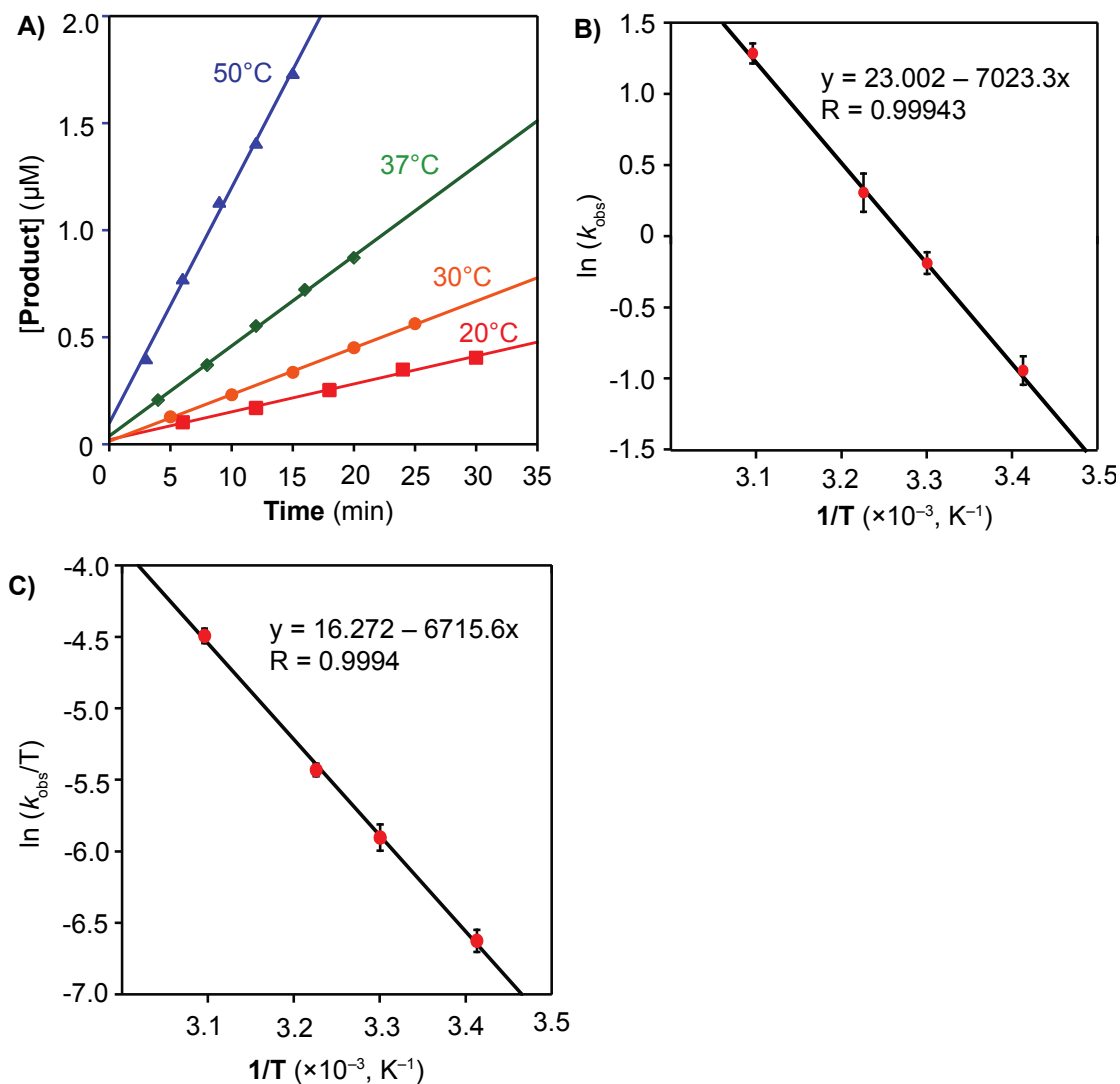


Figure A4.18. Temperature dependence studies of the reaction of benzaldehyde (6 mM) with complex **Ir18** (30 μM) and sodium formate (18 mM) in *t*-BuOH/PBS (1:9). The data show A) the change in the rates of product formation from 20–50°C; B) Arrhenius plot showing the dependence of k_{obs} as a function of temperature; and C) Eyring plot showing the dependence of k_{obs} as a function of temperature.

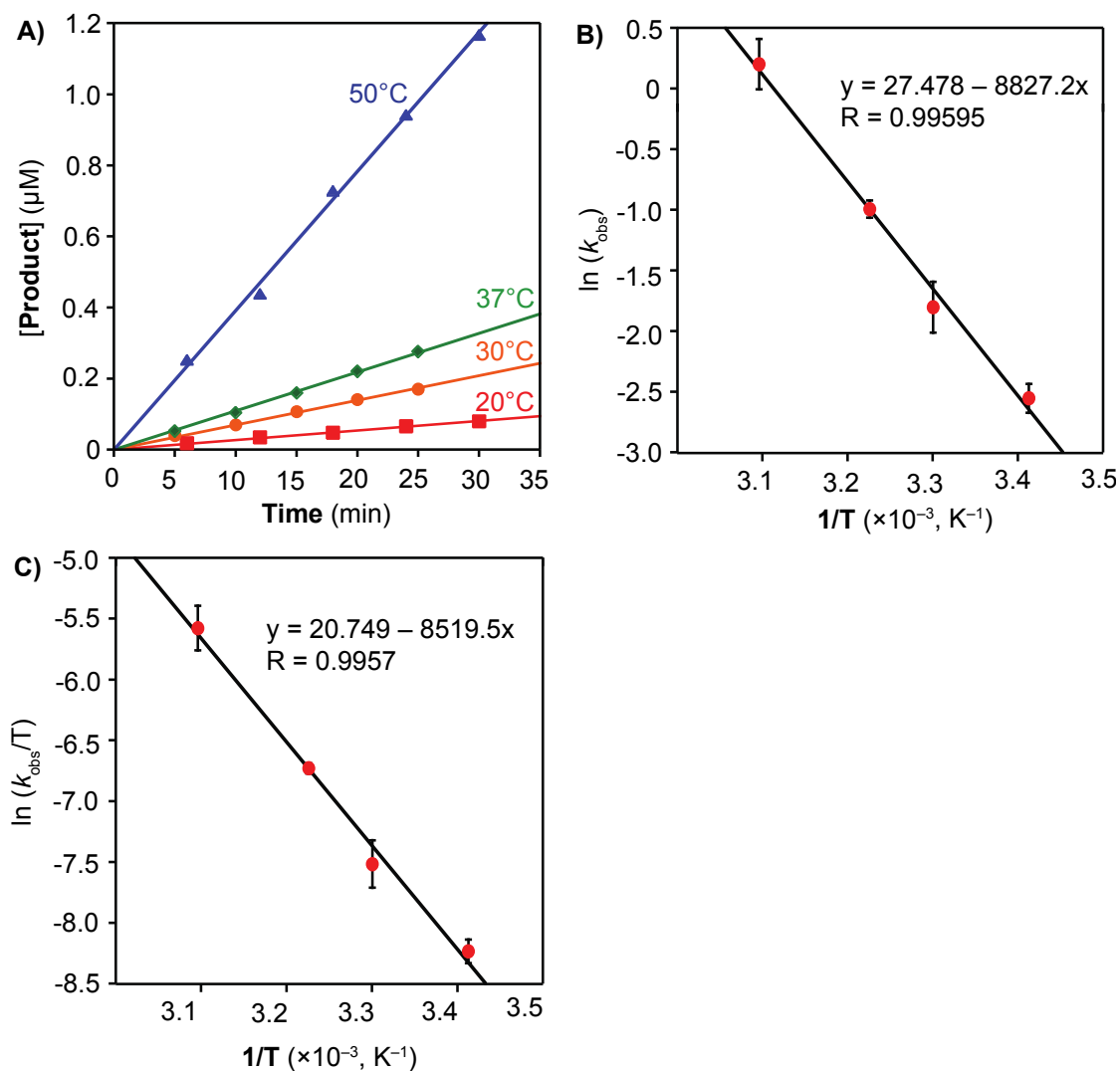


Figure A4.19. Temperature dependence studies of the reaction of benzaldehyde (6 mM) with complex **Ir17** (30 μM) and sodium formate (18 mM) in t-BuOH/PBS (1:9). The data show A) the change in the rates of product formation from 20–50°C; B) Arrhenius plot showing the dependence of k_{obs} as a function of temperature; and C) Eyring plot showing the dependence of k_{obs} as a function of temperature.

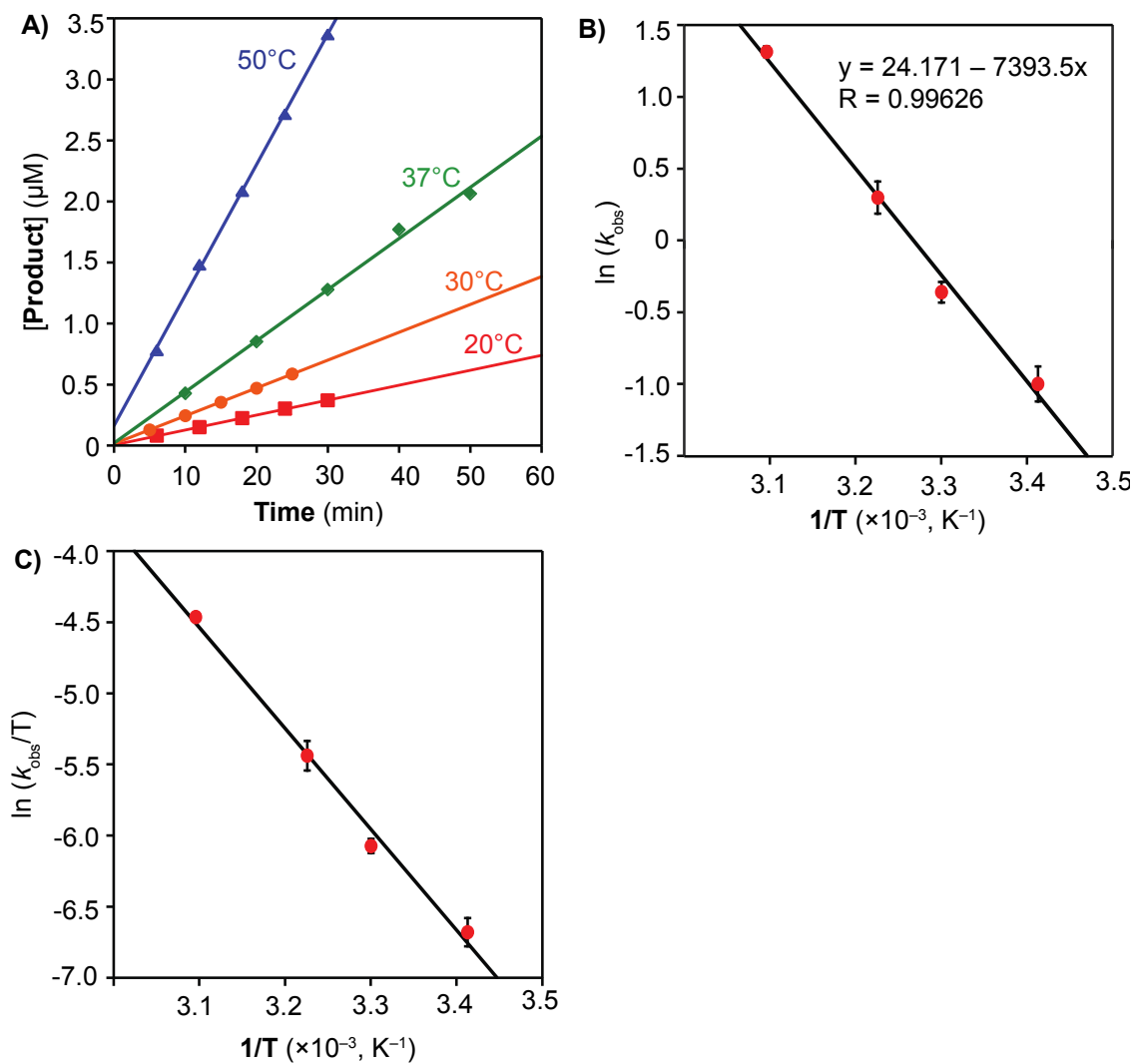


Figure A4.20. Temperature dependence studies of the reaction of benzaldehyde (6 mM) with complex **Ir20** (30 μM) and sodium formate (18 mM) in *t*-BuOH/PBS (1:9). The data show A) the change in the rates of product formation from 20–50°C; B) Arrhenius plot showing the dependence of k_{obs} as a function of temperature; and C) Eyring plot showing the dependence of k_{obs} as a function of temperature.

Chapter 5.

Iridium Complexes for Aldehyde Detoxification in Living Cells

5.1 Introduction

α,β -Unsaturated aldehydes, such as acrolein, crotonaldehyde, malondialdehyde, and 4-hydroxynonenal (4-HNE), are ubiquitous in living systems due to fatty acid peroxidation, carbohydrate oxidation, and absorption from the surrounding environment (air pollutant, smoking, food, drink, etc).¹⁻² They have been found to be associated with many metabolic diseases,³⁻⁴ neurodegenerative disorders,⁵ atherosclerosis,⁶ myocardial and cerebral ischemia,⁷ diabetes, and cancers.⁸⁻⁹ α,β -Unsaturated aldehydes are highly reactive compounds since their conjugated double bond and aldehyde functional groups are susceptible to nucleophilic attack to form adducts with DNA and proteins.¹⁰⁻¹¹ α,β -Unsaturated aldehydes, especially acrolein and 4-HNE, were found to be present at elevated levels in the brains of Alzheimer's patients,¹² which can produce cross-linked protein/DNA and cause protein aggregation.¹³⁻¹⁴ α,β -Unsaturated aldehydes can increase oxidative stress in cells through the formation of reactive oxygen species (ROS).^{3, 11, 14}

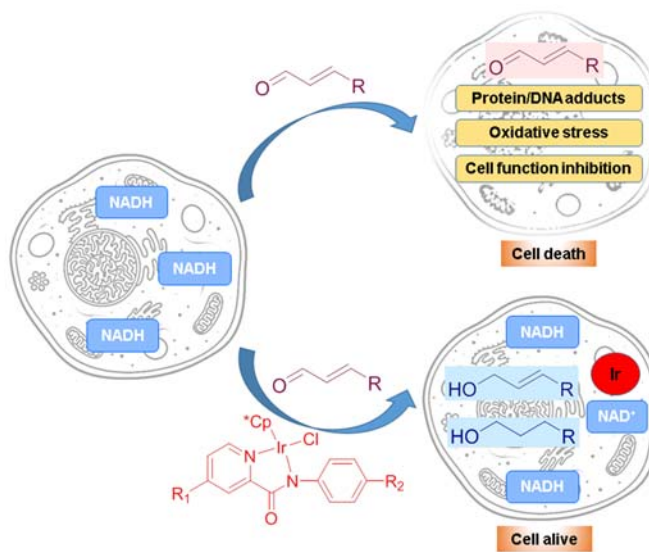
In most living systems, cytotoxic aldehydes can be detoxified by oxidoreductases such as glutathione-S-transferase, or by conjugation with small molecules such as thiols and amines.¹⁵ However, in neurodegenerative disorders like Alzheimer's and Parkinson's diseases, or inborn disorders like Sjögren-Larsson Syndrome¹⁶ and Succinic Semi-Aldehyde Dehydrogenase Deficiency,¹⁷ they can accumulate in the body due to defective aldehyde metabolism.

Aldehyde scavengers, or aldehyde traps, which are small molecules that can react with cytotoxic aldehydes, were introduced a few decades ago. The naturally occurring compoundarnosine and its synthetic histidyl-containing analogues, were shown to be effective in detoxifying α,β -Unsaturated aldehydes¹⁸⁻²³ Thiol and phenol-containing

compounds, such as L-cysteine, glutathione, hydrogen sulfide, and phloretin, have also been utilized for aldehyde detoxification.²⁴⁻²⁶ Although several aldehyde traps are currently in phase 3 clinical trials,²⁷⁻²⁸ they still have limitations such as having stoichiometric reactivity, or are prone to degradation by metabolism and exflux by excretion.²⁹⁻³¹

Transfer hydrogenation catalysts, such as those based on Ru, Ir, and Rh, are capable of converting aldehydes to alcohols.³²⁻³⁵ We previously reported a series of Cp*Ir catalysts with pyridinecarboxamidate ligands for reducing 4-HNE to their alcohols using NADH in cell culture media.³⁶ We also utilized these iridium catalysts to perform intracellular transfer hydrogenation, which converted a dimly emissive bodipy-aldehyde substrate to a strong fluorescent bodipy-alcohol product.³⁷

This chapter will describe the effect of iridium complexes in preventing/detoxifying cytotoxic aldehydes in mouse fibroblast and human neuroblastoma cells (Scheme 5.1). The efficacy of these iridium catalysts will also be compared with conventional aldehyde scavengers in the detoxification of α,β -unsaturated aldehydes.

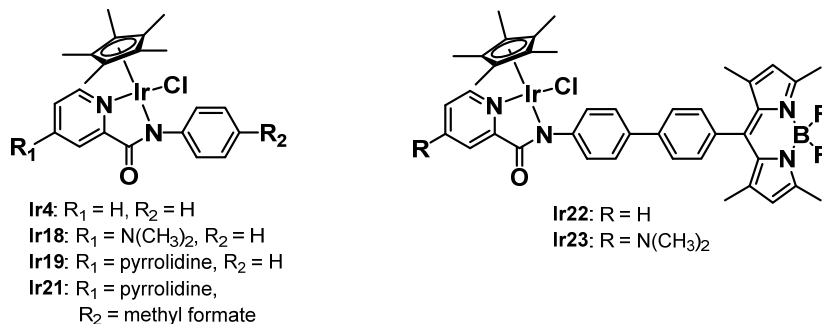


Scheme 5.1. Proposed aldehyde detoxification pathway of iridium complexes inside cells.

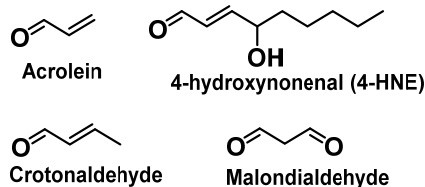
5.2 Iridium Complexes Synthesis and In Vitro Transfer Hydrogenation of Toxic Aldehydes

Previously, we discovered that pentamethyl-cyclopentadienyl (Cp*) iridium complexes that are ligated by *N*-phenyl-2-pyridinecarboxamidate (**Ir4**) can be activated by attaching electron donating groups to the pyridine ring at the *para* position. For example, complexes **Ir18**, **Ir19**, and **Ir21** (Chart 5.1A) showed better catalyst activities compared to **Ir4** under physiologically relevant conditions.³⁸

A) Ir complexes



B) Substrates



C) Aldehyde scavengers

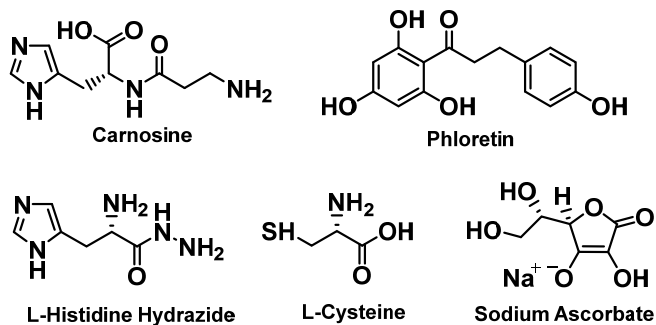
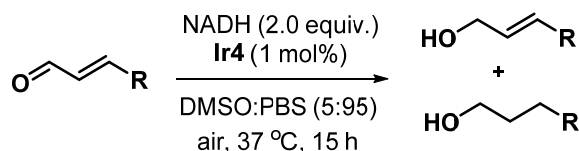


Chart 5.1. Compounds used in this study

To study the distribution and catalyst accumulation inside cells, we also employed iridium catalysts **Ir22** and **Ir23** with bodipy dyes connected to the phenyl ring of the pyridinecarboxamidate ligand at the *para* position (Chart 5.1A).³⁹ These fluorogenic catalyst analogues displayed similar catalytic activity as their parent catalysts.³⁹

The iridium complexes were first tested for aldehyde transfer hydrogenation in the reaction flasks using cell culture media. **Ir4** was found to convert 4-HNE to 4-hydroxynon-2-en-1-ol (88% yield) and 4-hydroxynonan-1-ol (6% yield) in t-BuOH/M199 (5:95) after 15 h at 37 °C, with 1 mol% catalyst and 2.0 equiv. of NADH.³⁶ **Ir4** was able to promote the reduction of a dimly emissive bodipy-aldehyde substrate to a strong fluorescent bodipy-alcohol inside NIH-3T3 mouse fibroblast cells without any added hydride source.³⁷

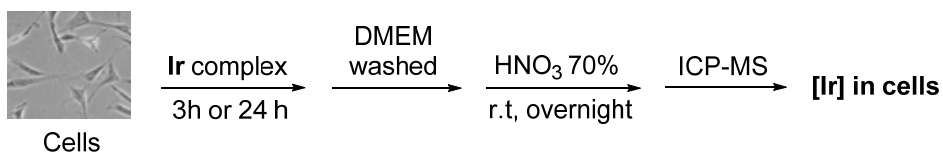


Scheme 5.2. In vitro hydrogenation of toxic aldehyde. Reaction conditions: Aldehyde (5 μmol), NADH (15 μmol), Ir catalyst (0.05 μmol), DMSO:PBS (5:95, 2.5 mL), 37 °C, 15 h. Yields were determined by ¹H NMR using an internal standard.

In the present work, we carried out transfer hydrogenation of crotonaldehyde and acrolein by **Ir4**/NADH in PBS (Scheme 5.2). Interestingly, no aldehydes and unsaturated alcohols were found in the reaction mixture, but saturated alcohol products were formed at low yields (13.3% for crotonaldehyde, and 9.4% for acrolein). We speculate that the low yields might be because of the evaporation of starting materials/products due to their volatility or that other side reactions are also occurring.

5.3 Accumulation of Iridium Complexes in Cells

Beside high activity, the catalysts should also show good cellular uptake to have good biocompatibility. To determine the efficiency of cellular uptake, inductively coupled plasma-mass spectrometry (ICP-MS) was used to quantify the amount of Ir catalysts that are taken up by cells. In these experiments, cells were incubated with Ir complexes for various lengths of time, digested by treatment with concentrated nitric acid, and then the resulting solution was analyzed by ICP-MS for iridium (Scheme 5.3).



Scheme 5.3. Procedure for determining iridium accumulation inside cells.

For cellular studies, we used mouse fibroblast (NIH 3T3) and human neuroblastoma (SH-SY5Y) to conduct aldehyde detoxification experiments. NIH 3T3 was chosen for all of our initial studies because of its robustness, fast growth rate, and availability. SH-SY5Y was selected for additional experiments because they are neuron-like cells, and thus, are more relevant biological models for studying neurodegenerative development.

In NIH 3T3 cells, iridium accumulation varied depending on the amount and length of time the cells were exposed to the Ir complexes. Treatment with 10 μM of iridium complex and after 3 hours incubation led to Ir accumulation of up to 303 ng Ir per 10^6 cells (Figure 5.1A). Increasing the incubation time of iridium complexes to 24 hours can increase the uptake to 715 ng Ir/ 10^6 cells. Treatment with 20 μM of iridium complex and

after 3 hours incubation, iridium accumulation was measured to be up to 918 ng Ir/10⁶ cells (Figure 5.1B). Increasing the incubation time of the iridium complexes to 24 hours increase uptake to 1380 ng Ir/10⁶ cells. **Ir21** and **Ir22** showed very high accumulation in cells compared to the other complexes. **Ir18** showed the lowest accumulation out of all the complexes tested. As shown in Figure 5.1C, increasing the incubation concentration of iridium complexes from 10 μ M to 20 μ M increased Ir cellular accumulation by \sim 3x in NIH 3T3 cells.

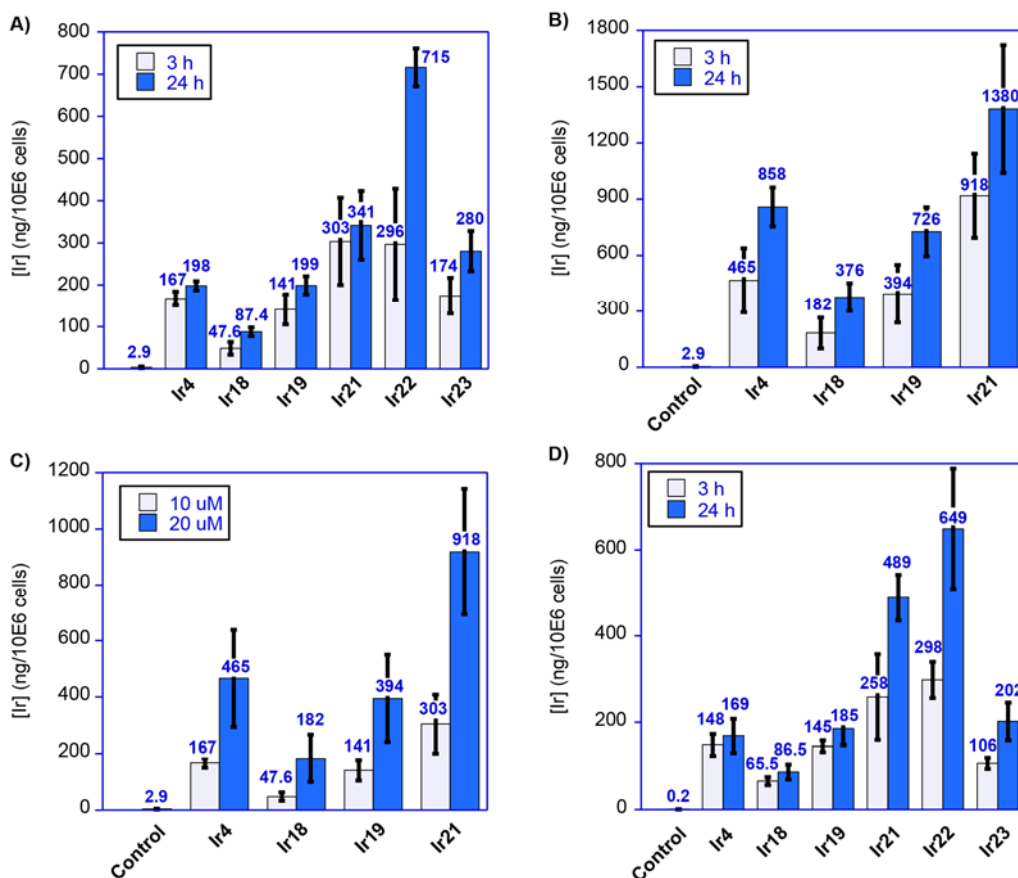
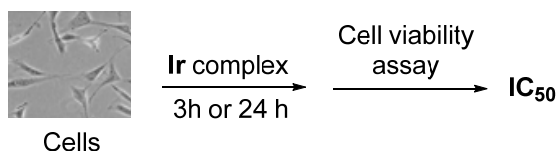


Figure 5.1. ICP-MS results for iridium. A) Iridium accumulation inside NIH 3T3 cells (10 μ M Ir incubation); B) Iridium accumulation inside NIH 3T3 cells (20 μ M Ir incubation); C) Iridium accumulation inside NIH 3T3 cells (3 h Ir incubation); D) Iridium accumulation inside SH-SY5Y cells (5 μ M Ir incubation).

We obtained similar results using SH-SY5Y cells. If the iridium complexes were incubated in SH-SY5Y cells at 5 μM concentration for 3 hours, the Ir concentration was measured to be 65.5-298 ng Ir/ 10^6 cells (Figure 5.1D). Increasing the incubation time of iridium complexes to 24 hours increase the amount iridium accumulation by about 2x. Similar as in the NIH 3T3 cell line, **Ir21** and **Ir22** had the highest accumulation in SH-SY5Y, with 694 ng Ir/ 10^6 cells for **Ir22** (5 μM , 24 h incubation). In contrast, **Ir18** showed the lowest accumulation (86.5 ng Ir/ 10^6 cells with 5 μM and 24 h incubation).

5.4 Toxicity of Iridium Complexes

Next, the cytotoxicity of the Ir complexes was determined in both NIH 3T3 and SH-SY5Y cell lines. For these experiments, cells were incubated with Ir complexes at various concentrations for different length of time. The samples were then analyzed using sulforhodamine B (SRB) cytotoxicity assay, and the half maximal inhibitory concentration (IC_{50}) were calculated (Scheme 5.4).



Scheme 5.4. Procedure for determining toxicity of iridium complexes.

In NIH 3T3, our iridium catalysts showed similar toxicity, with $\text{IC}_{50(3\text{h})} = 40 \mu\text{M}$ for the most toxic (**Ir22**), and $\text{IC}_{50(3\text{h})} = 81 \mu\text{M}$ for the least toxic (**Ir18**) (Figure 5.2). Increasing the incubation time of iridium complexes to 24 h led to slight lowering of the IC_{50} (5-30%), possibly due to greater accumulation of the iridium complexes.

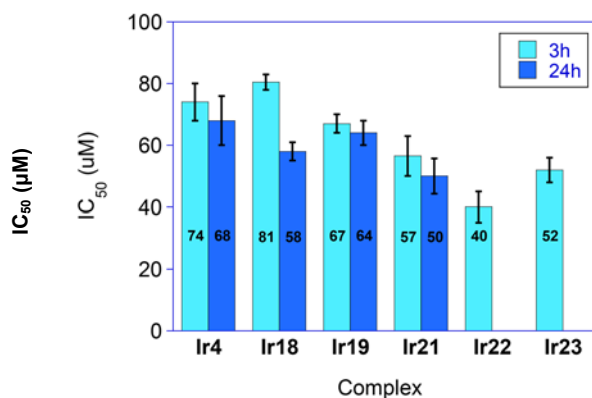


Figure 5.2. IC₅₀ of iridium complexes in NIH 3T3 cell lines.

The iridium catalysts were more toxic toward SH-SY5Y cells, by about 2x compared to in NIH 3T3 cells. The most toxic complex (**Ir22**) has IC₅₀ (3h) = 26 µM, and the least toxic complex (**Ir18**) has IC₅₀ (3h) = 43 µM (Figure 5.3).

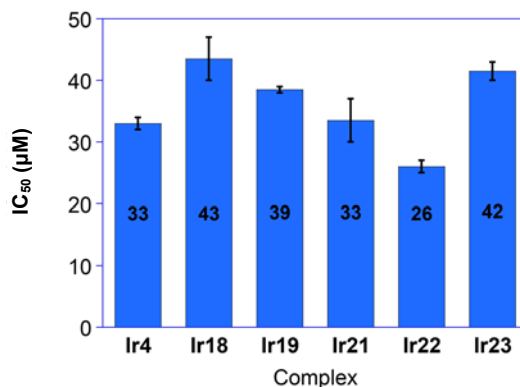


Figure 5.3. IC₅₀ of iridium complexes in SH-SY5Y cell lines.

Since our Ir complexes can consume NADH in cells, they may effect their intrinsic cellular metabolism. To minimize this possibility, we measured the IC₅₀ of Ir complexes in the presence of added sodium formate so that endogenous NADH does not get consumed. Interestingly, with relatively high concentration of sodium formate (1 mM), our Ir

complexes did not show significant changes in their IC_{50} . As shown in Figure 5.4, the IC_{50} of the Ir complexes with and without added sodium formate are very similar.

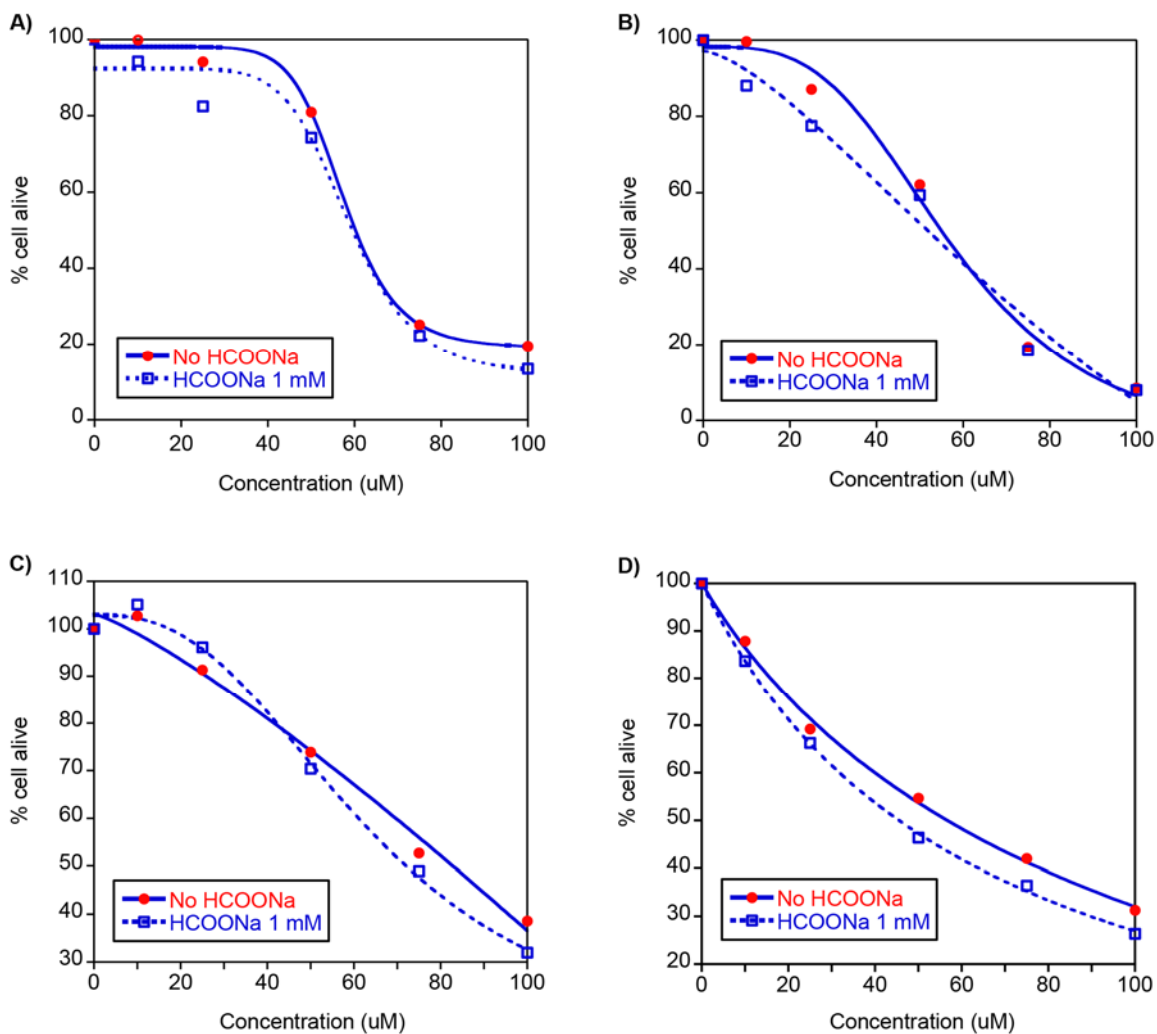
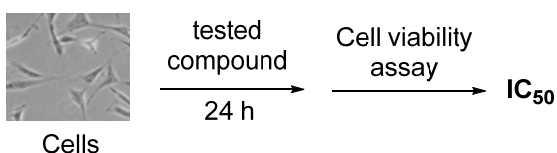


Figure 5.4. IC_{50} of Iridium complexes in NIH 3T3 cell line with and without sodium formate addition. A) Complex Ir4; B) Complex Ir18; C) Complex Ir19; D) Complex Ir21.

5.5 Toxicity of Aldehydes, Their Alcohol Products and Aldehyde Scavengers

The IC_{50} values of the cytotoxic aldehydes, their alcohol products, and aldehyde scavengers were also determined (Scheme 5.5 and Figure 5.5). We observed that the alcohols were much less toxic to the cells compared to their parent aldehydes, and saturated alcohols have 2-7.5 times higher IC_{50} than their corresponding unsaturated alcohols. These compounds showed greater toxicity in SH SY-5Y cells compared to NIH 3T3 cells.



Scheme 5.5. Procedure for determining toxicity of aldehydes and other compounds.

Out of all the aldehydes tested, acrolein showed the highest toxicity, and malondialdehyde showed the lowest toxicity, which is consistent with reported results. The well-studied aldehyde scavenger carnosine is relatively non-toxic with $IC_{50} > 10$ mM. As expected, L-cysteine and sodium ascorbate are also non-toxic with $IC_{50} > 10$ mM and > 5 mM, respectively. Phloretin is more cytotoxic than the other aldehyde scavengers since its IC_{50} ranges from 230 to 370 μ M depend on the cell line.

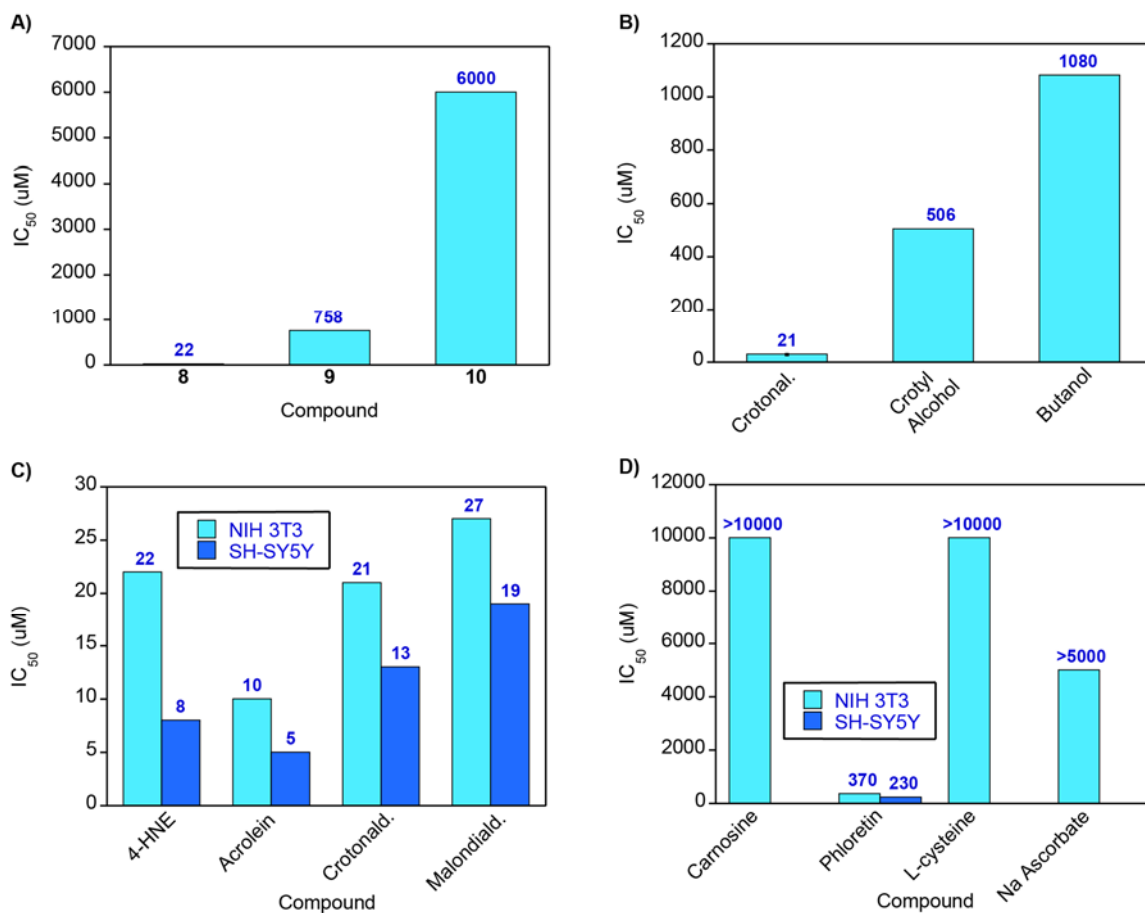
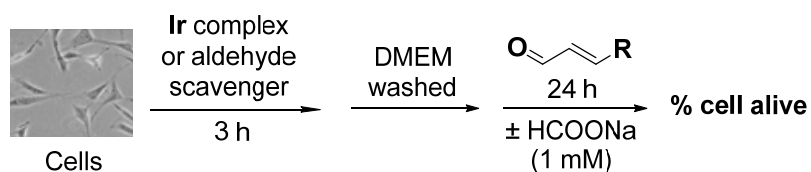


Figure 5.5. IC₅₀ of aldehydes, alcohol and aldehyde scavengers. A) Compare IC₅₀ of 4-HNE and its alcohols in NIH 3T3 cell line; B) Compare IC₅₀ of crotonaldehyde and its alcohols in NIH 3T3 cell line; C) Differences in IC₅₀ of toxic aldehydes in NIH 3T3 and SH-SY5Y cell lines; D) IC₅₀ of aldehyde scavengers in NIH 3T3 and SH-SY5Y cell lines.

5.6 Aldehyde Detoxification by Iridium Complexes and Aldehyde Scavengers

In the co-treatment experiments, cells were first incubated with an iridium complex or aldehyde scavenger, then washed twice with cell culture media DMEM to remove the extracellular compound, and then incubated with toxic aldehyde for 24 hours. After the desired treatment time, the cells were washed with DMEM again before analyzing by the SRB assay (Scheme 5.6).



Scheme 5.6. Procedure for aldehyde detoxification in cells.

As illustrated in Figure 5.6, cells that were pre-treated with Ir displayed ~1.1-1.8x greater viability in the presence of cytotoxic aldehydes compared to those that were untreated. Addition of sodium formate increased the viability by an additional ~10-20%, presumably because formate can increase the rates of transfer hydrogenation.

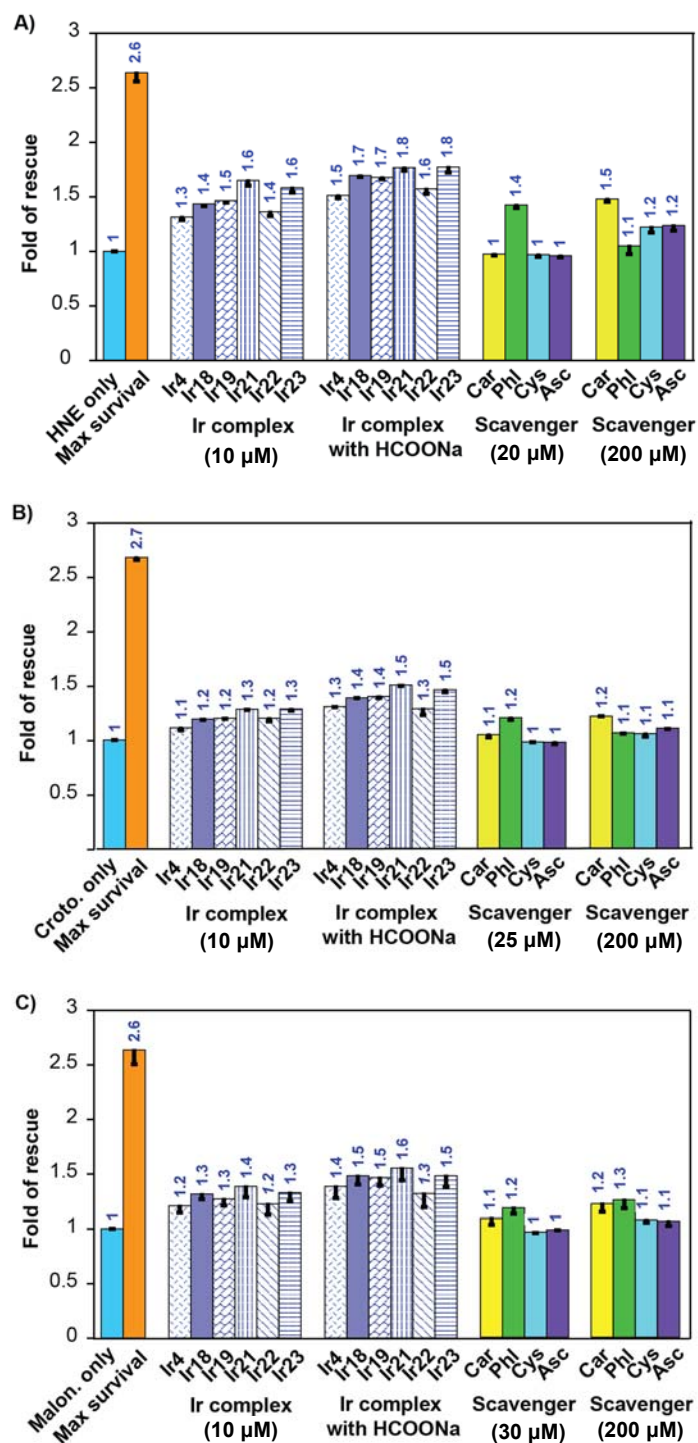


Figure 5.6. Compare iridium complexes and aldehyde scavengers in rescue NIH 3T3 cells from toxic aldehydes. A) 4-HNE (20 μ M); B) Crotonaldehyde (25 μ M); C) Malondialdehyde (30 μ M). Incubation conditions: Ir complex (10 μ M), HCOONa (1mM). Abbreviations: Croto. = crotonaldehyde, Malon. = malondialdehyde, Car = carnosine, Phl = phloretin, Cys = L-cysteine, Asc = sodium ascorbic.

In general, aldehyde were less effective at rescuing cells than the Ir complexes. Phloretin is the most potent compared to other aldehyde scavengers, and almost as effective as the Ir catalysts. However, phloretin is more toxic at high concentrations (200 μM). Carnosine showed almost no cell-protecting effects at low concentrations but can rescue cells at high concentrations. L-cysteine and sodium ascorbate, on the other hand, displayed poor aldehyde scavenger activity (less than 10% cell rescue).

The detoxification capabilities of both Ir complexes and aldehyde scavengers are higher for 4-HNE, lower for crotonaldehyde and malonaldehyde, and insignificant for acrolein. As shown in Figure 5.7, only **Ir21** showed 10% cell rescue compared to the acrolein-only treated cells. The other Ir complexes were inactive, and cells that were treated with **Ir22** showed even greater cell death (possibly due to its higher toxicity than other Ir complexes). This result can be explained by the high reactivity of acrolein, which was reported to react 110-150 times faster than 4-HNE with the thiol group of cysteine.⁵

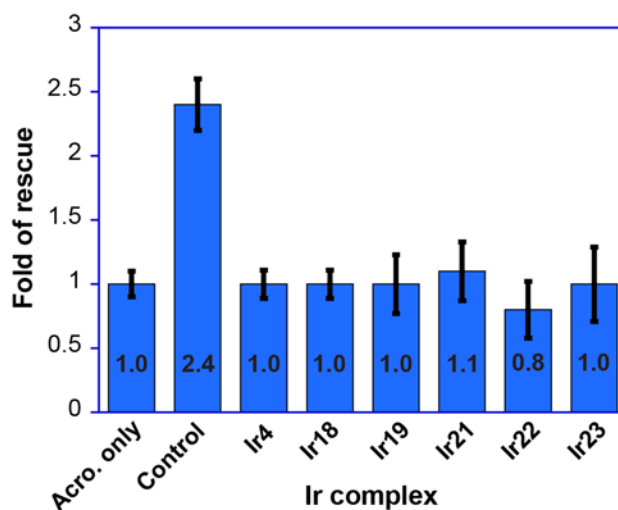


Figure 5.7. Iridium complexes in rescue NIH 3T3 cells from acrolein. Incubation conditions: Ir complex (10 μM , 3 h), HCOONa (1mM), acrolein (15 μM , 24 h).

Similar results were obtained in SH-SY5Y cell lines. The Ir complexes showed the highest activity for 4-HNE detoxification, with up to 2.3 folds increase in cell survival relative to the 4-HNE-only treated group. Lower activity was observed in crotonaldehyde and malondialdehyde detoxification, and no effect was observed for acrolein (Figure 5.8). Once again, the aldehyde scavengers were less effective than the Ir catalysts. The best aldehyde scavengers (phloretin and carnosine) showed 1.4-4.5 folds increase in the rescue of cells from 4-HNE and malondialdehyde, and 1.2-1.3 folds increase in the rescue of cells from crotonaldehyde.

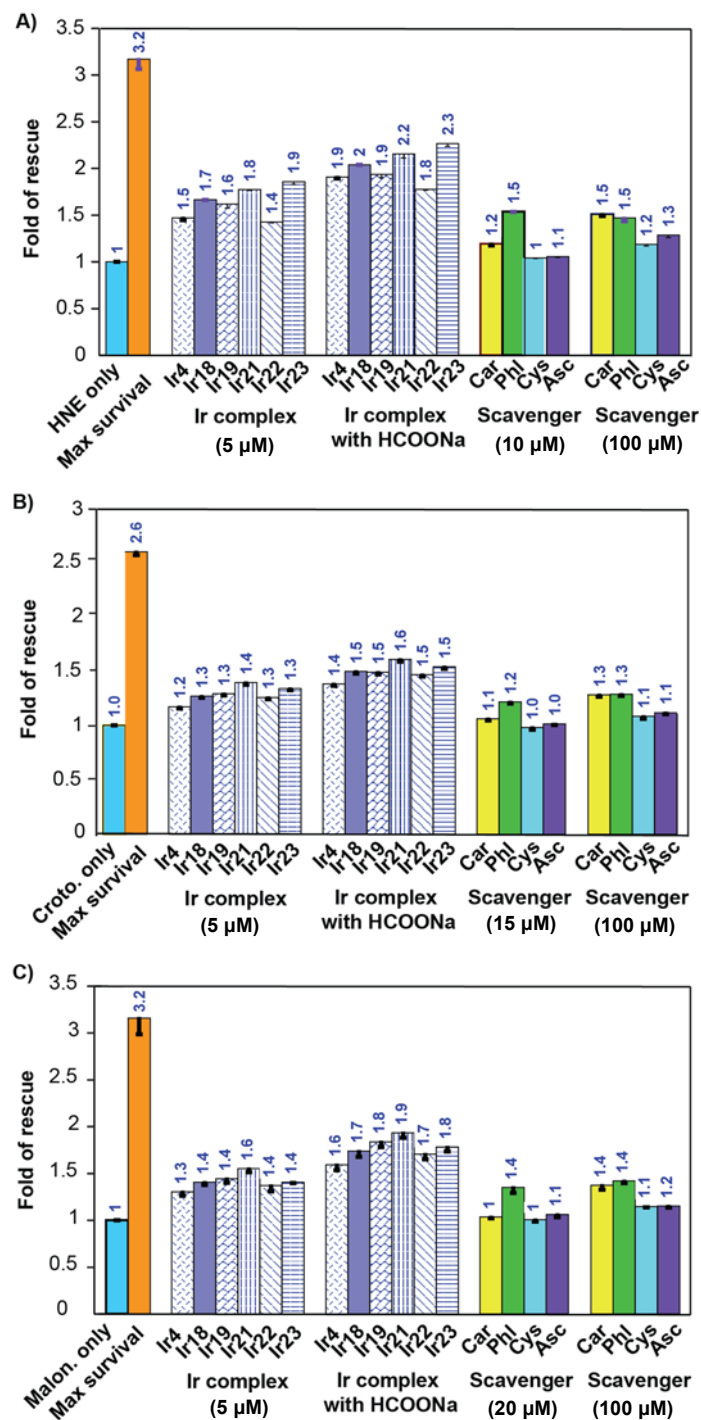


Figure 5.8. Compare iridium complexes and aldehyde scavengers in rescue SH-SY5Y cells from toxic aldehydes. A) 4-HNE (10 μM); B) Crotonaldehyde (15 μM); C) Malondialdehyde (20 μM). Incubation conditions: Ir complex (5 μM), HCOONa (1mM). Abbreviations: Croto. = crotonaldehyde, Malon. = malondialdehyde, Car = carnosine, Phl = phloretin, Cys = L-cysteine, Acs = sodium ascorbic.

5.7 Conclusion and Future Work

This work demonstrates that our Ir complexes are able to prevent/reduce toxicity of cytotoxic aldehydes inside living cells using either naturally-occurring NADH or extracellular hydride sources like sodium formate. The iridium complexes showed better aldehyde detoxification ability compared to well-known aldehyde scavengers such as carnosine or phloretin. These results suggest that aldehyde detoxification using a catalytic approach may have therapeutic advantages over conventional approaches.

To complete this study, we plan to perform additional experiments in the near future. First, we will use liquid chromatography–mass spectrometry (LC-MS) to quantify the amount of products formed from transfer hydrogenation in cells. Second, we will perform reactive oxygen species (ROS) quantification assays to compare the ROS levels in cells when treated with toxic aldehydes with and without iridium catalysts. This studies may help us to understand the biological effects of the Ir complexes in intracellular aldehyde detoxification. Third, we will employ flow cytometry to evaluate the differences in the cell cycles of toxic aldehyde treated cells with and without pre-treated Ir catalysts. Fluorescent substrates could also be used to study their distribution and retention inside cells. The prevention/detoxification effect of iridium catalysts can also be tested with endogenously-generated toxic aldehydes. In such studies, the Ir catalysts could be kept inside the cell culture media, which will help to maintain a critical catalyst concentration inside cells.

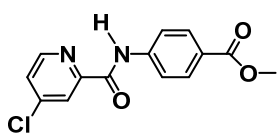
5.8 Experimental

General. Commercial reagents were used as received without further purification. Acrolein, crotonaldehyde, carnosine, L-cysteine, phloretin, and sodium ascorbate were purchased from commercial sources. The iridium complexes **Ir4**,³⁸ **Ir18**,³⁸ **Ir19**,³⁸ **Ir22**,³⁹ **Ir23**³⁹, 4-HNE⁴⁰ and malondialdehyde⁴¹⁻⁴² were prepared as reported procedures. NIH 3T3 and SH-SY5Y cell lines were obtained from American Type Culture Collection (ATCC).

Physical Methods. A Varian 810 instrument was used to acquire inductively coupled plasma-mass spectrometry (ICP-MS) analyses. Liquid chromatography-mass spectrometry (LC-MS) was analyzed by an Agilent 6460 Triple Quad. All cell images were obtained using an Olympus IX83 microscope equipped with a 20x air objective.

Synthesis

Preparation of methyl 4-[4-chloro-2-pyridine-2-amido]benzoate. In a 200 mL round



bottom flask, 4-chloro-2-pyridinecarboxylic acid (10.0 mmol, 1.0 equiv.) was dissolved in ~100 mL anhydrous dichloromethane, cooled in an ice bath for ~ 15 min before triethyl amine (20.0 mmol, 2.0 equiv.) was added. 15 min later, ethyl chloro formate (13.0 mmol, 1.3 equiv.) was added, then reaction was stirred in ice bath for another 30 min before adding methyl 4-aminobenzoate (6.0 mmol, 0.6 equiv.). Reaction was stirred in ice bath for an hour and room temperature overnight. Reaction mixture was extracted with water, organic phase was separated, dried over sodium sulfate, and then evaporated to dryness. The crude product was purified by washing with diethyl ether follow by recrystallizing in dichloromethane to get a white solid (1205 mg, 69 % yield). ¹H NMR (CDCl₃, 500 MHz): 10.09 (s, 1H), 8.52 (d, *J* = 5.2 Hz, 1H), 8.29

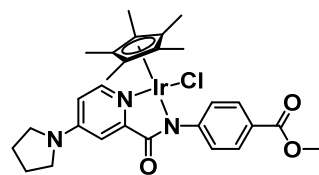
(d, $J = 2.0$ Hz, 1H), 8.07 (d, $J = 8.6$ Hz, 2H), 7.84 (d, $J = 8.6$ Hz, 2H), 7.51 (dd, $J = 5.2, 2.0$ Hz, 1H), 3.91 (s, 3H). ^{13}C NMR (CDCl_3 , 126 MHz): 166.7, 161.1, 150.9, 149.0, 146.5, 141.6, 131.1, 127.1, 126.0, 123.3, 119.1, 52.2 ppm.

Preparation of methyl 4-[4-(1-pyrrolidinyl)-2-pyridine-2-amido]benzoate. In a high-



pressure glass tube, methyl 4-[4-(1-pyrrolidinyl)-2-pyridine-2-amido]benzoate (1.0 mmol, 1 equiv.) and pyrrolidine (1.7 mL, 20 equiv.) were combined with 5.0 mL of acetonitrile. This tube was sealed tightly, and stirred at 120°C overnight. After removing the solvent under vacuum, the resulting off white solid was washed by methanol (10 mL x 3 times) to get a white solid (263 mg, 81% yield). ^1H NMR (CDCl_3 , 500 MHz): 10.37 (s, 1H), 8.14 (d, $J = 5.7$ Hz, 1H), 8.04 (d, $J = 8.5$ Hz, 2H), 7.84 (d, $J = 8.5$ Hz, 2H), 7.39 (s, 1H), 6.46 (dd, $J = 5.7, 2.1$ Hz, 1H), 3.90 (s, 3H), 3.37 (s, 4H), 2.04 (t, $J = 6.5$ Hz, 4H). ^{13}C NMR (CDCl_3 , 126 MHz): 166.8, 163.3, 152.9, 149.3, 148.0, 142.2, 130.8, 125.2, 118.8, 108.8, 105.6, 51.9, 47.2, 25.4 ppm.

Preparation of [Cp*Ir(*N*-(4-methylbenzoate)-2-(4-(1-pyrrolidinyl)-2-pyridine)carboxamidate)Cl] (**Ir21**). In a 50 mL schlenk flask, 20 mL of



ethanol was purged with nitrogen for about 10 min. $[\text{Cp}^*\text{IrCl}_2]_2$ (0.12 mmol, 1.0 equiv.) and the ligand (0.24 mmol, 2.0 equiv.) were added and stirred for 15 min at 80°C. The reaction mixture was treated with ammonium hexafluorophosphate (0.60 mmol, 5.0 equiv.) and stirred overnight at 80°C. The ethanol solvent was removed by rotary evaporation and then the solid residual was redissolved in 20 mL of dichloromethane and washed with water (3×20 mL). The organic

phase was separated, dried over sodium sulfate, and then evaporated to dryness. The crude product was purified by silica column (100% ethyl acetate, then 10% methanol/90%ethyl acetate) to get a bright yellow solid (151 mg, 91 % yield). ¹H NMR (CDCl₃, 500 MHz): 8.04 (d, *J* = 6.6 Hz, 1H), 7.98 (d, *J* = 8.4 Hz, 2H), 7.75 (d, *J* = 8.4 Hz, 2H), 7.17 (s, 1H), 6.49-6.45 (m, 1H), 3.89 (s, 3H), 3.43 (s, 4H), 2.05 (s, 4H), 1.38 (s, 15H) ppm. ¹³C NMR (CDCl₃, 126 MHz): 169.5, 167.4, 153.6, 153.4, 152.6, 148.8, 129.7, 127.2, 125.2, 110.1, 109.2, 85.8, 51.9, 47.7, 25.4, 8.6 ppm.

Procedure for In vitro Transfer Hydrogenation Studies. Aldehyde (5 μmol in DMSO, 1.0 equiv.), NADH (7.6 mg, 10 μmol, 2.0 equiv.), and iridium catalyst (0.05 μmol in DMSO, 20 μM, 1 mol%.) were combined in 2.5 mL of DMSO:PBS (5:95) in a 1 dram glass vial. The vial was tightly sealed with Teflon tape, and the reaction mixture was stirred at 37°C for 15 h before the organic products were extracted into deuterated chloroform with hexamethylbenzene (3 μmol, 0.6 equiv.) as an internal standard. The conversions and reaction yields were then determined from the proton NMR spectra.

ICP-MS Analysis. Cells were cultured in tissue culture plates (Corning 3595) at 37°C under a 5% CO₂ atmosphere. When 70-80% confluence was achieved, the old medium was aspirated and replaced by new cell culture medium with the test compound. At the end of the treatment period, the cells were detached by trypsin, then both cell culture medium (with some floating SH-SY5Y cells) and trypsinized cells were combined to be counted using a BIO-RAD TC10 automated cell counter. The sample was then centrifuged and the supernatant was removed. The cell pellet was then washed twice with fresh cell culture medium (vortexed, centrifuged, and then the supernatant was removed), and one more time

with phosphate buffered saline (PBS). The cell pellets were digested with 0.5 mL of 70% traced metal-free distilled HNO₃ at room temperature overnight. 6.5 mL of HPLC grade H₂O was added to each sample to obtain 5% HNO₃ final concentration. The cloudy solutions were then centrifuged to get clear samples for ICP-MS analysis. The final concentration of iridium was calculated by this equation: [Ir] (ng/10⁶ cells) = [Total Ir]/[Total cells], and total Ir (ng) = [Ir] (in ppb) x 10³ x 0.007 (L).

Cytotoxicity Sulforhodamine B (SRB) assay. Cells were seeded in a 96-well plate (7,000-10,000 cells/well) and incubated at 37 °C in a culture incubator with a humidified atmosphere containing 5% CO₂ to allow cells to adhere to the bottom of the wells (~15 hours with NIH 3T3, and ~48 hours with SH-SY5Y). Stock solutions of tested compound were prepared in DMSO or PBS, then diluted in cell culture media (Dulbecco's Modified Eagle Medium (DMEM):F12 (1:1) supplemented with 10% fetal bovine serum (FBS) and 1% penicillin-streptomycin 100X solution) to make a series of desired concentrations. Old cell culture medium was then removed and replaced by new cell culture media with test compounds at different concentrations, and cells were incubated for a desired time. The solutions were then aspirated and the cells were washed with fresh cell culture medium before 100 µL of cell culture medium (with no FBS) was added to each well, followed by 50 µL of fixative reagent (Cytoscan™ SRB Cytotoxicity Assay, G-Biosciences, catalog # 786-213). The 96 well plate was kept at 4 °C in 1 hour, then the cells was washed 3 times with distilled water before drying 2-3 hours at 37 °C. 100 µL of sulforhodamine B (SRB) dye solution was then added to each well and the 96 well plate was kept in the dark at room temperature for 30 minutes. The cells was then washed 4 times with 1x dye wash solution before drying 2-3 hours at 37 °C. 200 µL of SRB solubilization buffer was added to each

well, mixed by pipetting up and down to dissolve the dye completely. The absorbance of the 96-well plate was then measured at 495 nm to determine the amount of rhodamine complex formed. Cell viability was considered to be proportional to the absorbance of the wells. The absorbance value of the wells containing only solubilization buffer (background) was subtracted from those of the wells containing treated and control cells. Percentage cell viability was calculated using the following equation: $(A_{\text{conc}}/A_{\text{control}}) \times 100\%$, where A_{conc} is the absorbance at a specific probe concentration and A_{control} is the absorbance of the untreated cells sample. IC_{50} value was calculated from the sigmoidal curve fit of this data at 50% cell alive.

Cytotoxicity MTS assay. Cells were seeded and treated with a test compound in the same way as in the SRB assay. At the end of the treatment period, old medium was aspirated, and 100 μL of fresh cell culture medium containing 20% of 3-(4,5-dimethylthiazol-2-yl)-5-(3-carboxymethoxyphenyl)-2-(4-sulfophenyl)-2H-tetrazolium (MTS assay, Abcam catalog # ab197010) was added to each well. After 1 h, the absorbance of the 96-well plate was measured at 495 nm to quantify orange-brown formazan complex formed. Cell viability was considered to be proportional to the absorbance of the wells. The absorbance value of all control and treated wells was subtracted by the average absorbance value of the wells containing no cell but only solution of MTS (background). Percent cell viability was calculated using the following equation: $(A_{\text{conc}}/A_{\text{control}}) \times 100\%$, where A_{conc} is the absorbance at a certain concentration of tested compound, and A_{control} is the absorbance of the untreated wells. IC_{50} value was calculated from the sigmoidal curve fit of this data at 50% cell viability.

Aldehyde Detoxification. Cells were seeded in 96-well plate (~7,000 cells/well) and incubated at 37 °C with 5% CO₂ for ~15 hours (with NIH 3T3), or ~48 hours (with SH-SY5Y). The old cell culture medium was aspirated, and the new one with Iridium complex or aldehyde scavenger was added. At the end of the treatment period, the medium was removed, and cells were washed twice with fresh cell culture medium. The new cell culture medium with toxic aldehyde was then added, and cells were incubated at 37 °C with 5% CO₂ for 24 hours. Cell viability was then checked by SRB assay as described previously. The detoxification effect of iridium complex or aldehyde scavenger was then calculated as ratio of percentage of viable cells in treated wells and percentage of viable cells in negative control wells (with only toxic aldehyde). Positive control (with no added compound) was set as 100% cell viability.

5.9 References

1. Schauenstein, E. E., H.; Zollner, H. , Aldehydes in Biological Systems: Their Natural Occurances and Biological Activities. *Pion Limited: London* **1977**.
2. Witz, G., Biological interactions of α,β -unsaturated aldehydes. *Free Radical Biology and Medicine* **1989**, 7 (3), 333-349.
3. Dalleau, S.; Baradat, M.; Guéraud, F.; Huc, L., Cell death and diseases related to oxidative stress: 4-hydroxynonenal (HNE) in the balance. *Cell death and differentiation* **2013**, 20 (12), 1615-1630.
4. Csala, M.; Kardon, T.; Legeza, B.; Lizák, B.; Mandl, J.; Margittai, É.; Puskás, F.; Száraz, P.; Szelényi, P.; Bánhegyi, G., On the role of 4-hydroxynonenal in health and disease. *Biochimica et Biophysica Acta (BBA) - Molecular Basis of Disease* **2015**, 1852 (5), 826-838.
5. Dang Thanh, N.; Madeleine, A.; Ven, M.; Charles, R., Potential Role of Acrolein in Neurodegeneration and in Alzheimers Disease. *Current Molecular Pharmacology* **2010**, 3 (2), 66-78.

6. Poli, G.; Schaur, R. J.; Siems, W. G.; Leonarduzzi, G., 4-Hydroxynonenal: A membrane lipid oxidation product of medicinal interest. *Medicinal Research Reviews* **2008**, *28* (4), 569-631.
7. Lee, S. E.; Park, Y. S., Role of lipid peroxidation-derived α , β -unsaturated aldehydes in vascular dysfunction. *Oxidative medicine and cellular longevity* **2013**, *2013*, 629028-629028.
8. West, J. D.; Ji, C.; Duncan, S. T.; Amarnath, V.; Schneider, C.; Rizzo, C. J.; Brash, A. R.; Marnett, L. J., Induction of Apoptosis in Colorectal Carcinoma Cells Treated with 4-Hydroxy-2-nonenal and Structurally Related Aldehydic Products of Lipid Peroxidation. *Chemical Research in Toxicology* **2004**, *17* (4), 453-462.
9. Zhong, H.; Yin, H., Role of lipid peroxidation derived 4-hydroxynonenal (4-HNE) in cancer: focusing on mitochondria. *Redox biology* **2015**, *4*, 193-199.
10. Sayre, L. M.; Lin, D.; Yuan, Q.; Zhu, X.; Tang, X., Protein Adducts Generated from Products of Lipid Oxidation: Focus on HNE and ONE. *Drug Metabolism Reviews* **2006**, *38* (4), 651-675.
11. Grimsrud, P. A. X., H.; Griffin, T. J.; Bernlohr, D. A., Oxidative Stress and Covalent Modification of Protein with Bioactive Aldehydes. *J. Biol. Chem.* **2008**, *283*, 21837-21841.
12. Bradley, M. A.; Xiong-Fister, S.; Markesbery, W. R.; Lovell, M. A., Elevated 4-hydroxyhexenal in Alzheimer's disease (AD) progression. *Neurobiology of Aging* **2012**, *33* (6), 1034-1044.
13. Schaur, R. J.; Siems, W.; Bresgen, N.; Eckl, P. M., 4-Hydroxy-nonenal-A Bioactive Lipid Peroxidation Product. *Biomolecules* **2015**, *5* (4), 2247-2337.
14. Siegel, S. J.; Bieschke, J.; Powers, E. T.; Kelly, J. W., The oxidative stress metabolite 4-hydroxynonenal promotes Alzheimer protofibril formation. *Biochemistry* **2007**, *46* (6), 1503-1510.
15. Xie, Z.; Baba, S. P.; Sweeney, B. R.; Barski, O. A., Detoxification of aldehydes by histidine-containing dipeptides: From chemistry to clinical implications. *Chemico-Biological Interactions* **2013**, *202* (1), 288-297.
16. Cho, K. H.; Shim, S. H.; Kim, M., Clinical, biochemical, and genetic aspects of Sjögren-Larsson syndrome. *Clinical Genetics* **2017**, *93* (4), 721-730.
17. Kim, K.-J.; Pearl, P. L.; Jensen, K.; Snead, O. C.; Malaspina, P.; Jakobs, C.; Gibson, K. M., Succinic semialdehyde dehydrogenase: biochemical-molecular-clinical disease mechanisms, redox regulation, and functional significance. *Antioxidants & redox signaling* **2011**, *15* (3), 691-718.
18. Aldini, G.; Carini, M.; Beretta, G.; Bradamante, S.; Facino, R. M., Carnosine is a quencher of 4-hydroxy-nonenal: through what mechanism of reaction? *Biochemical and Biophysical Research Communications* **2002**, *298* (5), 699-706.
19. Guiotto, A.; Calderan, A.; Ruzza, P.; Osler, A.; Rubini, C.; Jo, D.-G.; Mattson, M. P.; Borin, G., Synthesis and Evaluation of Neuroprotective α,β -Unsaturated Aldehyde

- Scavenger Histidyl-Containing Analogues of Carnosine. *Journal of Medicinal Chemistry* **2005**, *48* (19), 6156-6161.
20. Galvani, S.; Coatrieux, C.; Elbaz, M.; Grazide, M.-H.; Thiers, J.-C.; Parini, A.; Uchida, K.; Kamar, N.; Rostaing, L.; Baltas, M.; Salvayre, R.; Nègre-Salvayre, A., Carbonyl scavenger and antiatherogenic effects of hydrazine derivatives. *Free Radical Biology and Medicine* **2008**, *45* (10), 1457-1467.
 21. Bertinaria, M.; Rolando, B.; Giorgis, M.; Montanaro, G.; Guglielmo, S.; Buonsanti, M. F.; Carabelli, V.; Gavello, D.; Daniele, P. G.; Fruttero, R.; Gasco, A., Synthesis, Physicochemical Characterization, and Biological Activities of New Carnosine Derivatives Stable in Human Serum As Potential Neuroprotective Agents. *Journal of Medicinal Chemistry* **2011**, *54* (2), 611-621.
 22. Aloisi, A.; Barca, A.; Romano, A.; Guerrieri, S.; Storelli, C.; Rinaldi, R.; Verri, T., Anti-Aggregating Effect of the Naturally Occurring Dipeptide Carnosine on A β 1-42 Fibril Formation. *PLOS ONE* **2013**, *8* (7), e68159.
 23. Maheshwari, M.; Roberts, J. K.; DeSutter, B.; Duong, K. T.; Tingling, J.; Fawver, J. N.; Schall, H. E.; Kahle, M.; Murray, I. V. J., Hydralazine Modifies A β Fibril Formation and Prevents Modification by Lipids in Vitro. *Biochemistry* **2010**, *49* (49), 10371-10380.
 24. Barreca, D.; Currò, M.; Bellocco, E.; Ficarra, S.; Laganà, G.; Tellone, E.; Laura Giunta, M.; Visalli, G.; Caccamo, D.; Galtieri, A.; Ientile, R., Neuroprotective effects of phloretin and its glycosylated derivative on rotenone-induced toxicity in human SH-SY5Y neuronal-like cells. *BioFactors* **2017**, *43* (4), 549-557.
 25. Falletti, O.; Cadet, J.; Favier, A.; Douki, T., Trapping of 4-hydroxynonenal by glutathione efficiently prevents formation of DNA adducts in human cells. *Free Radical Biology and Medicine* **2007**, *42* (8), 1258-1269.
 26. LoPachin, R. M.; Gavin, T., Molecular Mechanisms of Aldehyde Toxicity: A Chemical Perspective. *Chemical Research in Toxicology* **2014**, *27* (7), 1081-1091.
 27. <https://clinicaltrials.gov/ct2/show/NCT03131154>, accessed on December 26, 2018.
 28. <https://www.aldeyra.com/development-status/>, accessed on December 26, 2018.
 29. Zhu, Q.; Sun, Z.; Jiang, Y.; Chen, F.; Wang, M., Acrolein scavengers: Reactivity, mechanism and impact on health. *Molecular Nutrition & Food Research* **2011**, *55* (9), 1375-1390.
 30. Vidal, N.; Cavaille, J. P.; Graziani, F.; Robin, M.; Ouari, O.; Pietri, S.; Stocker, P., High throughput assay for evaluation of reactive carbonyl scavenging capacity. *Redox Biology* **2014**, *2*, 590-598.
 31. Rizzo, W. B., Fatty aldehyde and fatty alcohol metabolism: Review and importance for epidermal structure and function. *Biochimica et Biophysica Acta (BBA) - Molecular and Cell Biology of Lipids* **2014**, *1841* (3), 377-389.
 32. Wang, D.; Astruc, D., The Golden Age of Transfer Hydrogenation. *Chemical Reviews* **2015**, *115* (13), 6621-6686.

33. Ogo, S.; Makihara, N.; Watanabe, Y., pH-Dependent Transfer Hydrogenation of Water-Soluble Carbonyl Compounds with $[\text{Cp}^*\text{IrIII}(\text{H}_2\text{O})_3]^{2+}$ ($\text{Cp}^* = \eta^5\text{-C}_5\text{Me}_5$) as a Catalyst Precursor and HCOONa as a Hydrogen Donor in Water. *Organometallics* **1999**, *18* (26), 5470-5474.
34. Betanzos-Lara, S.; Liu, Z.; Habtemariam, A.; Pizarro, A. M.; Qamar, B.; Sadler, P. J., Organometallic Ruthenium and Iridium Transfer-Hydrogenation Catalysts Using Coenzyme NADH as a Cofactor. *Angewandte Chemie International Edition* **2012**, *51* (16), 3897-3900.
35. Ngo, A. H.; Bose, S.; Do, L. H., Intracellular Chemistry: Integrating Molecular Inorganic Catalysts with Living Systems. *Chemistry – A European Journal* **2018**, *24* (42), 10584-10594.
36. Ngo, A. H.; Ibañez, M.; Do, L. H., Catalytic Hydrogenation of Cytotoxic Aldehydes Using Nicotinamide Adenine Dinucleotide (NADH) in Cell Growth Media. *ACS Catalysis* **2016**, *6* (4), 2637-2641.
37. Bose, S.; Ngo, A. H.; Do, L. H., Intracellular Transfer Hydrogenation Mediated by Unprotected Organoiridium Catalysts. *Journal of the American Chemical Society* **2017**, *139* (26), 8792-8795.
38. Ngo, A. H., Do, L. H., Optimization of Half-Sandwich Iridium Transfer Hydrogenation Catalysts Guided by Kinetic and Thermodynamic Studies. *Manuscript submitted for publication*.
39. Bose, S.; Do, L. H., *Unpublished results*.
40. Gardner, H. W.; Bartelt, R. J.; Weisleder, D., A facile synthesis of 4-hydroxy-2(E)-nonenal. *Lipids* **1992**, *27* (9), 686-689.
41. Yates, S. A.; Dempster, N. M.; Murphy, M. F.; Moore, S. A., Quantitative analysis of malondialdehyde-guanine adducts in genomic DNA samples by liquid chromatography/tandem mass spectrometry. *Rapid Communications in Mass Spectrometry* **2017**, *31* (9), 762-770.
42. Kaykhani, M.; Yahyavi, H.; Hashemi, M.; Khoshroo, M. R., A simple graphene-based pipette tip solid-phase extraction of malondialdehyde from human plasma and its determination by spectrofluorometry. *Analytical and Bioanalytical Chemistry* **2016**, *408* (18), 4907-4915.

Chapter 5 Appendix

Table A5.1 Accumulation of Iridium in NIH 3T3 Cells

A) 10 μ M Iridium Complexes Incubation

Time (hours)	Complex	ICP-MS (ppb)	Total Ir (ng)	Total Cells ($\times 10^6$)	[Ir] (ng/ 10^6 cells)	Average [Ir] (ng/ 10^6 cells)	SD
Control		0.0	0.3	0.306	1.1	2.9	1.7
		0.2	1.5	0.286	5.1		
		0.1	0.7	0.288	2.4		
24	Ir4	4.9	34.5	0.185	186.7	197.7	11.0
		4.0	28.3	0.136	208.6		
	Ir18	2.1	15.0	0.166	90.3	87.4	10.3
		2.3	15.9	0.161	98.4		
		1.0	7.1	0.097	73.6		
	Ir19	1.2	8.4	0.037	227.1	198.8	21.5
		3.2	22.5	0.129	175.1		
		3.0	20.8	0.107	194.3		
	Ir21	3.3	23.2	0.055	422.4	341.1	81.4
		1.3	8.9	0.034	259.7		
	Ir22	18.3	127.8	0.178	716.8	715.4	45.2
		8.2	57.1	0.087	659.3		
		21.1	147.6	0.192	770.0		
	Ir23	5.4	37.8	0.109	346.8	280.1	47.6
		6.3	43.9	0.173	254.1		
2.8		19.6	0.082	239.4			
3	Ir4	2.4	16.6	0.087	190.1	167.2	16.7
		1.1	8.0	0.050	160.5		
		1.0	7.0	0.047	150.9		
	Ir18	0.4	3.0	0.077	38.9	47.6	15.3
		0.4	2.7	0.039	69.0		
		1.0	6.7	0.192	34.8		
	Ir19	1.5	10.7	0.056	190.4	141.0	36.1
		0.6	4.0	0.038	105.3		
		0.6	4.2	0.033	127.3		
	Ir21	4.0	27.9	0.127	220.0	303.3	103.6
		3.0	21.0	0.047	449.3		
		1.6	11.3	0.047	240.6		
	Ir22	10.7	74.8	0.157	475.9	296.1	132.4
		3.3	22.8	0.091	251.2		
		4.2	29.5	0.183	161.1		
Ir23	1.6	10.9	0.086	127.3	173.6	42.8	
	2.0	14.1	0.086	163.0			
	2.7	18.7	0.081	230.6			

B) 20 μ M Iridium Complexes Incubation

Time (hours)	Complex	ICP-MS (ppb)	Total Ir (ng)	Total Cells ($\times 10^6$)	[Ir] (ng/ 10^6 cells)	Average [Ir] (ng/ 10^6 cells)	SD
24 h	Ir4	25.4	178.1	0.183	971.4	858.0	103.3
		20.2	141.6	0.161	881.1		
		8.8	61.8	0.086	721.4		
	Ir18	2.7	18.6	0.061	304.6	376.3	75.2
		6.5	45.5	0.095	480.2		
		4.0	28.2	0.082	344.0		
	Ir19	13.6	94.9	0.105	903.3	726.2	130.1
		12.0	84.0	0.141	594.6		
		6.0	42.1	0.062	680.7		
Ir21	13.0	91.1	0.049	1860.8	1380.3	340.7	
	5.9	41.5	0.037	1110.1			
	6.6	45.9	0.039	1169.9			
3 h	Ir4	7.1	50.0	0.108	463.0	465.3	172.7
		10.5	73.7	0.109	677.9		
		1.1	8.0	0.031	255.0		
	Ir18	1.8	12.5	0.083	150.4	182.3	82.8
		5.0	35.1	0.119	295.9		
		1.6	11.4	0.113	100.7		
	Ir19	4.4	31.1	0.051	611.4	393.9	155.5
		2.6	18.0	0.058	313.1		
		7.4	51.8	0.201	257.1		
Ir21	9.4	65.9	0.073	905.4	917.7	224.2	
	8.8	61.8	0.052	1198.3			
	10.8	75.8	0.117	649.5			

Table A5.2 Accumulation of Iridium in SH-SY5Y Cells

Time (hours)	Complex	ICP-MS (ppb)	Total Ir (ng)	Total Cells (x 10 ⁶)	[Ir] (ng/10 ⁶ cells)	Average [Ir] (ng/10 ⁶ cells)	SD
Control		0.004	0.031	0.1680	0.18	0.23	0.05
		0.004	0.030	0.1067	0.28		
24	Ir4	2.957	20.698	0.1177	175.90	168.6	39.2
		1.328	9.295	0.0793	117.27		
		2.004	14.027	0.0660	212.52		
	Ir18	1.566	10.960	0.1056	103.79	86.5	17.3
		0.892	6.247	0.0903	69.21		
	Ir19	2.618	18.325	0.1240	147.79	185.4	37.6
		3.520	24.641	0.1105	223.07		
	Ir21	10.364	72.548	0.1667	435.29	488.8	53.5
		10.820	75.740	0.1397	542.29		
	Ir22	10.458	73.206	0.1437	509.55	648.7	139.2
		10.588	74.116	0.0941	787.91		
	Ir23	1.755	12.285	0.0849	144.64	201.8	43.6
1.655		11.585	0.0462	250.58			
2.481		17.366	0.0827	210.07			
3	Ir4	1.473	10.311	0.0839	122.90	147.9	25.1
		5.457	38.199	0.2208	173.00		
	Ir18	0.809	5.666	0.1011	56.06	65.5	9.4
		0.871	6.094	0.0813	74.92		
	Ir19	3.561	24.928	0.1577	158.04	145.1	13.0
		1.486	10.399	0.0787	132.08		
	Ir21	2.738	19.166	0.1203	159.27	258.3	99.0
		10.670	74.690	0.2090	357.37		
	Ir22	1.206	8.442	0.0330	256.08	297.8	41.7
		2.418	16.928	0.0499	339.47		
Ir23	1.186	8.302	0.0886	93.74	106.4	12.7	
	1.636	11.452	0.0962	119.04			

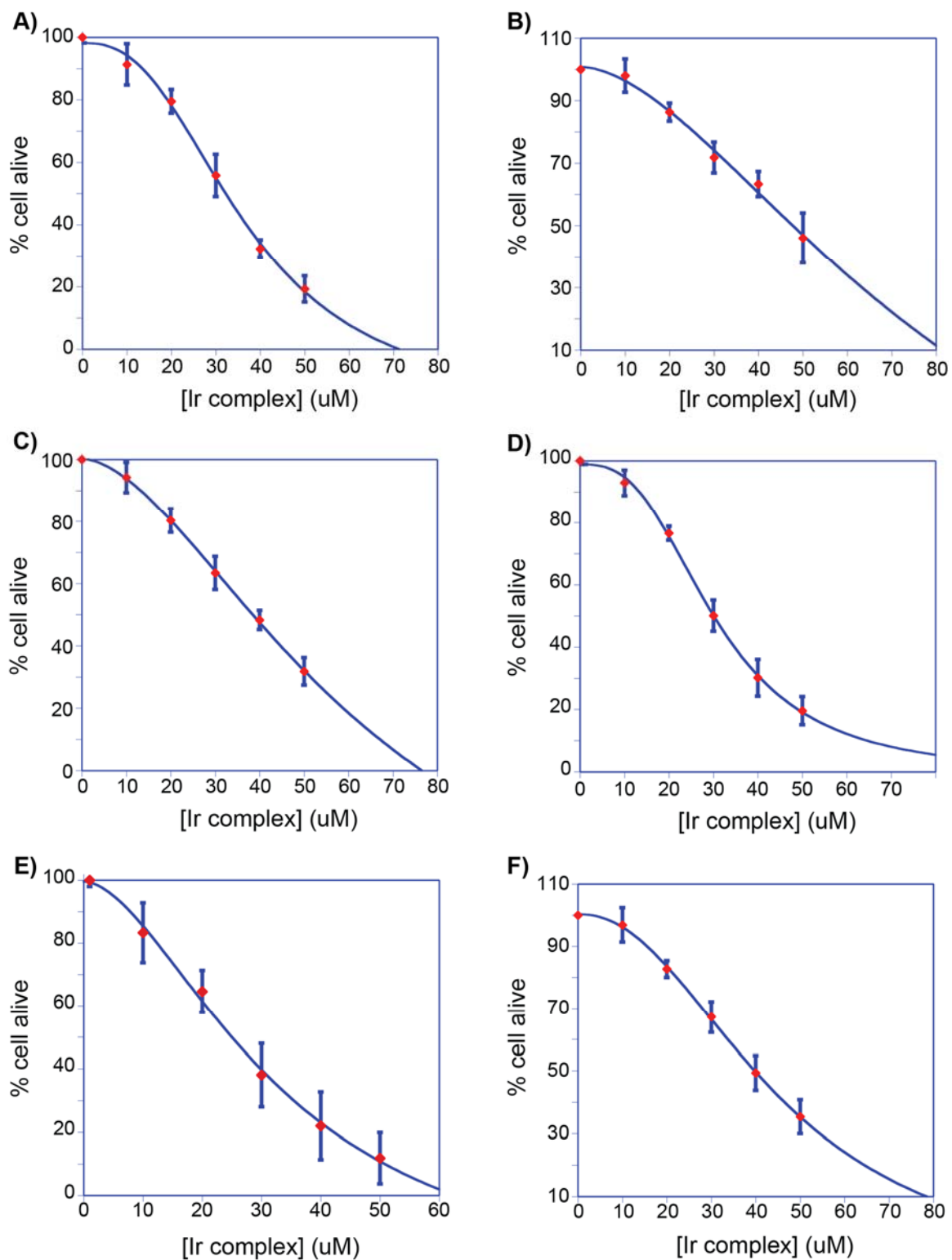


Figure A5.1. IC_{50} of Iridium complexes in SH-SY5Y cell line. A) Complex **Ir4**; B) Complex **Ir18**; C) Complex **Ir19**; D) Complex **Ir21**; E) Complex **Ir22**; F) Complex **Ir23**.

Chapter 6.

Iridium Complexes for Aldehyde Detoxification in Zebrafish

6.1 Introduction

Zebrafish (*Danio rerio*, also called Zebra Danio) are small freshwater fish from the southeastern Himalayan region in Asia, that are commonly used as whole organism models in biological research. Since the size of a mature fish is only about 3 to 4 cm long, it does not require large tanks to grow and is inexpensive to maintain.¹ Zebrafish have fast development time (hatches in 2-3 days), short generation time (matures in about 3 months), and produce a large number of offsprings (up to 200 eggs per batch from one pair of parents).¹⁻² Another advantage of zebrafish is the optical transparency of their embryos and young larvae, and even adults in some transparent mutants. The transparent fish allow easy visualization of their internal organs and make it possible to observe developmental changes. Zebrafish embryos are much larger in size (~ 650 μm in diameter) and grow out side of the mother so they are much easier to study than mouse embryos, which are smaller (~ 90 μm in diameter) and develop inside the animal.³ Zebrafish also have high genetic homology (~ 70%) to humans, which means that biological studies conducted in fish could have relevance to people.⁴

Zebrafish has been used in fish research since the 1980's⁵ and has become popular as a model organism for developmental, toxicological, and transgenic studies.^{1-2, 6-8} Because they have short life cycles, zebrafish is not only suitable for acute toxicity studies, but also useful for revealing potential long-term effects.⁷ Zebrafish have been used to evaluate the toxicity profiles of anticancer prodrugs,⁹⁻¹¹ antibacterial agents,¹²⁻¹³ insecticides,¹⁴⁻¹⁵ nanoparticles,¹⁶⁻¹⁸ and environmental toxins.¹⁹⁻²⁰ In 2004, Willett and co-workers developed a series of zebrafish bioassays for testing neurotoxic compounds, which includes protocols for visual assessment, quantification of motor neurons, and teratogenic

index (or teratogenicity).²¹ In 2013, Bondesson and co-workers also utilized zebrafish in their systematic analysis of toxicity and teratogenicity of 133 chemicals, which allowed them to rank the toxicity and evaluate the potential of these environmental pollutants in causing developmental defects.²²

α,β -unsaturated aldehydes, such as acrolein, crotonaldehyde, and 4-hydroxynonenal (4-HNE), have been found to be associated with many metabolic diseases, neurodegenerative disorders, and cancers due to their reactive unsaturated double bonds and aldehyde groups.²³⁻²⁶ In the following study, we used zebrafish as the model organism to evaluate the ability of Ir complexes to protect living organisms from cytotoxic α,β -unsaturated aldehydes.

6.2 Accumulation of Iridium Complexes in Zebrafish

To investigate how much iridium can be taken up by zebrafish, we incubated the fish with different concentration of Ir complexes for various times, and then measured their Ir concentrations by inductively-coupled plasma mass spectrometry (ICP-MS).

As shown in Table 6.1, accumulation of the iridium complexes inside zebrafish ranges from 2.9 to 52.9 ng per 100 fish. Different iridium complexes had different accumulation amounts, presumably due to their differences in hydrophobicity and charge (Figure 6.1A). Treating the fish with higher concentration (up to 50 μ M) can enhance their accumulation (Figure 6.1B). However, the iridium accumulation level does not increase linearly with increasing incubation time (Figure 6.1C), possibly because the iridium complexes could also diffuse out of the fish.

Table 6.1. Iridium Accumulation in Zebrafish.

<i>Ir complex</i>	<i>Incubation concentration</i>	<i>Incubation time</i>	<i>[Ir]⁽¹⁾ (ng/100 fish)</i>	<i>SD⁽²⁾</i>
None			1.6	3.4
			0.8	1.4
Ir2	10 μ M	3 h	2.9	5.6
Ir4	10 μ M	3 h	6.8	3.9
		1 h	24.1	2.3
	30 μ M	3 h	35.4	5.8
		5 h	26.3	5.2
50 μ M	3 h	52.9	7.7	
Ir18	10 μ M	3 h	10.1	4.7

(1) Data collected from single sample.

(2) Standard deviation was calculated from 3 runs.

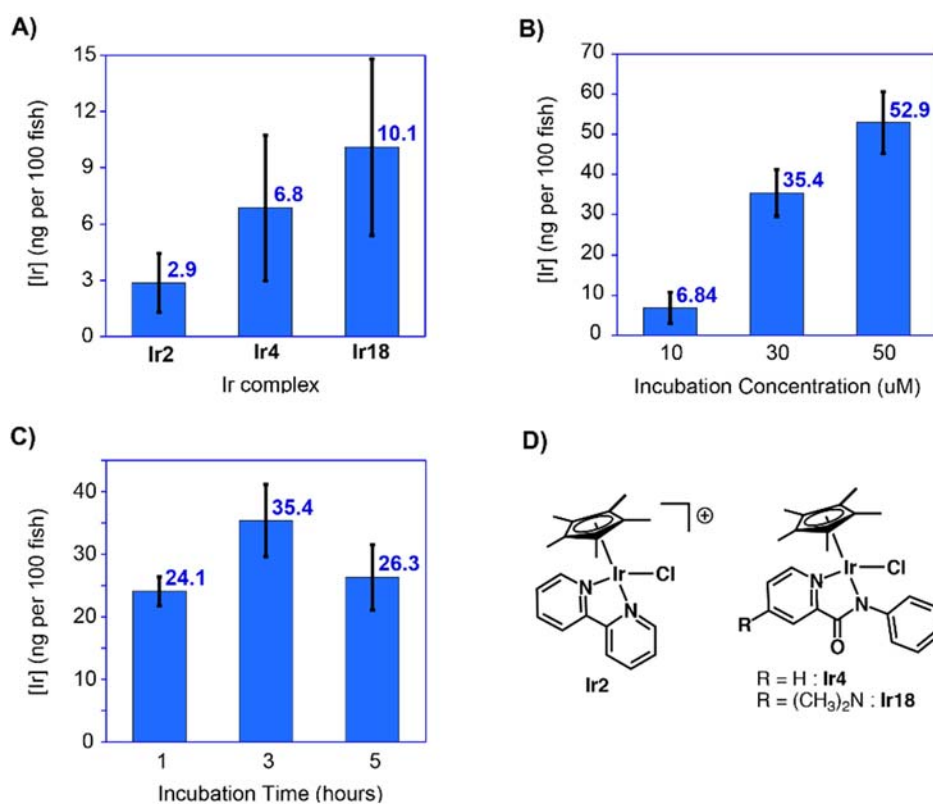
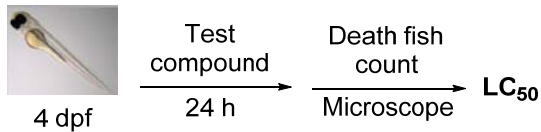


Figure 6.1. Iridium accumulation in zebrafish: A) Comparison of Ir complexes (10 μ M of catalyst, 3 h incubation); B) Comparison of incubation concentration (**Ir4** complex, 3 h incubation); C) Comparison of incubation time (**Ir4** complex, 30 μ M); D) Structures of Ir complexes used in zebrafish studies.

6.3 Toxicity of Iridium Complexes



Scheme 6.1. Procedure for determining toxicity of iridium complexes in zebrafish.

Although the iridium complexes that we tested shared similar structures, their zebrafish toxicity varied greatly. The lethal concentration required to kill 50% of zebrafish (LC_{50}) in 24 h were found to be $44 \pm 6 \mu\text{M}$ for **Ir18**, $78 \pm 18 \mu\text{M}$ for **Ir4**, and $5160 \pm 1173 \mu\text{M}$ for **Ir2** (Scheme 6.1 and Figure 6.2). This variation is most likely due to differences in the overall charge of the iridium complexes (**Ir2** is +1 while **Ir4** and **Ir18** are neutral). Interestingly, the complex has lowest iridium accumulation (**Ir2**) was the least toxic, whereas the complex with the highest iridium accumulation (**Ir18**) was the most toxic.

For the zebrafish studies described below, we employed low concentrations of Ir complexes ($5 \mu\text{M}$, $\leq 1/9 LC_{50}$), to minimize any Ir toxicity to the fish.

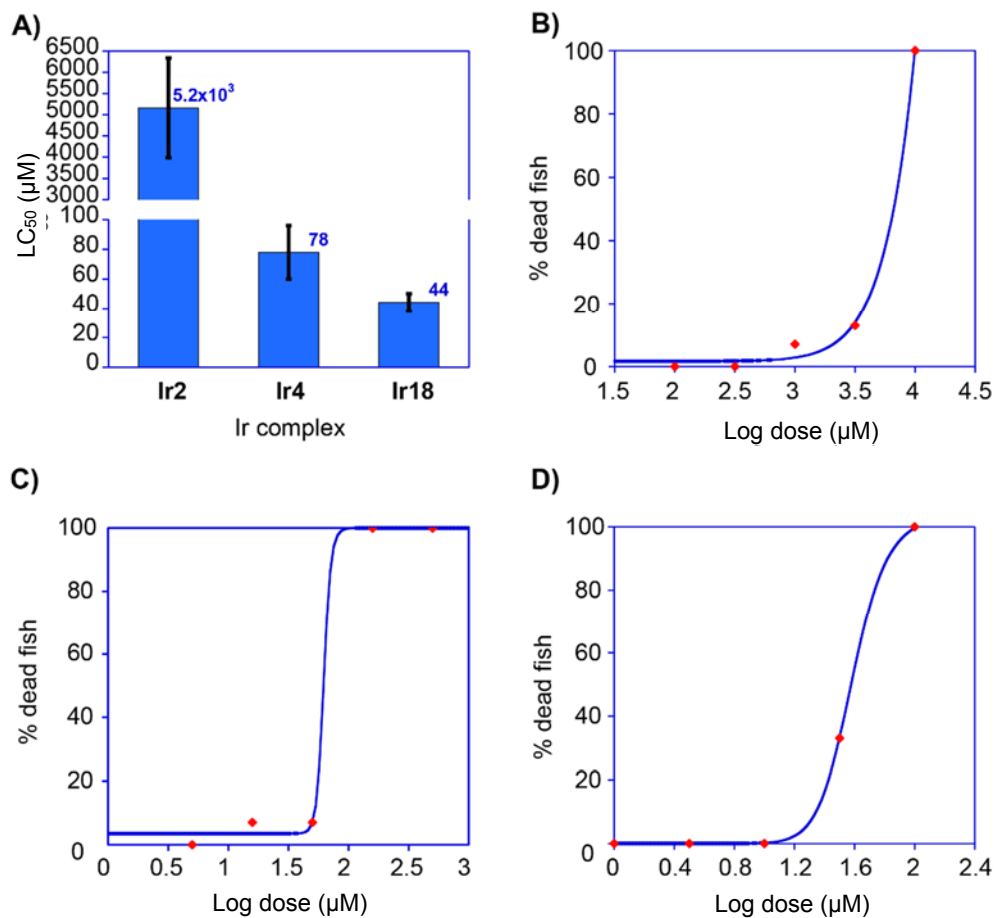


Figure 6.2. Toxicity of iridium complexes: A) Comparison of toxicity of all tested Ir complexes (24 h incubation, average results from 3 independent runs); B) LC₅₀ (24 h) of **Ir2**; C) LC₅₀ (24 h) of **Ir4**; C) LC₅₀ (24 h) of **Ir18**.

6.4 Toxicity of Acrolein and Alcohol Products

Before evaluating the ability of our Ir complexes to rescue zebrafish from toxic acrolein, we wanted to compare the toxicity of acrolein and its saturated and unsaturated alcohol products. As shown in Figure 6.3, acrolein is much more toxic compared to the alcohols. The LC_{50} (24 h) = $2.8 \pm 0.4 \mu\text{M}$ for acrolein, $3250 \pm 313 \mu\text{M}$ for allyl alcohol, and $134,000 \pm 31,000 \mu\text{M}$ for propanol. These results suggest that catalytic conversion of acrolein to non-toxic alcohols could be a viable approach to detoxification.

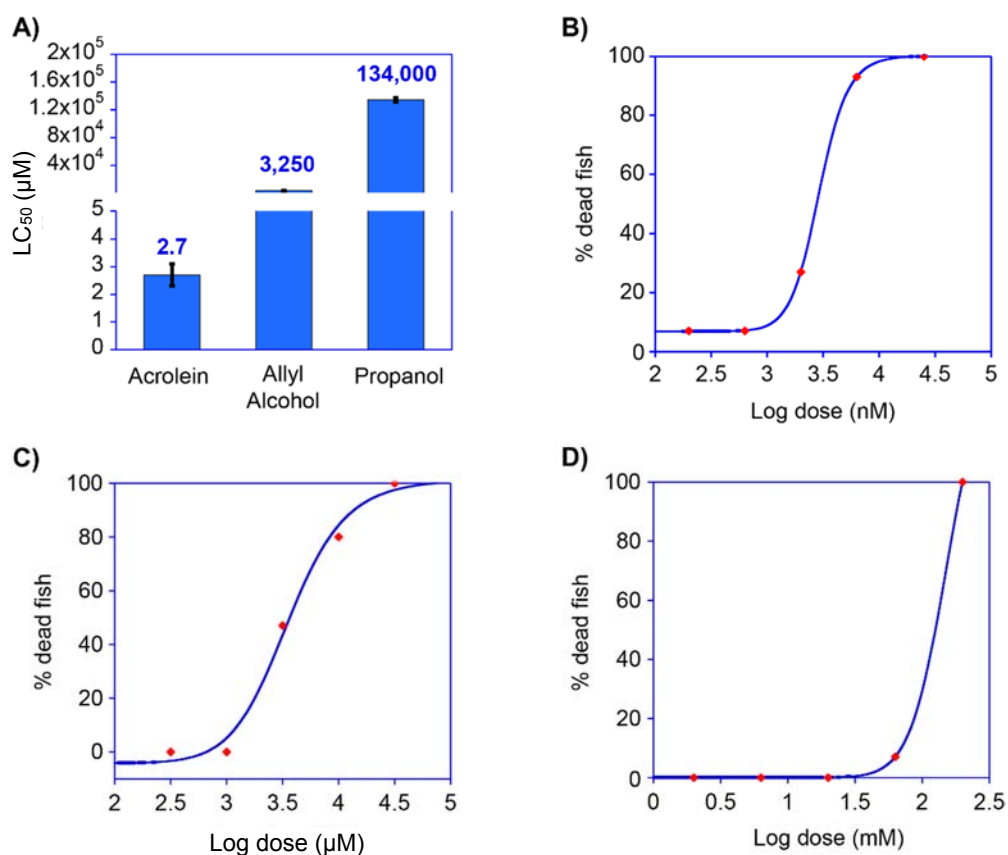
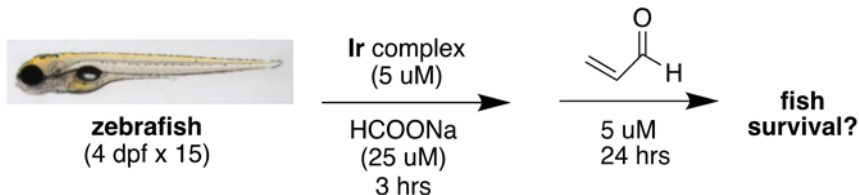


Figure 6.3. Toxicity of acrolein and its alcohol products: A) Comparison of toxicity of 3 tested compounds (24 h incubation, average results from 3 independent runs); B) LC_{50} (24 h) of acrolein; C) LC_{50} (24 h) of allyl alcohol; C) LC_{50} (24 h) of propanol.

6.5 Aldehyde Detoxification by Iridium Complexes in Zebrafish



Scheme 6.2. Procedure for aldehyde detoxification by iridium complexes in zebrafish.

In these studies, groups of fifteen zebrafish (4 dpf, days post fertilization) were treated with either **Ir2**, **Ir4** or **Ir18**, with or without addition of sodium formate as the hydride source, for 3 h. For some of the treatment groups, a washing procedure was performed to remove excess iridium complexes that were not taken up by the fish. The zebrafish were then grown in embryo medium (E3) containing 5 μM of acrolein for 24 h, at that time the number of dead fish were counted visually by a microscope (Figure 6.4).

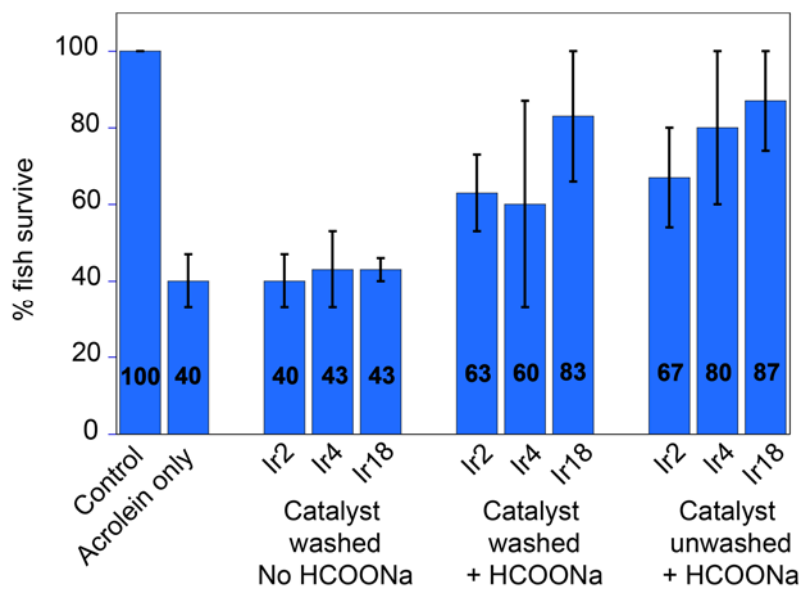


Figure 6.4. Effect of Ir SIMCats on zebrafish exposed to acrolein. Results were calculated from 2 independent runs, with 15 fish (4 dpf) per group per run.

Compared to the acrolein-only treatment group (6 out of 15 survived, or 40% survival), the presence of the Ir complexes and sodium formate increased the percentage of fish survival (60-87%). The removal of excess iridium before the addition of acrolein provided a lower level (4-20% less) of protection against the cytotoxic aldehyde. Addition of sodium formate (25 μM) helped to improve the fish survival by up to 20%, probably through the acceleration of both iridium-hydride formation and subsequent acrolein reduction. Among the iridium complexes tested, **Ir18** provided the highest level of protection (up to 17% higher compared to **Ir4**, and up to 20% higher compared to **Ir2**), which correlated well with their catalytic activities described in chapter 4.

6.6 Conclusion and Future Work

In summary, we have demonstrated that zebrafish are capable of taking up our organoiridium complexes. These iridium complexes, with LC_{50} values ranging from 44 μM to 5,200 μM , are shown to rescue up to 2.2 times, or 47% more zebrafish when treated with acrolein compared to those in control groups. Although these results are too preliminary to draw any definitive conclusions, they suggest that our Ir complexes are promising candidates for further aldehyde detoxification studies.

In future work, several different research avenues can be pursued. For example, other α,β -unsaturated aldehydes should be tested, such as 4-HNE, crotonaldehyde, or malondialdehyde. Fluorescent iridium complexes and substrates could be used to study their distribution and retention inside the fish. Experiments should be performed to measure fish hatching rates, hatching ratios, and other physiological characteristics to evaluate the potential of iridium complexes in preventing developmental defects in zebrafish. The

neurotoxicity of α,β -unsaturated aldehydes and detoxification ability of Iridium complexes could be assessed by motor neurons quantification or teratogenic index determination.

6.7 Experimental

Zebrafish for this study (transparent mutant type, *Nacre*) is available through the collaboration with Dr. Maria Bondesson from Center for Nuclear Receptors and Cell Signaling, University of Houston. The fish were kept in the zebrafish facility and taken care by staffs there, but were chosen, mated, and collected embryos by ourselves.

Zebrafish breeding and embryo collection: Fish are bred in spawning traps (for 8-12 fish) or spawning tanks (for 30-100 fish), with male and female ratio of 1:2. The fish were transferred from fish tanks to spawning vessels around 5 pm, and around 10 am the next day (~1 h after the fish are exposed to light) the eggs were collected. After collection using a net, the eggs were rinsed thoroughly with egg medium to remove any scales and feces. About 50-100 eggs were transferred to each petri dish with ~15 mL of embryo medium (i.e. E3 water, which include 83 μM NaCl, 2.8 μM KCl, 167 μM HEPES, 5.5 μM $\text{MgSO}_4 \cdot 7\text{H}_2\text{O}$, and 5.5 μM $\text{CaCl}_2 \cdot 6\text{H}_2\text{O}$). The eggs were checked under a microscope to remove all dead/deformed eggs, then incubated at 28.5°C. The embryos were examined every 24 h to remove all dead embryos until they are ready for experimentation.

LC₅₀ studies: Experiments were performed in 6 well plates (VWR cat # 10861-554). A group of 15 healthy fish (4 dpf, days post fertilization) were chosen and transferred to each well along with 3.0 mL of E3 water. Stock solutions of test compounds were prepared in DMSO, then diluted in E3 water to get the desired concentrations (DMSO was kept $\leq 1\%$ to minimize toxicity to the fish). A control well, which do not have any test compound,

was included in each plate. The plates were covered with sealing films to prevent spilling and cross-contamination between wells and then placed in an incubator at 28.5°C. After various incubation times, the fish were checked under microscope to assess their physical health (shape, movement, heart beat) and to count the number of dead fish.

ICP-MS preparation: A group of 100 zebrafish (4 dpf) was used for each experiment. After treated with an iridium complex for a certain amount of time, the fish were washed 3 times with E3 medium, then transferred to a 1 dram glass vial. The E3 medium in the vial was removed and then 350 µL of HNO₃ 65% was added to digest the fish overnight. The next day, the yellow slurry mixture (digested fish) was transferred to a 15 mL Falcon centrifuge tube, diluted with 4.5 mL of double distilled water, and centrifuged at 1500 rpm for 10 min. The clear, light yellow supernatant was then collected and ICP-MS was performed to analyze the concentration of iridium. The Ir concentrations were calculated using this equation:

$$[\text{Ir}] \text{ (ng/100 fish)} = [\text{Ir}] \text{ (in ppb)} \times 10^3 \times 0.00485 \text{ (L)}$$

Aldehyde Detoxification. Experiments were performed in 6 well plates (VWR cat # 10861-554). A group of 15 healthy fish (4 dpf, days post fertilization) were chosen and transferred to each well along with 3.0 mL of E3 water. Stock solutions of Iridium complex was prepared in DMSO, then diluted in E3 water to get the desired concentrations (DMSO was kept ≤ 1% to minimize toxicity to the fish). A control well, which do not have any test compound, was included in each plate. After 3 h, E3 water with Iridium complex was removed, and the fish were washed twice with fresh E3 water. The new E3 water with toxic aldehyde was then added, and the plates were covered with sealing films to prevent spilling

and cross-contamination between wells and then placed in an incubator at 28.5°C. After various incubation times, the fish were checked under microscope to assess their physical health (shape, movement, heart beat) and to count the number of dead fish.

6.8 References

1. Lele, Z.; Krone, P. H., The Zebrafish as a Model System in Developmental, Toxicological and Transgenic Research. *Biotechnology Advances* **1996**, *14* (1), 57-72.
2. Roper, C.; Tanguay, R. L., Chapter 12 - Zebrafish as a Model for Developmental Biology and Toxicology. In *Handbook of Developmental Neurotoxicology (Second Edition)*, Slikker, W.; Paule, M. G.; Wang, C., Eds. Academic Press: **2018**, 143-151.
3. Linney, E.; Upchurch, L.; Donerly, S., Zebrafish as a Neurotoxicological Model. *Neurotoxicology and Teratology* **2004**, *26* (6), 709-718.
4. Lee, J.; Freeman, J. L., Zebrafish as a Model for Developmental Neurotoxicity Assessment: The Application of the Zebrafish in Defining the Effects of Arsenic, Methylmercury, or Lead on Early Neurodevelopment. *Toxics* **2014**, *2* (3), 464-495.
5. Laale, H. W., The biology and use of zebrafish, *Brachydanio rerio* in Fisheries Research. *Journal of Fish Biology* **1977**, *10* (2), 121-173.
6. Teraoka, H.; Dong, W.; Hiraga, T., Zebrafish as a Novel Experimental Model for Developmental Toxicology. *Congenital Anomalies* **2003**, *43* (2), 123-132.
7. Froehlicher, M.; Liedtke, A.; Groh, K. J.; Neuhauss, S. C. F.; Segner, H.; Eggen, R. I. L., Zebrafish (*Danio rerio*) neuromast: Promising Biological Endpoint Linking Developmental and Toxicological Studies. *Aquatic Toxicology* **2009**, *95* (4), 307-319.
8. McCollum, C. W.; Ducharme, N. A.; Bondesson, M.; Gustafsson, J.-A., Developmental Toxicity Screening in Zebrafish. *Birth Defects Research Part C: Embryo Today: Reviews* **2011**, *93* (2), 67-114.
9. Zon, L. I.; Peterson, R. T., In vivo drug discovery in the zebrafish. *Nature Reviews Drug Discovery* **2005**, *4*, 35-44.
10. Lenis-Rojas, O. A.; Fernandes, A. R.; Roma-Rodrigues, C.; Baptista, P. V.; Marques, F.; Pérez-Fernández, D.; Guerra-Varela, J.; Sánchez, L.; Vázquez-García, D.; Torres, M. L.; Fernández, A.; Fernández, J. J., Heteroleptic Mononuclear Compounds of Ruthenium(II): Synthesis, Structural Analyses, In Vitro Antitumor Activity and In Vivo Toxicity on Zebrafish Embryos. *Dalton Transactions* **2016**, *45* (47), 19127-19140.
11. Ma, L.; Lin, X.; Li, C.; Xu, Z.; Chan, C.-Y.; Tse, M.-K.; Shi, P.; Zhu, G., A Cancer Cell-Selective and Low-Toxic Bifunctional Heterodinuclear Pt(IV)–Ru(II) Anticancer Prodrug. *Inorganic Chemistry* **2018**, *57* (5), 2917-2924.

12. Zhang, J.; Qian, J.; Tong, J.; Zhang, D.; Hu, C., Toxic Effects of Cephalosporins with Specific Functional Groups as Indicated by Zebrafish Embryo Toxicity Testing. *Chemical Research in Toxicology* **2013**, *26* (8), 1168-1181.
13. Zou, Y.; Zhang, Y.; Han, L.; He, Q.; Hou, H.; Han, J.; Wang, X.; Li, C.; Cen, J.; Liu, K., Oxidative Stress-Mediated Developmental Toxicity Induced By Isoniazide in Zebrafish Embryos and Larvae. *Journal of Applied Toxicology* **2017**, *37* (7), 842-852.
14. Xu, C.; Zhao, M.; Liu, W.; Chen, S.; Gan, J., Enantioselectivity in Zebrafish Embryo Toxicity of the Insecticide Acetofenate. *Chemical Research in Toxicology* **2008**, *21* (5), 1050-1055.
15. Ma, X.; Li, H.; Xiong, J.; Mehler, W. T.; You, J., Developmental Toxicity of a Neonicotinoid Insecticide, Acetamiprid to Zebrafish Embryos. *Journal of Agricultural and Food Chemistry* **2019**, *67* (9), 2429-2436.
16. Fako, V. E.; Furgeson, D. Y., Zebrafish as a Correlative and Predictive Model for Assessing Biomaterial Nanotoxicity. *Advanced Drug Delivery Reviews* **2009**, *61* (6), 478-486.
17. Pham, D.-H.; De Roo, B.; Nguyen, X.-B.; Vervaele, M.; Kecskés, A.; Ny, A.; Copmans, D.; Vriens, H.; Locquet, J.-P.; Hoet, P.; de Witte, P. A. M., Use of Zebrafish Larvae as a Multi-Endpoint Platform to Characterize the Toxicity Profile of Silica Nanoparticles. *Scientific Reports* **2016**, *6*, 37145.
18. Aerle, R.v.; Lange, A.; Moorhouse, A.; Paszkiewicz, K.; Ball, K.; Johnston, B. D.; de-Bastos, E.; Booth, T.; Tyler, C. R.; Santos, E. M., Molecular Mechanisms of Toxicity of Silver Nanoparticles in Zebrafish Embryos. *Environmental Science & Technology* **2013**, *47* (14), 8005-8014.
19. He, Z.; Zhu, R.; Xu, X.; Song, S.; Chen, J.; Xia, M., Ozonation Combined with Sonolysis for Degradation and Detoxification of m-Nitrotoluene in Aqueous Solution. *Industrial & Engineering Chemistry Research* **2009**, *48* (12), 5578-5583.
20. Riu, A.; McCollum, C. W.; Pinto, C. L.; Grimaldi, M.; Hillenweck, A.; Perdu, E.; Zalko, D.; Bernard, L.; Laudet, V.; Balaguer, P.; Bondesson, M.; Gustafsson, J.-A., Halogenated Bisphenol-A Analogs Act as Obesogens in Zebrafish Larvae (*Danio rerio*). *Toxicological sciences : an official journal of the Society of Toxicology* **2014**, *139* (1), 48-58.
21. Ton, C.; Lin, Y.; Willett, C., Zebrafish as a Model for Developmental Neurotoxicity Testing. *Birth Defects Research Part A: Clinical and Molecular Teratology* **2006**, *76* (7), 553-567.
22. Ducharme, N. A.; Peterson, L. E.; Benfenati, E.; Reif, D.; McCollum, C. W.; Gustafsson, J.-Å.; Bondesson, M., Meta-Analysis of Toxicity and Teratogenicity of 133 Chemicals from Zebrafish Developmental Toxicity Studies. *Reproductive Toxicology* **2013**, *41*, 98-108.

23. Dalleau, S.; Baradat, M.; Guéraud, F.; Huc, L., Cell Death and Diseases Related to Oxidative Stress: 4-Hydroxynonenal (HNE) in the Balance. *Cell death and differentiation* **2013**, *20* (12), 1615-1630.
24. Bradley, M. A.; Xiong-Fister, S.; Markesbery, W. R.; Lovell, M. A., Elevated 4-hydroxyhexenal in Alzheimer's Disease (AD) progression. *Neurobiology of Aging* **2012**, *33* (6), 1034-1044.
25. Dang Thanh, N.; Madeleine, A.; Ven, M.; Charles, R., Potential Role of Acrolein in Neurodegeneration and in Alzheimers Disease. *Current Molecular Pharmacology* **2010**, *3* (2), 66-78.
26. Siegel, S. J.; Bieschke, J.; Powers, E. T.; Kelly, J. W., The Oxidative Stress Metabolite 4-hydroxynonenal Promotes Alzheimer Protofibril Formation. *Biochemistry* **2007**, *46* (6), 1503-1510.